Purdue University
Purdue e-Pubs

Open Access Dissertations | Theses and Dissertations

8-2016

Development of orthogonally crosslinked thiol-ene hydrogels for encapsulation of pancreatic beta-cells

Han Shih
Purdue University

Follow this and additional works at: https://docs.lib.purdue.edu/open_access_dissertations

 Part of the Biomedical Engineering and Bioengineering Commons

Recommended Citation
Shih, Han, "Development of orthogonally crosslinked thiol-ene hydrogels for encapsulation of pancreatic beta-cells" (2016). *Open Access Dissertations*. 846.
https://docs.lib.purdue.edu/open_access_dissertations/846

This document has been made available through Purdue e-Pubs, a service of the Purdue University Libraries. Please contact epubs@purdue.edu for additional information.

Graduate School Form
30 Updated 12/26/2015

PURDUE UNIVERSITY
GRADUATE SCHOOL
Thesis/Dissertation Acceptance

This is to certify that the thesis/dissertation prepared

By Han Shih

Entitled

DEVELOPMENT OF ORTHOGONALLY CROSSLINKED THIOL-ENE HYDROGELS FOR ENCAPSULATION OF PANCREATIC β-CELLS

For the degree of Doctor of Philosophy

Is approved by the final examining committee:

Chien-Chi Lin
Co-chair

Alyssa Panitch
Co-chair

Raghavendra G. Mirmira

Dong Xie

To the best of my knowledge and as understood by the student in the Thesis/Dissertation Agreement, Publication Delay, and Certification Disclaimer (Graduate School Form 32), this thesis/dissertation adheres to the provisions of Purdue University's "Policy of Integrity in Research" and the use of copyright material.

Approved by Major Professor(s): Chien-Chi Lin

Approved by: George R. Wodicka 7/5/2016

Head of the Departmental Graduate Program Date

DEVELOPMENT OF ORTHOGONALLY CROSSLINKED THIOL-ENE HYDROGELS FOR ENCAPSULATION OF PANCREATIC β-CELLS

A Dissertation
Submitted to the Faculty
of
Purdue University
by
Han Shih

In Partial Fulfillment of the
Requirements for the Degree
of
Doctor of Philosophy

August 2016
Purdue University
West Lafayette, Indiana

ACKNOWLEDGEMENTS

I would like to acknowledge my dissertation advisor, Dr. Chien-Chi Lin, for his assistance, guidance and supervision during the entire course of this research and dissertation work. Dr. Lin generously shared with me his research experience and taught me useful knowledge and skills that I am always thankful and grateful for. He has given me plenty of opportunities to conduct excellent research and make me an independent researcher. I would not be able to excel without his support and training.

I would also like to thank my advisory committee members, Dr. Alyssa Panith, Dr. Dong Xie and Dr. Raghu Mirmira, for their time and insight for this dissertation work. In addition, I am thankful to have the opportunities to work with many excellent researchers in the Lin lab. Special thanks go to Dr. Changseok Ki, Dr. Tsai-Yu Lin, Mr. Zachary Munoz, and Ms. Tanja Greene for their friendship and support. Also, I would like to thank Ms. Sandra May for being patient and informative in assisting a distant student like myself.

Finally, I express my gratitude to my family and friends for their support and encouragement. In particularly, I want to thank my sister - Han Shih and Zachary Bart for their patience, understanding and company throughout my graduate study.

TABLE OF CONTENTS

Page

LIST OF TABLES v

LIST OF FIGURES vi

LIST OF ABBREVIATIONS xviii

NOMENCLATURE xix

ABSTRACT xx

1. INTRODUCTION 1

2. DYNAMIC CONTROL OF DEGRADABLE THIOL-ENE HYDROGELS 4
   - 2.1 Abstract 4
   - 2.2 Introduction 5
   - 2.3 Thiol-ene Hydrogel Network Crosslinking 12
   - 2.4 Degradation of Thiol-ene Hydrogel 17
   - 2.5 Applications of Thiol-ene Hydrogels in Controlled Release and Tissue Engineering 26
   - 2.6 Conclusion 30

3. VISIBLE LIGHT-INITIATED INTERFACIAL THIOL-ENE PHOTOPOLYMERIZATION FOR FORMING ISLET SURFACE CONFORMAL COATING 31
   - 3.1 Abstract 31
   - 3.2 Introduction 31
   - 3.3 Results and Discussion 33
   - 3.4 Materials and Methods 47
   - 3.5 Conclusion 53

Page

4. PHOTO-CLICK HYDROGELS PREPARED FROM FUNCTIONALIZED CYCLODEXTRIN AND POLY(ETHYLENE GLYCOL) FOR DRUG DELIVERY AND IN SITU CELL ENCAPSULATION....54
4.1 Abstract....54
4.2 Introduction....55
4.3 Results and Discussion....58
4.4 Materials and Methods....79
4.5 Conclusion....85

5. IMPROVING GELATION EFFICIENCY AND CYTOCOMPATIBILITY OF VISIBLE LIGHT POLYMERIZED THIOL-NORBORNENE HYDROGELS VIA ADDITION OF SOLUBLE TYROSINE....86
5.1 Abstract....86
5.2 Introduction....87
5.3 Results and Discussion....89
5.4 Materials and Methods....103
5.5 Conclusion....109

6. TUNING STIFFNESS OF CELL-LADEN HYDROGEL VIA HOST-GUEST INTERACTIONS....110
6.1 Abstract....110
6.2 Introduction....110
6.3 Results and Discussion....115
6.4 Materials and Methods....128
6.5 Conclusion....135

7. CONCLUSIONS AND RECOMMENDATION....136

LIST OF REFERENCES....139

VITA....158

LIST OF TABLES

Table		Page
Table 1.1	Advantages and disadvantages of microencapsulation and macroencapsulation	2
Table 2.1	Characteristics of step-growth Michael-type and thiol-ene hydrogels	16
Table 5.1	Area of norbornene peaks integrated from ^{1}H NMR results (Figure 5.4)	94
Table 5.2	Mouse primer sequences used in real time PCR	109
Table 6.1	Mouse primer sequences used in real time PCR	135

LIST OF FIGURES

Figure		Page
Figure 2.1	Schematics of hydrogels formed by: (A) Chain-growth photopolymerization using linear homo-bifunctional macromer to produce a heterogeneous network. (B) Step-growth photopolymerization of multifunctional and mutually reactive monomers. An idealized network structure is produced using a stoichiometric molar ratio of the two functional groups	6
Figure 2.2	Photo-cleavage of type I photoinitiator I-2959 (A) and LAP (B)	7
Figure 2.3	Structures of PEGDA (A), PEGDM (B), and acryalted PLA-PEG-PLA (C)	8
Figure 2.4	(A) Mechanism of radical-mediated thiol-ene photo-click reaction. (B) Synthesis route of PEG-tetra-ester-norbornene (PEG4eNB). (C) Synthesis route of PEG-tetra-amide-norbornene (PEG4aNB)	11
Figure 2.5	In situ rheometry of step-growth hydrogels: (A) Thiol−ene photoclick polymerization (4 wt % PEG4NB-DTT). UV light was turned on at 30 s. (B) Michael-type addition (4 wt % PEG4A-DTT). Temperature reached 37 °C at 15 s	14
Figure 2.6	Effect of PEG4NB macromer concentration on thiol-ene hydrogel equilibrium swelling (left y-axis) and elastic modulus (right y-axis). Swelling ratio of an ideal network was calculated based on the molecular weight between crosslinks ($\overline{M_c}$) of given macromer molecular weights (MW_{PEG4NB} = 20 kDa, MW_{DTT} = 154 Da) and functionalities (f_{PEG4NB} = 4, f_{DTT} = 2)	17

Figure Page

Figure 2.7 Effect of buffer pH on mass swelling ratio of 4 wt% PEG4NB-DTT hydrogels. Symbols represent experimental data while dashed curves represent exponential curve fitting to the experimental data. The apparent degradation rate constants (k_{hyd}) for gels degraded in pH 7.4 and pH 8.0 were 0.024 ± 0.001 and 0.057 ± 0.002 day^{-1} , respectively. Solid curves represent model predictions with best-fit kinetic rate constants: $k'_{pH\ 7.4} = 0.011\ day^{-1}$ and $k'_{pH\ 8.0} = 0.027\ day^{-1}$. No curve fitting or model prediction was made for gels degraded in pH 6.0 due to the stability of gels in acidic conditions 20

Figure 2.8 Effect of chymotrypsin concentration on mass loss of PEG4NB-CGGYC hydrogel (4wt% PEG4NB, N = 3, mean ± SEM)..... 22

Figure 2.9 (A) Schematic of visible light mediated photo-crosslinking and UV-mediated photodegradation of step-growth thiol-ene hydrogels crosslinked by PEG4NB and photolabile peptide CGOGC (O: L-2-nitrophenylalanine). (B) Effect of different wavelength UV lights (302 or 365 nm, 10 mW/cm^2) on reduction of residual hydrogel mass (N = 3, mean ± SEM)..... 24

Figure 2.10 Effect of peptide crosslinkers on PEG4NB-peptide hydrogels erosion/degradation. PEG4NB hydrogels crosslinked by different percentage of chymotrypsin sensitive (CGGYC) and non-degradable (CGGGC) peptides. Figure legends indicate the percent molar ratio of CGGYC:CGGGC..... 25

Figure 2.11 (A) Schematics of a thiol-ene cross-link. Arrows indicate potential cleavage sites. (B) Different modes of thiol-ene hydrogel degradation. PEG-ester-norbornene (R = O) or PEG-amide-norbornene (R = NH) can be used to construct gels with different hydrolytic degradability (only one arm is shown). With a proper combination of macromer and cross-linker, thiol-ene hydrogels can undergo different modes of degradation and produce different degradation products 29

Figure Page

Figure 3.1 (A) Schematic of visible light-initiated interfacial chain-growth (top) or step-growth thiol-ene (bottom) photopolymerization (EY: eosin-Y). (B) Viability of aggregates after non-gelling interfacial photopolymerization reactions (Green: live cells. Red: dead cells. Scales: 100 μm) 35

Figure 3.2 Schematic of visible light-mediated interfacial thiol-ene photopolymerization and conformal coating on β-cell aggregates or islets via: (A) one-step or (B) two-step coating method 37

Figure 3.3 (A) Schematic of visible light-initiated step-growth orthogonal thiol-ene reaction to form idealized hydrogel network. (B) Representative phase-contrast images of the conformal coated aggregates. (C) Representative live/dead stained images of the conformal coated aggregates (Scales: 50μm). (D-F) Effects of coating methods on (D) the cumulative distribution of conformal gel coating thickness, (E) the average coating thickness, and (F) the percent of coated aggregates. (G) Effect of aggregate diameter on thiol-ene conformal coating thickness. (One-step: 20 wt% PEG8NB-DTT and 30 seconds of light exposure. Two-step: 20 wt% PEG8NB-DTT, 3.4 kDa PEGdSH and 30 seconds of light exposure. Mean ± SEM, n > 200 aggregates) 38

Figure 3.4 (A-C) Representative phase-contrast images of MIN6 cell aggregates with thiol-ene conformal gel coating (two-step coating method). PEGdSH MW: (A) 2 kDa, (B) 3.4 kDa, and (C) 10 kDa. Arrows and dashed lines indicate the boundary of the hydrogel coating (Scales: 50 μm). (D-F) Parameters affecting thiol-ene conformal coating thickness: (D) molecular weight of PEGdSH, (E) photopolymerization time, and (F) concentration of macromer PEG8NB. Coating conditions: (A-D) 20 wt% of PEG8NB-DTT and 30 seconds of light exposure. (E) 3.4 kDa of PEGdSH and 30 seconds of light exposure. (F) 20 wt% of PEG8NB-DTT and 3.4 kDa of PEGdSH (Mean ± SEM, n > 200 aggregates) 39

Figure 3.5 Effects of molecular weight of PEGdSH on (A) cumulative distribution of conformal gel coating thickness, and (B) percent of coated aggregates. (20 wt% of PEG8NB-DTT, $R_{[PEG8NB]:[DTT]}$ = 1, 30 seconds of light exposure. Mean ± SEM) 40

Figure Page

Figure 3.6 Effects of PEG8NB concentration in the precursor solution on (A) cumulative distribution of conformal gel coating thickness, and (B) percent of coated aggregates. (MW of PEGSH = 3.4 kDa, $R_{[PEG8NB]:[DTT]}$ = 1 , 30 seconds of light exposure. Mean ± SEM) 41

Figure 3.7 Effects of polymerization time on (A) cumulative distribution of conformal gel coating thickness, and (B) percent of coated aggregates. (MW of PEGSH = 3.4 kDa, 20 wt% of PEG8NB-DTT, $R_{[PEG8NB]:[DTT]}$ = 1. Mean ± SEM) 41

Figure 3.8 (A) Effect of PEG8NB concentration on the mesh size (ξ) of hydrogels. The mesh size of an ideal network (ξ_{ideal}) was determined by Flory-Rehner equations (Equation 3.1 to 3.6). The experimental mesh size (ξ_{exp}) was calculated from the swelling ratio of PEG8NB-DTT hydrogels at different macromer contents (Equation 3.4, 3.5 & 3.6). Diameter of insulin was obtained from reference [124]. (B) Effect of PEG8NB concentration on the diffusion coefficient (D_g) of insulin in swollen hydrogel. The diffusion coefficient of insulin in pure solvent is obtained from reference [6] and the calculation of D_g was based on Lustig-Peppes model in reference [130]. (PEG8NB-DTT, 0.1 mM of eosin-Y, 5 minutes of light exposure, N = 5. Mean ± SEM) 44

Figure 3.9 (A) Schematic representation of thiol-ene hydrogels formed by hydrolytically degradable PEG8NB and non-degradable PEGa8NB. Effects of PEG macromer on (B) gel fraction, and (C) hydrolytic degradability of hydrogels. (20 wt% PEG8NB or PEGa8NB-DTT, 0.1 mM of eosin-Y, 5 minutes of light exposure, N = 5. Mean ± SEM) 45

Figure Page

Figure 3.10 (A) Representative live/dead stained images of non-coated and coated CD1 mice islets (24 hours after coating). (B-C) Representative phase contrast images of non-coated (top) and coated (bottom) CD1 mice islets on day 2 (B), and day 14 (C). Arrows and dashed lines in (b-c) indicate the boundary of the hydrogel coating (Scales: 50 μm). (D-E) *In vitro* glucose stimulated insulin secretion (GSIS) of isolated islets on (d) day 2 and (E) day 14. Asterisks indicate statistical significance between 2.5 and 25 mM of glucose within each group (Mean ± SEM, $p < 0.05$). Coating conditions: 3.4 kDa PEGdSH, 20 wt% PEGa8NB-DTT, 25 seconds light exposure 46

Figure 3.11 *In vitro* glucose stimulated insulin secretion (GSIS) index of CD1 murine islets. GSIS index is the normalization of insulin secreted at high glucose to low glucose. (Coating conditions: 3.4 kDa PEGdSH, 20 wt% PEGa8NB-DTT and 25 seconds light exposure. Mean ± SEM) 47

Figure 4.1 (A) Schematics of βCD modifications. (i) NaH, DMF, room temperature; (ii) allylbromide, DMF, room temperature; (iii) thioacetic acid, I-2959, UV (365 nm, 10 mW/cm^2), 30 min; (iv) sodium hydroxide (aq.), followed by neutralization with hydrogen chloride. ^1H NMR of (B) βCD, (C) βCD-AE, and (D) βCD-SH (dissolved in $(CD_3)_2SO$) 59

Figure 4.2 Mass spectroscopy of CD derivatives. (A) Mass-to-charge (m/z) for un-modified βCD (B-D) βCD-AE with increasing feed ratio of NaH and allylbromide (B: 2.3-, C: 4.5-, and D: 11.3-fold) 60

Figure 4.3 Thiol-content on βCD, βCD-AE, and βCD-SH measured by Ellman's assay 60

Figure Page

Figure 4.4 (A) Scheme of light and radical mediated thiol-allylether gelation. (B) *In situ* photorheometry of thiol-allylether photopolymerization (G': storage modulus; G": loss modulus) between PEG8SH and βCD-AE. (C) *In situ* photorheometry of solution containing PEG8SH and βCD. (D) Scheme of light and radical mediated thiol-norbornene gelation. (E) *In situ* photorheometry of thiol-norbornene photopolymerization PEG8NB and βCD-SH. (F) *In situ* photorheometry of solution containing PEG8NB and βCD (5 wt% PEG8SH or PEG8NB, 24 mg/mL of βCD-AE or βCD-SH, 1 mM LAP). Light (365 nm, 10 mW/cm^2) was turned on at 30 seconds (dotted line). N = 3, error bars were omitted for clarity 62

Figure 4.5 *In situ* photorheometry showing the evolution of storage modulus (G') and loss modulus (G") of thiol-allylether photopolymerization at 5 wt% PEG8SH and various CD-AE concentration in the precursor solution (1 mM LAP, 365nm light at 10 mW/cm^2). Light was turned on at 30 seconds (dotted line). N = 3, error bars were omitted for clarity 63

Figure 4.6 Evaluation of potential LAP/CD complex formation using reverse-phase HPLC. (A) 0.1mM LAP was injected into C18 analytical column using acetonitrile/ phosphate buffer (35/65) as the mobile phase. The mobile phase also contained different concentrations of βCD as indicated. Absorbance was measured at 280 nm. N = 3, error bars were omitted for clarity. (B) Elution time corresponds to maximum absorbance of LAP. (Mean ± SD, N = 3) 65

Figure 4.7 *In situ* photorheometry of thiol-ene hydrogels crosslinked by βCD-SH and (A) PEG4NB (20 kDa), (B) PEG8NB (40 kDa) or (C) PEG8NB (20 kDa). (5 wt% PEGNB, [thiol] = [norbornene], 1 mM LAP). Light (365 nm, 10 mW/cm^2) was turned on at 30 seconds (dotted line). N = 3, error bars were omitted for clarity 67

Figure Page

Figure 4.8 Effect of crosslinker on (A) gel fraction, (B) elastic modulus at equilibrium gel swelling, (C) shear modulus as a function of time, and (D) swelling ratio as a function of time. Asterisks indicate statistical significance ($p < 0.05$, 5 wt% 20 kDa PEG8SH or PEG8NB, 1 mM LAP, 365 nm light, intensity at 5 mW/cm^2, mean ± SD, N = 3) 69

Figure 4.9 Effect of crosslinker on shear modulus as a function of time in pH 9 PBS. (5 wt% 20 kDa PEG8SH or PEG8NB, 1 mM LAP, 365 nm light, intensity at 5 mW/cm^2, mean ± SD, N = 3) 70

Figure 4.10 (A) Photographs of thiol-allylether hydrogels incubated in curcumin suspended ddH_2O for 8 hours (top) and after DMSO-treatment (bottom). (B) Curcumin uptake in hydrogels formed by 5 wt% PEG8SH with 3.4 kDa of PEGAE or 24 mg/mL βCD-AE (1 mM LAP, 365 nm light at 10 mW/cm^2) 71

Figure 4.11 (A) Photographs of thiol-allylether hydrogels: (1) immediately after photopolymerization, (2) after incubating in curcumin solution for 36 hours, (3) after 100 hours of release in pH 7.4 PBS, and (4) after an additional 100 hours of release in DMSO (scale: 5 mm). (B) Effect of crosslinker on curcumin uptake in the gel. (C) Curcumin release from thiol-allylether hydrogel formed by 5 wt% PEG8SH with 3.4 kDa of PEGAE or 24 mg/mL βCD-AE (1 mM LAP, 365 nm light at 10 mW/cm^2) 73

Figure 4.12 Effect of crosslinker on the cytocompatibility of thiol-ene hydrogels on MIN6 β-cells. (A) Representative confocal z-stack images of MIN6 cells stained with live/dead staining kit on day 1 and day 10. MIN6 cells were encapsulated (2×10^6 cells/mL) in thiol-ene hydrogels crosslinked by DTT, CD-SH or CD-AE. (B) Cells viability as assessed by Alamarblue® reagent. (C) Normalized insulin secretion. All gel formulations contained 5 wt% 20 kDa PEG8SH or PEG8NB, 1 mM LAP, and 365 nm light at 5 mW/cm^2 (Scales: 100 μm) 75

Figure Page

Figure 4.13 Effect of crosslinker on the intracellular ATP content of MIN6 β-cells encapsulated in thiol-ene hydrogels. ATP contents were measured by CellTiter-Glo® reagent (mean ± SD, N = 3). All gel formulations contained 5 wt% 20kDa PEG8SH or PEG8NB, 1 mM LAP, and 365nm light at 5 mW/cm^2 76

Figure 4.14 Effect of crosslinker on elastic modulus at equilibrium swelling. Asterisk indicates statistical significant between crosslinker βCD-SH and DTT, R < 0.05. (5 wt% PEG4NB$_{20kDa}$, [thiol] = [norbornene] = 10 mM, 1 mM LAP, light intensity at 10 mW/cm^2, mean ± SD, N = 3) 77

Figure 4.15 Effect of crosslinker on the cytocompatibility of thiol-ene hydrogel on MIN6 β-cells. (A) Representative confocal z-stack images of MIN6 stained with live/dead staining kit on day 1 and 10. MIN6 were encapsulated (2×10^6 cells/mL) in thiol-ene hydrogels crosslinked by βCD-SH (left column) or DTT (right column). MIN6 β-cells viability measured by (B) CellTiter-Glo®, and (C) Alamarblue® reagent (mean ± SD, N = 3). All gel formulations contained 5 wt% PEG4NB$_{20kDa}$, [thiol] = [norbornene] = 10 mM, 1 mM LAP, and light at 5 mW/cm^2. (Scale: 100 μm) 78

Figure 5.1 (A) Scheme of visible light and eosin-Y mediated thiol-norbornene gelation. (B, C) *In situ* photorheometry of thiol-norbornene photopolymerization between 3wt% PEG8NB and 6mM CGGGC in the presence of 0 mM (B), and 1 mM of tyrosine (C). G': storage modulus; G": loss modulus. Eosin-Y: 0.1 mM. Light intensity: 70,000 lux. N = 3. Error bars were omitted for clarity. In collaboration with Hung-Yi Liu 91

Figure 5.2 *In situ* photorheometry of thiol-norbornene photopolymerization between 5wt% PEG4NB$_{20kDa}$ and 5 mM of DTT or di-cysteine containing peptide in the presence of 0.1 mM eosin-Y. G': storage modulus. Light intensity: 70,000 lux. N = 3. Error bars were omitted for clarity 92

Figure 5.3 Thiol conversion quantified by Ellman's assay. The right panel shows the shaded region in the left plot. (3.4 wt% PEGdNB$_{6kDa}$, 12 mM L-cysteine, 0.1 mM eosin-Y. Tyrosine was added at indicated concentration, N = 3). In collaboration with Hung-Yi Liu 93

Figure Page

Figure 5.4 Effect of tyrosine on norbornene conversion determined by ^{1}H NMR using non-gelling components: PEGdNB$_{6kDa}$ (3.6 wt%), soluble cysteine (12 mM), eosin-Y (0.1 mM), and tyrosine from 0 mM to 10 mM (from top to bottom). All prepared with D_2O (at 4.8 ppm). The integration of the areas under the norbornene peaks are reported in Table 5.1 94

Figure 5.5 (A) Photograph of hydrogels at equilibrium swelling. UV-vis spectra of eosin-Y before (thick blue) and after (thin red) visible light exposure for 5 minutes in the presence of PEGdNB, CGGGC, and varied concentrations of tyrosine. Tyrosine concentration: (B) 0 mM, (C) 0.1 mM, (D) 1 mM, and (E) 10 mM. Eosin-Y concentration in all measurements: 0.1 mM. (3.4 wt% PEGdNB$_{6kDa}$ or 3 wt% PEG8NB$_{20kda}$, 6 mM CGGGC, 0.1 mM eosin-Y, 400-700 nm light, intensity at 70,000 lux, mean ± SD, N = 3) 95

Figure 5.6 UV-vis spectra of eosin-Y before (thick blue) and after (thin red) visible light exposure for 5 minutes in the presence of PEGdNB, mono-cysteine, and varied concentrations of tyrosine. Tyrosine concentration: (A) 0 mM, (B) 0.02 mM, (C) 0.2 mM, and (D) 2 mM. Eosin-Y concentration in all measurements: 0.02 mM (N = 3) 96

Figure 5.7 Effect of tyrosine on (A) gel fraction, (B) elastic modulus at equilibrium gel swelling, and (C) swelling ratio as a function of time. (3 wt% PEG8NB, 6 mM CGGGC, 0.1 mM eosin-Y, 400-700 nm light, intensity at 70000 lux, mean ± SD, N = 3) In collaboration with Hung-Yi Liu 97

Figure 5.8 Effect of macromer concentration (A), and the ratio of norbornene to thiol (B) on the elastic modulus of PEG-peptide hydrogels. (3 wt% PEG8NB, 6 mM CGGGC, 0.1 mM eosin-Y, 400-700 nm light, intensity at 70000 lux, mean ± SD, N = 3) In collaboration with Hung-Yi Liu 98

Figure 5.9 Effect of tyrosine concentration on the degradability of PEG-peptide hydrogels. All gel formulations contained β-cells at 5×10^6 cells/mL, 3.5 wt% PEG8aNB, 7 mM KCYIGSRCK, 0.1 mM eosin-Y, and 400-700 nm light at 70000 lux 100

Figure Page

Figure 5.10 Effect of tyrosine on the cytocompatibility of MIN6 β-cells. (A) Representative confocal z-stack images of MIN6 cells stained with live/dead staining kit on day 1 (Scales: 100 μm). (B) Cells viability as assessed by Alamarblue® reagent. (C) Glucose stimulated insulin secretion (25 mM of glucose) normalized by cell metabolic activity. * indicates comparison between day 1 and day 10, while % indicates comparison between 0 to 1 mM of tyrosine, $p < 0.05$. All gel formulations contained β-cells at 5×10^6 cells/mL, 3.5 wt% PEG8aNB, KCYIGSRCK, 0.1 mM eosin-Y, and 400-700 nm light at 70000 lux. Ratio of [thiol] to [norbornene] was 1 and 0.85 for 0 mM and 1 mM of tyrosine, respectively 101

Figure 5.11 Effect of tyrosine on the mRNA expression of MIN6 β-cells. mRNA level of (A) Ins and (B) Pdx1 evaluated by qPCR. Actβ was used as a house keeping gene. * indicates comparison between day 1 and day 10, while % indicates comparison between 0 to 1 mM of tyrosine, $p < 0.05$. All gel formulations contained β-cells at 5×10^6 cells/mL, 3.5 wt% PEG8aNB, KCYIGSRCK, 0.1 mM eosin-Y, and 400-700 nm light at 70000 lux. Ratio of [thiol] to [norbornene] was 1 and 0.85 for 0 mM and 1 mM of tyrosine, respectively 102

Figure 5.12 Effect of tyrosine on the cytocompatibility of CD1 mouse islets. (A) Representative confocal z-stack images of islets stained with live/dead staining kit on day 1. (B) Glucose stimulated insulin secretion normalized by ATP content per gel (day 1). Gel formulations: 3.5 wt% PEG8aNB, KCYIGSRCK, 0.1 mM eosin-Y, and 400-700 nm light at 70000 lux (Scales: 100 μm) 103

Figure 6.1 **(**A**)** Schematics of thiol-allylether photo-click reaction using photoinitiator LAP and long-wave ultraviolet light exposure (365 nm, 10 mW/cm^2). (B-D) Chemical structures of the major macromers used, including TPVA (B), PEG4AE (C), and βCDAE (D) 113

Figure Page

Figure 6.2 (A) ^{1}H NMR of βCD (top), and βCD-AE (bottom). Prepared with D_2O (at 4.79 ppm). (B) Mass spectroscopy of βCDAE 114

Figure 6.3 Estimation of βCD-immobilization post-gelation: (A) gel fraction; (B) normalized thiol concentration measured by Ellman's assay; and (C) ATR-FTIR characterization. 2.5 wt% TPVA at 0.8 mM PEG4AE and 27.6 mM βCDAE ($R_{[allylether]/[thiol]}$ = 0.8) or βCD in the precursor solution (1 mM LAP, 365nm light at 10 mW/cm^2) 116

Figure 6.4 *In situ* photorheometry showing storage modulus (G') and loss modulus (G") of thiol-allylether photopolymerization (A) at 2.5wt% TPVA and 27.6 mM βCDAE; and (B) at 0.8 mM PEG4AE and 27.6 mM βCDAE in the precursor solution (1 mM LAP, 365nm light at 10 mW/cm^2). Light was turned on at 30 seconds (dotted line) 117

Figure 6.5 (A) Schematic of a reversible βCD/AD complex. (B) Chemical structure of PEG4AD. (C) *In situ* stiffening of hydrogel through incubating βCD-containing gel in PEG4AD solution. Gel softening could be achieved by incubating the stiffened gel in PBS or solution containing unmodified βCD. (D) *In situ* stiffening using PEG4AD (10 kDa) at different concentration. (E) Tuning the initial stiffness and dynamic stiffening of hydrogels through adjusting the content of PEG4AE in the pre-polymer solution. (Mean ± SD, N = 3, * indicates $p<0.05$) 119

Figure 6.6 Frequency sweep rheometry of thiol-allylether hydrogels before (A), and after (B) incubating in PEG4AD. Error bars omitted for clarity 120

Figure 6.7 (A) Effect of gel treatment conditions on the elastic modulus of thiol-allylether hydrogel. Right panel: timeline for the treatments of hydrogels. (B) Reversibly tuning the elastic moduli of thiol-allylether hydrogel. 5 wt% of PEG4AD (10 kDa) and 5 wt% of 4-arm PEG (10 kDa), respectively. Right panel: timeline for the treatments of hydrogels (2.5 wt% TPVA, 0.8 mM PEG4AE and 27.6 mM βCDAE, Mean ± SD, N = 3, * indicates $p<0.05$) 121

Figure Page

Figure 6.8 Effect of thiol-allylether hydrogel stiffness on the cytocompatibility of MIN6 β-cells. (A) Representative confocal z-stack images of MIN6 cells stained with live/dead staining kit on day 1 and day 10. MIN6 cells were encapsulated (2×10^6 cells/mL) in thiol-allylether hydrogels. (B) Cells viability as assessed by Alamarblue® reagent. (C) Normalized insulin mRNA expression on day 10. All gel formulations contained β-cells at 2×10^6 cells/mL, 2.5wt% TPVA, 0.6/0.8/1mM PEG4AE and 27.6 mM βCDAE, 1 mM LAP, and 365 nm light at 5 mW/cm^2 (Scales: 200 μm) 123

Figure 6.9 Effect of PEG4AD and βCD on the stiffening and softening of thiol-allylether hydrogel via CD-AD interactions. All gel formulations contained 2×10^6 cells/mL β-cells, 2.5 wt% TPVA, 0.8 mM PEG4AE and 27.6 mM βCDAE, 1 mM LAP, and 365 nm light at 10 mW/cm^2 (N = 3) 126

Figure 6.10 (A) Effect of PEGAD on the cytocompatibility of MIN6 β-cells. Cells viability as assessed by MTT. PEGAD (10 kda) was used. (B) Effect of PEG4AD (10 kDa) on the Ins mRNA expression. Cells were all cultured on 2D TCP 126

Figure 6.11 Effect of PEG4AD stiffening and βCD softening on the cytocompatibility and functions of MIN6 β-cells. (A) Representative confocal z-stack images of MIN6 cells stained with live/dead staining kit on day 8 with or without PEG4AD stiffening (i & ii) and on day 11 with or without βCD softening (iii & iv). (B) Cells viability as assessed by CellTiter Glo® reagent. (C) Insulin mRNA expression was normalized to condition (i). All gel formulations contained 2.5 wt% TPVA, 0.8 mM PEG4AE and 27.6 mM βCDAE, 1 mM LAP, 2×10^6 cells/mL, and 365 nm light at 5 mW/cm^2 (Scales: 200 μm). Mean ± SD, N = 3, * or $^{\#}$ indicate $p<0.05$ compared to condition i and iii, respectively..... 127

Figure 6.12 (A) Degree of TPVA thiolation measured by Ellman's assay. (B) ^{1}H NMR of TPVA prepared with D_2O (at 4.79 ppm)..... 129

Figure 6.13 ^{1}H NMR of (A) PEG4AE (20 kDa), and (B) PEG4AD (10k Da). All dissolved in $CDCl_3$ (at 7.26 ppm) 131

LIST OF ABBREVIATIONS

Symbol	Description
βCD	Beta-cyclodextrin
βCDAE	Beta-cyclodextrin conjugated with allylether
βCDSH	Beta-cyclodextrin conjugated with thiol
CGGGC	5-mer peptide cysteine-glycine-glycine-glycine-cysteine
DTT	Dithiothreitol
LAP	Lithium arylphosphinate
MIN6	Mouse insulinoma cells
NVP	1-vinyl-2 pyrrolidinone
PEG4aNB	Poly(ethylene glycol)-tetra-amide-norbornene
PEG8aNB	Poly(ethylene glycol)-octa-amide-norbornene
PEG4AD	Poly(ethylene glycol)-tetra-adamantane
PEG4AE	Poly(ethylene glycol)-tetra-allylether
PEG4NB	Poly(ethylene glycol)-tetra-norbornene
PEG8NB	Poly(ethylene glycol)-octa-norbornene
PEGDA	Poly(ethylene glycol)-di-acrylate
PEGdNB	Poly(ethylene glycol)-di-norbornene
PVA	Poly(vinyl alcohol)
TPVA	Thiolated poly(vinyl alcohol)

NOMENCLATURE

Symbol	Unit	Description
G’	Pa	Storage or elastic modulus
G”	Pa	Loss or viscous modulus
W_{Dry}	mg	Dried polymer weight
$W_{Swollen}$	mg	Swollen weight
$\overline{M_c}$	Da	Average molecular weight between crosslinks
MW_A	Da	Molecular weight of macromer
MW_B	Da	Molecular weight of crosslinker
$\overline{v_1}$	cm^3/g	Specific volume of water
$\overline{v_2}$	cm^3/g	Specific volume of PEG
V_1	$cm^3/mole$	Molar volume of water
$k’$	day^{-1}	Pseudo-first order ester bond hydrolysis rate constant
Ξ	nm	Mesh size
q		Mass swelling ratio
f_A		Number of reactive functionality for macromer
f_B		Number of reactive functionality for crosslinker
ν_c		Density of elastically active chains
ν_2		Polymer volume fraction
χ_{12}		Flory-Huggins interaction parameter for a PEG-H_2O system

ABSTRACT

Shih, Han. Ph.D., Purdue University, August 2016. Development of Orthogonally Crosslinked Thiol-ene Hydrogels for Encapsulation of Pancreatic β-cells. Major Professor: Chien-Chi Lin.

Type I diabetes mellitus (T1DM) is an autoimmune disease caused by auto-reactive T-cell-mediated destruction of insulin-producing β-cells. Effective encapsulation strategies can protect the transplanted islets from direct attack by host immune cells while maintaining insulin secretion. To achieve this goal, I have developed a hydrogel conformal coating using a visible light-mediated interfacial thiol-ene photopolymerization. Unlike conventional chain-growth visible light polymerizations, no additional cytotoxic co-initiator or co-monomer was required in thiol-ene gelation scheme for rapid gelation. More importantly, islets coated with thiol-ene gel maintained their viability and function *in vitro*. In addition to microencapsulate β-cells, the second objective of my dissertation focuses on developing a macroencapsulation technique using thiol-ene hydrogel with bioactivity and anti-inflammatory property. While islet transplantation holds potential in permanently reversing T1DM, this procedure initiates a cascade of inflammatory processes. To address this issue, we have developed thiol-ene hydrogel crosslinked by thiolated β-cyclodextrin (βCD). The conjugation of amphiphilic βCD affords enhanced loading and prolonged release of curcumin, an anti-inflammatory drug candidate but with poor water solubility. In addition, bioactive peptide such laminin-derived peptide flanked with two cysteine residues could be readily incorporated through orthogonal crosslinking, thus mimicking extracellular microenvironment in the pancreatic islets. Finally, in order to provide coated β-cells with an ideal biomechanical microenvironment, it is essential to identify a suitable gel stiffness to support the viability

and functions of β-cells. To this end, a thiol-allylether hydrogel with on-demand tunable matrix stiffness was developed. Specifically, host molecule βCD was immobilized in the hydrogel network to provide binding sites for soluble guest molecule poly(ethylene glycol)-adamantane. Gel stiffness was tuned through introducing reversible host-guest interactions. After *in situ* stiffening of the cell-laden hydrogel, the encapsulated β-cells showed increased in insulin mRNA expression, suggesting the profound impact of matrix stiffness on pancreatic β-cell fate.

CHAPTER 1
INTRODUCTION

In 2012, 29.1 million of Americans were diagnosed with diabetes. Among them, 1.3 million have suffered from Type 1 diabetes mellitus (T1DM), which is an autoimmune disorder caused by auto-reactive T-cells that destroy insulin-producing pancreatic β-cells in the islets of Langerhans [1]. The destruction of β-cells leads to inadequate insulin secretion, which leads to hyperglycemia. Current standard of therapy to restore glucose homeostasis is through multiple daily insulin injections or implantation of insulin delivery devices [2]. However, tight glycemic control through insulin administration requires frequent monitoring of blood glucose levels. In addition, patients experience various degrees of discomfort from exogenous insulin delivery. While whole pancreas or islet transplantation can provide T1DM patients with insulin-independence, these approaches are reserved for diabetic patients with hypoglycemia unawareness due to a significant shortage of donor organs [3-5]. The outcome of islet transplantation, however, is heavily influenced by blood mediated inflammatory response (IBMIR), which can destroy more than half of the transplanted islets shortly after surgery [6-8]. Furthermore, patients receiving donor islets are required to undergo lifelong immunosuppressant therapy. In order to improve the lifespan of transplanted islets, scientists and engineers have been developing encapsulation technologies to separate allogenic or even xenogenic islets from host tissues [9-18]. To this end, microencapsulation and macroencapsulation strategies have been introduced as devices to improve the outcome of islet transplantation [19-24]. Table 1.1 summarizes the advantages and disadvantages of each encapsulation approach. A successful permselective immune isolation barrier should be able to prevent infiltration of host immune cells while permitting facile exchange of nutrients and metabolites,

including oxygen, glucose, and insulin [2]. More importantly, this encapsulation strategy should support the survival and preserve the functions of cells.

Table 1.1. Advantages and disadvantages of microencapsulation and macroencapsulation techniques

	Microencapsulation	Macroencapsulation
Advantages	▪ Reduced diffusion barrier ▪ Low transplant volume	▪ Easy to retrieve transplant ▪ Easy to incorporate biomolecules ▪ Easy to characterize material properties
Disadvantages	▪ Difficult to retrieve transplants ▪ Difficult to incorporate biomolecules ▪ Difficult to characterize physical properties of materials	▪ Hindered permeability ▪ Higher transplant volume

The global goal for this dissertation is to develop microencapsulation and macroencapsulation techniques for synthesizing biomimetic materials to overcome some of the challenges facing islet transplantation. Thiol-ene hydrogels formed by radical mediated photopolymerizations have emerged as a versatile biomaterial platform for controlled release and tissue engineering applications. Chapter 2 of this dissertaion includes the mechanisms and the applications of thiol-ene photopolymerization. During my graduate studies, I have developed a cytocompatible visible light mediated step-growth thiol-ene polymerization scheme. The focus of this dissertation was to capitalize on this innovative gelation chemistry for the development of microencapsulation and macroencapsulation techniques to encapsulate β-cells. The following specific objectives are proposed:

Objective 1: Establish a visible light mediated interfacial thiol-ene photopolymerization for microencapaulation of islets. In Chapter 3, a cytocompatible visible light-mediated interfacial thiol-norbornene photopolymerization scheme was

developed for creating hydrogel conformal coating on pancreatic islets. I investigated the tunability of this microencapsulation technique, as well as the viability and function of coated islets.

Objective 2: Synthesize biomimetic and anti-inflammatory thiol-ene hydrogel for macroencapsulation of β-cells. To suppress the potential inflammatory response, I have developed thiol-ene hydrogel crosslinked by either thiolated β-cyclodextrin (βCD) derivative (Chapter 4). βCD derivatives were synthesized and characterized for the crosslinking of βCD-PEG hybrid hydrogels via radical-mediated thiol-ene photopolymerizations. Further investigation was conducted on the delivery of a model hydrophobic drug, and the testing of the cytocompatibility of these step-growth hydrogels. To introduce biofunctionality to the otherwise inert thiol-ene hydrogels, in Chapter 5, a laminin-derived peptide flanked with two cysteine residues were readily incorporated through orthogonal crosslinking to recapitulate islets extracellular microenvirnment to support β-cells survival.

Objective 3: Investigate the effect of biomechanical stimulus on the survival of β-cells. Utilizing thiol-ene hydrogel that contains chemically immobilized βCDs, the mechanical properties of the hydrogels could be tuned via host-guest interactions between βCD and adamantane functionalized PEG. The development and cytocompatibility of this hydrogel platform were included in Chapter 6. Most importantly, I evaluated the effect of biomechanical changes on the viability and functions of β-cells.

CHAPTER 2
DYNAMIC CONTROL OF DEGRADABLE THIOL-ENE HYDROGELS

2.1 Abstract

Thiol-ene hydrogels formed by radical mediated photopolymerizations have emerged as a versatile biomaterial platform for controlled release and tissue engineering applications. In this step-growth photopolymerization scheme, multi-arm poly(ethylene glycol)-norbornene (PEGNB) reacts with dithiol or bis-cysteine containing cross-linkers to form chemically cross-linked hydrogels. Thiol-ene hydrogels can be prepared via UV light or visible light irradiation, depending on the type of photoinitiator used. Thiol-ene reaction is not oxygen inhibited, which yields a rapid gelation kinetics. The step-growth polymerization affords an idealized network structure with independently tunable biochemical and biophysical matrix properties. Thiol-ene hydrogels can be rendered completely non-degradable, degradable only by hydrolysis, proteolysis, photolysis, or by the combination of different mechanisms. If PEG-ester-norbornene (PEGeNB) is used, the gels can be degraded hydrolytically due to the presence of ester bonds within the macromer. On the other hand, the use of PEG-amide-norbornene (PEGaNB) renders the gels hydrolytically stable. If cell-mediated or user-controlled gel degradation is desired, bis-cysteine peptide linker containing enzyme-sensitive or photolabile sequence can be used to cross-linked the gels. The capability of thiol-ene hydrogels to undergo diverse gelation and degradation permits researchers to design versatile hydrogel matrices suitable for protein delivery and three dimensional (3D) cell culture. Due to the

Chaper 2 here is as appeared in Chapter 12 by H. Shih and C. Lin, *Biodegradable Polymers*. Volume 2: New Biomaterial Advancement and Challenges, Editor: Chu CC. Nova Science Publishers. 2015, (ISBN: 978-1-63483-652-4)

orthogonal nature of the thiol-ene reaction, post-gelation modification in the presence of cells can be easily achieved, given that sufficient norbornene groups are available following the initial gelation. This attractive feature allows researchers to introduce biochemical motifs, in a spatial-temporally controlled manner, to guide cell morphogenesis in 3D.

2.2 Introduction

2.2.1 Photopolymerization to Prepare Hydrogels

Photo-initiated radical polymerizations have received significant attention for *in situ* cell encapsulation and controlled delivery of biological molecules, in large part due to rapid and ambient gelation conditions and the stability of the covalently crosslinked networks [25-30]. Synthetic macromers are increasingly developed for radical-mediated hydrogel synthesis. Depending on the reactivity of the macromer functional groups, hydrogels can be prepared from chain-growth, step-growth, or mixed-mode photopolymerization [31]. In chain-growth photopolymerization (Figure 2.1A), vinyl monomers/macromers are cross-linked into hydrogels due to propogation of carbonyl radicals across the unsaturated vinyl groups. In step-growth photopolymerization, cross-linking occurs between two mutually reactive groups located on multi-functional macromers (Figure 2.1B). A mixed-mode polymerization is the combination of both chain-growth and step-growth polymerizations, given that the macromer used (e.g., poly(ethylene glycol) diacrylate) possesses reactivity in both mechanisms [32].

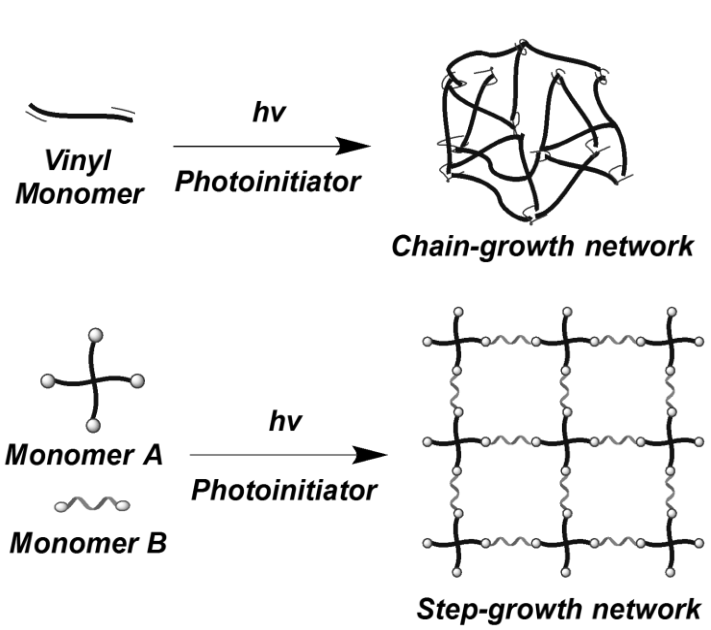

Figure 2.1. Schematics of hydrogels formed by: (A) Chain-growth photopolymerization using linear homo-bifunctional macromer to produce a heterogeneous network. (B) Step-growth photopolymerization of multifunctional and mutually reactive monomers. An idealized network structure is produced using a stoichiometric molar ratio of the two functional groups.

2.2.2 Photoinitiation Systems for the Polymerization of Hydrogels

Radical-mediated photopolymerization is a well-established technique to prepare hydrogels for biomedical applications. Typically, a light source that emits lights in the cytocompatible wavelengths (e.g., $\lambda > 365$ nm) is used to excite photoinitiator molecules. Following light exposure, a type I or cleavage-type photoinitiator (Figure 2.2) readily absorbs photons from the light source and decomposes into two primary radicals to initiate gelation [33]. On the other hand, a type II photoinitiator abstracts hydrogen from a co-initiator, thus generating secondary radicals that initiate crosslinking [33-35]. Adequate solubility of a photoinitiator in an aqueous solution and sufficiently high molar absorptivity at cytocompatible wavelengths are major factors concerning the suitability of a photoinitiator to initiate photopolymerization for preparing cytocompatiblie hydrogel. Only a few photoinitiators fulfill these criteria, such as type I initiators Irgacure-2959 (I-

2959, Figure 2.2A) [36, 37] and lithium arylphosphanate (LAP, Figure 2.2B) [38], as well as type II initiator eosin-Y [34, 35, 39]. Commercially available I-2959 has low water solubility (< 0.5 wt%) and low molar absorptivity at cytocompatible wavelengths (e.g., at 365nm , $\varepsilon < 10$ $M^{-1}cm^{-1}$). In addition, I-2959 cannot be used in visible light-mediated photocrosslinking due to its near zero molar absorptivity at wavelengths higher than 400 nm. While LAP is highly water-soluble (> 5 wt%) and has high absorbance at 365 nm ($\varepsilon \sim 200$ $M^{-1}cm^{-1}$), its excitability in visible light range is limited ($\varepsilon \sim 30$ $M^{-1}cm^{-1}$ at 405 nm) [38]. On the other hand, type II photoinitiator such as eosin-Y is highly water soluble and can be readily excited by visible light ($\varepsilon > 100{,}000$ $M^{-1}cm^{-1}$ at 515 nm). Eosin-Y has been used to initiate the gelation of chain-growth poly(ethylene glycol) diacrylate (PEGDA) hydrogels. Unfortunately, a co-initiator (e.g., triethanolamine, TEA) is required for generating sufficient radicals and a co-monomer (e.g., 1-vinyl-2-pyrrolidinone, NVP) is often used to achieve high and rapid functional group conversion. The adjustment of various gelation components can be complicated and this is perhaps why UV-mediated photopolymerizations, even with potential biosafety concerns, is still a preferred method for preparing hydrogels.

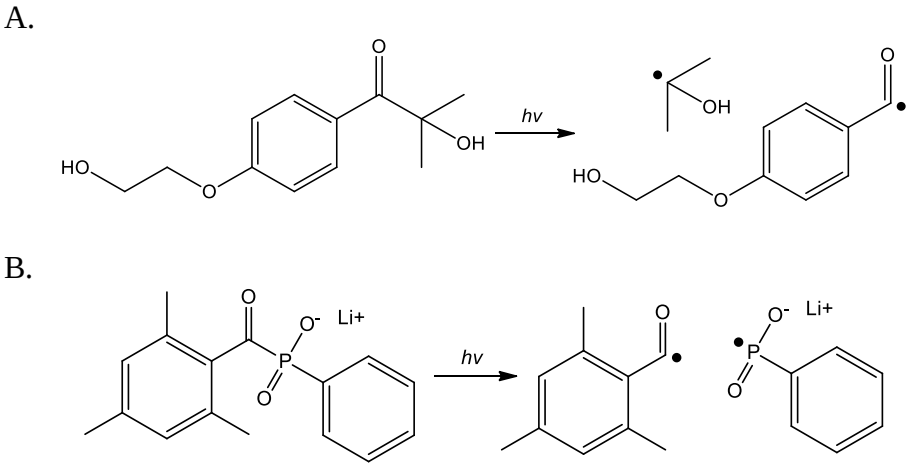

Figure 2.2. Photo-cleavage of type I photoinitiator I-2959 (A) and LAP (B).

Chain-growth polymerized network

Hydrogels crosslinked by radical-mediated chain-growth photopolymerization have been used for numerous drug delivery and tissue engineering applications. In general, any hydrophilic macromer with terminal or internal vinyl groups can be cross-linked into hydrogel via chain-growth polymerization, as long as the vinyl groups are capable of undergoing homopolymerization. Poly(ethylene glycol) diacrylate or dimethacrylate (PEGDA or PEGDM, Figure 2.3) are among the most commonly used macromers for preparing chain-growth hydrogels. Typically, a cleavage type photoinitiator is used in conjunction with a UV light source to generate radicals for initiating the cross-linking process. This reaction can be carried out in aqueous solution and under mild reaction conditions, making it suitable for in situ protein or cell encapsulation. The crosslinking density of the chain-growth hydrogels can be tuned by adjusting light exposure time or by altering the concentrations of the starting macromers. However, free radicals initially generated from photoinitiators have long half-life in chain-growth polymerization due to the continuous propagation of the radical species along the vinyl groups [40]. When performing *in situ* cell or protein encapsulation, these radicals may increase cellular damage, protein denaturation, or undesired protein-polymer reactions.

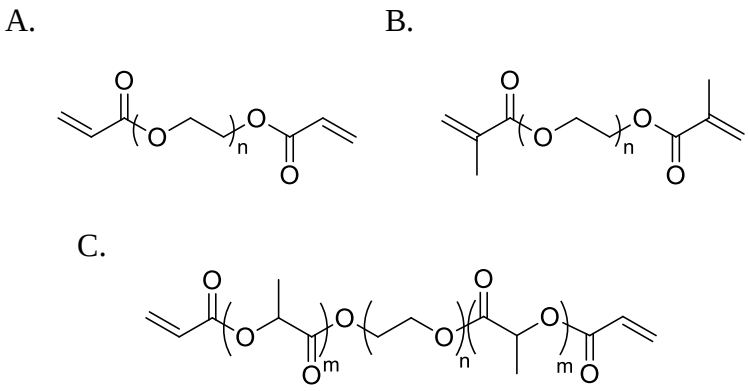

Figure 2.3. Structures of PEGDA (A), PEGDM (B), and acryalted PLA-PEG-PLA (C).

Furthermore, these chain-growth hydrogels are typically non-degradable in a mild aqueous environment. Degradable hydrogels are particularly useful as provisional

matrices for tissue regeneration and as carriers for controlled protein delivery [41-44]. Among all degradation mechanisms, hydrolytic degradation of synthetic hydrogels has received significant attention due to the simplicity of hydrolysis mechanism and well-defined polymer chemistry [45-47]. Although it is possible to render PEG hydrogels degradable, it requires the synthesis of macromers with build-in degradability. For example, hydrolytically degradable block co-polymer such as PLA-PEG-PLA (PLA: polylactic acid) can be synthesized through ring-opening co-polymerization of PEG and lactide. After end-capping the linear co-polymer with acrylates, the resulting macromers (Figure 2.3C) can be polymerized into a chain-growth network with various degrees of hydrolytic degradability, depending on the number of lactide units incorporated in the PLA blocks. Hydrogels prepared from these block copolymers are hydrolyzed to form lactic acid and PEG [45, 46]. The hydrolytic degradation rate of these hydrogels could be tuned and predicted by using copolymers with different lengths of lactide repeating units [45, 46].

In addition to the PLA-PEG-PLA copolymers, other hydrolytically labile hydrogels were prepared by incorporating ester bonds to the termini of PEG macromers prior to acrylation or methacrylation [48, 49]. Regardless of their degradability, homopolymerized vinyl-based hydrogels contain heterogeneous and dense hydrophobic polyacryalte kinetic chains (Figure 2.1A) that may cause adverse effects on the stability of the encapsulated molecules. These high molecular weight polyacrylate kinetic chains are not degradable [50], which could cause difficulty in clearance *in vivo*.

Step-growth thiol-ene network

In addition to chain-growth photopolymerized network, hydrogels can also be prepared via a radical mediated step-growth photopolymerization. Anseth and colleagues introduced a new class of PEG-based hydrogels formed by radical-mediated orthogonal thiol-ene photo-click reaction [38]. In this system, low intensity and long wavelength (5 – 10 mW/cm^2, 365 nm) UV light was used to generate thiyl radicals from thiol-containing molecules (e.g., bis-cysteine-containing oligopeptides). These thiyl radicals react with ene moieties on norbornene-functionalized multi-arm PEG to create orthogonal thiol-

ether linkages and a step-growth network (Figure 2.4A). Central to this gelation scheme is the multi-arm PEG macromers, which can be synthesized through either esterification of hydroxyl-terminated multi-arm PEG with norbornene acid or amide bond formation between amine-terminated multi-arm PEG with norbornene acid. The thiol-ene hydrogels obtained from this thiol-ene photoclick chemistry can be degraded hydrolytically via ester bond hydrolysis if PEG-ester-norbornene (PEGeNB) is used to form thiol-ene hydrogels (Figure 2.4B). Conversely, the gels remain hydrolytically stable when PEG-amide-norbornene (PEGaNB) is used (Figure 2.4C). This thiol-ene reaction scheme preserves all advantages offered by photopolymerizations, including rapid, ambient, and aqueous reaction conditions, as well as spatial-temporal control over gelation kinetics. Furthermore, step-growth thiol-ene photo-click reactions are not oxygen inhibited [51], which is beneficial for achieving rapid gelation compared with acrylate-based chain-growth photopolymerizations at equivalent macromer functionality [52]. Comparing with step-growth Michael-type gelation, thiol-ene photo-click reactions have reduced disulfide bond formation due to radical-mediated cleavage [53], thus increasing the extent of crosslinking and higher mechanical properties at a similar macromer content [38]. Furthermore, the orthogonal and step-growth nature of norbornene-sulfhydryl reaction permits dynamic modification of hydrogel biochemical and biophysical properties in the presence of cells [38]. Several cell types have been encapsulated successfully using thiol-ene hydrogels, including human mesenchymal stem cells [54], fibroblasts [38, 55], fibrosarcoma [55], valvular insterstitial cells [56], and radical-sensitive pancreatic β-cells [52]. Enzymatically degradable peptides could be utilized to crosslink thiol-ene hydrogels for creating an enzyme-responsive hydrogel network [57].

A.

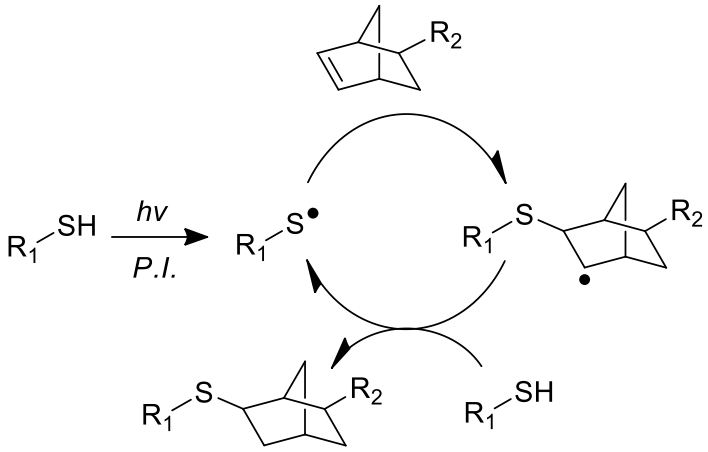

B. C.

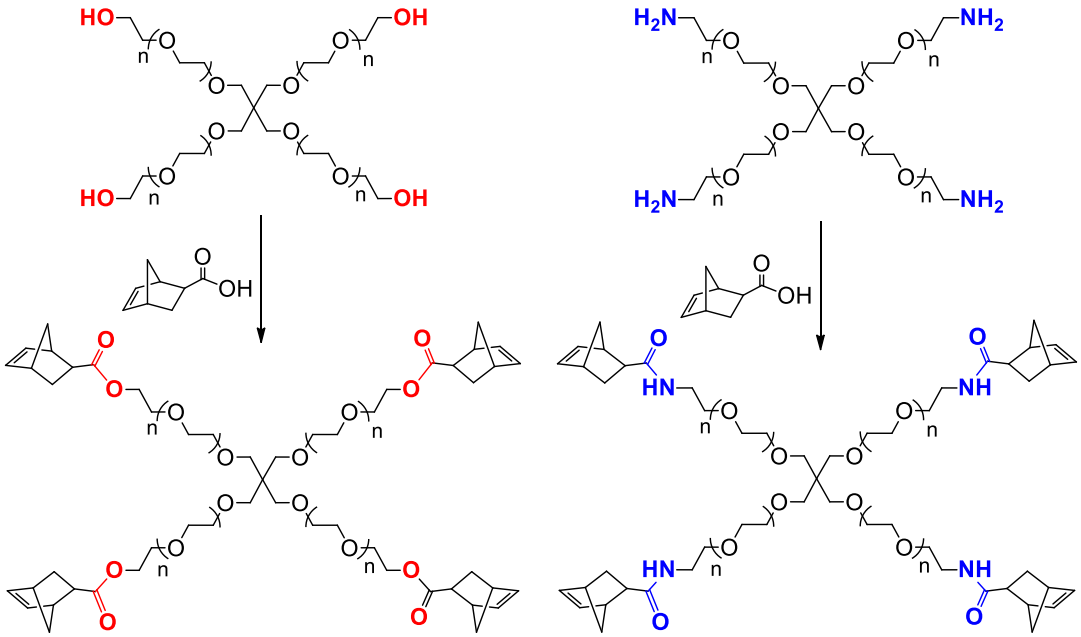

Figure 2.4. (A) Mechanism of radical-mediated thiol-ene photo-click reaction. (B) Synthesis route of PEG-tetra-ester-norbornene (PEG4eNB). (C) Synthesis route of PEG-tetra-amide-norbornene (PEG4aNB).

Early works on thiol-ene gelation have focused on the use of UV light and cleavage-type initiators. Recently, Lin and colleagues developed visible light mediated thiol-ene gelation using a type II photosensitizer eosin-Y as the sole photoinitiator [58, 59]. Mechanistically, visible light (400-700 nm) excites eosin to abstract hydrogen atoms from thiol-bearing molecules, which generate thiyl radicals that cross-link with norbornene groups through the same radical-mediated thiol-ene photo-click reactions (Figure 2.4A). In this gelation scheme, no co-initiator or co-monomer is needed to achieve gelation, thus improves the cytocompatibility of the gelation system for *in situ* cell encapsulation (Shih and Lin, 2013).

2.3 Thiol-ene Hydrogel Network Crosslinking

2.3.1 Improved gelation kinetics and efficiency

Hydrogels can be prepared by photopolymerization through either a chain-growth or a step-growth mechanism. While conventional chain-growth radical photopolymerization is sensitive to inhibition by molecular oxygen, orthogonal thiol-norbornene or thiol-ene photo-click reaction is not oxygen inhibited. Therefore, it yields rapid gelation kinetics and higher degree of functional group conversion [51, 60]. Experimentally, it was determined that at the same functional group concentration, the gelation of step-growth thiol-norbornene reaction occurs 20-time faster than acrylate-based chain-growth photopolymerization (e.g., gel points of 3 to 7 seconds for thiol-norbornene reaction and 1 to 2 minutes for acrylate-based homopolymerization). Hydrogels prepared from thiol-norbornene photopolymerization of PEG-based macromers also have higher gel fraction and stiffness compared with acrylate-based hydrogels with the same functional group concentrations [52]. For example, step-growth hydrogels prepared from PEG4NB and a peptide cross-linker Cys-Gly-Gly-Tyr-Cys exhibited consistently high gel fractions of 92-95%, whereas chain-growth hydrogels based on homopolymerization of PEGDA only yielded gel fractions of 63-84%.

Hydrogels with high gel fraction are desirable because the unreacted macromer components (due to lower gelation efficiency) may leach out from the hydrogels and complicated experimental results, especially for *in vivo* studies.

2.3.2 Improved network ideality

While both are initiated from light-induced radical-mediated photopolymerization, step-growth thiol-norbornene hydrogels formed with multi-arm PEG-norbornene (e.g., PEG4NB) have a completely different network structure compared with chai-growth homopolymerization of PEGDA. Another hydrogel system formed by a step-growth reaction is the Michael-type addition reaction. For example, multi-arm PEG-acrylate or PEG-vinylsulfone reacts orthogonally with thiol-terminated cross-linkers to yield a step-growth hydrogel network [61]. Although these step-growth hydrogels are useful in *in situ* cell encapsulation and protein delivery, they are known to have slower gelation kinetics at a physiological pH (minutes to hours) as compared with radical-mediated step-growth thiol-ene gelation (seconds to minutes). Recently, Shih and Lin compared the gelation kinetics of PEG-based hydrogels formed by these two types of step-growth polymerized hydrogels, namely radical-mediated thiol-ene photo-click reaction and Michael-type conjugation addition [62]. In this study, 4-arm PEG-norbornene (PEG4NB) and 4-arm PEG-acrylate (PEG4A) having the same molecular weight (MW_A = 20 kDa) and functionality (f_A = 4) were used as the macromers, while dithiothreitol (DTT) was used as a bi-functional (f_B = 2) cross-linker in both systems. *In situ* rheometry was used to monitor the gelation kinetics. As shown in Figure 2.5, the radical-mediated thiol-norbornene gelation exhibited much faster (>250-fold faster) gel points when compared with gelation caused by Michael-type addition reaction. Michael-type hydrogels formed from PEG4A and DTT also had a significantly lower shear modulus upon complete gelation.

A. B.

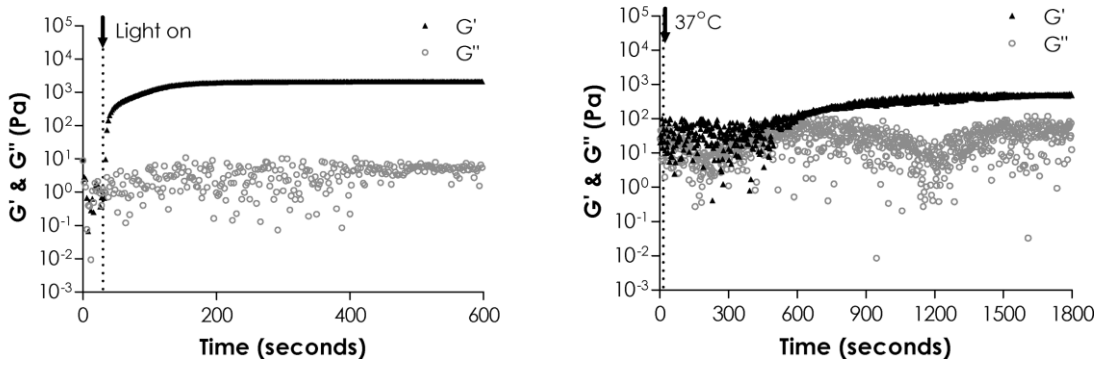

Figure 2.5. In situ rheometry of step-growth hydrogels: (A) Thiol−ene photoclick polymerization (4 wt % PEG4NB-DTT). UV light was turned on at 30 s. (B) Michael-type addition (4 wt % PEG4A-DTT). Temperature reached 37 °C at 15 s [62].

Apart from the difference in gelation kinetics, these two step-growth gelation systems (i.e., thiol-norbornene and thiol-acrylate Michael-type) also exhibit different degrees of network non-ideality. In principle, hydrogels prepared from an orthogonal reaction should have the same network structure if there is no non-ideality in polymerization. Specifically, at an identical macromer concentration and without any structural defect, hydrogels crosslinked by these macromers should have the same degree of crosslinking, which can be estimated by measuring hydrogel equilibrium swelling ratio (q):

$$q = \frac{W_{Swollen}}{W_{Dry}} \tag{2.1}$$

where $W_{Swollen}$ is hydrogel swollen weight and W_{Dry} is the dried polymer weight.

A perfectly crosslinked (or 'ideal') thiol-ene or Michael-type hydrogel network without defects can be estimated by means of hydrogel equilibrium swelling [63]. Considering the structural information of the step-growth hydrogels (i.e., macromer molecular weight and functionality), the average molecular weight between crosslinks ($\overline{M_c}$) is defined as [63]:

$$\overline{M_c} = 2(\frac{MW_A}{f_A} + \frac{MW_B}{f_B}) \tag{2.2}$$

Here, MW_A and MW_B represent the molecular weight of PEG4NB (or PEG4A) and crosslinker, respectively. f_A and f_B are the number of reactive functionality for PEG4NB (or PEG4A) and crosslinker. With a known $\overline{M_c}$, the ideal network crosslinking

density or density of elastically active chains (v_c) and polymer volume fraction (v_2) can be calculated based on the Flory-Rehner theory [64]:

$$v_c = \frac{V_1}{\overline{M_c}\,\overline{v_2}} = \frac{-[\ln(1-v_2)+v_2+\chi_{12}v_2^{\,2}]}{v_2^{\,1/3}-\frac{2v_2}{f_A}} \tag{2.3}$$

Here, $\overline{v_2}$ is the specific volume of PEG (0.92 cm^3/g at 37 °C), V_1 is the molar volume of water (18 cm^3/mole) and χ_{12} is the Flory-Huggins interaction parameter for a PEG-H_2O system (0.45). After obtaining v_2, ideal hydrogel mass swelling ratio q can be obtained using the following equation:

$$v_2 = \frac{\overline{v_2}}{(q-1)\overline{v_1}+\overline{v_2}} \tag{2.4}$$

where $\overline{v_1}$ is the specific volume of water (1.006 cm^3/g at 37 °C).

Based on Equation (2.2), the molecular weight between crosslinks ($\overline{M_c}$) of these two step-growth hydrogel systems without defect should be identical (neglecting the minor difference in the molecular weight of norbornene and acrylate moiety) and was calculated as 10,154 Da (Table 2.1). Thus, the ideal crosslinking density or density of crosslinked elastic chains (v_c) for these step-growth hydrogels was estimated to be 1.93×10^{-3} using Equation (2.3). Accordingly, the mass swelling ratio of a perfectly crosslinked step-growth hydrogel ($q_{eq,\ \text{ideal}}$) was calculated as 9.6 using Equations (2.3) and (2.4) (Table 2.1 and dashed line in Figure 2.6). Experimentally, however, we found that thiol-ene hydrogels, when compared to Michael-type gels at identical macromer compositions, had lower mass swelling ratio (28.5 ± 2.2 vs. 44.5 ± 3.8) at the equilibrium state [62]. This indicates that radical mediated thiol-ene hydrogels exhibit higher degree of network ideality compared to gels formed from Michael-type addition. These results confirmed a previous notion that radical-mediated thiol-ene reaction, when compared to Michael-type conjugation reaction, produce step-growth hydrogels with faster gelation kinetics, less structural defects, higher degree of crosslinking, and improved gel mechanical properties [41, 65].

Table 2.1. Characteristics of step-growth Michael-type and thiol-ene hydrogels [62]

	$\overline{M_c}$ (Da)	$q_{eq,\ ideal}$	$q_{eq,\ actual}$
PEG4A* (Michael-type)	10,154	9.6	44.5 ± 3.8
PEG4NB* (Thiol-ene)	10,154	9.6	28.5 ± 2.2

*4-arm PEG-derivatives (4 wt%, 20 kDa), crosslinked by DTT.

2.3.3 Tunable crosslinking density of thiol-norbornene hydrogels

Based on the Flory-Rehner theory, an 'ideal' step-growth network with a fixed macromer composition and without defect should only have a single equilibrium swelling ratio [62]. With the same gel formulation, the swelling ratio should be independent of macromer concentrations at equilibrium swelling state. However, the experimental equilibrium mass swelling ratios of thiol-norbornene hydrogels exhibited high dependency on PEG4NB macromer concentration, indicating the existence of network non-ideality (Figure 2.6). For instance, when the concentration of PEG4NB macromer was increased from 4 wt% to 20 wt%, swelling ratios decreased from ~29 to ~12 and approached ideal equilibrium swelling ratio (~9.6). Hydrogels with lower swelling ratios (at higher macromer contents) had higher elastic moduli. This inverse relationship was commonly observed in chain-growth polymerized hydrogel networks. The result suggested a higher possibility of network defects formed at lower PEG4NB contents. When cross-linked at a low macromer concentration, step-growth photopolymerization tends to yield more intramolecular reactions (i.e., primary cycles) [63, 66, 67] . On the other hand, at a higher macromer concentration, the probability of forming intermolecular cross-linking increases. The outcomes of increased intramolecular reactions at lower macromer concentrations include higher gel swelling and lower gel modulus (Figure 2.6). Although thiol-ene hydrogels contain network defects at lower polymer contents, the stiffness of these hydrogels is physiologically relevant (shear moduli between 1 to 10 kPa) and ideal for studying the influence of matrix stiffness on cell fate processes [68, 69].

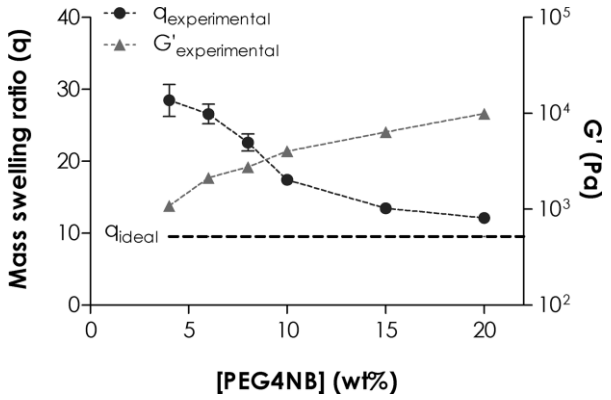

Figure 2.6. Effect of PEG4NB macromer concentration on thiol-ene hydrogel equilibrium swelling (left y-axis) and elastic modulus (right y-axis). Swelling ratio of an ideal network was calculated based on the molecular weight between crosslinks ($\overline{M_c}$) of given macromer molecular weights (MW_{PEG4NB} = 20 kDa, MW_{DTT} = 154 Da) and functionalities (f_{PEG4NB} = 4, f_{DTT} = 2) [62].

2.4 Degradation of Thiol-ene Hydrogel

2.4.1 Hydrolytic degradation

In addition to the chain-growth polymerized hydrogels, step-growth polymerized gels could also be rendered hydrolytically degradable. For example, Hubbell and co-workers developed Michael-type addition hydrogels through nucleophilic reactions between acrylates on multi-arm PEG macromer and sulfhydryl groups on the crosslinkers [63]. Thioether-ester linkages formed between acrylate and sulfhydryl moieties were hydrolytically labile and the degradation rates of these hydrogels could be tuned by controlling macromer concentration and functionality. Bowman and colleagues performed experimental and theoretical investigations on hydrolytic degradation of step-growth thiol-acrylate and thiol-allylether photopolymers [66, 70-72]. Degradation was readily tuned and predicted using monomers with different concentration, functionality, and degradability. Leach and colleagues developed hydrolytically degradable Michael-type hydrogels based on 4-arm PEG-vinylsulfone (PEGVS) and PEG-diester-dithiol [73, 74]. Degradation of these step-growth hydrogels was altered by tuning the number of

methylene groups between the thiol and ester moieties in the PEG-diester-dithiol linkers. In the above examples, acidic by-products (i.e., carboxylic acid) are obtained from the ester hydrolysis mechanism.

Due to the presence of thio-ester bond forming between thiol and backbone PEG, thiol-ene hydrogels can be rendered hydrolytically degradable. Metters and Hubbell previously established a statistical-*co*-kinetic model for predicting the hydrolytic degradation of step-growth Michael-type hydrogels. Due to structural similarities between step-growth Michael-type and thiol-ene hydrogels, Shih and Lin utilized this model to study the hydrolytic degradation of step-growth thiol-ene hydrogels and showed the high predictability of thiol-ene hydrogels. Based on this model, the degradation of thiol-ene hydrogels was assumed to be purely due to ester bond hydrolysis with a pseudo-first order degradation kinetics [45, 46]. With this assumption, the fraction of hydrolyzed ester bonds (P_{Ester}) at any given time in the system is expressed as:

$$P_{Ester} = 1 - \frac{[Ester]}{[Ester]_0} = 1 - e^{-k't} \tag{2.5}$$

Here, k' is the pseudo-first order ester bond hydrolysis rate constant [Ester] and $[Ester]_0$ are the current and initial numbers of intact ester bonds in the system.

The fraction of intact elastic chains (i.e., crosslinkers such as DTT or bis-cysteine containing peptides) within these crosslinked networks at any given time is expressed as:

$$1 - P_{Chain} = (1 - P_{Ester})^N = e^{-Nk't} \tag{2.6}$$

where N is the number of degradable units (i.e., ester bonds) connected to one elastic chain (e.g., N = 2 for the case of PEG4NB-DTT hydrogels).

To obtain the degree of crosslinking in the system, one must also consider the connectivity of multi-arm PEG macromers. For an ideal step-growth network, the fraction of f_A-armed macromer with i arms still connected to the network at any time point during ester hydrolysis is expressed as [63]:

$$F_{i,f_A} = \frac{f_A!}{(f_A - i)!i!} P_{chain}^{(f_A - i)} (1 - P_{chain})^i \tag{2.7}$$

The crosslinking density of the degrading network is expressed as:

$$\nu_c = \left(\sum_{i=3}^{f_A} \frac{i}{2} F_{i,f_A}\right)[A]_0 \tag{2.8}$$

Here, $i \geq 3$ because any f_A-arm ($f_A \geq 3$) macromer with only two arms connected to intact elastic chains forms an extended loop, rather than a crosslink. $[A]_0$ represents the concentration of f_A-arm macromers (e.g., PEG4NB) in the equilibrium swelling state before the onset of network degradation, which is correlated to the crosslinking density of a network:

$$v_{c,0} = \frac{f_A}{f_B}[A]_0 \tag{2.9}$$

When the functionalities of the macromer and crosslinker (f_A = 4 and f_B = 2) are taken into account, the crosslinking density of a perfectly crosslinked thiol-ene network in the equilibrium state could be derived from Equations (2.3) to (2.9) and expressed as:

$$v_c = (6e^{-3Nk't} - 4e^{-4Nk't})[A]_{0,actual} \tag{2.10}$$

For gels with non-idealities or structural defects, $[A]_{0,actual}$ is obtained using actual crosslinking density as:

$$[A]_{0,actual} = \frac{v_{c,actual}}{v_{c,ideal}}[A]_0 \tag{2.11}$$

where $v_{c,actual}$ represents the experimental crosslinking density converted from experimental mass swelling ratio using Equations (2.3) and (2.4) and $v_{c,ideal}$ represent ideal crosslinking density calculated based on the molecular weight between cross-links: $\overline{M_c}$.

The hydrolytic degradation of thiol-ene hydrogels was found to be pH-dependent. It was demonstrated that PEG4NB-DTT hydrogels incubated in acidic condition (pH 6.0) had an almost constant swelling ratio over a 45-day period, whereas hydrogels with the same compositions exhibited increasing swelling over time in slightly basic conditions (pH 7.4 and pH 8.0) (Figure 2.7). If the degradation follows the same ester hydrolysis mechanism at an elevated pH value (e.g., from pH 7.4 to pH 8.0), degradation profiles at different pH values could be described using a pseudo-first order equation [76]:

$$[Ester] = [Ester]_0 e^{-k'[OH^-]t} \tag{2.12}$$

Through experimental curve fitting, it was shown that the degradation of thiol-ene hydrogels was not solely governed by simple ester bond hydrolysis and other factors could also play a role on the degradation rate of these thiol-ene hydrogels. A potential explanation for this phenomenon is base-catalyzed oxidation of thioether bond forming

between norbornene and thiol groups, which may be promoted at higher pH values. Another possible reason for the lower-than-predicted degradation rate at higher pH values was that the degradation process produced acidic by-products, which decreased acidity and retarded the degradation.

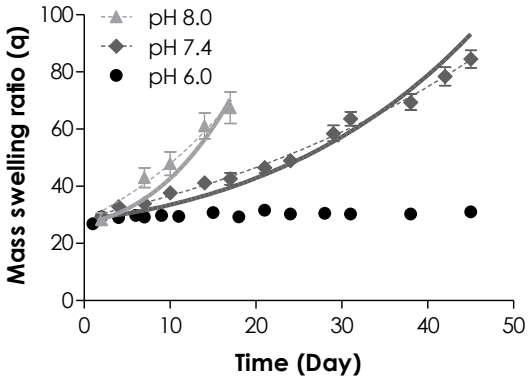

Figure 2.7. Effect of buffer pH on mass swelling ratio of 4 wt% PEG4NB-DTT hydrogels. Symbols represent experimental data while dashed curves represent exponential curve fitting to the experimental data. The apparent degradation rate constants (k_{hyd}) for gels degraded in pH 7.4 and pH 8.0 were 0.024 ± 0.001 and 0.057 ± 0.002 day^{-1}, respectively. Solid curves represent model predictions with best-fit kinetic rate constants: $k'_{\text{pH 7.4}}$ = 0.011 day^{-1} and $k'_{\text{pH 8.0}}$ = 0.027 day^{-1}. No curve fitting or model prediction was made for gels degraded in pH 6.0 due to the stability of gels in acidic conditions.

In addition to the influence of pH, degradation rate of thiol-ene hydrogels can be affected by other factors such as macromer concentrations. Theoretically, thiol-ene hydrogels formed at a higher macromer concentration have a higher degree of network crosslinking. The later property is directly correlated to the concentration of thiol-ether-ester bonds formed in the network. Experimentally, it was demonstrated that given the same amount of time and hydrated environment, thiol-ene hydrogels with higher degree of network crosslinking would degrade slower. The degree of network crosslinking can also be altered by changing the ratio of thiol to ene. At higher thiol-to-ene ratio, higher network crosslinking (e.g., higher $[A]_0$) led to slower rate of degradation. Furthermore, hydrolytic degradation rate of thiol-ene hydrogels can be affected by the sequence of bis-cysteine-bearing peptide linker. Hydrogels crosslinked by peptides containing aromatic

(e.g., Cys-Gly-Gly-Tyr-Cys or CGGYC) or hydrophobic (e.g., Cys-Gly-Gly-Leu-Cys or CGGLC) residues yielded slower degradation rates compared to gels crosslinked by peptide linker without side group (i.e, Cys-Gly-Gly-Gly-Cys or CGGGC), potentially due to steric hindrance and hydrophobic effect of tyrosine and leucine residues that retarded degradation [62].

2.4.2 Enzymatic degradation

Thiol-ene hydrogels can be rendered enzymatic degradable when protease sensitive peptides are used as gel cross-linkers. The termini of these peptides are usually flanked with cysteine residues to provide sylfhldryl groups needed for the orthogonal thiol-ene photo-click reactions. Enzyme-sensitive thiol-ene hydrogels can serve as carriers for delivering therapeutic agents in response to specific enzymatic activity, which causes cleavage of the peptide cross-linkers. For example, Aimetti *et al* reported a human neutrophile elastase (HNE) responsive thiol-ene hydrogels for delivering therapeutic agents on demand [57]. Lin *et al.* reported a cymotrypsin degradable peptide (i.e., Cys-Gly-Gly-Tyr-Cys, CGGY↓C) for enzyme responsive recovery of pancreatic β-cell aggregates from thiol-ene hydrogels [52]. In Figure 2.8, a linear relationship for hydrogel mass loss as a function of time suggests that the enzymatic degradation of thiol-ene hydrogels was governed by a surface erosion mechanism. A significantly faster rate of erosion was observed when hydrogels were incubated in solution with higher chymotrypsin concentration [52].

In addition to utilizing a surface erosion mechanism to release drugs or cells, thiol-ene hydrogels can also be used to study cellular behaviors, such as proliferation and migration that are related to local enzymatic reactions. During these processes, cells can secrete enzymes such as the matrix metalloproteinases (MMPs). When a hydrogel is cross-linked with a peptide senstive to MMPs, the local protease activity can cause peptide cleavage and reduction in local gel cross-linking density. This process permits the cells to explore their neighboring matirx, which has been shown to improve tissue regeneration [77]. In particular, bis-cysteine MMP sensitive peptide (i.e.,

KCGPQG↓IWGQCK) has been used as a crosslinker for encapsulating cells in thiol-ene hydrogels [54]. It has been shown that cells, such as hMSCs or pancreatic cancer PANC-1 cells, secrete MMPs to cleave thiol-ene hydrogels as they spread or proliferate [54, 78, 79]. Although this type of enzymatic degradation is mostly restricted to local cellular activites, significant reduction in bulk gel mechanical properties could also be observed after prolong culture.

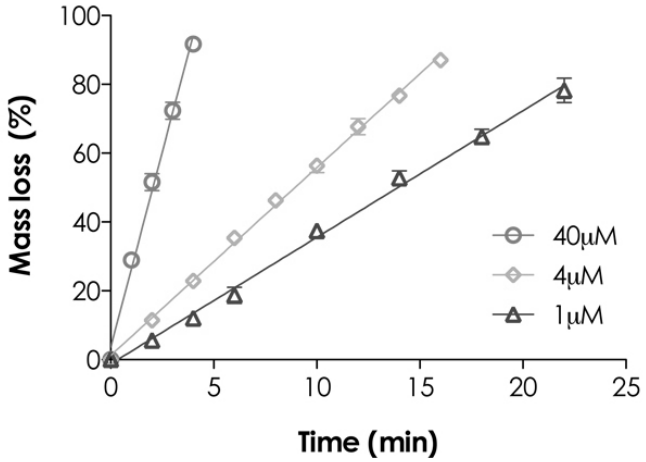

Figure 2.8. Effect of chymotrypsin concentration on mass loss of PEG4NB-CGGYC hydrogel (4wt% PEG4NB, N = 3, mean ± SEM) [52].

2.4.3 Photolytic degradation

There is a growing interest in the development of biomimetic materials with dynamically tunable gel properties during the course of the studies. For example, macromers with photolabile groups can be used to fabricate hydrogels with dynamically tunable cross-linking density. This will allow users to change gel biomechanical (i.e., reduction of gel cross-linking density) or biochemical properties (e.g., removal of pendent bioactive motifs) through additional light-mediated bond cleavage. Additionally, drugs or cells immobilized/entrapped within a photodegradable gel can be released on demand via light-induced matrix degradation. The cleavage of photolabile linkers can lead to the reduction of matrix stiffness that allow one to observe the influence of matrix properties on cell fate processes [80, 81].

Currently available photolabile units often contain an *ortho*-nitrobenzyl (*o*-NB) moiety that is highly susceptible to UV light. The absorbance of *o*-NB-containing macromers usually peaks between 280-400 nm [81-84]. When exposing to lights at these wavelengths, *o*-NB groups are effectively photo-lysed. This photolysis reaction liberates the initially immobilzied molecules or reduces the gel cross-linking density. Current methods to prepare photodegradable hydrogels are restricted to non-photo-mediated process, such as redox reactions, thermal polymerizations, Michael-type conjugations, or orthogonal 'click' chemistries [53, 75, 81, 85-87]. Photodegradable hydrogels can also be synthesized by photopolymerization, given that an appropriate photopolymerization system is utilized such that the photodegradable unit remain intact during network formation. Ki *et al.* recently reported the synthesis of photodegradable step-growth thiol-ene hydrogels by visible light-initiated thiol-ene photo-click reactions. A visible light source was utilized to excite eosin-Y, which initiated the cross-linking of PEG4NB and linker dithiothreitol (DTT) [80]. This new step-growth hydrogel system preserves the favorable preoperties offered by photochemistry, including photopolymerization and photodegradtion. Visible light wavelengths (400-700nm) were used to photopolymerized the thiol-ene hydrogels, whereas an orthogonal wavelength (302nm and 365nm) was used to cleave the peptide linker (Cys-Gly-NPA-Gly-Cys) containing a photolabile amino acid, L-2-nitrophenylalanine (NPA) (Figure 2.9A). The rate of hydrogel degradation was easily manipulated by wavelength and UV light intensity. As shown in Figure 2.9B, shorter wavelength and higher light intensity resulted in faster rate of photolysis. The applications of this simple photodegradable thiol-ene hydrogel include patterning of bioactive motifs in a spatial-temporal fashion, and releasing of biomolecules that are tethered with photolabile group.

A.

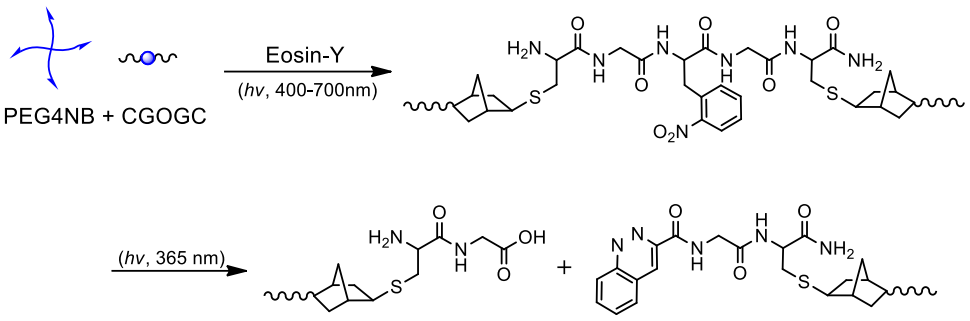

B.

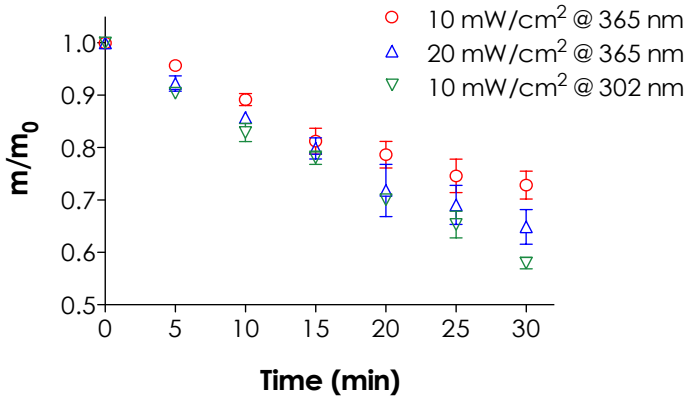

Figure 2.9. (A) Schematic of visible light mediated photo-crosslinking and UV-mediated photodegradation of step-growth thiol-ene hydrogels crosslinked by PEG4NB and photolabile peptide CGOGC (O: L-2-nitrophenylalanine). (B) Effect of different wavelength UV lights (302 or 365 nm, 10 mW/cm^2) on reduction of residual hydrogel mass (N = 3, mean ± SEM) [80].

2.4.4 Multifaceted degradation mechanisms

While the radical-mediated thiol-ene hydrogels can be designed to be degraded via hydrolysis, proteolysis, or photolysis, it is also possible to combine several degradation mechanisms into one hydrogel matrix. For instance, a simple dual-mode enzymatic and hydrolytic degradable hydrogel was created without altering hydrogel molecular structure or hydrophilicity [62]. As shown in Figure 2.10, thiol-ene hydrogels were cross-linked by non-cleavable CGGGC and chymotrypsin-sensitive CGGY↓C peptides at various compositions [62]. When these gels were exposed to chymotrypsin

solution, hydrogels containing high percentage of CGGYC cross-linker (100−75%) eroded in a surface erosion mechanism, evidenced by linearly increasing mass loss profiles with time. When the total content of CGGYC peptide was decreased to 50 and 25%, chymotrypsin treatment led to increased gel mass (i.e., negative mass loss). This indicated the protease treatment led to a "loosened" gel structure and increased water uptake. Under this condition, the degradation mode was likely transitioned from a surface erosion mechanism to a bulk degradation mechanism. On the other hand, chymotrypsin treatment had no effect on the swelling or mass loss of thiol-ene hydrogels cross-linked by purely non-chymotrypsin sensitive linker (CGGGC). These results suggested that by combining peptide cross-linkers with various protease sensitivities, the degradation behaviors of thiol-ene hydrogels could be manipulated between surface erosion and bulk degradation for dynamically controlled growth factors or drug delivery.

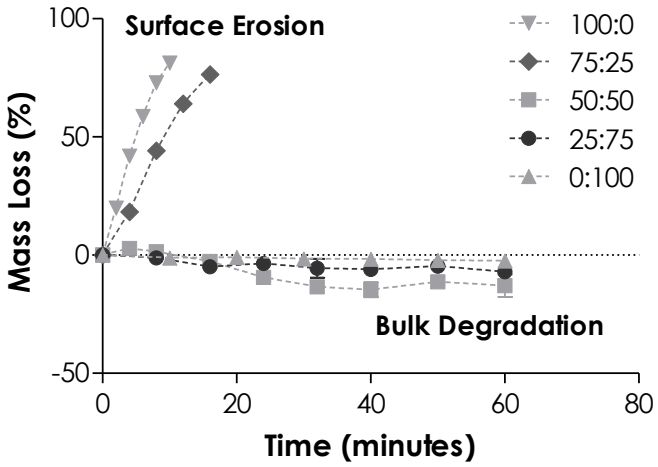

Figure 2.10. Effect of peptide crosslinkers on PEG4NB-peptide hydrogels erosion/degradation. PEG4NB hydrogels crosslinked by different percentage of chymotrypsin sensitive (CGGYC) and non-degradable (CGGGC) peptides. Figure legends indicate the percent molar ratio of CGGYC:CGGGC. (4 wt% PEG4NB-peptide hydrogels, pH 7.4, N = 4) [62]

2.5 Applications of Thiol-ene Hydrogels in Controlled Release and Tissue Engineering

2.5.1 Protein delivery

Protein therapeutics (e.g., gorwth factors, cytokines, chemokines, etc.) play an important role in promoting wound healing and tissue regeneration. *In situ* encapsulation of proteins in chemically cross-linked hydrogels has been a favorable option due to the simplicity of material prepration and drug loading process. Releasing proteins from a hydrgoel can positively affect the healing/regeneration process of a damaged or diseased tissue. When co-encapsulated with cells, the network-entrapped proteins can also direct cell fate processes within the hydrogels. However, maintaining the structural integrity and bioactivity of a protein-based biomacromolecule during network corss-linking has proven a challenging task, in large part due to the presence of reactive radical species [40, 57]. For example, Lin and Metters demonstrated a significant reduction of structural and functional integrity of model proteins bovine serum albumin (BSA) and lysozyme in chain-growth photopolymerized PEGDA hydrogels, as well as the effect of photoinitiators on protein bioactivity [88]. McCall and Anseth later compared the influence of chain-growth and step-growth photopolymerized hydrogels on the stability of lysozyme and transforming growth factor β (TGFβ) [40]. A 1000-fold increase in bioactive protein recovery was observed in thiol-ene hydrogels compared to chain-growth PEGDA hydrogels. Results of this study demonstrated that thiol-ene click reactions are capable of forming a cross-linked network more rapidly at a lower initiator concentration and with little to no impact on protein bioactivity. The highly efficient and orthogonal thiol-ene reaction, together with its non-oxygen inhibited nature, preserves the structure and function of sensitive proteins.

In addition to preserving the bioactivity of encapsulated proteins, thiol-ene hydrogels are also a class of versatile matrices for sustained and stimuli-responsive protein delivery. For example, Aimetti *et al.* have developed an enzyme-responsive thiol-ene hydrogels with potential for delivering anti-inflammatory drugs in responding to human neutrophil elastase (HNE), a protease secreted by neutrophil [57]. The hydrogels

were cross-linked by low molecular weight PEGNB macromer and HNE-sensitive bis-cysteine-bearing peptides. The sequences of HNE-sensitive peptide substrates were systematically altered, from which to identify appropricate sequences for rapid linker cleavage and subsequent liberation of the otherwise entrapped proteins. The release of model protein was purely governed by matrix cleavage and proceeded in a surface erosion manner. Ideally, this system can be used to release anti-inflammatory drugs upon the onset of inflammation.

Thiol-ene hydrogels could also be formulated into microgels. Murphy and colleagues used aqueous two-phase separation, in conjunction with radical-mediated thiol-ene photopolymerization, to prepare micro-scale hydrogels [89]. Affinity peptides capable of sequestering vascular endothelial growth factor (VEGF) were also immobilized within the permeable hydrogels. This molecular sequestering approach increased the binding and sustained the release of VEGF *in vitro*, which affected the proliferation of human umbilical vein endothelial cells. More recently, Fraser et al. prepared microgels formed by visible light mediated thiol-ene photopolymerization using eosin-Y as the photoinitiator [90]. Through a sequential thiol-ene polymerization, a thin gel coating was formed on the core microgels. Although not demonstrated in that publication, the multilayer microgels can be used to regulate the rate of drug release.

2.5.2 3D cell culture

In addition to the mild and rapid reaction kinetics, radical-mediated thiol-ene hydrogels have high cytocompatibility for cells derived from either mesenchymal or epithelial origins. Thiol-ene hydrogels have been used to encapsulate a host of mammalian cells, including fibroblasts [38, 55], valvular interstitial cells (VICs) [56], HT1080 fibroscarcoma [55], human mesnechymal stem cells [54, 78], pancreatic β-cells [52], pancreatic ductal epithelial cells [79, 91], and embryonic stem cells [92]. Thiol-ene hydrogels impreganated with bone morphogenic protein 2 (BMP2) have also been used to accelerate bone healing (as compared to commercially available BME-2 delivery matrix) *in vivo*. Although the cross-linking of thiol-ene hydrogels is initiated by light sensitive

photoinitiators, the concentration of radicals needed to initiate rapid gelation is orders of magnitude lower than that in chain-growth polymerization, in large part due to the non-oxygen-inhibited nature of thiol-ene reaction. This is significant because during the encapsulation process, some cells are prone to damage induced by free radicals. Insulin producing β-cells are one type of radical-sensitive cells. Lin and colleagues compared the differentces in chain-growth PEGDA and step-growth thiol-ene hydrogels in terms of gelation kinetics and cytocompatibility using a pancreatic β-cell line, MIN6. It was found that thiol-ene hydrogels were more cytocompatible than conventional PEGDA hydrogels for MIN6 cells. Furthermore, β-cells were able to proliferate into spheroids within these thiol-ene hydrogels [52, 59]. The cell spheroids could be recovered upon enzymatic-mediated cleavage of the step-growth hydrogel network.

Using PEG-norbornene macromers and protease-sensitive peptides as the gel cross-linkers, local matrix remodeling can be dictated by local cellular activity. Thiol-ene hydrogels can also be prepared to be degradabled hydrolytically and/or proteolytically, or completely non-degradable (Figure 2.11). The tunable degradability of the thiol-ene hydrogels allows one to examine the influence of microscale network properties on the encapsulated cell fate. For example, Anseth and colleages utilized thiol-ene hydrogels with different degree of matrix metalloproteinase (MMP) degradability to evaluate the potential of thiol-ene hydrogels as a 3D cell culture platform. MMP-sensitive peptide flanked with terminal cysteines (e.g., KCGPQGIWGQCK) was mixed with non-labile PEG-dithiol in different ratios [54]. The resulting thiol-ene hydrogels exhibited different degrees of protease sensitivity. The facile incorporation of CRGD motifs rendered the gel adhesive to the encapsulated human mesenchymal stem cells (hMSCs). Results showed that thiol-ene hydorgels were highly suitable for culturing and differentiate hMSCs. Following Anseth's work, a recent study utilized two PEGNB macromers that are hydrolytically labile or hydrolytically stable to evaluate the effects of single-mode (purely hydrolytic or enzymatic) or dual-mode (hydrolytic and enzymatic) network degradation on hMSCs viability and morphology [78]. It was found that dual-mode degradable thiol-ene hydrogels provided a more cytocompatible environment for promoting cell survival, proliferation, and morphogenesis in 3D. The results in the study

demonstrated significant influence of network degradation and cell-mediated matrix remodeling on cell fate process.

A.

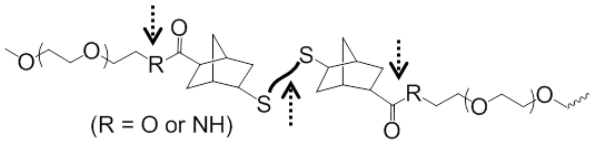

B.

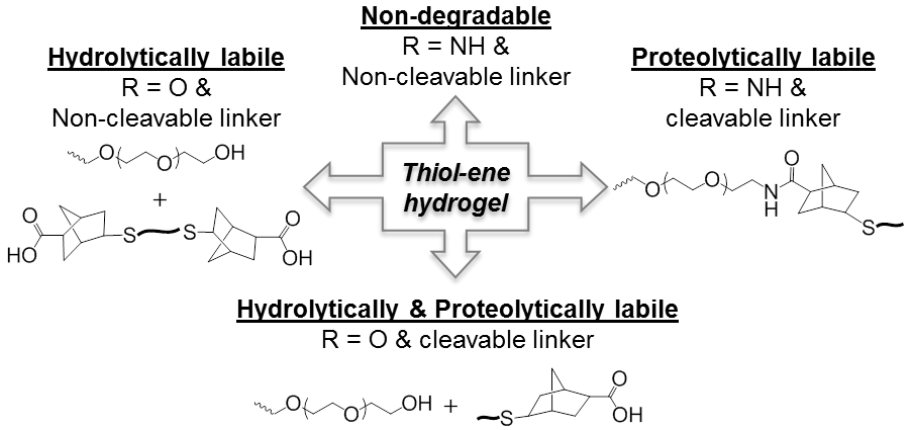

Figure 2.11. (A) Schematics of a thiol-ene cross-link. Arrows indicate potential cleavage sites. (B) Different modes of thiol-ene hydrogel degradation. PEG-ester-norbornene (R = O) or PEG-amide-norbornene (R = NH) can be used to construct gels with different hydrolytic degradability (only one arm is shown). With a proper combination of macromer and cross-linker, thiol-ene hydrogels can undergo different modes of degradation and produce different degradation products.

Recently, thiol-ene hyodrgels were used to study cancer cells in 3D. Lin and colleagues have established a highly tunable biomimetic thiol-ene hydrogel platform for studying the growth and morphogenesis of pancreatic ductal epithelial cells in 3D [79, 91]. The thiol-ene hydrogels were tuned to render the otherwise inert PEG environment responsive to epithelial cell morphogenesis. The growth and morphological changes in PANC-1 cells, a pancreatic ductal adenocarcinoma cell line, were affected by macromer molecular weight, gel stiffness, cross-linker chemistry, and additional cell-matrix interaction. The use of MMP-sensitive or RGDS-immobilized gels promoted the formation of cyst-like cell clusters, whereas the cell clusters proliferated from single cells

were more compact and exhibited epithelial cell phenotype in non-MMP sensitive or YIGSR-immobilized gels [79]. Furthermore, thiol-ene PEG-peptide hydrogels serve as a promising platform for evaluating the efficacy of peptide drugs toward pancreatic cancer cells in 3D. The viability of PANC-1 cells under the influence of epidermal growth factor receptor (EGFR) inhibition was altered by the dosage of the inhibitor and by the conditions of the matrix in which the cells reside [91]. The use of 3D hydrogel matrices with adaptable and well-defined biophysical and biochemical properties may facilitate the identification of anti-cancer drugs that are effective in tumor tissues but with minimal side effects to normal tissues.

2.6 Conclusion

In summary, thiol-ene hydrogels formed by radical mediated photopolymerizations have emerged as a versatile biomaterial platform for controlled release of therapeutics and tissue engineering applications. Thiol-ene hydrogels have improved network crosslinking than the conventional chain-growth PEGDA and step-groth Michael-type addition hydrogels. Depending on the type of photoinitiator used, thiol-ene hydrogels can be prepared via UV light or visible light irradiation. Thiol-ene hydrogels can be rendered completely non-degradable, degradable only by hydrolysis, proteolysis, photolysis, or by the combination of different mechanisms. The diverse gelation and degradation of thiol-ene hydrogels offer researchers a new platform to design hydrogel matrices suitable for protein delivery and three dimensional cell culture.

CHAPTER 3
VISIBLE LIGHT-INITIATED INTERFACIAL THIOL-ENE PHOTOPOLYMERIZATION FOR FORMING ISLET SURFACE CONFORMAL COATING

3.1 Abstract

A visible light-mediated interfacial thiol-ene photopolymerization scheme was developed for creating an immunoisolation coating on islets. Islets were stained with photoinitiator eosin-Y, followed by sequential incubations in macromer solutions. Upon visible light exposure, a step-growth thiol-ene hydrogel was formed around islets. The coated islets maintained viable *in vitro*.

3.2 Introduction

Type 1 diabetes mellitus (T1DM) is an autoimmune disorder caused by auto-reactive T-cells that destroy insulin-producing pancreatic β-cells in the islets of Langerhans [1, 93-95]. The direct outcome of β-cell destruction is hyperglycemia due to the lack of insulin secretion. Current gold standard of therapy to restore glucose homeostasis is insulin administration, such as insulin injections or implantation of insulin delivery devices [2]. However, tight glycemic control through insulin administration requires frequent monitoring of blood glucose levels, and all forms of exogenous insulin therapy cause various degrees of patient discomfort. While whole pancreas or islet transplantation can provide T1DM patients with insulin-independence, these approaches

Chaper 3 here is as appeared in H. Shih, R.G. Mirmira and C. Lin, *Journal of Materials Chemistry B*, 2015(3) 170-175

are reserved for diabetic patients with hypoglycemia unawareness due to a significant shortage of donor organs [3-5, 96, 97]. In addition, patients transplanted with allogenic islets are required to receive prolonged immunosuppressant therapy, which unfortunately cannot prevent instant blood mediated inflammatory response (IBMIR) that often destroys more than half of the transplanted islets shortly after surgery [6-8].

In a hope to improve the lifespan of transplanted islets, scientists and engineers have been developing encapsulation technologies to immunoisolate allogenic or even xenogenic islets from host tissues [9-18]. A few critical considerations of islet encapsulation are the cytocompatibility of the encapsulation process, the stability of the coating, and the permeability of the barrier. A successful permselective immune isolation barrier should be able to prevent infiltration of host immune cells while permitting facile exchange of nutrients and metabolites, including oxygen, glucose, and insulin [2]. Existing encapsulation technologies include macromolecular self-assembly [13, 15, 98], cell surface engineering [13], and covalent crosslinking of hydrogels [2, 99]. For example, islets can be encapsulated in polyplexes formed by layer-by-layer (LbL) self-assembly between ionic macromolecules (e.g., polyanionic alginate with divalent barium or calcium cation) [100-102]. Recent work has explored multi-layer coatings formed by affinity binding between labeled macromers (e.g., biotinylated-PEG-N-hydroxysuccinimide, streptavidin, and biotin-peptide) [103, 104], and hydrogen bonding between polar macromers (e.g., poly(N-vinylpyrrolidone) and tannic acid) [105]. The long-term stability of these physically assembled coatings depends highly on the micro-environmental conditions in the transplantation site, such as pH and ionic strength [106, 107]. Alternatively, islets can be encapsulated through cell surface engineering. In one example, islets were functionalized with hetero-bifunctional maleimide-poly(ethylene glycol)-lipid (maleimide-PEG-lipid), which was subsequently reacted with thiol-containing molecules via thiol-maleimide Michael-type addition [20, 108, 109]. The drawbacks of this maleimide-based coating chemistry are slow gelation rate (from minutes to hours) [63, 73, 110], and potential cytotoxicity of maleimide moieties that may not be ideal for islet cell encapsulation [111].

Hubbell and colleagues pioneered an islet conformal coating technique based on visible light-initiated chain-growth photopolymerization [9, 19, 112-115]. The coating process starts with staining islets with a type II photoinitiator, eosin-Y. The stained islets are then incubated in a precursor solution containing macromer PEG-diacrylate (PEGDA), co-initiator triethanolamine (TEA), and co-monomer N-vinylpyrrolidone (NVP). Upon exposure to a visible light source, eosin-Y on islet surface initiates interfacial photopolymerization. Thickness of the coating could be controlled by light exposure time, as well as the concentrations of PEGDA macromer, co-initiator, and co-monomer [112]. Although this technique achieved early success in animal and non-human primate models [116], the chain-growth polymerization scheme suffers from the potential cytotoxicity of co-monomer and co-initiator [117, 118], as well as the formation of a heterogeneous network containing hydrophobic polyacrylate kinetic chains [50]. Since the chain-growth polymerization is initiated from islet surface, the gelation yielded a dense hydrogel layer immediately adjacent to the cell surface [19]. The gradient of crosslinking density would complicate the permeability of nutrients, oxygen, and insulin [119], all of which are essential in maintaining islet survival and functions.

3.3 Results and Discussion

Unlike a chain-growth network that contains heterogeneous cross-links, the step-growth thiol-norbornene photo-click reaction produces orthogonal cross-links with enhanced cytocompatibility [40, 52, 59]. We recently reported a visible light mediated step-growth thiol-ene hydrogelation without using co-monomer (NVP) and cytotoxic co-initiator (TEA) [59]. We hypothesized that this visible light initiated orthogonal thiol-ene reaction could be adapted to form interfacial islet surface conformal coating. Prior to testing this hypothesis, we evaluated the cytocompatibility of this cell surface initiated thiol-ene photopolymerization. Here, we used MIN6 cell aggregates generated from rotating suspension culture as the cell model. These aggregates were cultured in high glucose DMEM supplemented with 50 μM β-mercaptoethanol, 10 % fetal bovine serum

(FBS, Gibco), and 1× antibiotic-antimycotic (Invitrogen) and maintained at 37 ^{o}C and 5 % CO_2. Since different compositions are required for chain-growth and step-growth coating chemistries, in this study, we used non-gelling components (e.g., PEGMA or PEGdNB) to examine the cytocompatibility of these coating chemistries (Figure 3.1A) under similar radical concentrations. After 10 days in culture, MIN6 β-cell aggregates (average aggregate diameter ~100 μm) were retrieved from media, washed with HBSS and stained with 10 mM of eosin-Y (Fisher Scientific) for 5 minutes. After staining, aggregates were washed 3 times with HBSS to remove excess eosin-Y and were transferred to non-gelling precursor solutions containing: (i) 16 wt% $PEGMA_{2kDa}$ (Monomer-Polymer), 50 mM of TEA, and 9 mM of NVP, or (ii) 20 wt% $PEGdNB_{10kDa}$ [120] and dithiothreitol (DTT, Fisher Scientific) at a unity functional group molar ratio ($R_{[thiol]/[ene]}$ = 1).These tubes were exposed to visible light using a fiber optic microscope illuminator (wavelength: 400 to 700 nm, AmScope) for 1 minute. In Figure 3.1B and 3.1C, aggregates were recovered in culture media for 1 hour, followed by staining with live/dead staining reagents (i.e., 0.25 μL/mL Calcein AM and 2 μL/mL Ethidium homodimer-3, respectively) for 1 hour before imaging with a confocal microscope (Olympus Fluoview, FV1000). Similar to our previous work on bulk cell encapsulation using UV-light irradiation [52], visible light-based chain-growth photopolymerization (initiated by eosin-Y/TEA/NVP) was less cytocompatible compared with the step-growth photopolymerization initiated by eosin-Y and DTT. As shown in Figure 3.1B (left), numerous dead cells were found on the surface of MIN6 cell aggregates in the visible light-based chain-growth polymerization system, which was attributed to the high concentrations of radical species in the chain-growth polymerization, [40] as well as the potential cytotoxicity of TEA [117, 118]. In contrast, the visible light-initiated orthogonal step-growth thiol-ene reaction caused less cell death (Figure 3.1B, right) [52, 59]. Due to technical difficulties in quantifying aggregates viability, aggregates viability is only qualitatively analysed using live/dead staining.

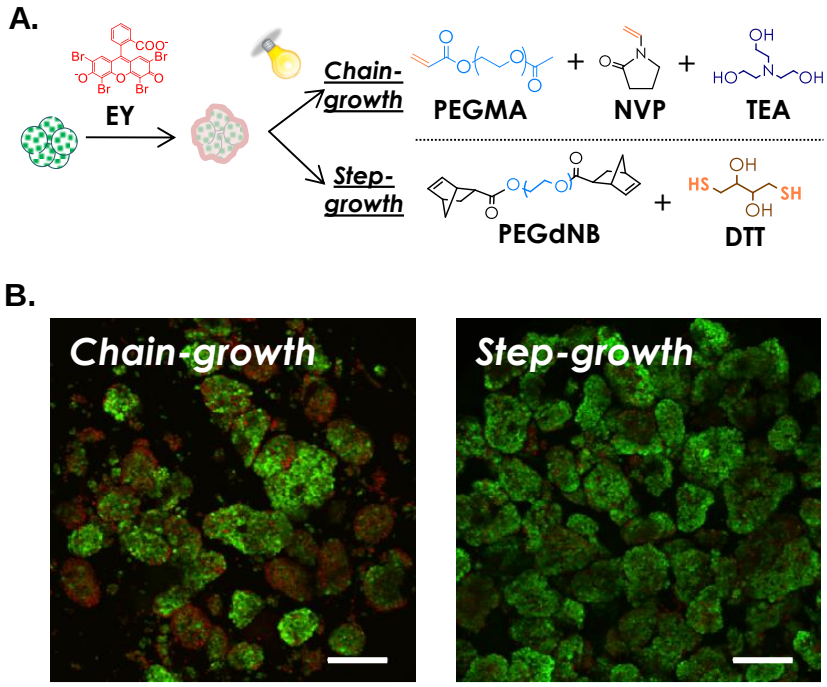

Figure 3.1. (A) Schematic of visible light-initiated interfacial chain-growth (top) or step-growth thiol-ene (bottom) photopolymerization (EY: eosin-Y). (B) Viability of aggregates after non-gelling interfacial photopolymerization reactions (Green: live cells. Red: dead cells. Scales: 100 μm).

Next, we prepared interfacial thiol-ene coating on MIN6 β-cell aggregates. MIN6 β-cell aggregates were stained with 10 mM of eosin-Y for 5 minutes. Eosin-Y stained cell aggregates were washed three times with HBSS (centrifugation for 3 minutes at 500 rpm each), suspended in 50 μL of macromer solution contained 20 wt% 8-arm PEG-norbornene (PEG8NB) with stoichiometric ratio of thiol from DTT (Figure 3.2A & 3.3A), and exposed to bright visible light. Note that in all the coating experiments, aggregate density was fixed at approximately 500 aggregates/mL and more than 200 aggregates were analysed. Representative phase contrast images (Nikkon Eclipse *Ti*) revealed the formation of a thin thiol-ene hydrogel coating on β-cell aggregates after only 30 seconds of light exposure (Figure 3.3B, left). Furthermore, live/dead staining results showed that the coated β-cell aggregates remained viable (Figure 3.3C, left). This direct coating method (i.e., one-step incubation) produced a wider distribution of gel coating thickness, ranging from 20 μm to 60 μm (Figure 3.3D), which averaged to approximately 33 μm (Figure 3.3E) quantified by estimating circular diameter using NIS-Elements BR

3.2 software. In addition, the one-step method only yielded a coating efficiency of 64 % (Figure 3.3F), and there was a strong dependency between the coating thickness and the size of the cell aggregates (Figure 3.3G). Here, coating efficiency is the percent fraction of coated aggregates over the sum of coated and non-coated aggregates. While the one-step coating method is easy and cytocompatible to β-cell aggregates, it did not show high coating efficiency and consistency. Thus, it is essential to establish a coating strategy that provides high consistency and repeatability for isolated islets, which are heterogeneous in size (a few tens to a few hundreds micron) [121]. We hypothesized that the conformal coating results could be improved by providing additional thiols near the surface of the cell aggregates. These surface-anchored thiols could reduce the variability of coating thickness and increase coating/polymerization efficiency. Our recent work has shown that PEG exhibits affinity to eosin-Y [122]. Hence, we hypothesized that by incubating eosin-Y stained aggregates with PEG-di-thiol (PEGdSH) would allow PEGdSH to anchor on the surface of cell aggregates via affinity binding to cell surface adsorbed eosin-Y (Figure 3.2B). To test this hypothesis, stained aggregates were incubated in 20 wt% of PEGdSH for 5 minutes, and washed three times with HBSS before suspending in macromer solution containing PEG8NB with DTT (Figure 3.2B). After 30 seconds of light exposure, conformal hydrogel coating also formed on β-cell aggregates (Figure 3.3B, right). Two-step coating process is also cytocompatible to MIN6 aggregates (Figure 3.3C, right). More cell death observed in two-step coating potentially due to the increased in radical reactions on the surface of aggregates. This two-step incubation process produced thiol-ene conformal gel layer with a narrower distribution of coating thickness (Figure 3.3D, ~20 to 40 μm) and a lower average coating thickness (Figure 3.3E, ~ 26 μm). More importantly, the two-step coating method yielded higher coating efficiency (Figure 3.3F, 80 %) and a reduced dependency between coating thickness and the size of cell aggregates (Figure 3.3G).

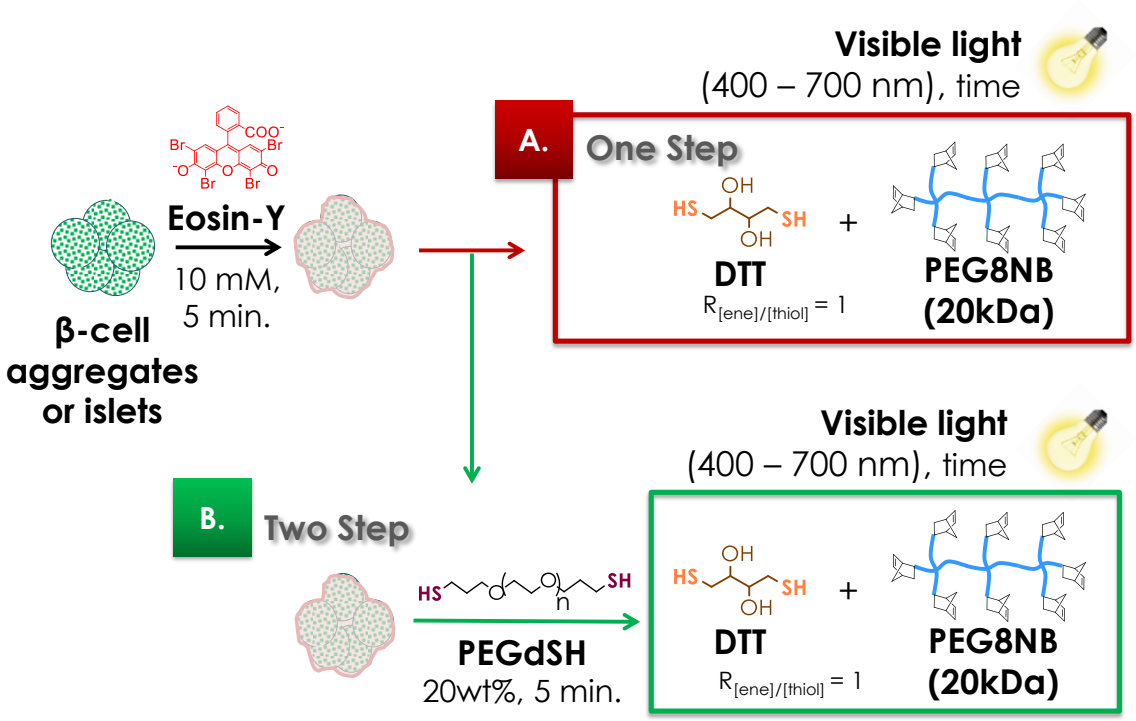

Figure 3.2. Schematic of visible light-mediated interfacial thiol-ene photopolymerization and conformal coating on β-cell aggregates or islets via: (A) one-step or (B) two-step coating method.

Results shown in Figure 3.3 have demonstrated the benefits and importance of additional PEGdSH incubation in interfacial thiol-ene photopolymerization. Therefore, we further investigated the effect of PEGdSH on coating thickness and efficiency. In general, the thiol-ene coating thickness decreased with increasing molecular weight (MW) of PEGdSH (i.e., from 35 μm, 26 μm, to 13 μm for 2 kDa, 3.4 kDa, and 10 kDa PEGdSH, respectively, Figure 3.4A-D & 3.5A). The use of higher MW of PEGdSH resulted in decreased coating efficiency (Figure 3.5B, from 98 % to 64 %). It is worth noted that in these experiments, the concentration of PEGdSH (20 wt%) as well as the stoichiometric ratio of thiol (from DTT) and norbornene (from PEG8NB) in the precursor solution were maintained. PEGdSH at a lower MW has higher thiol content when comparing with its counterpart at a higher MW and at the same macromer concentration. Therefore, increased coating thickness and efficiency at a lower PEGdSH MW were likely due to increased availability of thiols near the surface of the aggregates, which accelerated the thiol-ene cross-linking reaction.

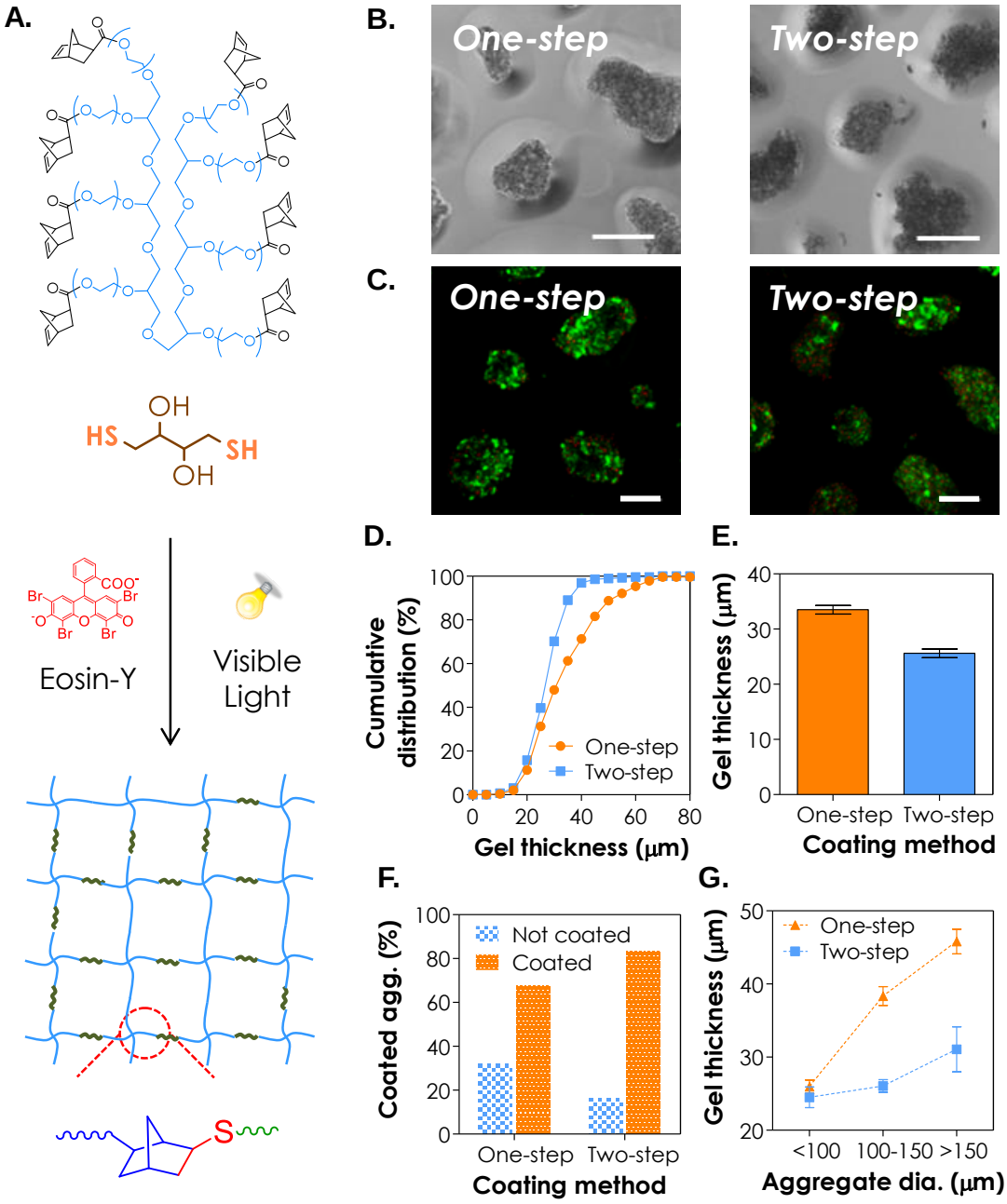

Figure 3.3. (A) Schematic of visible light-initiated step-growth orthogonal thiol-ene reaction to form idealized hydrogel network. (B) Representative phase-contrast images of the conformal coated aggregates. (C) Representative live/dead stained images of the conformal coated aggregates (Scales: 50μm). (d-f) Effects of coating methods on (D) the cumulative distribution of conformal gel coating thickness, (E) the average coating thickness, and (F) the percent of coated aggregates. (G) Effect of aggregate diameter on thiol-ene conformal coating thickness. (One-step: 20 wt% PEG8NB-DTT and 30 seconds of light exposure. Two-step: 20 wt% PEG8NB-DTT, 3.4 kDa PEGdSH and 30 seconds of light exposure. Mean ± SEM, n > 200 aggregates)

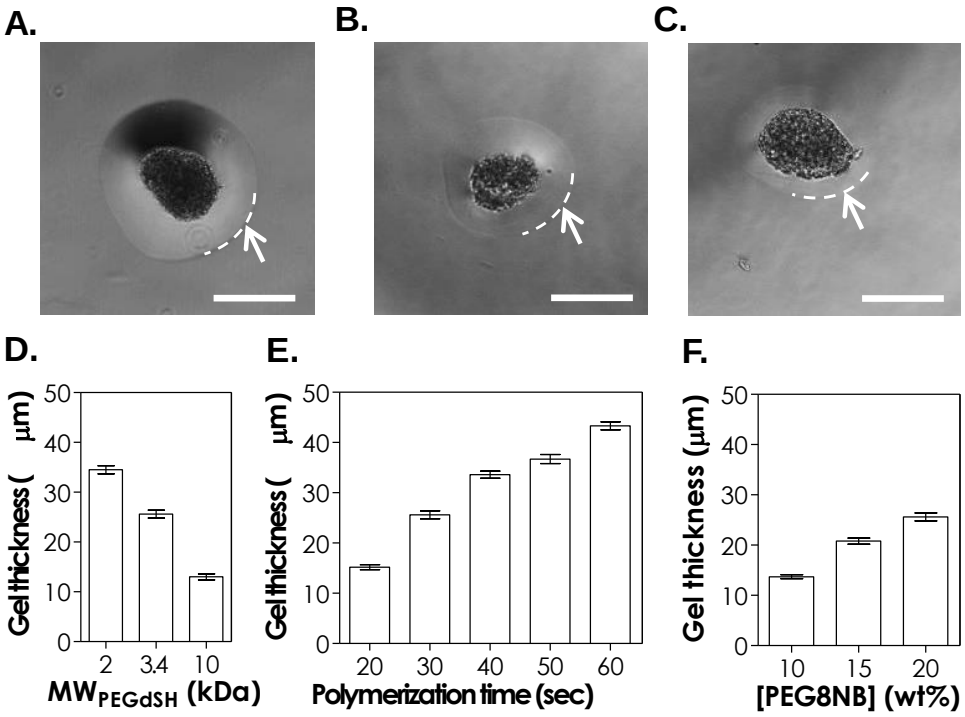

Figure 3.4. (A-C) Representative phase-contrast images of MIN6 cell aggregates with thiol-ene conformal gel coating (two-step coating method). PEGdSH MW: (A) 2 kDa, (B) 3.4 kDa, and (C) 10 kDa. Arrows and dashed lines indicate the boundary of the hydrogel coating (Scales: 50 μm). (D-F) Parameters affecting thiol-ene conformal coating thickness: (D) molecular weight of PEGdSH, (E) photopolymerization time, and (F) concentration of macromer PEG8NB. Coating conditions: (A-D) 20 wt% of PEG8NB-DTT and 30 seconds of light exposure. (E) 3.4 kDa of PEGdSH and 30 seconds of light exposure. (F) 20 wt% of PEG8NB-DTT and 3.4 kDa of PEGdSH (Mean ± SEM, n > 200 aggregates).

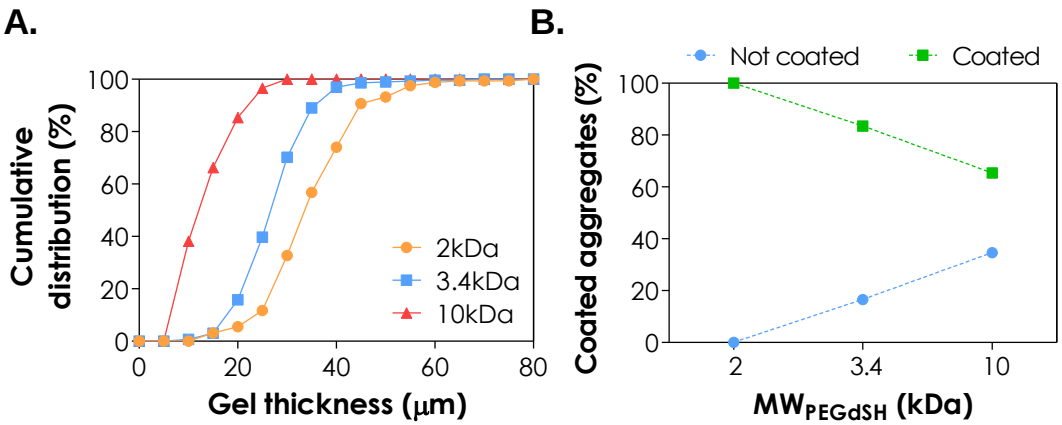

Figure 3.5. Effects of molecular weight of PEGdSH on (A) cumulative distribution of conformal gel coating thickness, and (B) percent of coated aggregates. (20 wt% of PEG8NB-DTT, $R_{[PEG8NB]:[DTT]}$ = 1, 30 seconds of light exposure. Mean ± SEM)

We also evaluated the influence of other parameters on the thiol-ene interfacial conformal coating. For example, when the polymerization time was increased from 20 to 60 seconds, gel thickness was increased from 15 to 43 μm (Figure 3.4E & 3.6). Longer polymerization time resulted in increasing coating efficiency (Figure 3.6B, from 53 % to 98 %) and the likelihood of encapsulating more than one aggregate per gel capsule (~20 % at 60 seconds). In addition, when the concentration of PEG8NB in the precursor solution was increased from 10 wt% to 20 wt%, gel thickness increased from 14 to 26 μm (Figure 3.4F & 3.7A). The use of a higher PEG8NB concentration also increased coating efficiency (from 24 % to 84 %, Figure 3.7B). Regardless of the coating thickness, our analysis showed that thiol-ene hydrogels have controllable mesh size depending on the concentration of PEG8NB used. Based on the Flory-Rehner theory of elasticity, the mesh size of a step-growth hydrogel with an ideal network (e.g., PEG8NB-DTT hydrogel, MW_{PEG8NB} = 20 kDa, MW_{DTT} = 154 Da, and f_{PEG8NB} = 8 and f_{DTT} = 2) is 9.1 nm (Equation 3.1 to 3.6) [123]. The mesh sizes of all thiol-ene hydrogels prepared here (Figure 3.8, from 15.1 nm to 9.9 nm for 5 to 20 wt% of PEG8NB, respectively) were all larger than the hydrodynamic radius (2.0 nm) and diameter (4.0 nm) of insulin [124]. This indicates that the diffusion of insulin from thiol-ene gel coating will not be significantly retarded.

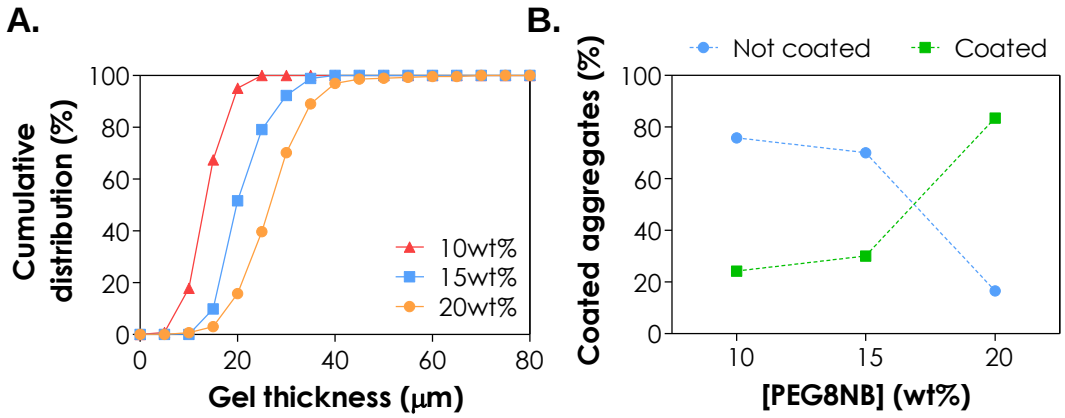

Figure 3.6. Effects of PEG8NB concentration in the precursor solution on (A) cumulative distribution of conformal gel coating thickness, and (B) percent of coated aggregates. (MW of PEGSH = 3.4 kDa, $R_{[PEG8NB]:[DTT]}$ = 1, 30 seconds of light exposure. Mean ± SEM)

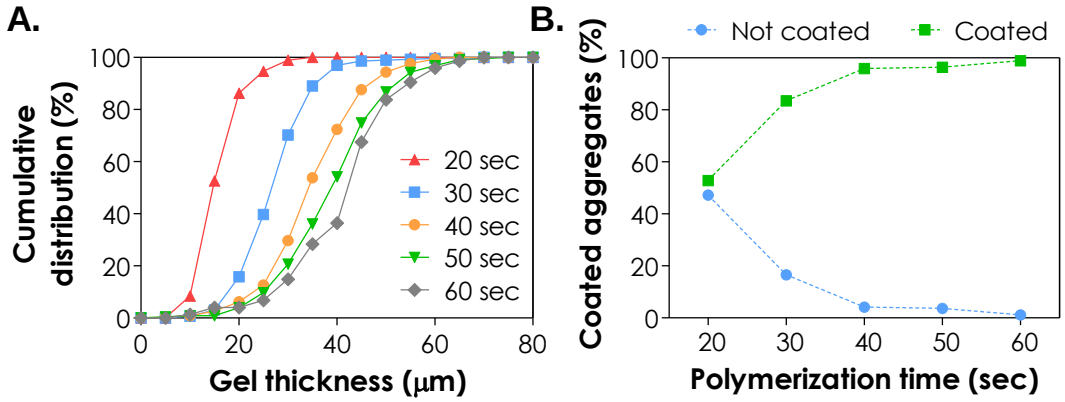

Figure 3.7. Effects of polymerization time on (A) cumulative distribution of conformal gel coating thickness, and (B) percent of coated aggregates. (MW of PEGSH = 3.4 kDa, 20 wt% of PEG8NB-DTT, $R_{[PEG8NB]:[DTT]}$ = 1. Mean ± SEM)

Following the optimization of interfacial thiol-ene photopolymerization conditions using MIN6 aggregates, we prepared orthogonal thiol-ene hydrogel conformal coating on isolated islets. CD1 mice (7- to 8-week old) were obtained from Charles River and islets were isolated from CD1 mice following established protocol [125]. Permission for animal studies was approved by Indiana University School of Medicine IACUC (protocol #10235-MD/R). CD1 murine islets were used in this study while the main macromer was replaced with hydrolytically stable 8-arm PEG-amide-NB (PEGa8NB, Figure 3.9A) [59]. It is worth noted that thiol-ene hydrogels formed from PEGa8NB have similar degree of cross-linking efficiency (i.e., gel fraction above 90 %) and swelling (up to 2 weeks) when compared with hydrolytically labile ester-containing PEG8NB (Figure 3.9). Specifically, hydrogels formed from hydrolytically labile PEG8NB showed significant degradation after three weeks. During the month-long incubation, no significant gel degradation was observed in gels formed from hydrolytically stable PEGa8NB (Figure 3.9C). As shown in Figure 3.10A, coated islets remained viable 24 hours post coating. Furthermore, the coated hydrogel layer maintained its stability throughout 2 weeks of *in vitro* culture (Figure 3.10B, 3.10C & 3.10D). The average thickness of coating was ~30 μm with 90% of coating efficiency (data not shown). In long-term *in vitro* culture of primary islets, the production of cellular debris and the darkening of islets core are common phenomena, likely due to necrosis in the isolated islets (Figure 3.10D) [126]. Clearly, the cellular debris was free floating in culture media with the non-coated islets. On the other hand, the dark debris was 'trapped' within the conformal coating layer on the coated islets. These results suggest that the coating serves as a bi-directional immuoisolation barrier as it not only blocks the infiltration of host immune cells, but also prevents the liberation of graft debris to the transplantation site that would otherwise trigger host immune response [127, 128]. To examine insulin secretion from the coated islets, glucose-stimulated insulin secretion (GSIS) was performed at day 2 and day 14 (Figure 3.10E & 3.10F). Here, glucose solution was prepared (2.5 or 25 mM of glucose) with Krebs-Ringer bicarbonate (KRB) buffer containing sodium chloride (23 mM), potassium chloride (1 mM), sodium bicarbonate (4.8 mM), magnesium chloride hexahydrate (0.2 mM), calcium chloride dehydrate (0.2

mM), 4-(2-hydroxyethyl)-1-piperazineethanesulfonic acid (HEPES, 0.5 mM) and bovine serum albumin (BSA, 0.1 vol%). The temperature of glucose solutions were equilibrated to 37 ^{o}C. Coated or non-coated islets were washed with HBSS, hand-picked and transferred into micro-centrifuge tube (30 islets per tube, N = 4 tubes per sample group). Islets were primed with 500 μL of low glucose solution for 1 hour at 37 ^{o}C and 5 % CO_2. Then, islets were incubated with 500 μL of low or high glucose solution (at 37 ^{o}C, 5 % CO_2) for 2 hours each. The glucose solution was collected after each glucose treatment. After glucose stimulation, islets were lysed with acid ethanol extraction buffer (75 vol% of ethanol, 1.5 vol% 1N hydrochloric acid and 23.5 vol% ddH_2O) and the samples were diluted accordingly with KRB mixture [129]. The amounts of insulin were quantified by mouse insulin ELISA kit (Mercodia) and normalized to their corresponding total insulin content (i.e., the sum of intracellular and secreted insulin). We found that the amounts of insulin secreted from the thiol-ene hydrogel coated islets were not statistically different from the non-coated islets. Within each non-coated or coated islets group, statistically significance ($p < 0.05$) was found between insulin secretion at 2.5 mM and 25 mM glucose. The GSIS index, which is the ratio of insulin secretion in high glucose buffer to low glucose buffer, showed no statistical significance between coated and non-coated islets throughout 2 weeks of *in vitro* culture (Figure 3.11). These results suggest that, after the thiol-ene interfacial coating process, the thiol-ene conformal gel coated islets preserved their responsiveness to glucose.

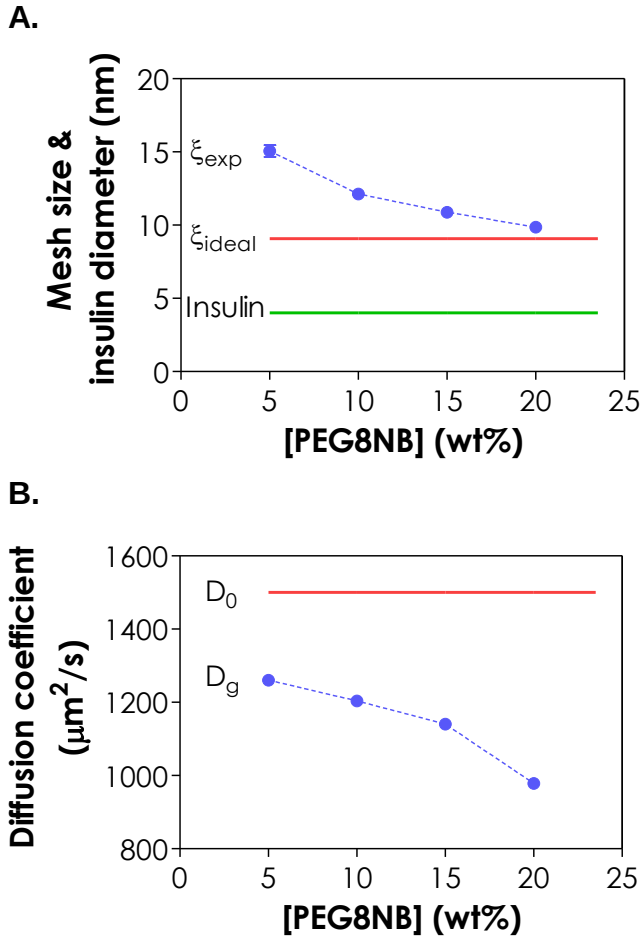

Figure 3.8. (A) Effect of PEG8NB concentration on the mesh size (ξ) of hydrogels. The mesh size of an ideal network (ξ_{ideal}) was determined by Flory-Rehner equations (Equation 3.1 to 3.6). The experimental mesh size (ξ_{exp}) was calculated from the swelling ratio of PEG8NB-DTT hydrogels at different macromer contents (Equation 3.4, 3.5 & 3.6). Diameter of insulin was obtained from reference [124]. (B) Effect of PEG8NB concentration on the diffusion coefficient (D_g) of insulin in swollen hydrogel. The diffusion coefficient of insulin in pure solvent is obtained from reference [6] and the calculation of D_g was based on Lustig-Peppes model in reference [130]. (PEG8NB-DTT, 0.1 mM of eosin-Y, 5 minutes of light exposure, N = 5. Mean ± SEM)

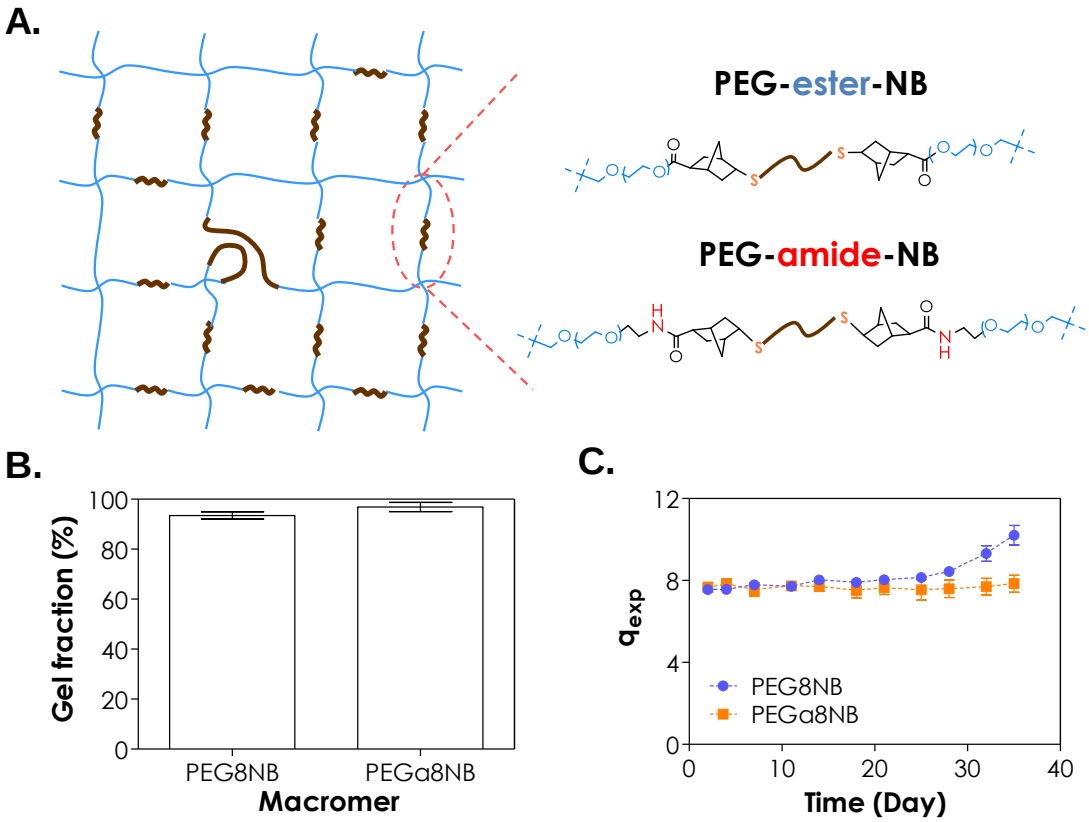

Figure 3.9. (A) Schematic representation of thiol-ene hydrogels formed by hydrolytically degradable PEG8NB and non-degradable PEGa8NB. Effects of PEG macromer on (B) gel fraction, and (C) hydrolytic degradability of hydrogels. (20 wt% PEG8NB or PEGa8NB-DTT, 0.1 mM of eosin-Y, 5 minutes of light exposure, N = 5. Mean ± SEM)

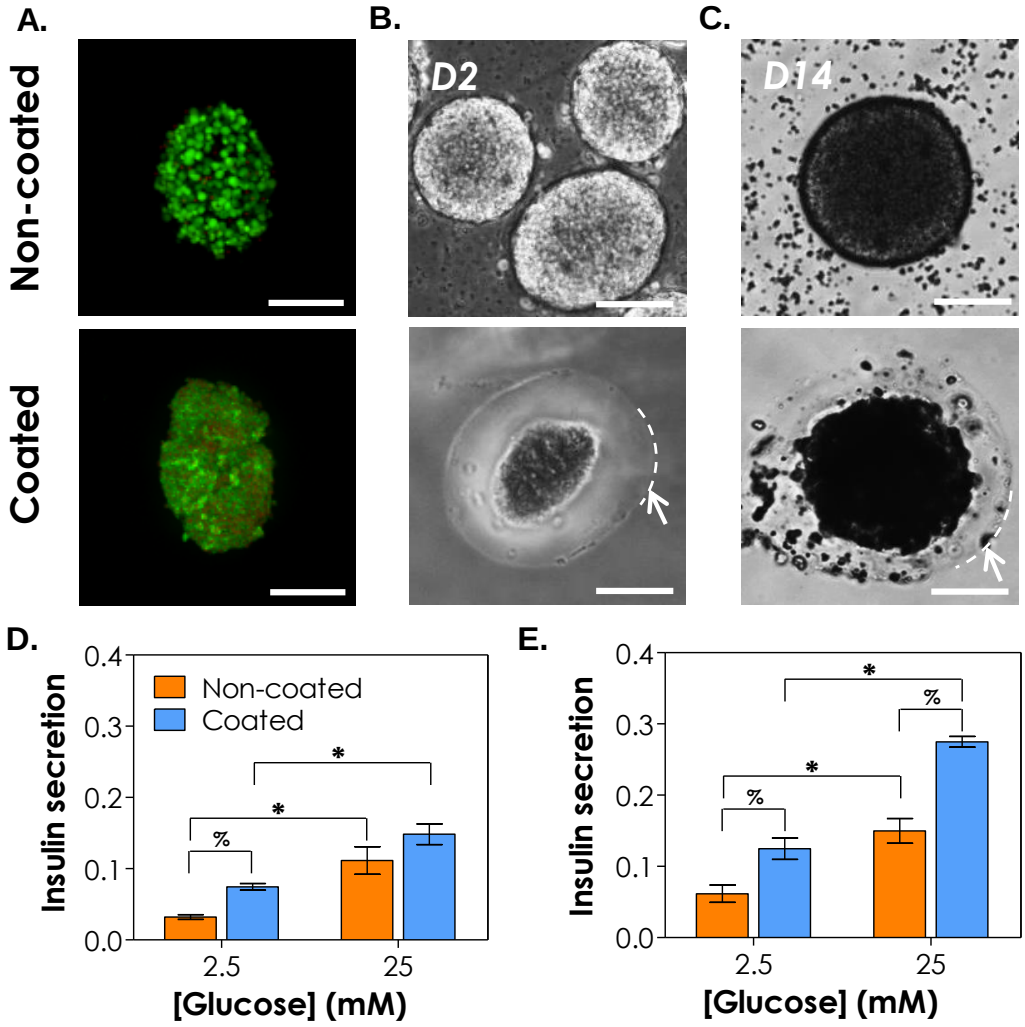

Figure 3.10. (A) Representative live/dead stained images of non-coated and coated CD1 mice islets (24 hours after coating). (B-C) Representative phase contrast images of non-coated (top) and coated (bottom) CD1 mice islets on day 2 (B), and day 14 (C). Arrows and dashed lines in (B-C) indicate the boundary of the hydrogel coating (Scales: 50 µm). (D-E) *In vitro* glucose stimulated insulin secretion (GSIS) of isolated islets on (D) day 2 and (E) day 14. Asterisks indicate statistical significance between 2.5 and 25 mM of glucose within each group (Mean ± SEM, $p < 0.05$). Coating conditions: 3.4 kDa PEGdSH, 20 wt% PEGa8NB-DTT, 25 seconds light exposure.

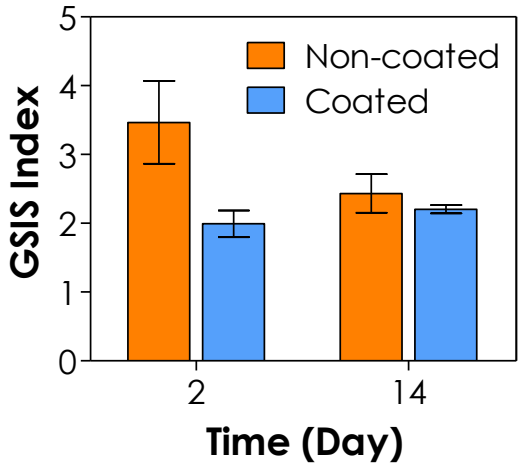

Figure 3.11. *In vitro* glucose stimulated insulin secretion (GSIS) index of CD1 murine islets. GSIS index is the normalization of insulin secreted at high glucose to low glucose. (Coating conditions: 3.4 kDa PEGdSH, 20 wt% PEGa8NB-DTT and 25 seconds light exposure. Mean ± SEM)

3.4. Materials and Methods

Materials: Eosin-Y disodium salt and DTT were purchased from Fisher Scientific. 8-arm PEG-hydroxyl (MW: 20 kDa) and 8-arm PEG-amine (MW: 20 kDa) were purchased from JenKem Technology USA. PEG-monoacrylate (MW: 2 kDa) was purchased from Monomer-Polymer. Linear raw PEG-hydroxyl (MW: 2, 3.4 or 10 kDa) and all other chemicals were obtained from Sigma-Aldrich unless noted otherwise. CD1 mice (7- to 8-week old) were obtained from Charles River as islet donors. Permission for animal studies was approved by Indiana University School of Medicine IACUC (protocol #10235-MD/R).

Synthesis of Poly(ethylene glycol)-ester-norbornene (PEGNB) macromer: Linear or 8-arm PEGNB was synthesized by reacting linear or 8-arm hydroxyl-terminated PEG with 5-norbornene-2-carboxylic acid (5-fold excess to hydroxyl group) in anhydrous dichloromethane (DCM) using N,N'-dicyclohexylcarbodiimide (DCC, 2.5-fold excess) as

a coupling reagent. Norbornene acid was mixed with DCC and stirred at room temperature for 1 hour. The resulting norbornene anhydride was filtered into an addition funnel and added drop wise into a flask containing linear (10 kDa) or 8-arm PEG (20 kDa), 4-(dimethylamino) pyridine (DMAP, 0.5-fold excess), and pyridine (5-fold excess) in anhydrous DCM. The flask was kept in an ice bath and the mixture was reacted for overnight in dark. The product was filtered and precipitated in cold ethyl ether on ice. After drying *in vacuuo*, PEGNB product was re-dissolved in water and dialyzed for 2 days (in pH 6 ddH_2O). ^1H NMR (Bruker 500) was used to confirm the degree of PEG functionalization (> 90 %).

Synthesis of Poly(ethylene glycol)-amide-octa-norbornene (PEGa8NB) macromer: Norbornene acid (5-fold excess to amine groups) was activated by HBTU/HOBT (5.5-fold excess to amine group) in dimethylformamide (DMF) for 3 minutes. With nitrogen gas purging, N,N-Diisopropylethylamine (DIEA, 6-fold excess to amine group) was added to the activated norbornene acid solution and stirred for 5 minutes. The solution was added drop wise to a two-neck flask containing PEG-octa-amine in DMF. After overnight reaction at room temperature, the product was precipitated in cold ethyl ether. After drying *in vacuuo*, PEGaNB product was re-dissolved in water and dialyzed for 2 days . ^1H NMR (Bruker 500) was used to confirm the degree of PEG functionalization (> 90 %).

Synthesis of PEGdSH macromer: PEGdSH was synthesized following established protocol. In brief, linear PEG (2, 3.4 or 10 kDa) was dissolved in anhydrous toluene and dried by evaporating toluene. Dried PEG was re-dissolved in anhydrous tetrahydrofuran (THF), to which sodium hydride (1.5-fold excess of hydroxyl group) was added slowly and the mixture was stirred until no hydrogen gas bubble was visible, the set up was purged with nitrogen gas in an oil bath at 40 °C. Allyl bromide (6-fold excess of hydroxyl group) was added drop wise to the PEG solution and the reaction was allowed to continue overnight in dark. Sodium bromide salt was filtered off to obtain a clear solution containing PEG-allylether (PEGdAE), which was precipitated out in cold ethyl ether,

filtered, and dried *in vacuuo*. Next, thiolacetic acid (2-fold excess to allylether group) was added slowly to dichloromethane (DCM) solution containing PEGdAE and photoinitiator Irgacure I-2959 (0.5 wt%). Photoconjugation was initiated by UV-light exposure (Omicure S1000, 365 nm and 10 mW/cm^2) for 15 minutes and continued for another 30 minutes after supplementing with another portion (0.5wt%) of I-2959. Linear PEG-thiolacetate was precipitated in cold ethyl ether, filtered, and dried *in vacuuo*. After re-dissolving PEG-thiolacetate in ddH_2O (30 mL), 15 mL of sodium hydroxide (2N) was added to the solution for 5 minutes. Then, equal amount of hydrochloride acid (2N) was added to neutralize PEG-thiolacetate solution. After dialysis for 2 days at room temperature, PEGSH was obtained from lyophilization. The purity (> 90 %) was characterized with H^1NMR Bruker 500).

Cytocompatibility of interfacial thiol-ene photopolymerization on β-cell aggregates or islets: MIN6 β-cell aggregates were formed on an orbital shaker in a non-treated tissue culture plate. These aggregates were cultured in high glucose DMEM supplemented with 50 μM β-mercaptoethanol, 10 % fetal bovine serum (FBS, Gibco), and 1× antibiotic-antimycotic (Invitrogen) and maintained at 37 ^oC and 5 % CO_2. After 10 days in culture, MIN6 β-cell aggregates (average aggregate diameter ~100 μm) were retrieved from media, washed with HBSS and stained with 10 mM of eosin-Y for 5 minutes. After staining, aggregates were washed 3 times with HBSS to remove excess eosin-Y and were transferred to non-gelling precursor solutions containing: (i) 16 wt% $PEGMA_{2kDa}$, 50 mM of TEA, and 9 mM of NVP, or (ii) 20 wt% $PEGdNB_{10kDa}$ and DTT at a unity functional group molar ratio ($R_{[thiol]/[ene]} = 1$). These tubes were exposed to visible light using a fiber optic microscope illuminator (wavelength: 400 to 700 nm, AmScope) for 1 minute. Aggregates were recovered in culture media for 1 hour, followed by staining with live/dead staining reagents (i.e., 0.25 μL/mL Calcein AM and 2 μL/mL Ethidium homodimer-3, respectively) for 1 hour before imaging with a confocal microscope (Olympus Fluoview, FV1000). Pancreatic islets were isolated from CD1 mice following established protocol [125]. These islets were cultured in RPMI media supplemented with 10 % fetal bovine serum, and 1× antibiotic-antimycotic. In a similar manner as described

above, islets were stained with live/dead dyes and evaluated viability with a confocal microscope.

Coating of β-cell aggregates or pancreatic islets: MIN6 β-cell aggregates or isolated CD1 islets were stained with 10 mM of eosin-Y for 5 minutes. For the one-step coating method, aggregates were washed three times with HBSS (centrifugation for 3 minutes at 500 rpm each) and suspended in 50 μL of macromer solution contained 20 wt% PEG8NB with stoichiometric ratio of thiol (from DTT) (Figure 3.2A). For the two-step coating method, stained aggregates/islets were incubated in 20 wt% of PEGdSH for 5 minutes, and washed three times with HBSS before suspending in macromer solution containing PEG8NB or PEGa8NB with DTT (Figure 3.2B). The mixture containing macromer components and stained aggregates/islets was exposed to visible light (between 20 to 60 seconds). In these experiments, aggregate/islet density was fixed at approximately 500 aggregates/mL. Coated aggregates or islets were imaged with phase-contrast microscope (Nikkon Eclipse *Ti*) and coating thickness was quantified by estimating circular diameter using NIS-Elements BR 3.2 software.

Glucose stimulated insulin secretion (GSIS) and ELISA: Glucose solution was prepared (2.5 or 25 mM of glucose) with Krebs-Ringer bicarbonate (KRB) buffer containing sodium chloride (23 mM), potassium chloride (1 mM), sodium bicarbonate (4.8 mM), magnesium chloride hexahydrate (0.2 mM), calcium chloride dehydrate (0.2 mM), 4-(2-hydroxyethyl)-1-piperazineethanesulfonic acid (HEPES, 0.5 mM) and bovine serum albumin (BSA, 0.1 vol%). The temperature of glucose solutions were equilibrated to 37 ^{o}C. Coated or non-coated islets were washed with HBSS, hand-picked and transferred into micro-centrifuge tube (30 islets per tube, N = 4 tubes per sample group). Islets were primed with 500 μL of low glucose solution for 1 hour at 37 ^{o}C and 5 % CO_2. Then, islets were incubated with 500 μL of low or high glucose solution (at 37 ^{o}C, 5 % CO_2) for 2 hours each. The glucose solution was collected after each glucose treatment. After glucose stimulation, islets were lysed with acid ethanol extraction buffer (75 vol% of ethanol, 1.5 vol% 1N hydrochloric acid and 23.5 vol% ddH_2O) and the samples were diluted accordingly with KRB mixture. The amounts of insulin were quantified by mouse

insulin ELISA kit (Mercodia) and normalized to their corresponding total insulin content (i.e., the sum of intracellular and secreted insulin).

Hydrogel fabrication and swelling: Step-growth thiol-ene hydrogels were formed by radical-mediated photopolymerization using 0.1 mM of eosin-Y under visible light exposure at an intensity of 70,000 Lux using a fiber optic microscope illuminator (AmScope) for 5 minutes. To quantify hydrogel swelling, circular hydrogel discs were prepared from 50 μL precursor solution. Immediately after gelation, hydrogels were incubated in ddH_2O at 37 ºC on an orbital shaker for 24 hours to remove sol fraction. Gels were then dried and weighed to obtain dried polymer weights (W_{Dry}). The dried polymers were incubated in 5 mL of buffer solution (pH 7.4 PBS) at 37 ºC on an orbital shaker. At specific time points, hydrogels were removed from the medium, blotted dry with Kimwipe, and weighed to obtain swollen weights ($W_{Swollen}$). Hydrogel mass swelling ratios (q_{exp}) were determined by a ratio of $W_{Swollen}$ to W_{Dry}.

Hydrogel mesh size: For an 'ideal' thiol-ene hydrogel network containing no structural defects, the ideal mesh size was determined with structural information. First, the average molecular weight between crosslinks ($\overline{M_c}$) is defined as [129]:

$$\overline{M_c} = 2\left(\frac{MW_A}{f_A} + \frac{MW_B}{f_B}\right) \tag{3.1}$$

Here, MW_A and MW_B represent the molecular weight of PEG8NB and crosslinker DTT, respectively. f_A and f_B are the number of reactive functionality for PEG8NB and DTT, which were 8 and 2, respectively. With a known $\overline{M_c}$, the ideal network crosslinking density or density of elastically active chains (v_c) and polymer volume fraction (v_2) can be calculated based on the Flory-Rehner theory [63]:

$$v_c = \frac{V_1}{\overline{M_c}\,\overline{v_2}} = \frac{-[\ln(1-v_2)+v_2+\chi_{12}{v_2}^2]}{{v_2}^{1/3}-\frac{2v_2}{f_A}} \tag{3.2}$$

Here, $\overline{v_2}$ is the specific volume of PEG (0.92 cm^3/g at 37 ºC), V_1 is the molar volume of water (18 cm^3/mole) and χ_{12} is the Flory-Huggins interaction parameter for a PEG-H_2O system (0.45). After obtaining v_2, ideal hydrogel mass swelling ratio q_{ideal} can be obtained using the following equation:

$$v_2 = \frac{\overline{v_2}}{(q_{ideal}-1)\overline{v_1}+\overline{v_2}} \tag{3.3}$$

where $\overline{v_1}$ is the specific volume of water (1.006 cm^3/g at 37 ºC).

The polymer volume fraction in the swollen state ($v_{2,s}$) was obtained using the following equation:

$$v_{2,s} = \frac{\frac{1}{\rho_2}}{\frac{q}{\rho_1}+\frac{1}{\rho_2}} \tag{3.4}$$

where ρ_1 and ρ_2 are the densities of the solvent and polymer, respectively. Here, q was either q_{ideal} or q_{exp}.

Second, the root-mean-squared end-to-end distance of network chains between two crosslinks in the neutral state or $(\overline{r_0^2})^{1/2}$ was determined based on:

$$(\overline{r_0^2})^{\frac{1}{2}} = l(C_n \frac{n\overline{M_c}}{M_r})^{\frac{1}{2}} \tag{3.5}$$

Here, C_n is the Flory characteristic ratio, l is the average bond length along the polymer backbone, and n is the number of chemical bonds within a repeating unit (e.g., n equals to 3 for PEG). M_r is the molecular weight of the repeating units of the polymer chain.

With calculated $v_{2,s}$ and $(\overline{r_0^2})^{1/2}$, mesh size of the hydrogel (ξ) was obtained as the product of the two parameters:

$$\xi = {v_{2,s}}^{-\frac{1}{3}}(\overline{r_0^2})^{\frac{1}{2}} \tag{3.6}$$

Diffusion coefficient of insulin: To estimate the diffusivity of insulin in a swollen hydrogel, a diffusivity model adapted by Lustig and Peppas was used [130]:

$$\frac{D_g}{D_0} = (1-\frac{r_s}{\xi})\exp[(-Y\left(\frac{v_{2,S}}{1-v_{2,S}}\right)] \tag{3.7}$$

where Dg is the insulin diffusion coefficient in the swollen thiol-ene hydrogel, D_0 is the diffusion coefficient of insulin in pure solvent (1500 μm^2/second) [131], and r_s is the hydrodynamic radius of insulin (2 nm) [124]. Here, Y is assumed to be 1 which is the ratio of the critical volume required for a successful movement of insulin and the average free volume per molecule of solvent.

Data Analysis: Data analysis was performed on Prism 5 software. Unless otherwise noted, all experiments were conducted independently for three times and the results were reported as mean ± SEM. Student's t-test was conducted for statistical analysis where

significance was reported for $p < 0.05$. For coating thickness characterizations, at least 200 aggregates were analyzed per experimental condition.

3.5 Conclusion

In summary, we have developed a visible light-mediated thiol-norbornene interfacial coating process to prepare step-growth conformal hydrogel coating on islet surface. Using MIN6 β-cell aggregates as a model, we evaluated the parameters critical in determining coating thickness (e.g., MW of PEGdSH, polymerization time, and macromer concentration). The results of live/dead staining and GSIS demonstrated high cytocompatibility of thiol-norbornene hydrogel coating on murine islets. This visible light mediated thiol-norbornene interfacial photopolymerization provides an alternate coating option and should be of great interest to the field of islet transplantation. Future work will focus on modifying thiol-norbornene gel formulation to create multi-functional immuno-isolation barrier, and on determining the inflammatory response and long-term efficacy of the transplanted coated islets on maintaining euglycemia.

CHAPTER 4
PHOTO-CLICK HYDROGELS PREPARED FROM FUNCTIONALIZED CYCLODEXTRIN AND POLY(ETHYLENE GLYCOL) FOR DRUG DELIVERY AND IN SITU CELL ENCAPSULATION

4.1 Abstract

Polymers or hydrogels containing modified cyclodextrin (CD) are highly useful in drug delivery applications as CD is a cytocompatible amphiphilic molecule that can complex with a variety of hydrophobic drugs. Here, we designed modular photo-click thiol-ene hydrogels from derivatives of βCD and poly(ethylene glycol) (PEG), including βCD-allylether (βCD-AE), βCD-thiol (βCD-SH), PEG-thiol (PEGSH), and PEG-norbornene (PEGNB). Two types of CD-PEG hybrid hydrogels were prepared using radical-mediated thiol-ene photo-click reactions. Specifically, thiol-allylether hydrogels were formed by reacting multi-arm PEGSH and βCD-AE, and thiol-norbornene hydrogels were formed by cross-linking βCD-SH and multi-arm PEGNB. We characterized the properties of these two types of thiol-ene hydrogels, including gelation kinetics, gel fractions, hydrolytic stability, and cytocompatibility. Compared with thiol-allylether hydrogels, thiol-norbornene photo-click reaction formed hydrogels with faster gelation kinetics at equivalent macromer contents. Using curcumin, an anti-inflammatory and anti-cancer hydrophobic molecule, we demonstrated that CD-crosslinked PEG-based hydrogels, when compared with pure PEG-based hydrogels, afforded higher drug loading efficiency and prolonged delivery *in vitro*. Cytocompatibility of these CD-crosslinked hydrogels were evaluated by *in situ* encapsulation of radical sensitive pancreatic MIN6 β-cells. All formulations and crosslinking conditions tested were cytocompatible for cell

---

Chaper 4 here is as appeared in H. Shih and C. Lin, *Biomacromolecules*, 2015(16) 1915-1923

encapsulation. Furthermore, hydrogels crosslinked by βCD-SH showed enhanced cell proliferation and insulin secretion as compared to gels crosslinked by either dithiothreitol (DTT) or βCD-AE, suggesting the profound impact of both macromer compositions and gelation chemistry on cell fate in chemically crosslinked hydrogels.

4.2 Introduction

As defined by the Food and Drug Administration (FDA), amphiphilic cyclodextrins (CDs) are a class of 'Generally Recognized as Safe (GRAS)' macromolecules [132-134]. The hydrophobic cavity of CD can accommodate a broad range of poorly soluble drugs through host-guest complex formation, whereas the hydrophilic surface of CD facilitates the dissolution of the CD-drug complex in aqueous solutions [135]. Three types of CD, α-, β-, and γ-CD (with 6, 7, and 8 repeating units of glycopyranose, respectively), are commonly used for increasing the solubility of hydrophobic drugs [136]. In addition to serving as a drug-dissolving agent, CDs can be easily modified for forming multifunctional macromolecules, including linear polymers and network hydrogels [137-139]. For example, hydroxyl groups of βCD could be functionalized with acrylate for crosslinking into hydrogel for binding and releasing anti-cancer drug, such as chlorambucil. The release rate was controlled by adjusting pH or degree of network crosslinking [140]. CD could also be functionalized with azide for chemical crosslinking with PEG-di-alkyne via the copper-catalyzed azide-alkyne cycloaddition (CuAAC) [141]. Unfortunately, copper is a cytotoxic metal that induces oxidative damage to cells [142]. Hence, CuAAC is mostly not compatible with live cell experiments [143]. Recently, Sanyal *et al.* reported the formation and characterization of Michael-type thiol-maleimide hydrogels using hepta-thiol-substituted βCD (βCD-SH_7) and linear poly(ethylene glycol)-maleimide (PEG-maleimide) [144]. However, maleimide group deprives topoisomerase II catalytic activity of cells that can lead to cell apoptosis [145] and the presence of unreacted maleimide might create adverse effects on cell viability [145, 146]. In addition, thiol-maleimide gelation proceeds via a nucleophilic

reaction that does not allow one to easily control polymerization kinetics. In this regard, Arslan *et al.* prepared CD-PEG hybrid hydrogels through photo-crosslinking of commercially available βCD-SH_7 and PEG-allylether and the hydrogels were used to deliver hydrophobic puerarin [147]. This hydrogel crosslinking, however, was carried out in an organic condition using dimethylformamide (DMF) as the solvent. As a result, this system was not compatible for *in situ* cell encapsulation.

In the past few years, we and other groups have explored the aqueous-based step-growth thiol-norbornene photo-click chemistry to prepare highly cytocompatible and tunable hydrogels for tissue engineering applications [148]. The gelation of thiol-norbornene hydrogels can be initiated by type I photoinitiator (e.g., Irgacure-2959 or lithium arylphosphinate (LAP)) under long wavelength, low intensity ultraviolet (UV) light irradiation (365 nm, 5–10 mW/cm^2). Thiol-norbornene gelation could also be initiated by visible light (400-700 nm) exposure with type II photoinitiator (e.g., eosin-Y or rose bengal) as the sole photosensitizer [58, 59]. The advantages of step-growth thiol-norbornene photopolymerization include rapid, ambient, and aqueous reaction conditions, as well as spatial-temporal control over gelation kinetics [36, 37, 120]. More importantly, thiol-norbornene hydrogels are highly cytocompatible even for radical-sensitive pancreatic β-cells [52, 149]. In addition to PEG-norbornene, other macromers containing non-homopolymerizable ‘ene’ moieties have been explored for forming step-growth thiol-ene hydrogels. For example, Kloxin and colleagues recently reported an aqueous thiol-allylether reaction to form thiol-ene hydrogel for *in situ* cell encapsulation. The radical-mediated thiol-allylether hydrogel was formed between multi-arm PEG-thiol (PEGSH) and bis-allyloxycarbonyl functionalized peptides [150]. This thiol-allylether gelation produced hydrolytically stable hydrogels that were cytocompatible for encapsulation of human mesenchymal stem cells (hMSCs).

Thiol-ene hydrogels have been exploited as platforms for encapsulating hydrophilic biomolecules, drugs, and cells. Since CDs are capable of increasing the solubility of poorly soluble molecules, a CD-crosslinked thiol-ene hydrogel can potentially be used to encapsulate and to deliver both hydrophilic and hydrophobic biomolecules. Furthermore, CD can be used to form supramolecular association with

selected hydrophobic molecules, such as adamantane. A CD-immobilized hydrogel formed by the aqueous thiol-ene photo-click reaction will not only permit in situ cell encapsulation, but may also allow researchers to create hydrogels with dynamically tunable properties in the presence of cells. As the first step toward achieving this goal, we report here the synthesis and characterization of βCD derivatives, the crosslinking of βCD-PEG hybrid hydrogels via radical-mediated thiol-ene photopolymerizations, the delivery of a model hydrophobic drug, and the cytocompatibility of these step-growth hydrogels. Specifically, a two-step synthesis procedure was developed for functionalizing βCD with the desired number of allylether, which could be used to form hydrolytically stable thiol-allylether photo-click hydrogel. Alternatively, allylether moieties could be further converted to thiols, which could be used to form thiol-norbornene hydrogels. Both thiol-ene gelation systems utilized a low concentration of LAP as the photoinitiator and the gelation was initiated via light exposure at 365 nm. We investigated the gelation kinetics and physical properties of these two types of thiol-ene hydrogels. Curcumin, a hydrophobic molecule with anti-inflammatory and anti-cancer potential, was used as a model drug to demonstrate the enhanced uptake and prolonged release of hydrophobic drug from CD-crosslinked thiol-ene hydrogels. Furthermore, the cytocompatibility of these step-growth CD-crosslinked thiol-ene hydrogels were evaluated via *in situ* encapsulation of radical-sensitive pancreatic MIN6 β-cells.

4.3 Results and Discussion

4.3.1 Preparation and characterization of βCD derivatives

A two-step process was employed to modify βCD with allylether moiety. First, NaH was added at different concentrations to activate hydroxyl groups on βCD (Figure 4.1A, step i). Following the secession of hydrogen gas, excess allyl bromide was added to the reaction mixture (Figure 4.1A, step ii) to afford βCD-AE. ^{1}H NMR results (Figure 4.1B) showed that allylether group was successfully introduced to βCD. Unexpected peaks between 4.1 to 4.3 ppm were likely due to regioisomerism. Peaks of similar intensities (i.e., 3.8 or 4.6 ppm) were likely due to the shifting of protons on βCD due to varied combinations of allylether positions. The modification was confirmed by mass spectroscopy analysis. The difference of the average molecular mass of βCD-AE and βCD was divided by the molecular mass of allylether (i.e., 40 Da) to estimate the degree of allylether functionalization. As the concentration of NaH or allylbromide to βCD was increased (from 0 to 11.3-fold, Figure 4.2), so was the detected mass of the modified βCD and the estimated degree of substitution (0, 1.5, 2.4 and 4.5, respectively). To obtain thiol-substituted βCD, βCD-AE was first photoconjugated with thioacetic acid via radical-mediated thiol-allylether addition (Figure 4.1A, step iii). The intermediate product, βCD-thioacetate, was hydrolyzed with sodium hydroxide, neutralized with hydrochloric acid, and purified via dialysis to obtain the final product, βCD-SH (Figure 4.1A, step iv). ^{1}H NMR results confirmed that allylether was replaced with thiol group (Figure 4.1B, bottom panel). The presence of thiol on modified βCD was further quantified by Ellman's assay (Figure 4.3). As the concentration of βCD-SH was increased from 0.02 to 1 mg/mL, the concentration of thiol detected increased linearly ($R^2 = 0.99$) from 0.006 ± 0.001 to 0.362 ± 0.005 mM. As expected, no thiol was detected from unmodified βCD or βCD-AE.

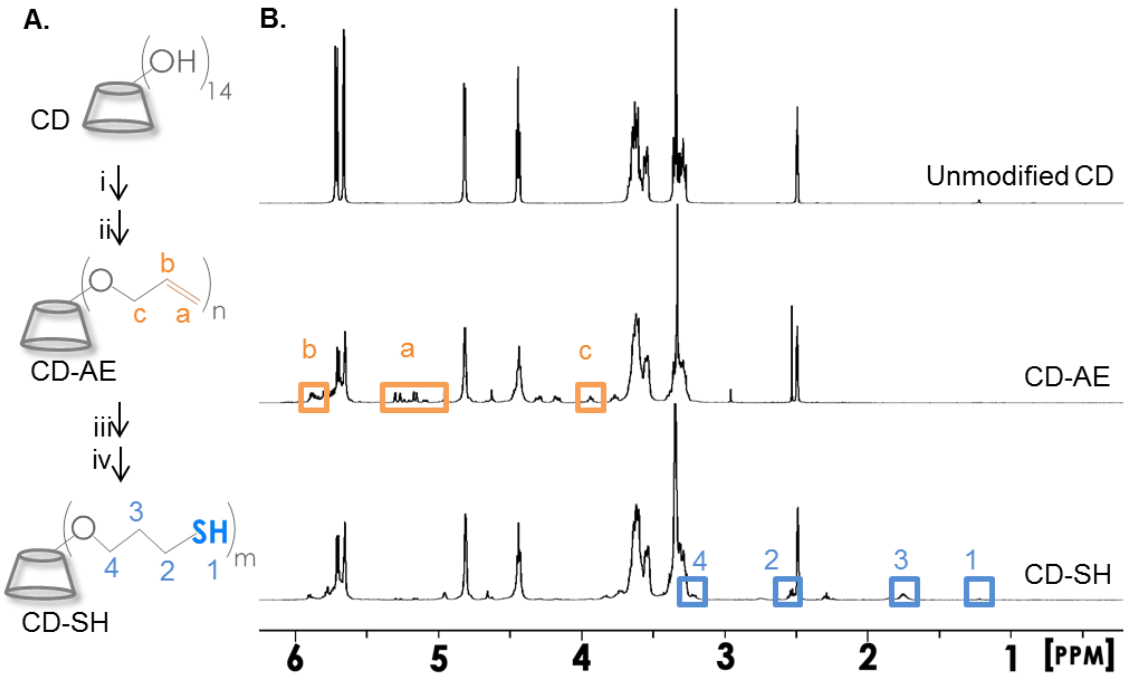

Figure 4.1. (A) Schematics of βCD modifications. (i) NaH, DMF, room temperature; (ii) allylbromide, DMF, room temperature; (iii) thioacetic acid, I-2959, UV (365 nm, 10 mW/cm^2), 30 min; (iv) sodium hydroxide (aq.), followed by neutralization with hydrogen chloride. ^{1}H NMR of (B) βCD, (C) βCD-AE, and (D) βCD-SH (dissolved in $(CD_3)_2SO$).

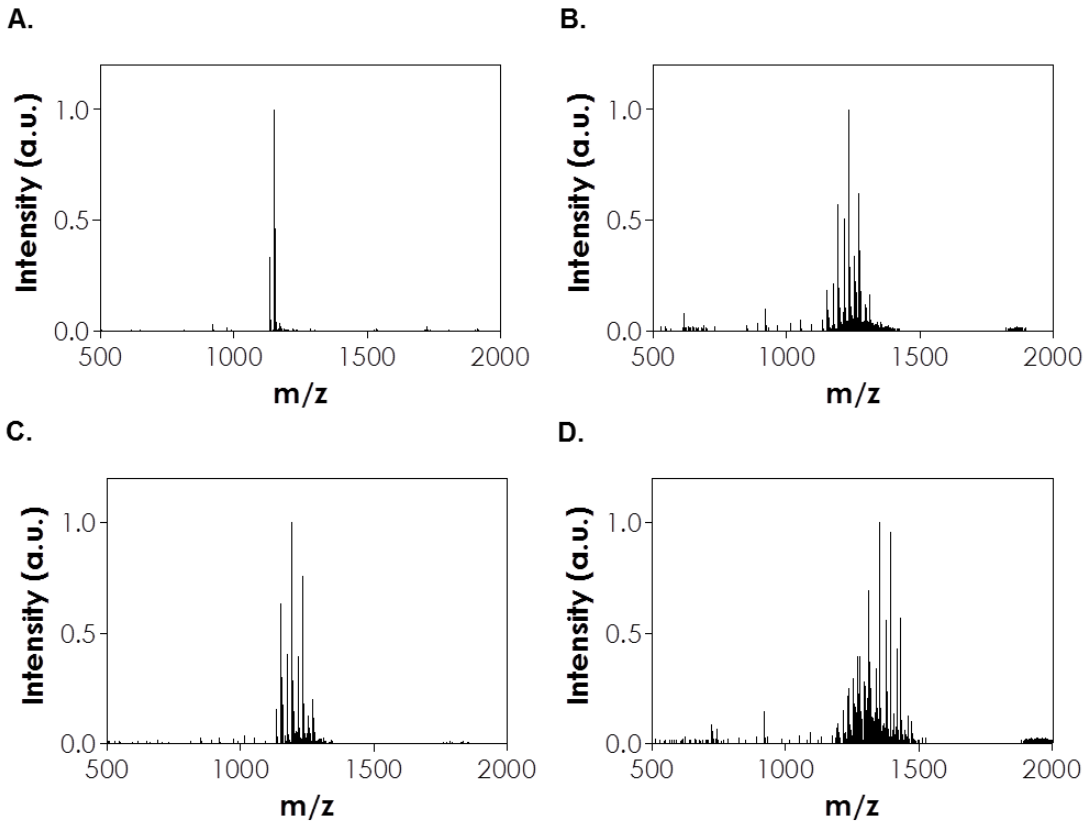

Figure 4.2. Mass spectroscopy of CD derivatives. (A) Mass-to-charge (m/z) for un-modified βCD (B-D) βCD-AE with increasing feed ratio of NaH and allylbromide (B: 2.3-, C: 4.5-, and D: 11.3-fold).

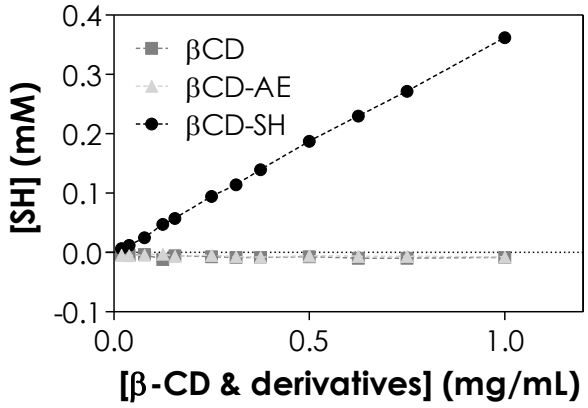

Figure 4.3. Thiol-content on βCD, βCD-AE, and βCD-SH measured by Ellman's assay.

4.3.2 Preparation of thiol-ene photo-click hydrogels

We next demonstrated the crosslinking of CD-PEG hybrid hydrogels using PEG8SH (M.W. 20 kDa) and βCD-AE through a radical-mediated thiol-allylether photo-click reaction (Figure 4.4) and the gelation was evaluated via *in situ* photorheometry (Figure 4.4B, 4.5). Specifically, 5 wt% of PEG8SH was cross-linked with different concentrations of βCD-AE (9 to 24 mg/mL). The gel points of all formulations evaluated were similar regardless of βCD-AE concentration in the precursor solution (gel point ~ 17 to 22 seconds, Figure 4.5). However, the formulation afforded the highest elastic modulus (~2.5 kPa at 300 second) at 24 mg/mL of βCD-AE (Figure 4.4B). Further increasing βCD-AE concentration did not yield higher gel modulus (data not shown). Controlled experiment using unmodified βCD with PEG8SH showed no sign of gelation even after 300 seconds of light exposure in the presence of photoinitiator (Figure 4.4C), suggesting that the gelation was not due to disulfide bond formation. Since 24 mg/mL of βCD-AE yielded the highest shear modulus of thiol-allylether hydrogel, we examined the gelation of thiol-norbornene hydrogel (Figure 4.4D) using this concentration (24 mg/mL) of thiol-substituted βCD (i.e., βCD-SH) and 5 wt% of 8-arm PEG-norbornene (PEG8NB, M.W. 20 kDa). Even with slightly lower degree of functionalization (~85 % on PEG8NB), the gelation of βCD-SH with PEG8NB still afforded a 5-fold faster gel point (Figure 4.4E, gel point ~3 seconds). However, the final shear modulus of thiol-norbornene hydrogel formed with βCD-SH and PEG8NB only reached about 1.1 kPa (Figure 4.4E). Control experiment showed that gelation was not possible when unmodified βCD was mixed with PEG8NB (Figure 4.4F) and subjected to the same radical-initiation conditions, indicative of the lack of either PEG8NB homopolymerization or gelation due to supramolecular assembly (or threading) between multi-arm PEG and βCD.

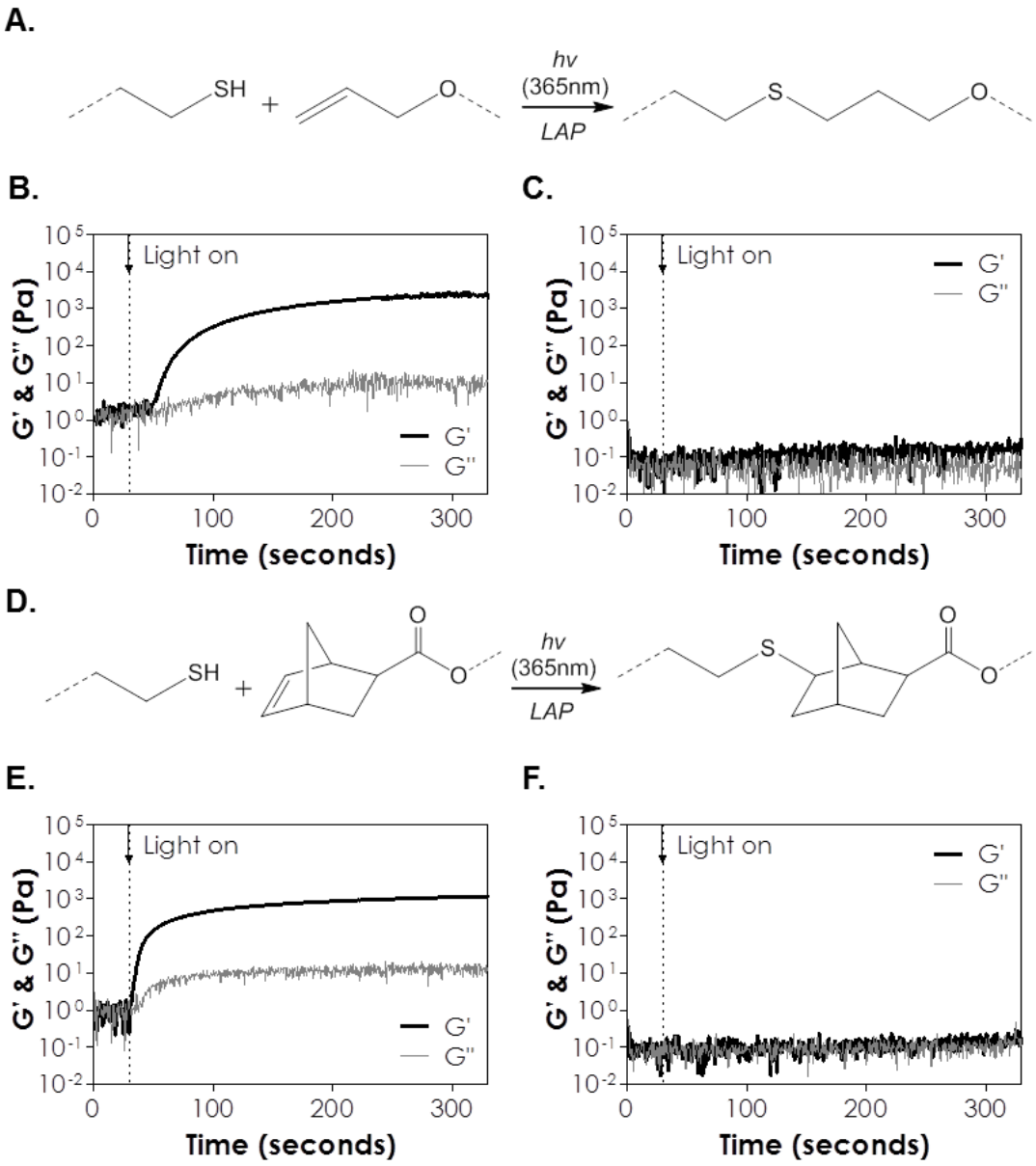

Figure 4.4. (A) Scheme of light and radical mediated thiol-allylether gelation. (B) *In situ* photorheometry of thiol-allylether photopolymerization (G': storage modulus; G": loss modulus) between PEG8SH and βCD-AE. (C) *In situ* photorheometry of solution containing PEG8SH and βCD. (D) Scheme of light and radical mediated thiol-norbornene gelation. (E) *In situ* photorheometry of thiol-norbornene photopolymerization PEG8NB and βCD-SH. (F) *In situ* photorheometry of solution containing PEG8NB and βCD (5 wt% PEG8SH or PEG8NB, 24 mg/mL of βCD-AE or βCD-SH, 1 mM LAP). Light (365 nm, 10 mW/cm^2) was turned on at 30 seconds (dotted line). N = 3, error bars were omitted for clarity.

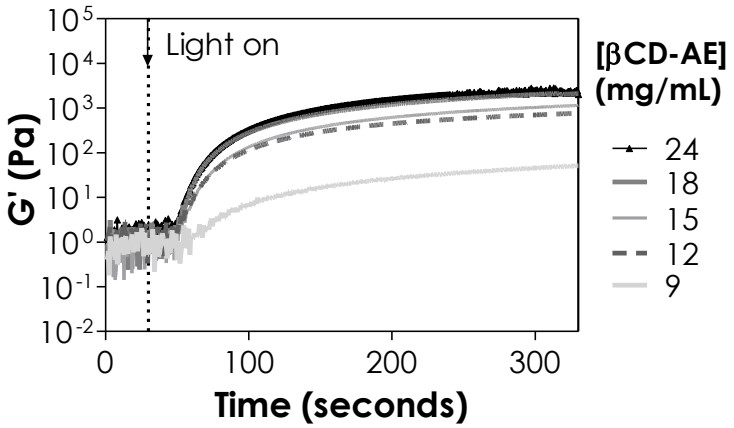

Figure 4.5. *In situ* photorheometry showing the evolution of storage modulus (G') and loss modulus (G") of thiol-allylether photopolymerization at 5 wt% PEG8SH and various CD-AE concentration in the precursor solution (1 mM LAP, 365nm light at 10 mW/cm^2). Light was turned on at 30 seconds (dotted line). N = 3, error bars were omitted for clarity.

The fast thiol-ene gelation using macromers functionalized with norbornene, a strained ene, is well-documented in the literature. For example, we have shown that PEG-peptide thiol-norbornene gelation could be achieved rapidly (gel point ~ 2-3 seconds) using low PEGNB and photoinitiator concentrations (e.g., 4 wt% PEG4NB$_{20kDa}$ with DTT or bis-cysteine peptides and 1 mM LAP) [62]. On the other hand, Kloxin and colleague designed a radical-mediated (1.1 mM of LAP) thiol-allylether hydrogel system using 10 wt% of PEG4SH (M.W. 20 kDa) with alloc-functionalized peptides and obtained a gel point of about 15 seconds [150]. While both allylether and norbornene react with thiol via a strictly step-growth mechanism (i.e., no homopolymerization between the ene groups) [151], the polymerization rate of thiol-norbornene is six times faster than that of thiol-allylether due to the unity ratio of thiyl radical propagation to chain transfer kinetic parameters (k_{pSC} /k_{CT}) [151]. It is worth noting that, while thiol-norbornene gelation was one order of magnitude faster than thiol-allylether gelation, the final gel shear modulus of the former was only about half of the latter. This could be explained by the fact that PEG8NB, which was synthesized in house, was lower in the degree of functionalization (85%, per 1H NMR) as compared with commercially acquired PEG8SH (>95%, per manufacturer's certificate of analysis, respectively).

Furthermore, since βCD-SH was modified from βCD-AE, it would make sense that gels crosslinked by βCD-SH would have a lower degree of crosslinking, and hence lower shear modulus, as compared with gels crosslinked by βCD-AE.

CD has been shown to assist the assembly of physical 'pseudo-polyrotaxane' hydrogel through interactions with PEG or block co-polymers of polypropylene oxide (PPO) and polyethylene oxide (PEO) (e.g., Pluronic). Previously, Cooper-White and colleagues reported supramolecular gelation of αCD with Pluronic co-polymers and concluded that the 'threading' induced gelation would only occur in the presence of 'poly-CD' aggregates, which was only apparent at a sufficiently high concentration of CD (at least 50-70 mg/mL) [152]. The gelation in the work presented here was purely based on thiol-ene photochemistry since the CD concentrations used in this study were less than 40 mg/mL and the fact that no gelation was observed by simply mixing unmodified βCD with PEGNB (Figure 4.4C). Another relevant work reported by Elisseeff and colleagues showed a tunable CD/PEG hybrid hydrogel crosslinked by chain-growth photopolymerization. It is worth noting that the functionalized βCD motifs were 'threaded' onto PEG-diacrylate after overnight incubation[153]. We believe that the threading of CD to PEG chains was minimal, if any, since we added βCD into the mixture right before photopolymerization in all experiments. Another potential complication is the formation of LAP/βCD complex. We performed isocratic HPLC using acetonitrile/phosphate buffer (35/65) containing βCD (0 to 10 mM) as the mobile phase. While the elution of LAP shifted slightly (Figure 4.6A), the elution time of injected LAP (0.1 mM) was not significantly different from each other regardless of βCD concentration (Figure 4.6B). Since the gelation was accomplished within 5 minutes, it is unlikely that the association between LAP and βCD, if any, would impede light-induced initiator breakdown and gelation. Furthermore, the potential association would also decrease after the photoinitiators were broken down into fragments upon light irradiation.

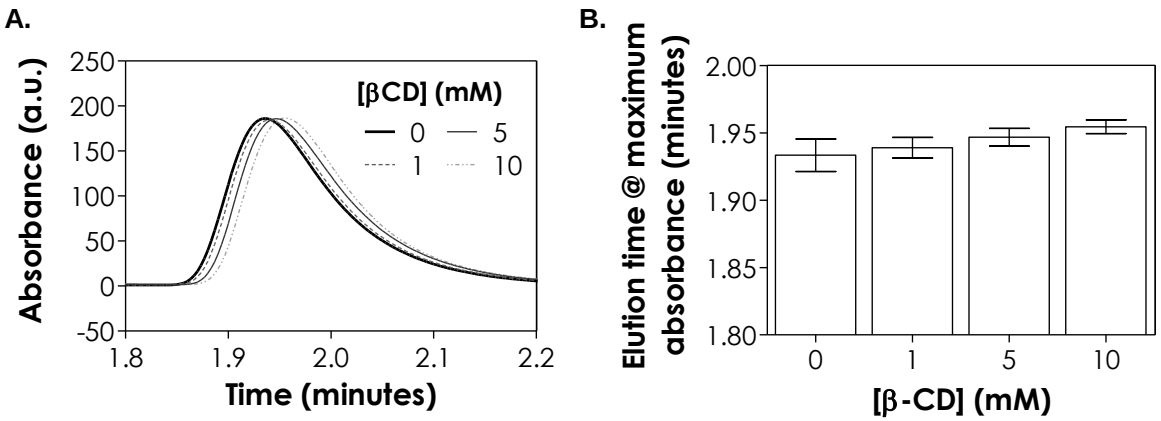

Figure 4.6. Evaluation of potential LAP/CD complex formation using reverse-phase HPLC. (A) 0.1mM LAP was injected into C18 analytical column using acetonitrile/phosphate buffer (35/65) as the mobile phase. The mobile phase also contained different concentrations of βCD as indicated. Absorbance was measured at 280 nm. N = 3, error bars were omitted for clarity. (B) Elution time corresponds to maximum absorbance of LAP. (Mean ± SD, N = 3)

4.3.3 Effects of macromer functionality and molecular weight on gelation kinetics

Since thiol-norbornene reaction exhibits faster gelation kinetics than thiol-allylether reaction, we evaluated the effects of PEGNB macromer functionality and molecular weight on the gelation of CD-based thiol-norbornene hydrogels (Figure 4.7). PEG4NB (M.W. 20 kDa, Figure 4.7A) and PEG8NB (M.W. 40 kDa, Figure 4.7B) were selected as these two macromers provided the same total concentration of norbornene at the same weight percentage (i.e., 10 mM at 5 wt%). Note that the molar ratio of norbornene to thiol was maintained at one, whereas the concentration of thiol from βCD-SH was determined by Ellman's assay (Figure 4.3). Since the average molecular weight per arm in these two macromers was the same (i.e., 5 kDa), the average molecular weight between crosslinks ($\overline{M_c}$) of the two was also the same (Eq. 3). This implied that the two sets of hydrogels would have the same ideal crosslinking efficiency (Eq. 4). Experimentally, however, we found that thiol-norbornene hydrogels cross-linked by PEG4NB (20 kDa) had a slightly slower gel point (~6 seconds) and a lower shear modulus (~1 kPa) when

compared with gels crosslinked by PEG8NB (40 kDa) (~4 seconds and ~3 kPa). These results was consistent with the trend found in previously reported step-growth Michael-type hydrogels [154]. Theoretically, step-growth hydrogels with the same $\overline{M_c}$ (Eq. 3) should have identical mesh size (Eq. 4) regardless of the macromer concentration. Experimentally, however, macromer with lower functionality formed hydrogel with higher swelling ratio compared with macromer with higher functionality [62, 63]. The phenomenon was attributed to network defects and inefficient cross-linking at lower macromer functionality. We also compared gelation kinetics of CD-based thiol-norbornene hydrogels using macromer PEG8NB with different molecular weight (Figure 4.7B & 4.7C). The gel point of hydrogel cross-linked by 20 kDa PEG8NB was 2.2–fold faster, and the elastic modulus was 1.5–fold higher, than the gels cross-linked by 40 kDa PEG8NB. These results were also expected because of the higher molarity of norbornene groups on 20 kDa PEG8NB at equivalent polymer weight content.

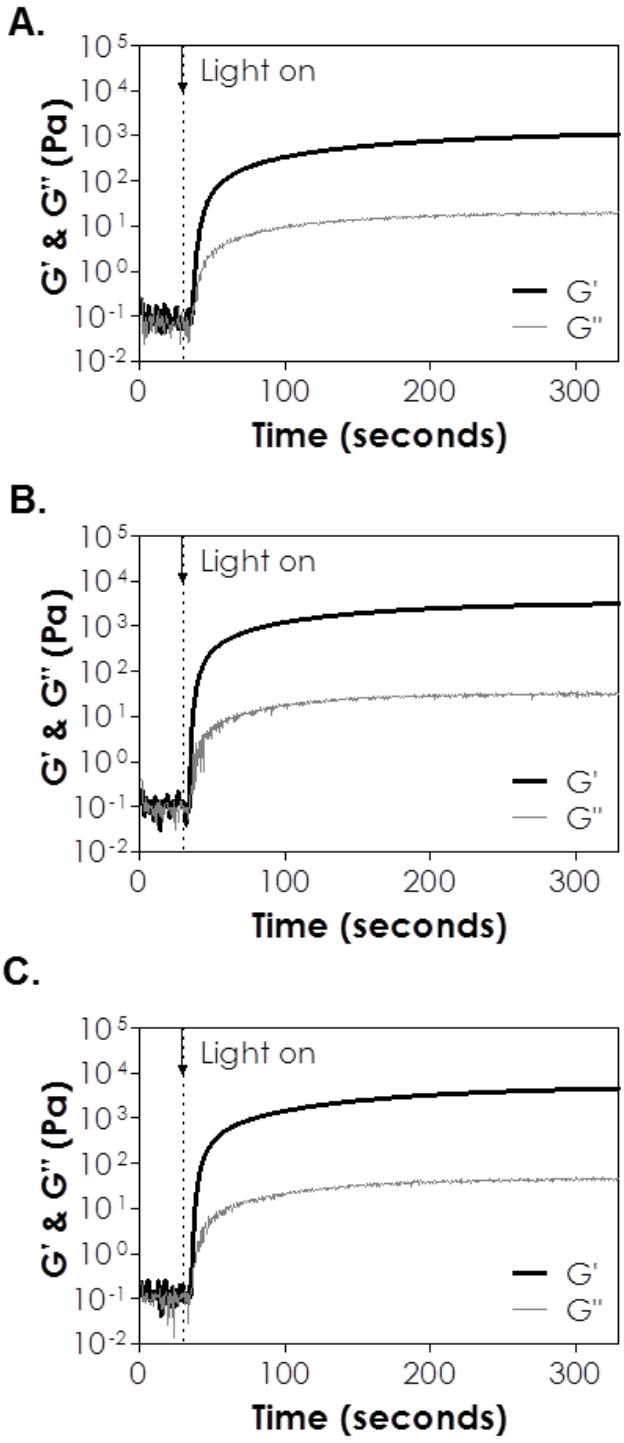

Figure 4.7. *In situ* photorheometry of thiol-ene hydrogels crosslinked by βCD-SH and (A) PEG4NB (20 kDa), (B) PEG8NB (40 kDa) or (C) PEG8NB (20 kDa). (5 wt% PEGNB, [thiol] = [norbornene], 1 mM LAP). Light (365 nm, 10 mW/cm^2) was turned on at 30 seconds (dotted line). N = 3, error bars were omitted for clarity.

4.3.4 Effects of cross-linker on hydrogel properties

After examining the effect of CD-PEG macromer formulations on gelation, we evaluated the influence of crosslinker on the physical properties of selective groups of thiol-norbornene hydrogels. Three sets of macromers were used: (1) DTT with PEG4NB (labelled as DTT in Figure 4.8), (2) βCD-SH with PEG4NB (labelled as CD-SH), and (3) PEG4SH with βCD-AE (labelled as CD-AE). As shown in Figure 4.8A, the gel fraction was not significantly different between the three groups (86 ± 3 %, 79 ± 8 %, and 74 ± 6 % for DTT, CD-SH, and CD-AE gel, respectively). However, the DTT gel exhibited the highest equilibrium shear modulus when compared with gels crosslinked with CD-SH or CD-AE (Figure 4.8B, ~7.1, 3.4, and 2.4 kPa for DTT, CD-SH and CD-AE gel, respectively). The differences in equilibrium shear moduli reflected the variation in network crosslinking density, which was affected by the types of thiol (i.e., DTT, CD-SH, or PEG4SH) and ene (i.e., norbornene or allylether) used in the formulations [62]. The lowest crosslinked CD-AE gels also had highest swelling ratio among the three groups (Figure 4.8D). Interestingly, even though the modulus of DTT gel was higher than that of CD-SH gel (Figure 4.8B & 4.8C), the swelling ratio of DTT gel was also 2-fold higher than that of CD-SH gel (Figure 4.8D). This result was contradictory to the inverse scaling of modulus and swelling ratio in chemically crosslinked hydrogels. A significantly lower swelling ratio for CD-SH gel might be a result of higher CD-SH concentration and mass (48 mg/mL) required for this formulation. As a comparison, the concentration of DTT used was only 1.5 mg/mL. Inclusion of higher content of amphiphilic CD in the gel formulations might profoundly impact the ability of these gels to imbibe water.

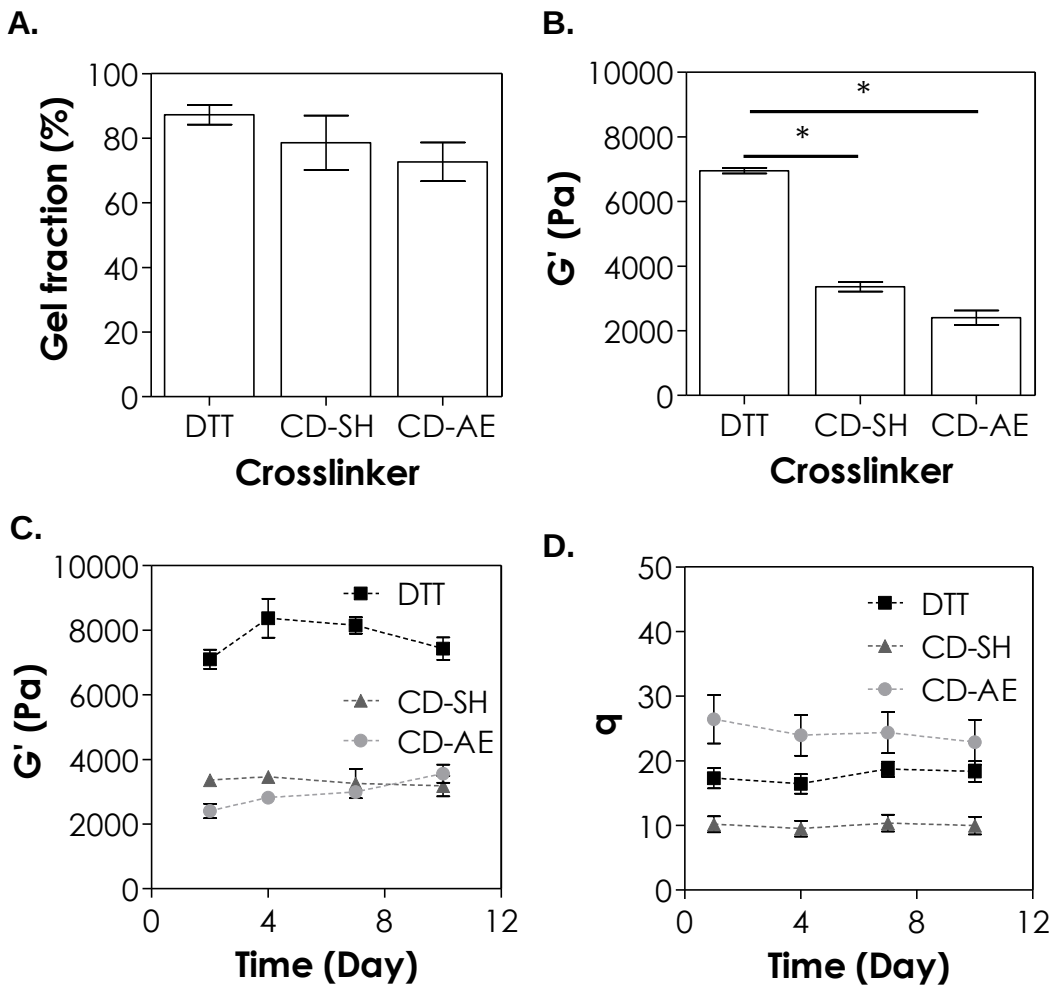

Figure 4.8. Effect of crosslinker on (A) gel fraction, (B) elastic modulus at equilibrium gel swelling, (C) shear modulus as a function of time, and (D) swelling ratio as a function of time. Asterisks indicate statistical significance ($p < 0.05$, 5 wt% 20 kDa PEG8SH or PEG8NB, 1 mM LAP, 365 nm light, intensity at 5 mW/cm^2, mean ± SD, N = 3).

The step-growth thiol-norbornene hydrogels were known to degrade hydrolytically if ester bonds were presence in the PEGNB macromers [62]. We evaluated the hydrolytic stability of the three groups of thiol-ene hydrogels (i.e., DTT, CD-SH, and CD-AE gel). The hydrolytic degradation of these thiol-ene hydrogels in neutral buffer solution (pH 7.4) was not significant as the modulus and swelling ratio remained relatively stable over 10 days (Figure 4.8C & 4.8D). We reason that this was because these gels were either highly crosslinked (G' ~7.1

kPa and 3.4 kPa for DTT and CD-SH gel, respectively) or contained no hydrolytically labile bonds (e.g., CD-AE thiol-allylether gel). We also conducted an accelerated hydrolysis study (Figure 4.9) by incubating these hydrogels in basic buffer (pH 9). As expected, a decline in G' over time was observed for DTT and CD-SH gels (both crosslinked with PEG4NB), indicative of base-catalysed hydrolysis of ester bonds in PEG4NB macromer (Figure 4.9). On the other hand, CD-AE gel remained intact over time (i.e., constant G') since thiol-allylether hydrogels did not contain hydrolytic degradable moieties.

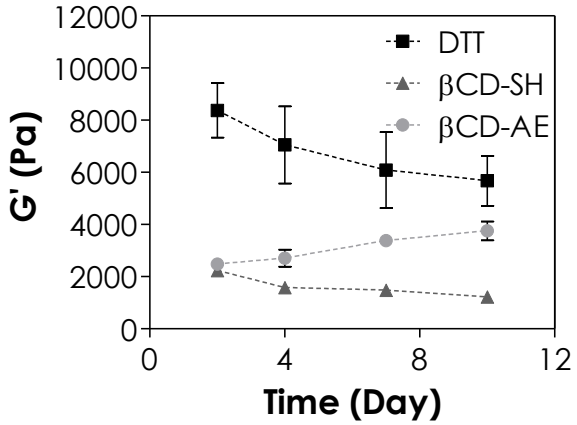

Figure 4.9. Effect of crosslinker on shear modulus as a function of time in pH 9 PBS. (5 wt% 20 kDa PEG8SH or PEG8NB, 1 mM LAP, 365 nm light, intensity at 5 mW/cm^2, mean ± SD, N = 3).

4.3.5 Uptake and release of hydrophobic curcumin from thiol-allylether hydrogels

One potential application of the CD-PEG hydrogel system is to deliver hydrophobic drugs. Many anti-inflammatory drugs, such as curcumin [155], are hydrophobic and hence have lower bioavailability *in vivo*. Curcumin has also been a subject of intensive research interest in diabetes because of its blood glucose lowering effect [156]. Since thiol-norbornene hydrogels would be hydrolyzed in basic buffer [62], we chose thiol-allylether hydrogels crosslinked by CD-AE and PEG4SH as a model gel system to demonstrate the enhanced uptake and sustained release effect of curcumin from

CD-PEG hybrid hydrogels. Pure PEG hydrogels crosslinked by PEGAE and PEG4SH under the same gelation conditions were used as control. The two sets of gels (labeled as PEGAE and CD-AE in Figure 4.10) were incubated in ddH_2O suspended with hydrophobic curcumin for 8 hours. As shown in the top panel of Figure 4.10A, hydrogels crosslinked with CD-AE appeared more yellowish when compared to hydrogels crosslinked with PEGAE, indicative of higher amount of curcumin (yellow in color) uptake due to the presence of chemically crosslinked CD in the gel. Subsequently, these gels were immersed in DMSO to completely liberate the curcumin. As shown in the bottom panel of Figure 4.10A, both sets of gels appear transparent and identical, indicating that all curcumin were released from the gels. The liberated curcumin was quantified via UV/vis absorbance measurement (Figure 4.10B). Compared to pure PEG hydrogels crosslinked with PEGAE and PEG4SH, hydrogels crosslinked with CD-AE were capable of loading twice as much curcumin (~9 and ~20 μg/gel for PEGAE and CD-AE gel, respectively).

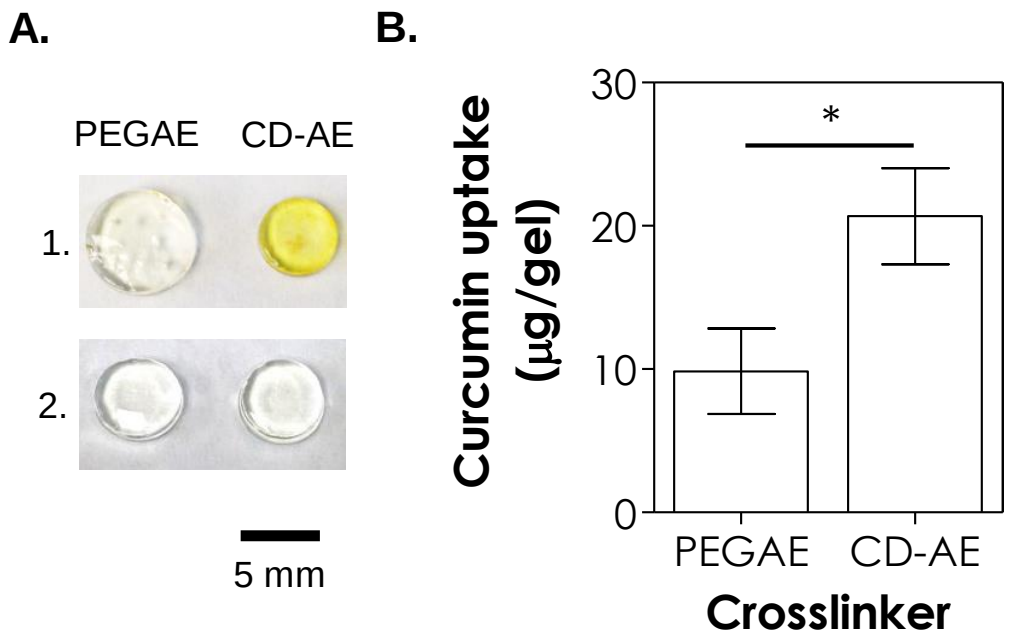

Figure 4.10. (A) Photographs of thiol-allylether hydrogels incubated in curcumin suspended ddH_2O for 8 hours (top) and after DMSO-treatment (bottom). (B) Curcumin uptake in hydrogels formed by 5 wt% PEG8SH with 3.4 kDa of PEGAE or 24 mg/mL βCD-AE (1 mM LAP, 365 nm light at 10 mW/cm^2).

Because the amount of curcumin loading in the control PEGAE gel was much lower than that in the CD-AE gel, it would be difficult to compare the release of curcumin from these two sets of gels. In order to form complex with βCD, Yadav *et al* employed the pH shifting method to solubilize curcumin in an alkaline solution with βCD [157]. Therefore, we believe that the alkaline condition did not affect the association of βCD and curcumin.To demonstrate the sustained delivery of curcumin from CD-crosslinked hydrogels, we performed drug-loading in alkaline curcumin solution for 36 hours (curcumin was dissolved in 0.5 N NaOH first, followed by diluting with pH 7.4 PBS). Prior to drug loading the two sets of gels were equally transparent (Figure 4.11A, panel 1). After drug loading (Figure 4.11A, panel 2), the two sets of thiol-allylether hydrogels were equally opaque, suggestive of similar curcumin intake. The similar amount of curcumin absorbed in the gels were quantified by DMSO treatment as described earlier (Figure 4.11B, 6.6 ± 1.1 and 6.9 ± 0.4 μg/gel for PEGAE and CD-AE gel, respectively). The gels were then incubated in buffer solution for curcumin release. Significantly more curcumin was released from hydrogels crosslinked by PEGAE than by CD-AE (Figure 4.11C, 85 % and 42 % of curcumin was released from PEGAE and CD-AE hydrogels after 10 hours, respectively). Over the course of first 100 hours, a 1.8-fold higher amount of curcumin was released from PEGAE-crosslinked gels than from CD-AE crosslinked gels (Figure 4.11C, 87 % and 49 %, respectively\). After the release study, CD-AE gel appeared slightly darker than PEGAE gel (Figure 4.11A, panel 3), suggesting that a higher amount of curcumin was still retained in this gel. However, after DMSO treatment for an additional 100 hours, the remaining curcumin were completely released from both sets of hydrogels (Figure 4.11C) and the appearances of the gels were similar in color (Figure 4.11A, panel 4).

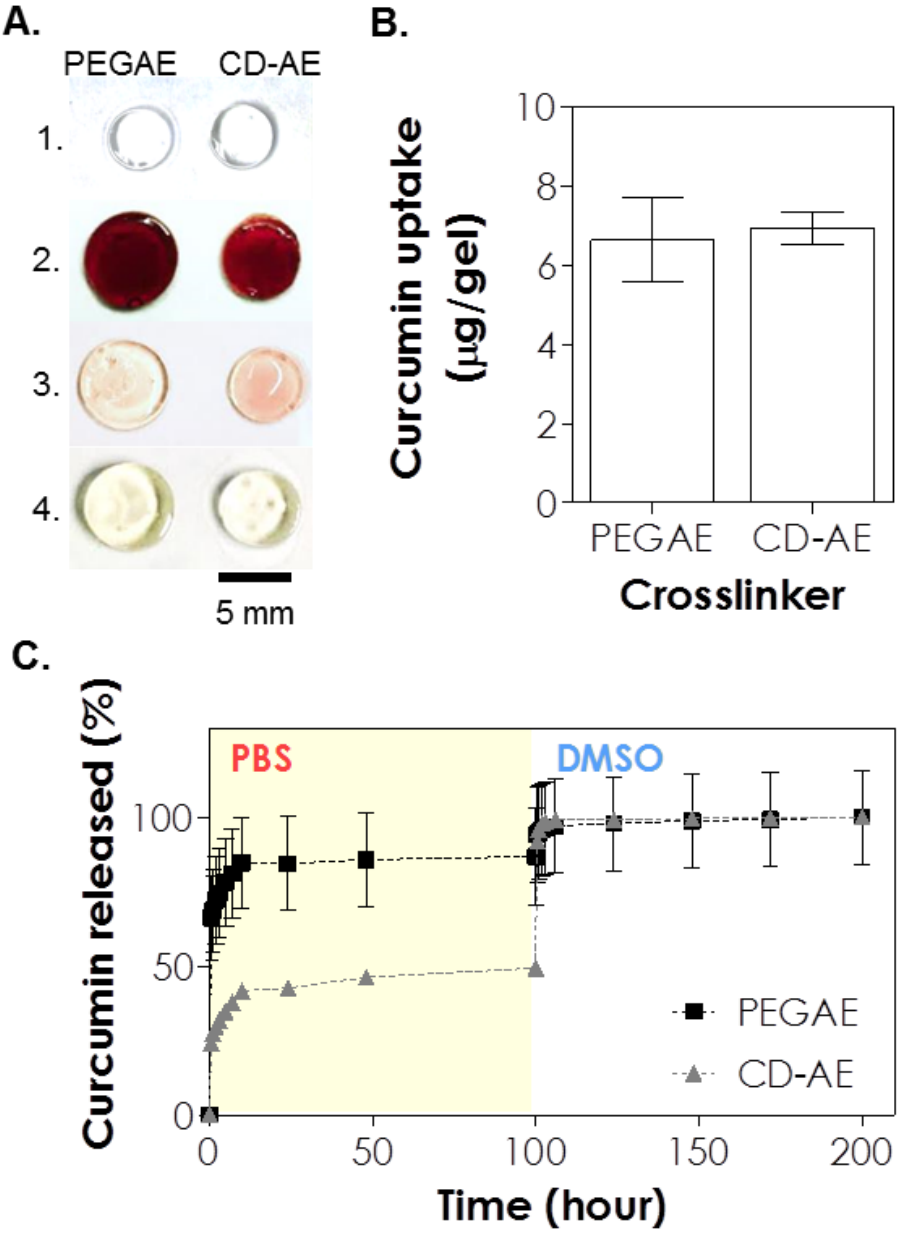

Figure 4.11. (A) Photographs of thiol-allylether hydrogels: (1) immediately after photopolymerization, (2) after incubating in curcumin solution for 36 hours, (3) after 100 hours of release in pH 7.4 PBS, and (4) after an additional 100 hours of release in DMSO (scale: 5 mm). (B) Effect of crosslinker on curcumin uptake in the gel. (C) Curcumin release from thiol-allylether hydrogel formed by 5 wt% PEG8SH with 3.4 kDa of PEGAE or 24 mg/mL βCD-AE (1 mM LAP, 365 nm light at 10 mW/cm^2).

The increase of curcumin solubility via guest-host interactions with CD is well documented [158-160]. In our study, CD-AE was employed as both a hydrogel crosslinker and a carrier for hydrophobic drug (i.e., curcumin). Compared to thiol-allylether hydrogels crosslinked by PEGAE, gels crosslinked by CD-AE accommodated significantly more curcumin due to the formation of inclusion complex. The presence of CD/curcumin inclusion complex also resulted in delayed/sustained release of curcumin from the CD-AE hydrogel. Since all curcumin absorbed in the gel could be liberated by DMSO, we believe that the retention of curcumin was purely due to inclusion complex formation but not Michael-type reaction occurred between curcumin and nucleophilic thiols in the gels [161],[162] . For the purpose of proof-of-concept, current study only demonstrated post-loading of curcumin by CD/PEG hydrogels. Future study will focus on pre-complexing functionalized CD with curcumin, which can be used as crosslinker to simultaneously encapsulate drugs and cells in a single reaction.

4.3.6 Cytocompatibility of CD-crosslinked thiol-ene hydrogels

Next, we evaluated the cytocompatibility of CD-crosslinked thiol-ene hydrogels using *in situ* encapsulation of pancreatic MIN6 β-cells at a relatively low cell density (2×10^6 cells/mL) [149]. Thiol-norbornene hydrogels crosslinked by DTT and PEG8NB (M.W. 20 kDa) were used as a control group as similar gelation formulation has been shown to be cytocompatible for radical-sensitive MIN6 β-cells [52]. One day after cell encapsulation, live/dead staining was performed and the results show that thiol-norbornene hydrogels crosslinked by CD-SH were highly cytocompatible for MIN6 cells (Figure 4.12A, ~83 % live cells), while hydrogels crosslinked by DTT or by CD-AE contained slightly more dead cells (Figure 4.12A, ~72 % and 73 % live cells for gels crosslinked by DTT and CD-AE, respectively). Regardless of the cross-linker used, MIN6 β-cells formed spherical aggregates in all hydrogels 10 days after cell encapsulation (Figure 4.12A, right panel). The average diameters of the spheroids were about 18 μm, 26 μm, and 32 μm for hydrogels crosslinked by DTT, CD-SH and CD-AE, respectively. We also quantified cell metabolic activity using CellTiter-Glo® (for

measuring intracellular ATP content) and AlamarBlue® regent (for measuring cell metabolic activity). In DTT or CD-AE crosslinked hydrogels, the intracellular ATP content increased from ~13 to 200 pmol of ATP per sample (Figure 4.13) from day 1 to day 10. The difference between DTT and CD-AE crosslinked hydrogels was not significantly on either day 1 or day 10. On the other hand, the amount of ATP increased from ~70 to 390 pmol per sample in hydrogels crosslinked by CD-SH (Figure 4.13). The increased in intracellular ATP was most likely due to the cell proliferation and the formation of multi-cell aggregates. Cell proliferation in CD-PEG hydrogels was verified by Alamarblue® reagent assay (Figure 4.12B) and the trends were consistent with live/dead staining and ATP assay.

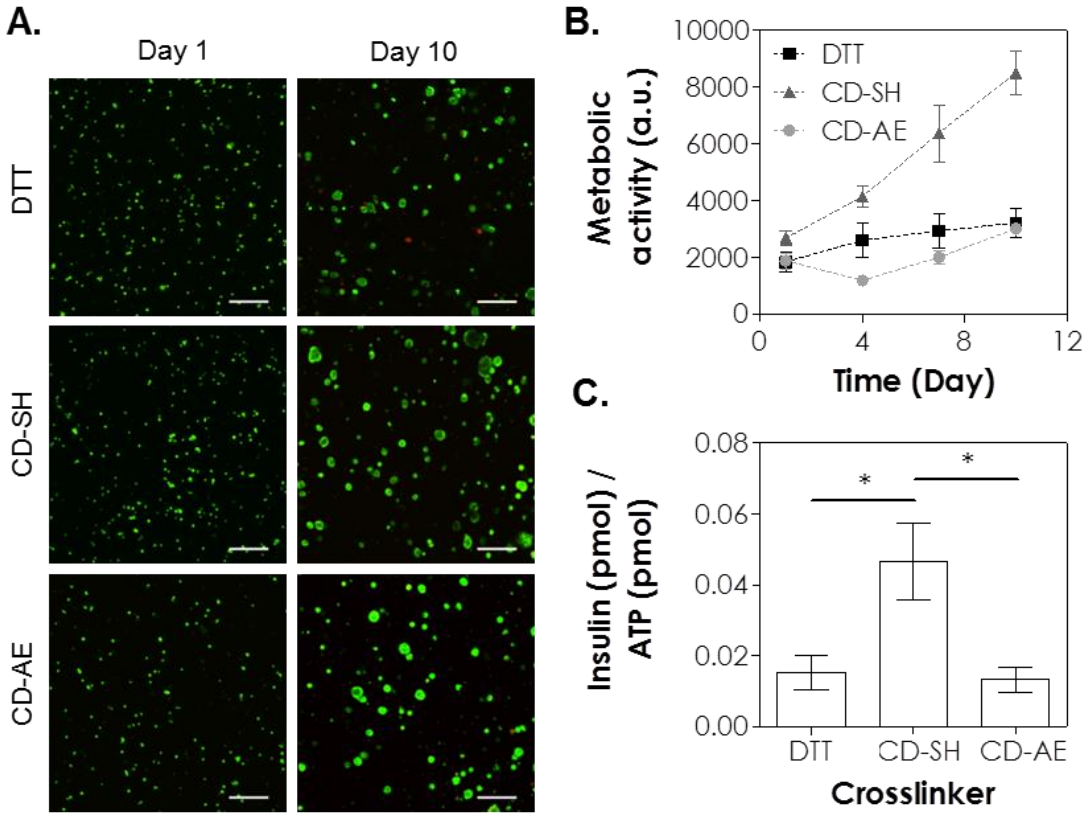

Figure 4.12. Effect of crosslinker on the cytocompatibility of thiol-ene hydrogels on MIN6 β-cells. (A) Representative confocal z-stack images of MIN6 cells stained with live/dead staining kit on day 1 and day 10. MIN6 cells were encapsulated (2×10^6 cells/mL) in thiol-ene hydrogels crosslinked by DTT, CD-SH or CD-AE. (B) Cells viability as assessed by Alamarblue® reagent. (C) Normalized insulin secretion. All gel formulations contained 5 wt% 20 kDa PEG8SH or PEG8NB, 1 mM LAP, and 365 nm light at 5 mW/cm^2 (Scales: 100 μm).

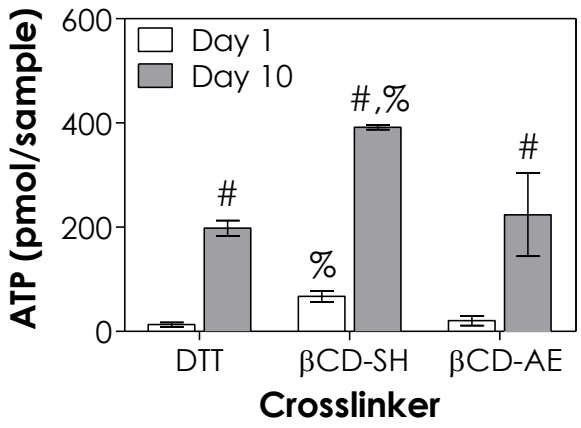

Figure 4.13. Effect of crosslinker on the intracellular ATP content of MIN6 β-cells encapsulated in thiol-ene hydrogels. ATP contents were measured by CellTiter-Glo® reagent (mean ± SD, N = 3). All gel formulations contained 5 wt% 20kDa PEG8SH or PEG8NB, 1 mM LAP, and 365nm light at 5 mW/cm^2.

Studies have shown that softer matrix and hydrolytic gel degradation promoted the phenotype, function, and proliferation of MIN6 βcells in 3D [52, 163]. The thiol-norbornene hydrogels in the current study were slightly stiffer (Figure 4.8B) and relatively stable at pH 7.4 over the course of 10 days (Figure 4.8C & 4.8D). Consistent with our published work using PEG-based thiol-norbornene hydrogels [62], the hydrolysis rate of CD-PEG hybrid hydrogels could be accelerated under basic condition (e.g., pH 9, Figure 4.9). On the other hand, thiol-allylether hydrogels remained hydrolytically stable (Figure 4.9). Therefore, compared to CD-SH crosslinked hydrogels, the slightly higher initial cell death (Figure 4.12A to 4.12C) in DTT-crosslinked hydrogels might be a result of higher gel stiffness. When we replaced PEG8NB with PEG4NB without changing macromer molecular weight (20 kDa) or content (5 wt%), the modulus of the hydrogels decreased by half (Figure 4.14, 3.1 kPa and 1.2 kPa for DTT and CD-SH cross-linked gels, respectively). Additional cell encapsulation studies using these softer gels showed improved viability of encapsulated MIN6 cells (Figure 4.15, top panel, >98 % viable cells). In addition to gel stiffness, the presence of active radicals could induce cellular damage during photo-encapsulation [164]. While thiol-allylether hydrogels crosslinked by CD-AE were softer than thiol-norbornene hydrogel crosslinked

by DTT (Figure 4.8B, ~2.4 kPa and 7.1 kPa for CD-AE and DTT gel, respectively), the viability of MIN6 cells was not much higher (Figure 4.12). We reason that the radical-sensitive MIN6 cells were exposed to active radicals for a longer time during the thiol-allylether gelation because of a much lower chain transfer kinetic constant, and hence the benefits of a softer gel on cell viability was offset by longer exposure of the cells to radical species.

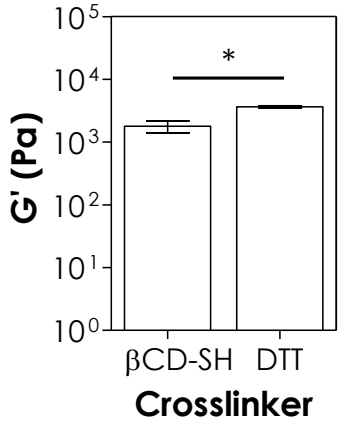

Figure 4.14. Effect of crosslinker on elastic modulus at equilibrium swelling. Asterisk indicates statistical significant between crosslinker βCD-SH and DTT, $R < 0.05$. (5 wt% $PEG4NB_{20kDa}$, [thiol] = [norbornene] = 10 mM, 1 mM LAP, light intensity at 10 mW/cm^2, mean ± SD, N = 3)

Finally, we evaluated function of encapsulated cells with static glucose stimulated insulin secretion (GSIS, Figure 4.12C). Since the viability of MIN6 cells varied among different conditions, the amount of insulin was normalized to the amount of intracellular ATP, which scales with cell number at day 10. Compared with thiol-ene hydrogels crosslinked by DTT or CD-AE, the secretion of insulin by MIN6 cells encapsulated in thiol-ene hydrogel crosslinked by CD-SH was about 3-fold higher than thiol-ene hydrogel crosslinked by DTT and CD-AE (Figure 4.12C, about 0.04 CD-SH, and 0.01 for DTT and βCD-AE). This functional assay result also concurs with the notion that softer gel matrix promotes phenotype of insulin secreting cells.

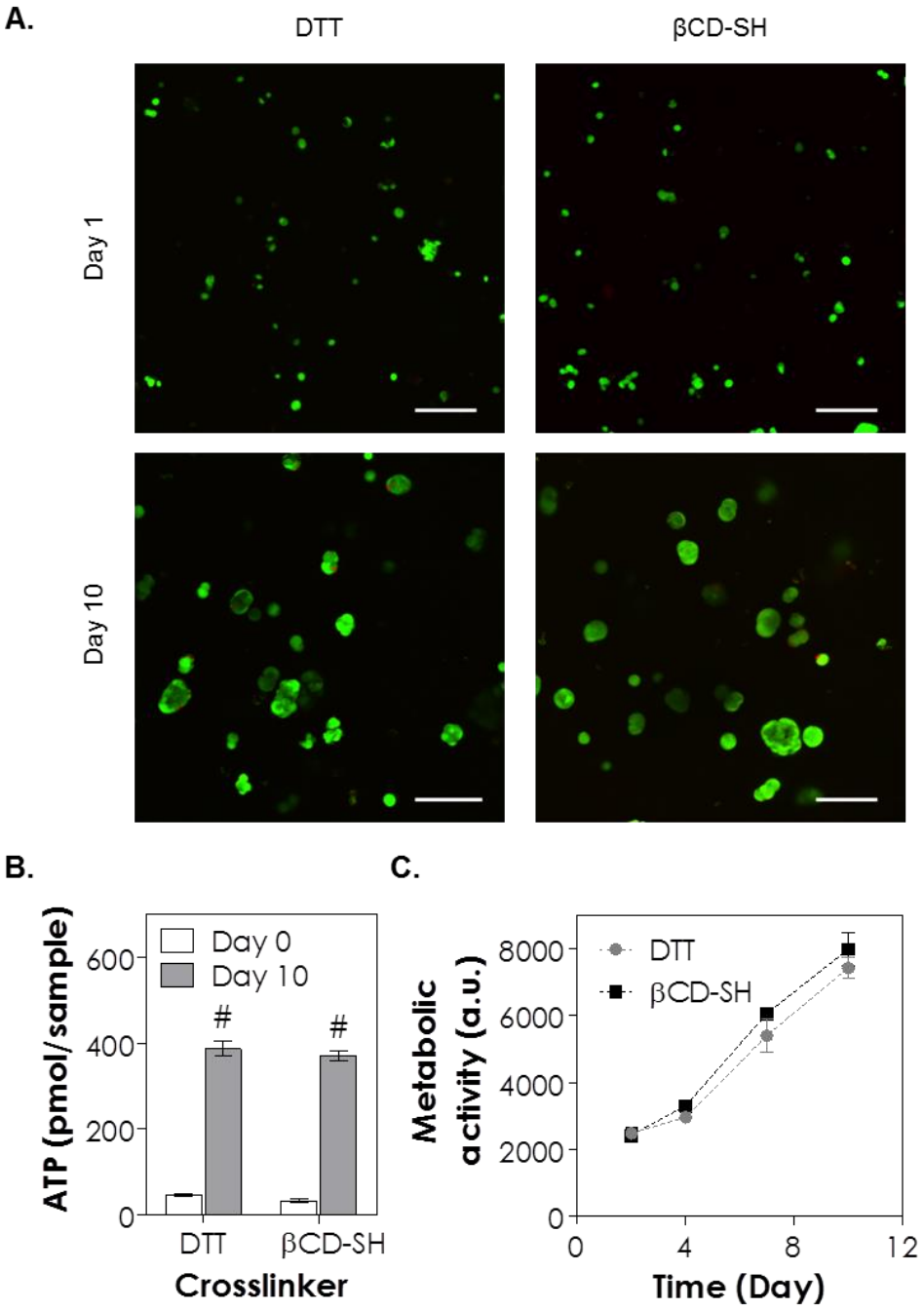

Figure 4.15. Effect of crosslinker on the cytocompatibility of thiol-ene hydrogel on MIN6 β-cells. (A) Representative confocal z-stack images of MIN6 stained with live/dead staining kit on day 1 and 10. MIN6 were encapsulated (2×10^6 cells/mL) in thiol-ene hydrogels crosslinked by βCD-SH (left column) or DTT (right column). MIN6 β-cells viability measured by (B) CellTiter-Glo®, and (C) Alamarblue® reagent (mean ± SD, N = 3). All gel formulations contained 5 wt% $PEG4NB_{20kDa}$, [thiol] = [norbornene] = 10 mM, 1 mM LAP, and light at 5 mW/cm^2. (Scale: 100 μm).

4.4. Materials and Methods

Materials: 4-arm PEG (20 kDa), 8-arm PEG (20 kDa and 40 kDa) and 8-arm PEG-thiol (PEG8SH, 20 kDa) were purchased from JenKem Technology USA. βCD was purchased from TCI America. 5-norbornene-2-carboxylic acid, N,N'-dicyclohexylcarbodiimide (DCC), 4-(dimethylamino) pyridine (DMAP), sodium hydride, and allyl bromide were obtained from Sigma-Aldrich. Dialysis membranes with MWCO 500-1000 Da and 6000-8000 Da were obtained from Spectrum Laboratories and Fisher Scientific, respectively. Other chemicals were purchased from Fisher Scientific unless noted otherwise.

Synthesis of photoinitiator and PEG macromers: The synthesis of photoinitiator lithium arylphosphonate (LAP) was described as reported elsewhere [38]. PEG-tetra-norbornene (PEG4NB, 20 kDa) and PEG-octa-norbornene (PEG8NB, 20 kDa and 40 kDa) were synthesized following an established protocol [120]. In brief, 5-norbornene-2-carboxylic acid (5-fold excess of OH group) and coupling reagent DCC (2.5-fold excess of OH group) were added to anhydrous dichloromethane (DCM). The mixture was purged with nitrogen and stirred at room temperature for 1 hour. The resulting norbornene anhydride was filtered into an addition funnel and added slowly to a flask containing PEG (4-arm or 8-arm), DMAP (0.5-fold of OH group), and pyridine (0.5-fold of OH group) dissolved in anhydrous DCM. The flask was purged with nitrogen, kept on ice and allowed to react overnight in dark. The product was precipitated in cold ethyl ether and collected by filtration. PEGNB product was re-dissolved in double distilled water (ddH_2O) and proceed with dialysis (MWCO 6000-8000 Da) for 2 days using slightly acidic ddH_2O (pH 6.8) to prevent ester hydrolysis of PEGNB. The pure product was obtained from lyophilization (degree of norbornene substitution >85 %). PEGNB: ^1H NMR ($CDCl_3$, 500 MHz): δ – 4.25 (m, 2H), 5.98 (m, 1H), 6.23 (m, 1H). PEG-allylether (PEGAE) was synthesized following a published protocol. Briefly, linear PEG (3.4 kDa) was dissolved in anhydrous toluene and dried with evaporation by reduced pressure. Dried PEG was re-dissolved in anhydrous tetrahydrofuran (THF).

Sodium hydride (1.5-fold excess of hydroxyl group) was added slowly to the PEG solution under continuous nitrogen purging at 40 °C. Upon complete liberation of hydrogen gas, allylbromide (6-fold excess of hydroxyl group) was added drop wise to the solution. After overnight reaction in dark, sodium bromide salt was filtered off to afford a PEG-allylether (PEGAE) solution. PEGAE was precipitated in cold ethyl ether, filtered and dried *in vacuuo*. The purity of PEGAE product was verified with H^1 NMR in $CDCl_3$ (96 %, Bruker 500). PEGAE: ^{1}H NMR ($CDCl_3$, 500 MHz): δ – 4.04 (m, 2H), 5.31 (m, 1H), 5.43 (m, 1H), 6.07 (m, 1H).

Synthesis of allylether or thiol functionalized βCD: βCD-AE was synthesized following a published protocol with slight modification [165]. βCD was dried in vacuum oven overnight and dissolved in 40 mL of anhydrous dimethylformamide (DMF) in a flask. While purging the flask with nitrogen, desired amount of sodium hydride (i.e., 2.3, 4.5 or 11.3-fold of [NaH] and [allylbromide] to [βCD]) was added slowly and the mixture was stirred until no hydrogen gas bubbles were visible (Figure 4.1A, step i). Allylbromide was added drop wise to the βCD solution using an addition funnel and the reaction was allowed to continue overnight in dark (Figure 4.1A, step ii). Next, the volume of βCD-AE mixture was reduced using a rotary evaporator. βCD-AE was precipitated in cold acetone twice and dried in a vacuum oven. βCD-AE: ^{1}H NMR ($(CD_3)_2SO$, 500 MHz): δ – 4.04 (m, 2H), 5.31 (m, 1H), 5.43 (m, 1H), 6.07 (m, 1H). The exact mass of βCD-AE was determined by using mass spectroscopy (Agilent Technologies 6520 Accurate-Mass Q-TOF LC/MS).

Next, thioacetic acid (2-fold excess to [βCD-AE]) was added slowly to 10 mL of DMF containing 1 g of βCD-AE and photoinitiator Irgacure I-2959 (0.5 wt%). Photo-conjugation was initiated by UV-light exposure (Omicure S1000, 365 nm and 10 mW/cm^2) for 15 minutes and continued for another 30 minutes after supplementing with another portion of 0.5 wt% I-2959 (Figure 4.1A, step iii). βCD-thiolacetate was precipitated in cold acetone, filtered, and dried in vacuum oven. After re-dissolving βCD-thioacetate in ddH_2O (10 mL), while purging with

nitrogen, 5 mL of sodium hydroxide (2 N) was added to the solution for 5 minutes to hydrolyze the thioacetate group. The solution was neutralized by adding equal volume of hydrochloride acid (2 N) solution, followed by dialysis (MWCO 500-1000) for 2 days at room temperature (Figure 4.1A, step iv). The product βCD-thiol (βCD-SH) was obtained from lyophilization. βCD-SH: ^{1}H NMR ($(CD_3)_2SO$, 500 MHz): δ – 1.3 (s, 1H), 1.76 (m, 2H), 2.53 (m, 2H), 3.35 (m, 2H). Ellman's assay was performed to determine the concentration of thiol in βCD-SH solution.

Hydrogel fabrication and characterizations: Step-growth thiol-ene hydrogels were formed by light mediated photo-click reactions using the following macromers: (1) PEG8SH (20 kDa) and βCD-AE, (2) PEG8NB (20 kDa) and βCD-SH, or (3) PEG8NB (20 kDa) and DTT. To obtain the best crosslinking efficiency in each gelation formulation, the stoichiometric ratio of thiol to ene was maintained at one. The concentration of PEGNB was adjusted based on ^{1}H NMR results to afford correct norbornene concentrations in the gelation mixtures. Photoinitiator LAP was added to the precursor solution (50 μL/gel) to afford a final concentration of 1 mM. The precursor solution was injected in between two glass slides separated by 1 mm thick spacers. Hydrogel slabs were prepared by exposing the solution to 365 nm light at 5 mW/cm^2 for 5 minutes. To characterize gel fractions, hydrogels were immediately dried in vacuuo after gelation. Dry mass ($W_{Dry,1}$) was measured and the dried polymers were incubated in ddH_2O at 37 ^oC on an orbital shaker for 24 hours to remove uncrosslinked (sol fraction) species. The swollen gels were dried again in vacuuo and weighed to obtain dried polymer weights ($W_{Dry,2}$). After swelling hydrogels in pH 7.4 PBS for two days, the swollen gel weights were measured ($W_{Swollen}$). Gel fractions were obtained by the ratio of the two dry masses (i.e., $W_{Dry,1}/W_{Dry,2}$). Hydrogel swelling ratios (q) were defined as the ratio of swollen gel mass to the second dried polymer mass (i.e., $W_{Swollen}/W_{Dry,2}$).

Crosslinking efficiency of thiol-ene hydrogel: The average molecular weights between crosslinks ($\overline{M_c}$) of thiol-ene hydrogels can be obtained from the structural information of the macromers (i.e., molecular weight and functionality) [63]:

$$\overline{M_c} = 2(\frac{MW_A}{f_A} + \frac{MW_B}{f_B}) \quad (4.1)$$

Here, MW_A and MW_B represent the molecular weight of PEGNB and βCD-SH, while f_A and f_B are the number of reactive functionality for PEGNB and βCD-SH, respectively. With a known $\overline{M_c}$, the ideal network crosslinking density or density of elastically active chains (v_c) and polymer volume fraction (v_2) can be calculated [64]:

$$v_c = \frac{V_1}{\overline{M_c}\overline{v_2}} \quad (4.2)$$

Here, $\overline{v_2}$ is the specific volume of PEG (0.92 cm^3/g at 37 ^oC), V_1 is the molar volume of water (18 cm^3/mole) and χ_{12} is the Flory-Huggins interaction parameter for a PEG-H_2O system (0.45).

In situ photo-rheometry was performed at room temperature on a Bohlin CVO 100 digital rheometer equipped with a light cure cell. A macromer solution (100 μL) was placed on a quartz plate in the light cure cell and irradiated with light (Omnicure S1000, 365 nm, 10 mW/cm^2) through a flexible light guide. Light was turned on 30 seconds after starting time-sweep measurement (10 % strain, 1 Hz frequency, and a gap size of 90 μm) using a 25 mm parallel plate geometry. Gel points (i.e., crossover time) were determined at the time when storage modulus (G') surpassed loss modulus (G").

Oscillatory rheometry in strain-sweep mode was used to obtain elastic modulus of the hydrogel. At equilibrium swelling (after 48 hours in pH 7.4 PBS), a biopsy punch was used to punch out circular gel discs (8 mm in diameter) from the gel slabs. Storage moduli of the hydrogels were measured using 8 mm parallel plate geometry with a gap size of 800 μm. The elastic moduli from at least three hydrogels for each gel formulation were recorded from the average of the linear viscoelastic region (LVR, linear portion of G' plotting against % strain).

Uptake and release of curcumin: Thiol-ene hydrogel discs (25 μL; 4.8 mm dia. × 1.1 mm height) were formed as described above using the following formulations: (1) PEG8SH (20 kDa) and βCD-AE, or (2) PEG8SH (20 kDa) and PEGAE (3.4 kDa). After photo-crosslinking, hydrogels were incubated in 2 mL of curcumin suspended in ddH_2O (2 mg/mL). After 8 hours, hydrogels were removed from the curcumin suspension, rinsed with ddH_2O, and placed individually in 1.6 mL tube. Hydrogels were individually incubated in 500 μL of DMSO. A portion of DMSO (200 μL) was collected and fresh DMSO (200 μL) was added every 24 hours for one week. The amount of released curcumin in DMSO was characterized via measuring absorbance at 430 nm using a microplate reader (BioTek®, Synergy HT).

In another experiment, hydrogels were transferred to 4 mL scintillation vials containing 400 μL of curcumin solution, which was prepared by dissolving curcumin in 0.5 N sodium hydroxide and then diluting with pH 7.4 PBS to a final concentration of 2 mg/mL. This pH shifting method to dissolve curcumin was adapted from Yadav *et al* [157]. After incubating the gels at room temperature for 36 hours, hydrogels were transferred to scintillation vials containing 400 μL of pH 7.4 PBS to rinse off the curcumin adsorbed on gel surface for 10 minutes. The solution was removed from the vials and 1 mL of pH 7.4 PBS was added to each vial for curcumin release study. Scintillation vials containing hydrogels were placed on an orbital shaker (60 rpm) at room temperature. At specific time points, 500 μL of solution was collected from each vial, and fresh 500 μL of pH 7.4 PBS was added back to the vial. After 48 hours, PBS was completely removed from the vials, and 1 mL of DMSO was added to each hydrogel to extract the remaining curcumin from the gels. At specific time points, 500 μL of DMSO was collected from each vial, and fresh DMSO was added back to the vial to maintain the total volume at 1 mL. The absorbance of all collected curcumin samples (from curcumin release and DMSO, 200 μL/sample) were measured using a microplate reader (BioTek®, Synergy HT) at 430 nm. Measured absorbance was blanked with either pH 7.4 PBS or DMSO, and correlated to standard curves with known

concentrations of curcumin. The cumulative uptake of curcumin per gel was the sum of curcumin released in PBS and DMSO.

Cell encapsulation and viability assay: Mouse insulinoma cells (MIN6, final cell density in the gels at 2×10^6 cells/mL) were suspended in polymer solutions containing 1 mM LAP and macromers, including: (1) $PEG8NB_{20kDa}$ with DTT, (2) $PEG8NB_{20kDa}$ with βCD-SH or (3) $PEG8SH_{20kDa}$ with βCD-AE. Precursor solution was exposed to light (365 nm, 5 mW/cm^2) for 5 minutes to obtain cell-laden hydrogels (25 μl/gel), which were maintained in high-glucose DMEM supplemented with 10 % fetal bovine serum (FBS), 50 μM β-mercaptoethanol, and 1× antibiotic-antimycotic. To characterize cell viability, cell-laden hydrogels were incubated in 500 μL Almarblue® reagent (10 % in cell culture medium) at 37 ºC and 5 % of CO_2. After 14 hours of incubation, 200 μl of media were transferred to a 96-well plate for fluorescence quantification (excitation: 560 nm and emission: 590 nm). To obtain qualitative cell viability, cells were stained with a live/dead staining kit (Calcein AM stained live cells green and Edithium homodimer stained dead cells red) and imaged with confocal microscopy. In each stained hydrogel, three images were taken at a step size of 10 μm for a total depth of 100 μm per image. The viability of MIN6 cells was quantified as the percent of live cells over the total number of live and dead cells.

Insulin secretion from MIN6 cells: Cell function was assayed by glucose stimulated insulin secretion (GSIS). Briefly, cell-laden hydrogels were rinsed with HBSS, followed by priming in Krebs-Ringer bicarbonate (KRB) buffer (23 mM sodium chloride, 1 mM potassium chloride, 4.8 mM sodium bicarbonate, 0.2 mM magnesium chloride hexahydrate, 0.2 mM calcium chloride dehydrate, 0.5 mM 4-(2-hydroxyethyl)-1-piperazineethanesulfonic acid and 0.1 vol% bovine serum albumin) containing 2.5 mM glucose for 1 hour at 37 ºC and 5 % CO_2. Then, the gels were incubated with 500 μL of low (2.5 mM) or high (25 mM) glucose KRB

for 2 hours each. The high glucose buffer solution was collected and subjected to insulin ELISA (Mercodia).

HPLC to evaluate potential LAP/CD complex formation: Isocratic HPLC was performed using acetonitrile and 0.05 M of pH 5 phosphate buffer at a ratio of 35 to 65 (vol.%) as the mobile phase. βCD was dissolved at different concentrations (0, 1, 5, and 10 mM) in the mobile phase. Photoinitiator LAP (dissolved at 0.1 mM in the same solvent as the mobile phase without βCD) was injected and run through an analytical C18 column at a flow rate of 1 mL/min. The elution of the samples were monitored at 280 nm.

Data analysis & statistics: All experiments were conducted independently for three times and results were reported as mean ± SD. Data was analyzed with student's t-test or two way ANOVA using GraphPad Prism 5 ($p < 0.05$).

4.5 Conclusion

In summary, we have synthesized step-growth thiol-ene photopolymerized hydrogel using derivatives of βCD and PEG. We found that thiol-norbornene hydrogels crosslinked by CD-SH and PEGNB exhibited faster gelation kinetics and higher crosslinking efficiency when comparing with thiol-allylether hydrogels crosslinked by PEGSH and CD-AE. Furthermore, the gelation kinetics of thiol-norbornene depended highly on the functionality of macromer used. In addition, CD/PEG hydrogels afforded higher loading, as well as prolonged and sustained delivery, of hydrophobic curcumin. The results of live/dead staining, cell viability assay, and GSIS demonstrated that cell viability was maintained in these hydrogels, but in some cases affected by hydrogel properties (e.g., stiffness). Future work will focus on utilizing this CD-based radical-mediated thiol-ene photopolymerized hydrogel as a delivery vehicle of hydrophobic biomolecules.

CHAPTER 5
IMPROVING GELATION EFFICIENCY AND CYTOCOMPATIBILITY OF VISIBLE LIGHT POLYMERIZED THIOL-NORBORNENE HYDROGELS VIA ADDITION OF SOLUBLE TYROSINE

5.1. Abstract

Hydrogels containing biomimetic or therapeutic peptides have been used widely for tissue engineering and drug delivery applications. An attractive technique to prepare peptide-immobilized hydrogels is photopolymerization, which offers rapid and spatial-temporally tunable gelation kinetics. Recently, our lab introduced a visible light mediated step-growth thiol-norbornene gelation scheme, in which eosin-Y was used as the sole photoinitiator. Compared with conventional visible light mediated chain-polymerizations where multiple initiator components are required, step-growth photopolymerized thiol-norbornene hydrogels are more cytocompatible for *in situ* encapsulation of radical sensitive cells, such as pancreatic β-cells. While prior work has demonstrated the efficient crosslinking of inert poly(ethylene glycol)-norbornene (PEGNB) hydrogels via visible light irradiation, no peptide linkers were used to render the otherwise inert hydrogel network bioactive. This contribution explored the crosslinking of various bis-cysteine containing peptides with macromer 8-arm PEGNB to form biomimetic hydrogels suitable for in situ cell encapsulation. Initial efforts to polymerize thiol-norbornene PEG-peptide hydrogels through visible light and eosin-Y mediated crosslinking encountered challenges in gelation efficiency. During the optimization processes, we found that the addition of soluble tyrosine during polymerization significantly improved the crosslinking efficiency of PEG-peptide hydrogels. In addition, soluble tyrosine drastically enhanced the cytocompatibility of the resulting PEG-peptide hydrogels, as demonstrated

by in situ encapsulation and culture of pancreatic β-cell line (MIN6) and primary mouse islets.

5.2. Introduction

Ongoing efforts in biomaterials science and engineering are the design of bioactive or biomimetic hydrogels for drug delivery and tissue engineering applications. Towards this end, hydrogels have been fabricated from naturally derived materials such as alginate [166], glycosaminoglycans [167-170], fibrin [171, 172], chitosan [173-175], dextran [176], collagen [177], and gelatin [178, 179]. Although hydrogels derived from natural matrices are inherently bioactive, it is difficult to tune their bioactivity, mechanics, and degradation features [180]. On the other hand, hydrogels prepared from purely synthetic polymers, such as polyethylene glycol (PEG) and polyvinyl alcohol (PVA), have high tunability in mechanical properties but they do not possess bioactive features necessary for promoting cell viability and function [181-183]. Hence, biomimetic peptides are routinely used to render the otherwise inert synthetic hydrogel bioactive.

A classical way of immobilizing peptides in synthetic hydrogel is through chain-growth copolymerization of acrylated macromers and acrylated peptides [184]. Alternatively, cysteine containing peptides could be readily crosslinked with acrylated macromers through a mixed-mode photopolymerization [185]. For example, Lin and Anseth incorporated cysteine-bearing glucagon-like peptide 1 (GLP-1C) into PEG-diacrylate (PEGDA) hydrogel to improve the viability and insulin secretion of encapsulated islets [186]. Alternatively, PEG-peptide hydrogel could be polymerized via Michael-type addition between nucleophilic macromers (e.g., acrylate, maleimide, or vinyl sulfone) and cysteine-containing peptides [73, 187-189]. For example, Garcia and colleagues synthesized bioactive PEG-peptide hydrogels using 4-arm PEG-maleimide with cysteine-containing protease-sensitive and integrin-binding peptides (i.e., CRGDS) to promote the performance of encapsulated islets *in vivo* [190]. While these PEG-peptide

hydrogels have found various successful applications, limitations and challenges exist. For instance, chain-polymerized hydrogels are known to form network containing heterogeneous and hydrophobic polyacrylate kinetic chains and high molecular weight degradation products [47, 191-193]. On the other hand, while Michael-type hydrogels were formed by orthogonal crosslinking, it is difficult to control gelation kinetics and the resulting gel network often contains high degrees of structural defects [63].

To overcome some of the above-mentioned issues, Anseth and colleagues introduced a new class of PEG-peptide hydrogels formed by radical-mediated step-growth thiol-norbornene photo-click reaction [38]. In this system, low intensity and long wavelength ultraviolet (UV) light (5–10 mW/cm^2, 365 nm) is used to generate primary radicals from photoinitiator lithium acylphosphinate (LAP) [38]. The radicals deprotonate protons from bis-cysteine-containing peptides, thus forming thiyl radicals capable of adding to norbornene in a strictly orthogonal fashion. The replenished carbonyl radicals are terminated through abstracting additional hydrogens from other thiol-containing molecules, hence completing the step-growth cycle. Similar to other photopolymerization schemes, the advantages of step-growth thiol-norbornene reaction include rapid, ambient, and aqueous reaction conditions, as well as spatial-temporal control over gelation kinetics [36, 37, 120]. Furthermore, thiol-norbornene photo-click reaction is not susceptible to oxygen inhibition, providing rapid gelation when comparing to acrylate-based chain-growth photopolymerizations at equivalent macromer concentration and functionality [51, 52]. Thiol-norbornene photo-click reactions also hinder disulfide bond formation due to radical-mediated cleavage [53], thus increasing the degree of crosslinking and improved mechanical properties [38].

While current thiol-norbornene hydrogels have shown to be cytocompatible for mammalian cells [38, 52, 54-56, 78, 79, 91, 92, 194], the use of UV-light still raised concerns of DNA and protein damage [195, 196]. Recently, our lab developed step-growth thiol-norbornene photo-click PEG-based hydrogels using a visible light source (400 nm to 700 nm) and type II photoinitiator eosin-Y [59]. This reaction scheme not only preserves all advantages offered by photopolymerization, but also eliminates the use of potentially cytotoxic components (i.e., co-initiator and co-monomer) used in the

conventional visible light polymerized chain-growth hydrogels. We have shown that purely synthetic hydrogels (i.e., PEGNB crosslinked with dithiothreitol, DTT) prepared through this reaction are highly cytocompatible for *in situ* encapsulation of pancreatic β-cells and human mesenchymal stem cells (hMSCs) [59]. In an attempt to create bioactive hydrogels using visible light thiol-norbornene photopolymerization, we replaced DTT with bis-cysteine-bearing peptides as the hydrogel crosslinker. However, we found that the gelation efficiency was influenced significantly on the sequence of the bis-cysteine peptides. During the optimization processes, we discovered that the addition of soluble amino acid containing aromatic side chain (e.g., tyrosine, and tryptophan) could improve the efficiency of cysteine deprotection to form thiyl radicals, implying that gelation efficiency would be different in the presence of soluble amino acids. To test this hypothesis, soluble tyrosine was added during visible light polymerization to form PEG-peptide hydrogel. We systematically studied the gelation kinetics and physical properties of PEG-peptide hydrogel. In addition, we evaluated the cytocompatibility of PEG-peptide hydrogels to both pancreatic β-cells and isolated mouse islets.

5.3. Results and Discussion

5.3.1. Tyrosine-assisted crosslinking of thiol-norbornene PEG-peptide hydrogels

To evaluate the influence of soluble tyrosine on gelation kinetics of PEG-peptide hydrogels formed by visible light mediated thiol-norbornene polymerization, hydrogel was crosslinked from a bis-cysteine-containing peptide (i.e., CGGGC) and PEG8NB in the presence of photoinitiator eosin-Y and visible light exposure (400-700 nm at 70,000 lux, Figure 5.1A). We found that PEG-peptide hydrogels crosslinked without soluble tyrosine had a gel point of about 100 seconds and an ultimate elastic modulus of ~100 Pa (Figure 5.1B). The poor gelation was unexpected as we had previously demonstrated rapid gelation using PEGNB with an inert crosslinker – DTT [59]. Since visible light-mediated thiol-norbornene gelation starts with the deprotonation of thiol group by excited

eosin-Y, we suspected that the poor gelation efficiency shown in Figure 5.1B might be a result of insufficient deprotonation of thiol groups on cysteine residues, which are part of the peptide sequence. Furthermore, we found that gelation efficiency depends highly on the sequence of the bis-cysteine peptide crosslinkers (Figure 5.2). Indeed, the influence of amino acids (e.g., tyrosine, tryptophan) on the half-life of eosin-Y radicals has been documented in the literature [195, 197]. Therefore, we hypothesized the addition of soluble tyrosine might improve the crosslinking efficiency of visible light-based thiol-norbornene hydrogels. To test this hypothesis, soluble tyrosine (e.g., 1 mM) was added during gelation, which was monitored by *in situ* photorheometry. With the addition of tyrosine, the gel point was five-fold faster (~22 seconds) than the gelation without tyrosine. Furthermore, the ultimate elastic modulus increased ten-fold to ~1000 Pa (Figure 5.1C). The significant improvement of gelation efficiency in the presence of soluble tyrosine was indicative of an accelerated deprotonation of peptide-bound cysteine side-chain and/or the thiol-norbornene coupling.

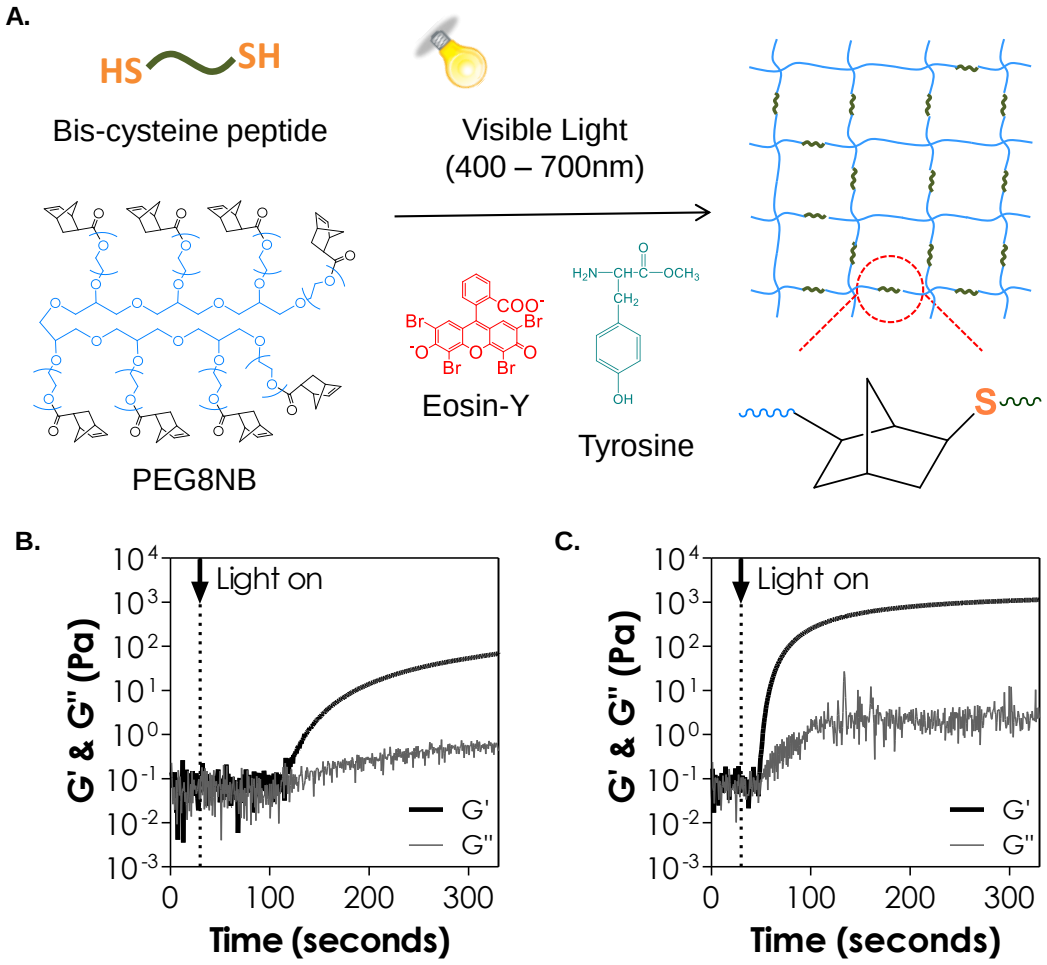

Figure 5.1. (A) Scheme of visible light and eosin-Y mediated thiol-norbornene gelation. (B, C) *In situ* photorheometry of thiol-norbornene photopolymerization between 3wt% PEG8NB and 6mM CGGGC in the presence of 0 mM (B), and 1 mM of tyrosine (C). G': storage modulus; G": loss modulus. Eosin-Y: 0.1 mM. Light intensity: 70,000 lux. N = 3. Error bars were omitted for clarity. In collaboration with Hung-Yi Liu.

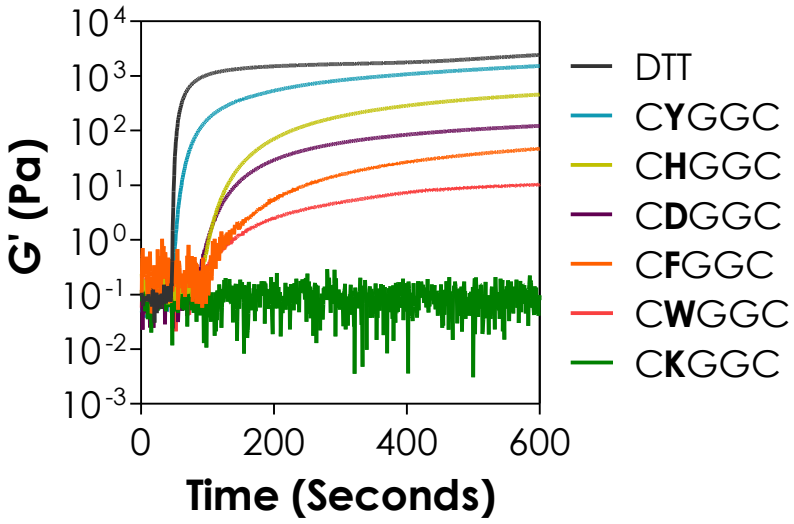

Figure 5.2. *In situ* photorheometry of thiol-norbornene photopolymerization between 5wt% $PEG4NB_{20kDa}$ and 5 mM of DTT or di-cysteine containing peptide in the presence of 0.1 mM eosin-Y. G': storage modulus. Light intensity: 70,000 lux. N = 3. Error bars were omitted for clarity.

To further examine the kinetics of tyrosine-assisted thiol-norbornene reaction, we characterized thiol and norbornene consumptions using precursor solution containing non-gelling components, including linear PEG-norbornene (PEGdNB. MW: 6 kDa), soluble cysteine, eosin-Y, and soluble tyrosine at different concentrations. After visible light exposure, the concentration of free thiol remaining in the solution was quantified by Ellman's reagent. Figure 5.3 shows that the rate of thiol conversion was faster at higher soluble tyrosine concentrations. At 20 seconds (where gel point was previously determined, Figure 5.1C), thiol conversion increased from 22 to 48 % as the concentration of tyrosine was increased from 0 to 10 mM (Figure 5.3, right panel). This higher thiol conversion rate in the presence of soluble tyrosine could explain the faster gel point shown in Figure 5.1C. Regardless of the amount of soluble tyrosine added, all non-gelling formulations eventually reached similar thiol conversion (~95% at 300 seconds of visible light exposure). Even though all non-gelling formulations had similar thiol conversion (Figure 5.3), hydrogels formed without soluble tyrosine showed lower ultimate elastic modulus than that formed in the presence of soluble tyrosine (Figure

5.1B). The faster gelation assisted by soluble tyrosine likely decreased network non-ideality, and hence higher gel modulus.

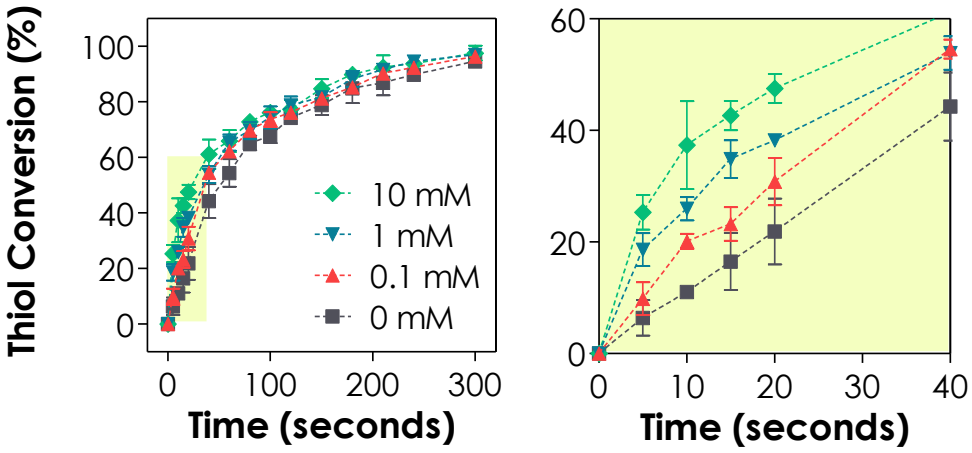

Figure 5.3. Thiol conversion quantified by Ellman's assay. The right panel shows the shaded region in the left plot. (3.4 wt% $PEGdNB_{6kDa}$, 12 mM L-cysteine, 0.1 mM eosin-Y. Tyrosine was added at indicated concentration, N = 3) In collaboration with Hung-Yi Liu.

In a separate experiment, we examined the consumption of norbornene in non-gelling samples using ^{1}H NMR. The areas under the norbornene signature peaks (Figure 5.4 and 5.5A, norbornene peaks: δ 5.8-6.2 ppm) were used to represent norbornene conversion. As the concentration of soluble tyrosine was increased from 0 to 10 mM (Figure 5.4A and 5.5B, tyrosine peaks: δ 6.8-7.2 ppm), the area under the norbornene signature peaks decreased from 1.86 to 0.37 a.u. (Table 5.1). When compared with unreacted PEGNB (Table 5.1, area under norbornene peaks: 7.05 a.u.), the norbornene consumption increased from 74 to 95 % when the concentration of soluble tyrosine was increased from 0 to 10 mM (Table 5.1). Since the step-growth thiol-norbornene reaction is strictly orthogonal (i.e., no homo-polymerization between norbornene groups under current experimental conditions), the amount of norbornene consumed after the reaction could be attributed to thiol-norbornene coupling.

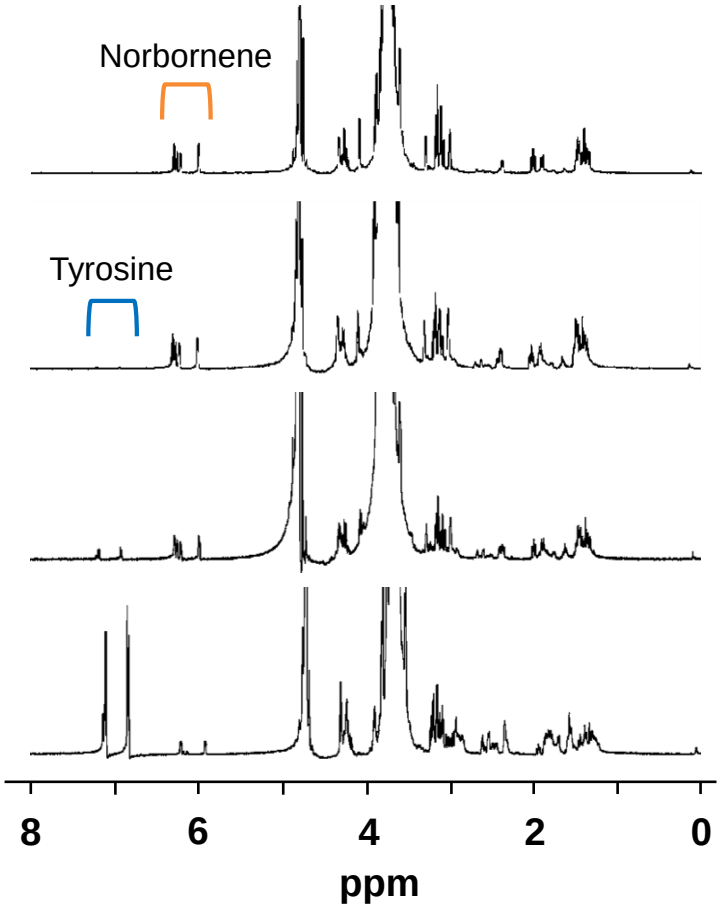

Figure 5.4. Effect of tyrosine on norbornene conversion determined by ^{1}H NMR using non-gelling components: $PEGdNB_{6kDa}$ (3.6 wt%), soluble cysteine (12 mM), eosin-Y (0.1 mM), and tyrosine from 0 mM to 10 mM (from top to bottom). All prepared with D_2O (at 4.8 ppm). The integration of the areas under the norbornene peaks are reported in Table 5.1.

Table 5.1. Area of norbornene peaks integrated from ^{1}H NMR results (Figure 5.4).

	[Tyrosine] (mM)	$Area_{Norbornene}$ (a.u.)	Norbornene conversion (%)
(-) reaction	0	7.05	0
(+) reaction	0	1.86	73.6
	0.1	1.84	74.0
	1	0.70	90.1
	10	0.37	94.8

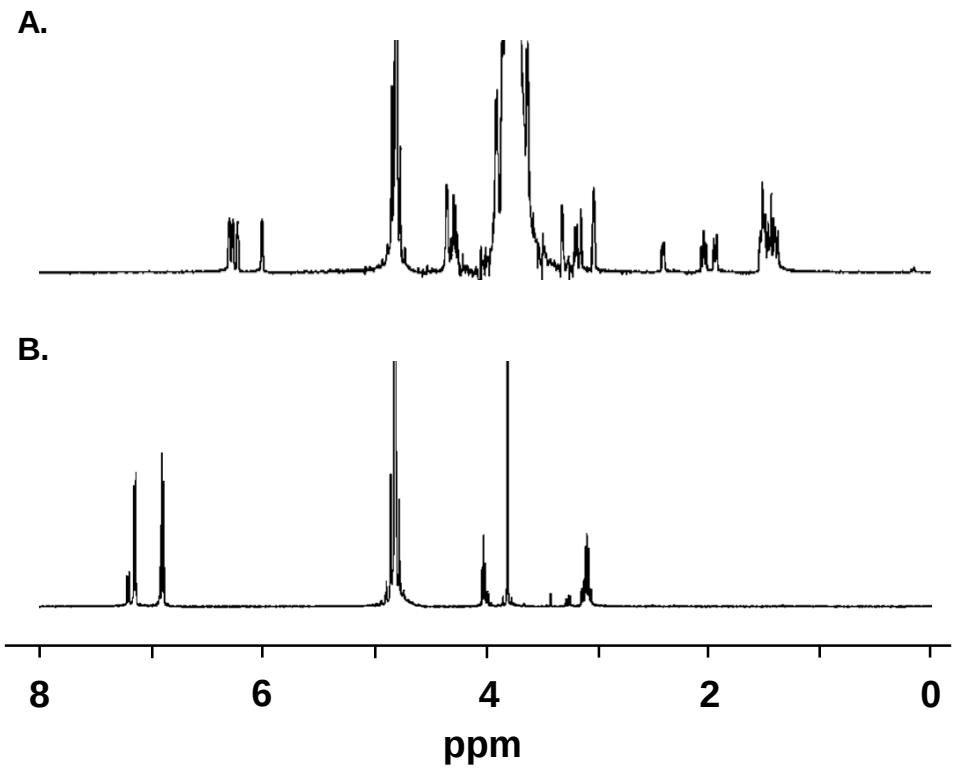

Figure 5.5. ^{1}H NMR of (A) $PEGdNB_{6kDa}$ and (B) L-tyrosine methyl ester. All prepared with D_2O (at 4.8 ppm).

5.3.2. Effect of tyrosine on the spectrophotometric properties of eosin-Y

In addition to the alteration of gel properties, we observed a decreased in the redness of hydrogels with increasing tyrosine used during gelation (Figure 5.6A). The color of the gels was due to the intrinsic color of eosin-Y sequestered within thiol-ene gel network during gelation [58]. Since the concentration of eosin-Y was the same across the four formulations, the disappearance of redness was potentially due to the quenching of eosin-Y by tyrosine through a proton-coupled electron transfer process [198, 199]. To verify this, we evaluated the spectrophotometric properties of precursor solution containing non-gelling components. Before exposing solution to light, the UV/Vis spectra of these solution were similar regardless of the concentration of tyrosine used (peak absorbance of

~0.5 at 516 nm, Figure 5.6B to 5.6D). However, after exposing the non-gelling solution to visible light, the reduction in peak absorbance (at 516 nm) with increasing concentration of tyrosine (Figure 5.6B to 5.6D, 0.25 to 0.18 a.u. for 0 mM to 10 mM of tyrosine, respectively) confirmed the quenching of eosin-Y by tyrosine.

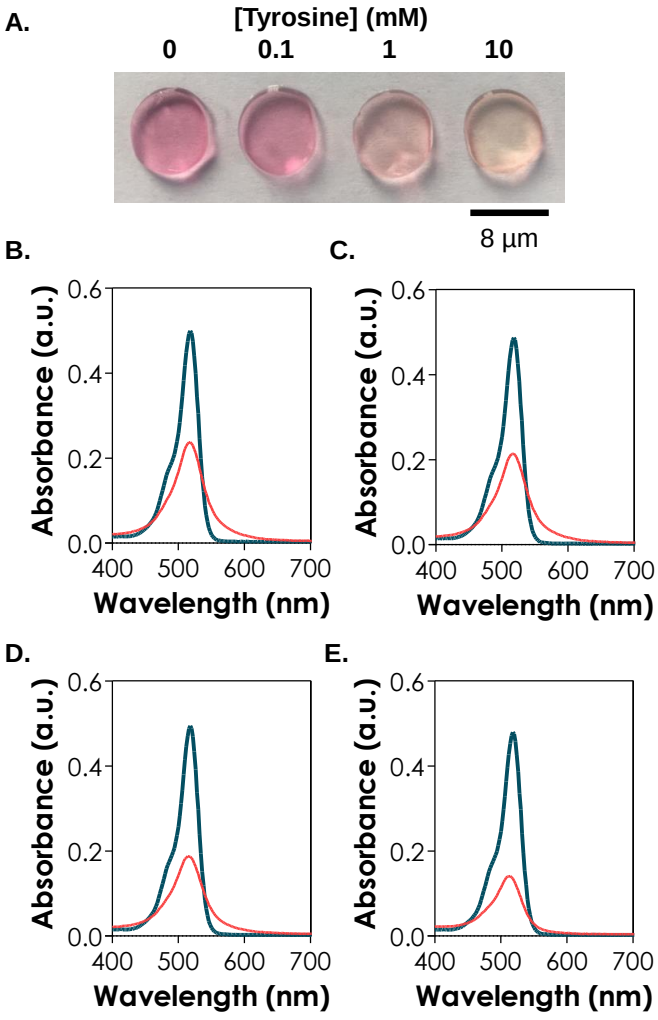

Figure 5.6. (A) Photograph of hydrogels at equilibrium swelling. UV-vis spectra of eosin-Y before (thick blue) and after (thin red) visible light exposure for 5 minutes in the presence of PEGdNB, CGGGC, and varied concentrations of tyrosine. Tyrosine concentration: (B) 0 mM, (C) 0.1 mM, (D) 1 mM, and (E) 10 mM. Eosin-Y concentration in all measurements: 0.1 mM. (3.4 wt% $PEGdNB_{6kDa}$ or 3 wt% $PEG8NB_{20kda}$, 6 mM CGGGC, 0.1 mM eosin-Y, 400-700 nm light, intensity at 70,000 lux, mean ± SD, N = 3).

5.3.3. Effect of tyrosine, macromer content and thiol-to-norbornene ratio on hydrogel properties

We further investigated hydrogel properties with respect to the concentration of soluble tyrosine added during gelation. Here, CGGGC was used as a model peptide for gel characterizations. As we increased the concentration of soluble tyrosine from 0 to 1 mM, gel fraction increased from 50 to 65 % (Figure 5.7A), elastic modulus increased from 1 to 3 kPa (Figure 5.7B), and equilibrium swelling ratio decreased from 16 to 10 (Figure 5.7C). These metrics were indicative of an improved crosslinking in the presence of soluble tyrosine. This implies that the network crosslinking density of these PEG-peptide hydrogels could be tuned easily with the amount of tyrosine added during reaction. Interestingly, further increasing tyrosine from 1 to 10 mM led to a decreased in gel fraction, elastic modulus and an increased in swelling ratio. The negative impact of high tyrosine concentration on gel properties was unexpected as the results obtained from thiol and norbornene consumption (Figure 5.3 and 5.4) showed a monotonic increase of functional group conversion. We hypothesize that the increased network non-idealities at high tyrosine content (i.e., 10 mM) was likely due to steric inference caused by tyrosine.

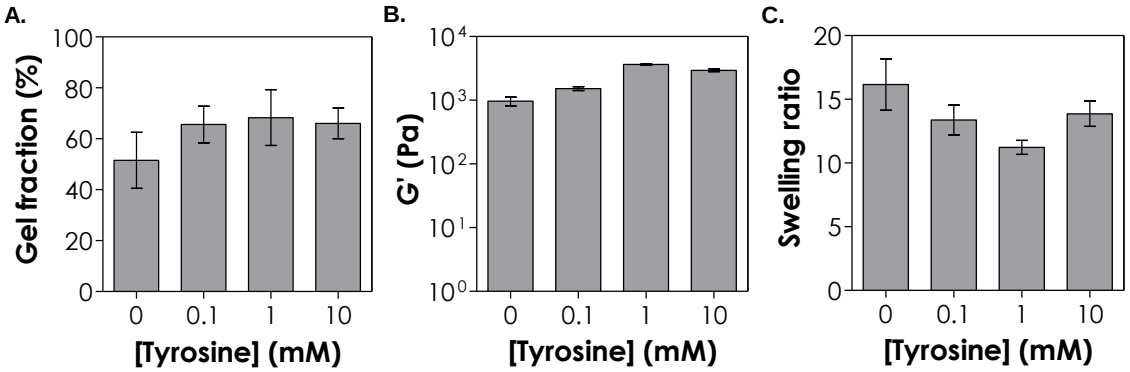

Figure 5.7. Effect of tyrosine on (A) gel fraction, (B) elastic modulus at equilibrium gel swelling, and (C) swelling ratio as a function of time. (3 wt% PEG8NB, 6 mM CGGGC, 0.1 mM eosin-Y, 400-700 nm light, intensity at 70000 lux, mean ± SD, N = 3). In collaboration with Hung-Yi Liu.

In addition to tuning gel properties by varying the concentration of soluble tyrosine, the physical properties of gels could also tuned by varying PEG8NB macromer and the ratio of ene to thiol. As PEG8NB concentration was increased from 3 to 9 wt%, there was a 25–fold increase in elastic modulus at equilibrium swelling (Figure 5.8A, from 1.3 to 32 kPa). In addition, increasing ratio of norbornene to thiol from 0.6 to 1 led to a 26–fold increase in elastic modulus at equilibrium swelling (Figure 5.8B, 0.05 to 1.3 kPa). These studies demonstrated the high tunability of visible light polymerized step-growth PEG-peptide hydrogels [59, 62].

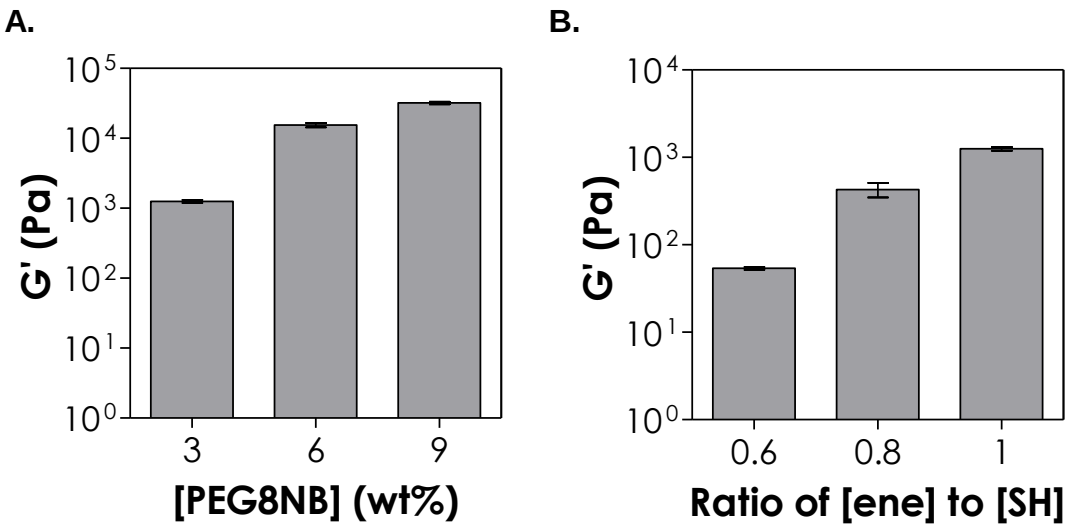

Figure 5.8. Effect of macromer concentration (A), and the ratio of norbornene to thiol (B) on the elastic modulus of PEG-peptide hydrogels. (3 wt% PEG8NB, 6 mM CGGGC, 0.1 mM eosin-Y, 400-700 nm light, intensity at 70000 lux, mean ± SD, N = 3). In collaboration with Hung-Yi Liu.

5.3.4. Cytocompatibility of PEG-peptide hydrogels

Next, we evaluated the cytocompatibility of thiol-ene hydrogel crosslinked in the presence of soluble tyrosine using *in situ* encapsulation of pancreatic MIN6 β-cells. Thiol-norbornene hydrogels were crosslinked by laminin-derived peptide (i.e., KC**YIGSR**CK) and non-degradable 8-arm PEGNB (PEG8aNB, 20 kDa) with or without adding soluble tyrosine. Here, laminin-derived peptide was used to mimic β-cells extracellular microenvironment [200-202]. To ensure that matrix stiffness would not a confounding factor when evaluating cellular fate, cell-laden hydrogels were formulated to have similar modulus (Figure 5.9, ~2 kPa), which was achieved through adjusting stoichiometric ratio of thiol to norbornene (i.e., $R_{[thiol]/[ene]}$ = 1 for gelation without tyrosine and 0.85 gelation with 1 mM of tyrosine). Hydrogels crosslinked with PEG8aNB were hydrolytically stable throughout the course of study (Figure 5.9). One day after cell encapsulation, live/dead staining was performed and more than 90 % of cells were stained green indicating that hydrogels were cytocompatible for *in situ* encapsulation of β-cells. However, we observed slightly more dead cells (stained red) when encapsulation was performed without tyrosine (Figure 5.10A, top). Regardless of the initial cell viability, β-cells formed cell spheroids after 10 days of culture in both formulations (Figure 5.10A, bottom). In addition, AlamarBlue® reagent was used to quantify metabolic activity of the cells encapsulated within the hydrogels. Compared with cells encapsulated in the absence of tyrosine, cells encapsulated in the presence of tyrosine showed higher cell metabolic activity throughout the course of study (Figure 5.10B). Most importantly, β-cells encapsulated in the presence of tyrosine had higher insulin secretion than cells encapsulated without the addition of tyrosine (Figure 5.10C, 2-fold and 3-fold higher on day 1 and 10, respectively). We examined the expression of insulin (*ins*) and pancreatic duodenal homeobox-1 (*pdx1*) on the mRNA level. These two genes were chosen because of their importance in glycemic control and in proliferation of pancreatic β-cells [203, 204]. The mRNA expression of *ins* and *pdx1* showed that the addition of tyrosine did not create adverse influence on β-cells (Figure 5.11). Together, the addition of soluble tyrosine increased cell viability, insulin secretion, and did not

negatively impact beta cell-related gene expression. These results were most likely due to faster gelation kinetics, which reduced exposure time of radicals on radical sensitive β-cells.

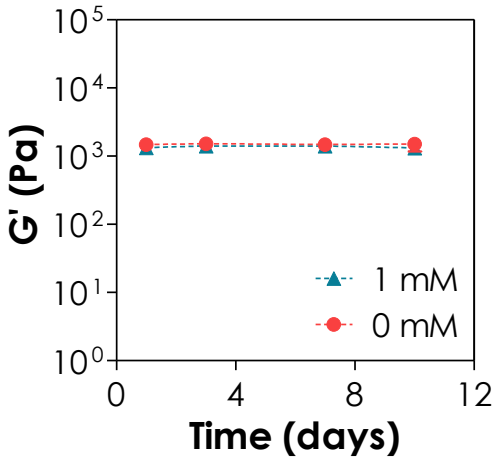

Figure 5.9. Effect of tyrosine concentration on the degradability of PEG-peptide hydrogels. All gel formulations contained β-cells at 5×10^6 cells/mL, 3.5 wt% PEG8aNB, 7 mM KCYIGSRCK, 0.1 mM eosin-Y, and 400-700 nm light at 70000 lux.

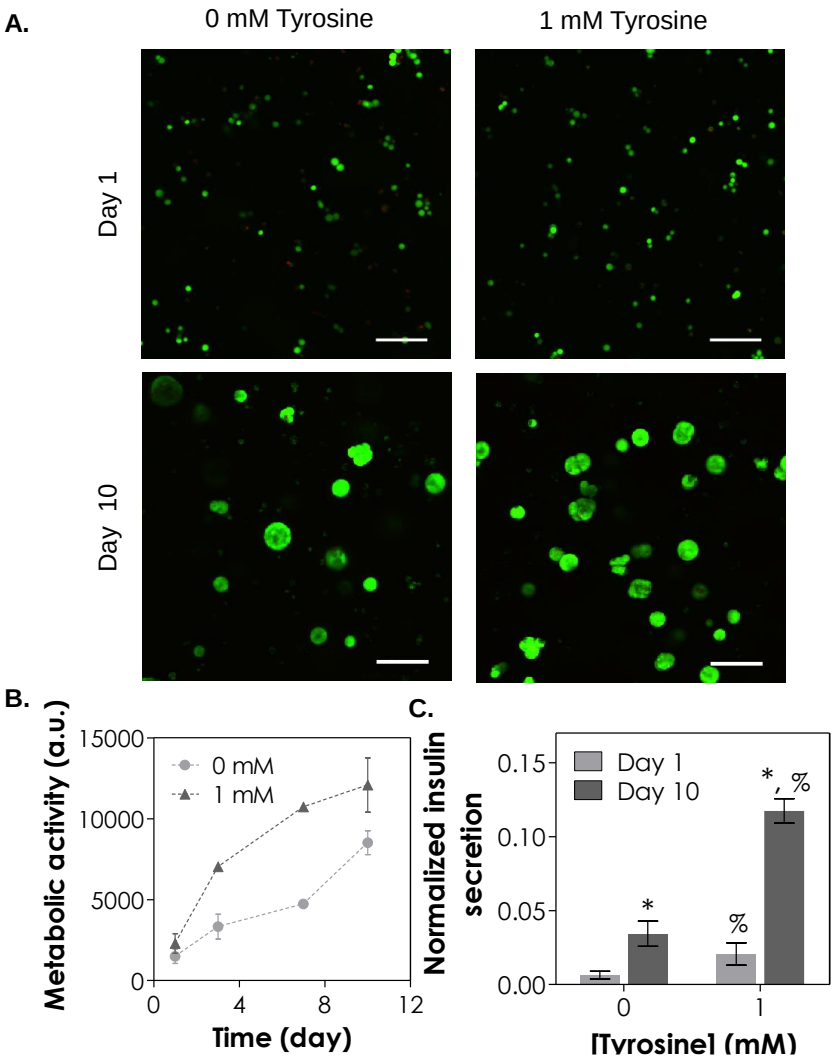

Figure 5.10. Effect of tyrosine on the cytocompatibility of MIN6 β-cells. (A) Representative confocal z-stack images of MIN6 cells stained with live/dead staining kit on day 1 (Scales: 100 μm). (B) Cells viability as assessed by Alamarblue® reagent. (C) Glucose stimulated insulin secretion (25 mM of glucose) normalized by cell metabolic activity. * indicates comparison between day 1 and day 10, while % indicates comparison between 0 to 1 mM of tyrosine, $p < 0.05$. All gel formulations contained β-cells at 5×10^6 cells/mL, 3.5 wt% PEG8aNB, KCYIGSRCK, 0.1 mM eosin-Y, and 400-700 nm light at 70000 lux. Ratio of [thiol] to [norbornene] was 1 and 0.85 for 0 mM and 1 mM of tyrosine, respectively.

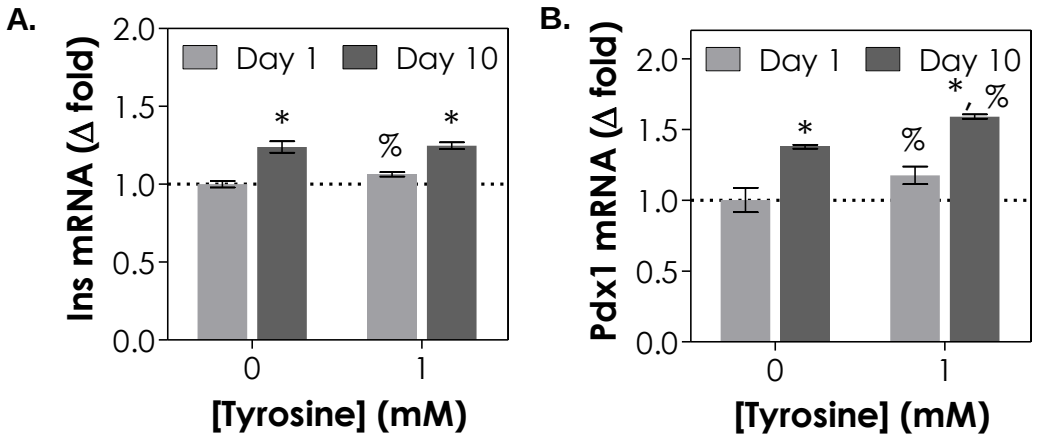

Figure 5.11. Effect of tyrosine on the mRNA expression of MIN6 β-cells. mRNA level of (A) Ins and (B) Pdx1 evaluated by qPCR. Actβ was used as a house keeping gene. * indicates comparison between day 1 and day 10, while % indicates comparison between 0 to 1 mM of tyrosine, $p < 0.05$. All gel formulations contained β-cells at 5×10^6 cells/mL, 3.5 wt% PEG8aNB, KCYIGSRCK, 0.1 mM eosin-Y, and 400-700 nm light at 70000 lux. Ratio of [thiol] to [norbornene] was 1 and 0.85 for 0 mM and 1 mM of tyrosine, respectively.

In addition to encapsulate β-cells, *in situ* cell encapsulation was also performed on islets isolated from CD1 mice. One day post encapsulation, live/dead images of encapsulated islets showed a significant amount of cell death (cells stained red) when islets were encapsulated without tyrosine (Figure 5.12A). When islets were challenged with glucose, only islets encapsulated in the presence of tyrosine showed a significant enhancement in insulin secretion (Figure 5.12B, 4-fold increased with 1 mM of tyrosine used). Collectively, the decreased cell viability and insulin-secreting function was potentially due to longer exposure of cells to radicals.

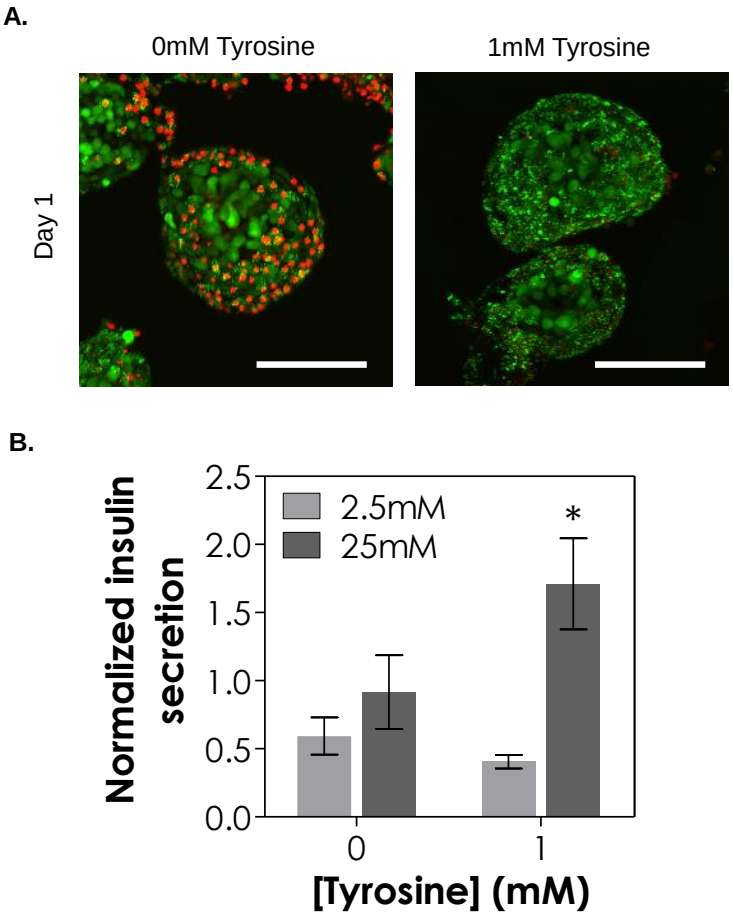

Figure 5.12. Effect of tyrosine on the cytocompatibility of CD1 mouse islets. (A) Representative confocal z-stack images of islets stained with live/dead staining kit on day 1. (B) Glucose stimulated insulin secretion normalized by ATP content per gel (day 1). Gel formulations: 3.5 wt% PEG8aNB, KCYIGSRCK, 0.1 mM eosin-Y, and 400-700 nm light at 70000 lux (Scales: 100 μm).

5.4. Materials and Methods

Materials: 8-arm PEG and PEG-amide were purchased from JenKem Technology USA. Fmoc-protected amino acids, HBTU, and HOBT were purchased from AnaSpec. Linear PEG (6 kDa), 5-norbornene-2-carboxylic acid, N,N'-dicyclohexylcarbodiimide (DCC), 4-(dimethylamino) pyridine (DMAP) were obtained from Sigma-Aldrich. Dialysis

membranes and other chemicals were obtained from Fisher Scientific unless noted otherwise.

PEGNB synthesis: Linear PEG-norbornene (PEGNB, 6 kDa) and PEG-octa-norbornene (PEG8NB, 20 kDa and 40 kDa) was synthesized following an established protocol [120]. In brief, 5-norbornene-2-carboxylic acid (5-fold excess of OH group) and coupling reagent DCC (2.5-fold excess of OH group) were added to anhydrous dichloromethane (DCM). The mixture was purged with nitrogen and stirred at room temperature for 1 hour. The resulting norbornene anhydride was filtered into an addition funnel and added slowly to a flask containing PEG, DMAP (0.5-fold of OH group), and pyridine (0.5-fold of OH group) dissolved in anhydrous DCM. The flask was purged with nitrogen, kept on ice and allowed to react overnight in dark. The reaction was repeated for the second time to improve the functionalization of norbornene on PEG. The product was precipitated in cold ethyl ether and collected by filtration. PEGNB product was re-dissolved in double distilled water (ddH_2O) and proceed with dialysis for 2 days using slightly acidic ddH_2O (pH 6.8) to prevent ester hydrolysis of PEG8NB. The pure product was obtained from lyophilization (degree of norbornene substitution >85 %). PEGNB: ^{1}H NMR ($CDCl_3$, 500 MHz): δ – 4.25 (m, 2H), 5.98 (m, 1H), 6.23 (m, 1H).

To synthesize hydrolytically stable PEG-amide-norbornene (PEGaNB), norbornene acid (5-fold excess to amine groups) was first activated by HBTU/HOBT (5.5-fold excess to amine group) in dimethylformamide (DMF) for 3 minutes. With nitrogen gas purging, N,N-Diisopropylethylamine (DIEA, 6-fold excess to amine group) was added to the activated norbornene acid solution and stirred for 5 minutes. The solution was added drop wise to a two-neck flask containing PEG-octa-amine in DMF. After overnight reaction at room temperature, the product was precipitated in cold ethyl ether. After drying *in vacuuo*, PEGaNB product was re-dissolved in water and dialyzed for 2 days. ^{1}H NMR (Bruker 500) was used to confirm the degree of PEG functionalization (> 90 %).

Peptide synthesis: All peptides were synthesized in an automated microwave-assisted peptide synthesizer (CEM Discover SPS attached with Liberty 1). Crude peptides were cleaved from resins using phenol, trifluoroacetic acid (TFA), triisopropylsilane (TIS), and ddH_2O. Cleaved peptides were precipitated in cold ethyl ether, collected through centrifugation, dried *in vacuuo*, and purified by reverse phase HPLC (PerkinElmer Flexar system). Peptide identity was confirmed by mass spectrometry (Agilent Technologies Model 1200-6520).

Hydrogel fabrication and characterization: Step-growth thiol-norbornene hydrogels were formed by visible light mediated photo-click reactions using PEG8NB and di-cysteine peptide (i.e., Cys-Gly-Gly-Gly-Cys or CGGGC) in the presence of 0.1 mM of eosin-Y. L-tyrosine methyl ester (i.e., soluble tyrosine) was added in selected formulations. The concentration of PEG8NB was adjusted based on ^{1}H NMR results to afford correct norbornene concentrations in the gelation mixtures. The precursor solution was injected in between two glass slides separated by 1 mm thick spacers or in 1 mL syringe mold with an open tip. Hydrogel crosslinking was initiated by exposing the solution to 400-700 nm light at 70,000 lux (equivalence of 10mW/cm^2 at 550nm) for 5 minutes. To characterize gel fractions, hydrogels were immediately dried in vacuuo after gelation. Dry mass ($W_{Dry,1}$) was measured and the dried polymers were incubated in ddH_2O at 37 ^oC on an orbital shaker for 24 hours to remove un-crosslinked (sol fraction) species. The swollen gels were dried again in vacuuo and weighed to obtain second dried polymer weights ($W_{Dry,2}$). Gel fractions were obtained by the ratio of the two dry masses (i.e., $W_{Dry,1}/W_{Dry,2}$). In selected experiments, gels were allowed to swell in pH 7.4 PBS for two days prior to obtaining swollen gel weights ($W_{Swollen}$). Hydrogel swelling ratios (q) were defined as the ratio of swollen gel mass to the second dried polymer mass (i.e., $W_{Swollen}/W_{Dry,2}$).

Rheometry: In situ photo-rheometry was performed at room temperature on a Bohlin CVO 100 digital rheometer equipped with a light cure cell. A macromer solution (100 µL) was placed on a quartz plate in the light cure cell and irradiated with the visible light

(400-700 nm, 70,000 lux) through a flexible light guide. Light was turned on 30 seconds after starting time-sweep measurement (5 % strain, 1 Hz frequency, and a gap size of 90 μm) using a 25 mm parallel plate geometry. Gel points (i.e., crossover time) were determined at the time when storage modulus (G') surpassed loss modulus (G").

Oscillatory rheometry in strain-sweep mode was used to obtain elastic modulus of the hydrogel. At equilibrium swelling (after 48 hours in pH 7.4 PBS), a biopsy punch was used to punch out circular gel discs (8 mm in diameter) from the gel slabs. Storage moduli of the hydrogels were measured using 8 mm parallel plate geometry with a gap size of 750 μm. The elastic moduli from at least three hydrogels for each gel formulation were recorded from the average of the linear viscoelastic region (LVR, linear portion of G' plotting against % strain).

Thiol and norbornene consumption: Eosin-Y (at 0.1 mM) and various components (i.e., $PEGdNB_{6kDa}$, L-cysteine HCl, and L-tyrosine methyl ester) were dissolved in PBS (pH 7.4) and exposed to visible light (400-700 nm, 70,000 lux). Concentrations of the components were equivalent to those used in gelation studies (final concentration of norbornene and thiol = 12 mM). To determine thiol-consumption, portions of non-gelling solution throughout 5 minutes of light exposure were collected, and the content of the free thiol was immediately assayed with Ellman's reagent buffer. The thiol concentration presented at the specific time was measured against a known standard (i.e., L-cysteine HCl). In a separate experiment, non-gelling precursor solutions (1 mL each) were lyophilized after exposing to light for 5 minutes. ^{1}H NMR was used to evaluate the signature peaks for norbornene (D_2O was used for dissolution). The areas of the norbornene peaks (δ 5.8-6.2 ppm) were obtained and all integrated areas obtained were further compared to the area under the norbornene peaks for pure PEGdNB at the same macromer concentration (Figure 5.5A and Table 5.1). Norbornene consumption was calculated using the difference in the area of the norbornene peaks before and after reaction over that before the reaction.

Spectrophotometric properties: Eosin-Y (at 0.1 mM) and various components (i.e., $PEGdNB_{6kDa}$, L-cysteine HCl, and L-tyrosine methyl ester) were dissolved in PBS (pH 7.4) and exposed to visible light for 5 minutes. Non-gelling components were used (e.g., PEGdNB and L-cysteine) to prevent gelation and to facilitate solution-based UV/Vis spectrometric measurements. Concentrations of the components were equivalent to those used in gelation studies (final concentration of norbornene and thiol = 12 mM). Using a microplate reader (BioTek Synergy HT) in UV/Vis absorption mode (wavelength between 400 and 700 nm at 2 nm increments), the absorbance spectra of the non-gelling solutions were measured before and after the exposure of light. To prevent saturation in absorbance, solution was diluted so the final concentration of eosin-Y is 0.02 mM.

Cell encapsulation and viability: Mouse insulinoma cells (MIN6, final cell density in the gels at 5×10^6 cells/mL) were suspended in polymer solutions containing 0.1 mM eosin-Y, PEG8aNB, and di-cysteine peptide (i.e., Lys-Cys-Tyr-Ile-Gly-Ser-Arg-Cys-Lys or KCYIGSRCK) with and without tyrosine. Precursor solution was exposed to the same visible light for 5 minutes to obtain cell-laden hydrogels (20 μl/gel), which were maintained in high-glucose DMEM supplemented with 10 % fetal bovine serum (FBS), 50 μM β-mercaptoethanol, and 1× antibiotic-antimycotic. Similar procedure was performed to encapsulate isolated CD1 islets. CD1 mice (7- to 8-week old) were obtained from Charles River and islets were isolated following established protocol [125]. Permission for animal studies was approved by Indiana University School of Medicine IACUC (protocol #10235-MD/R). Islets encapsulated gels were maintained in RPMI-1640 media supplemented with 10 % FBS, and 1× antibiotic-antimycotic. To characterize cell viability, cell-laden hydrogels were incubated in 500 μL Almarblue® reagent (10 % in cell culture medium) at 37 ^oC and 5 % of CO_2. After specific hours of incubation (16 hours for MIN6), 200 μl of media were transferred to a 96-well plate for fluorescence quantification (excitation: 560 nm and emission: 590 nm). To obtain qualitative cell viability, cells were stained with a live/dead staining kit (Calcein AM stained live cells green and Edithium homodimer stained dead cells red) and imaged with confocal microscopy (Olympus FV-1000 Laser Scanning Biological Microscope). For

MIN6 encapsulated gels, three images were taken at a step size of 10 μm for a total depth of 100 μm per image. For islets encapsulated gels, images were taken at a step size of 5 μm for a total depth of 50 μm per image.

Insulin secretion from islets: To access glucose stimulated insulin secretion (GSIS), cell-laden hydrogels were rinsed with HBSS, followed by priming in Krebs-Ringer bicarbonate *(*KRB) buffer (23 mM sodium chloride, 1 mM potassium chloride, 4.8 mM sodium bicarbonate, 0.2 mM magnesium chloride hexahydrate, 0.2 mM calcium chloride dehydrate, 0.5 mM 4-(2-hydroxyethyl)-1-piperazineethanesulfonic acid and 0.1 vol% bovine serum albumin) containing 2.5 mM glucose for 1 hour at 37 ^{o}C and 5 % CO_2. Then, the gels were incubated with 500 μL of low (2.5 mM) or high (25 mM) glucose KRB for 2 hours each. The low and high glucose buffer solutions were collected and analyzed using mouse insulin ELISA kit (Mercodia). Cell viability was further quantified by CellTiter Glo® assay (Promega). Insulin secretion obtained from ELISA was normalized by the respective ATP content of the cell-laden hydrogels.

mRNA isolation and rtPCR: In preparation for RNA isolation, cell-laden gels were rapidly frozen using liquid nitrogen and stored in -80 ^{o}C until use. Collected samples were processed following NucleoSpin® RNA protocols (Clontech). The concentrations of pure RNA were determined using NanoDrop 2000 Spectrophotometer (Thermo Scientific). RNA was reverse transcribed into cDNA using PrimeScript^{TM} RT Reagent Kit (Clontech). SYBR Premix Ex Taq II kit (Clontech) was used for quantitative real time PCR (Applied Biosystems 7500 Fast Real-Time PCR machine) for selected genes (Table 5.2). The results for gene of interests were internally normalized by a house keeping gene (i.e., β-actin), and further normalized to control (i.e., gels crosslinked without tyrosine on day 1).

Table 5.2. Mouse primer sequences used in real time PCR.

Gene Symbol	Primer Sequence	Reference
Actβ	TGAGAGGGAAATCGTGCGTG	[205]
	TGCTTGCTGATCCACATCTGC	
Ins	TGGCTTCTTCTACACACCCAAG	[206]
	ACAATGCCACGCTTCTGCC	
Pdx1	CGGACATCTCCCCATACGAAG	[207]
	CCCCAGTCTCGGTTCCATTC	

Data analysis: All experiments were conducted independently for three times and results were reported as mean ± SD. Data was analyzed with student's t-test using GraphPad Prism 5 ($p < 0.05$).

5.5. Conclusion

In summary, we have synthesized visible light mediated step-growth thiol-norbornene photopolymerized hydrogel using multi-arm PEGNB and di-cysteine containing peptides. We found that thiol-norbornene hydrogels crosslinked in the presence of soluble tyrosine exhibited faster gelation kinetics and higher crosslinking efficiency. Furthermore, the network crosslinking depended highly on the amount of tyrosine, concentration of macromer and the ratio of norbornene to thiol used. In addition, a series of cell viability tests revealed that hydrogels crosslinked in the presence of tyrosine preserved the viability and insulin secreting function of pancreatic β-cells and mouse islets. Together, this data show that PEG-peptide hydrogels formed by visible light mediated thiol-ene polymerization should be of great interest for drug delivery and tissue engineering applications.

CHAPTER 6
TUNING STIFFNESS OF CELL-LADEN HYDROGEL VIA HOST-GUEST INTERACTIONS

6.1 Abstract

We report a dynamic hydrogel system with on-demand tunable matrix stiffness. The hydrogels are formed by thiol-allylether photo-click reaction using thiolated poly(vinyl alcohol) (TPVA), 4-arm poly(ethylene glycol)-allylether (PEG4AE), and mono-functional β-cyclodextrin-allylether (βCDAE). Adamantane-functionalized 4-arm PEG (PEG4AD) is used to stiffen hydrogels, whereas unmodified βCD is used to induce gel softening. The stiffening and softening processes are fully reversible and these hydrogels are ideal for investigating the effect of matrix mechanics on cell fate processes.

6.2 Introduction

Dynamic cell-laden hydrogels are increasingly developed for studying the influence of matrix mechanics on cell fate processes [208]. For example, stiffness of a cell-laden hydrogel could be irreversibly decreased through user-controlled or cell-mediated matrix degradation [62, 209-211]. On the other hand, the crosslinking density of some hydrogels could be increased irreversibly by applying secondary photo-crosslinking in the presence of the primary cell-laden hydrogel network [212, 213]. One common feature of the aforementioned strategies is that the changes in matrix mechanics are irreversible, hence these matrices might not be ideal for studying the impact of

---

Chaper 6 here is as appeared in H. Shih and C. Lin, *Journal of Materials Chemistry B*, 2016, DOI: 10.1039/C6TB00890A

dynamic matrix stiffening on cellular mechanobiology [214, 215]. Here, we report a dynamic cell-laden hydrogel platform with post-gelation tunability in matrix stiffness, which is achieved by providing reversible host-guest interactions within the cell-laden hydrogel network. The hydrogels are prepared by a single step light-mediated thiol-allylether photo-click reaction using thiolated poly(vinyl alcohol) (TPVA), 4-arm poly(ethylene glycol)-allylether (PEG4AE), and β-cyclodextrin-allylether (βCDAE). The thiol-allylether photo-click gelation is compatible with *in situ* cell encapsulation and the stiffness of the hydrogel are tuned through non-covalent host-guest interactions between network-immobilized βCD and soluble 4-arm PEG-adamantane (PEG4AD) supplied on demand. The stiffening/softening processes are fully reversible by means of incubating gels in PEG4AD and βCD solutions, respectively. More importantly, the magnitude of the stiffness change can be tuned from several hundreds to a few kilo-Pascals, a range relevant to many cell fate processes [216].

The influence of matrix biomechanical properties on cell fate has been intensively studied in the past decade [214, 217-221]. In particular, the differentiation of mesenchymal stem cells (MSC) has been shown to depend on substrate stiffness [153, 216, 217, 222]. Furthermore, mechanical properties of tissues have been implicated in invasion and drug resistance of cancer cells [214, 215, 223-225], as well as in myofibroblastic activation of hepatic stellate cells and valvular interstitial cells [68, 226-228]. It is commonly accepted that a cell culture matrix should present relevant mechanical properties for maintaining appropriate cell phenotype [163, 229], and the ultra-stiff tissue culture plastics (TCP) fail to provide such a physiologically relevant context. On the other hand, commercially available three-dimensional (3D) cell culture matrices are mechanically unstable and with limited tunability in stiffness post-gelation [230]. In view of the challenges facing these cell culture platforms, the past decade has witnessed increasing interests in 3D cell culture matrices with tailor-made and dynamically tunable biophysical and biochemical properties [231, 232]. To affect cell fate processes in 3D, synthetic polymeric cell-laden hydrogels can be designed to undergo different modes of degradation, including hydrolytic, enzymatic, or photolytic degradation [62, 209-211]. Hydrogels can also be hardened through secondary radical-

mediated chain-growth or step-growth photopolymerizations [212, 213]. For example, the presence of excess unreacted vinyl groups in the primary hydrogel network permits additional crosslinking reactions for network stiffening [212, 213]. Although this approach readily increases hydrogel crosslinking density and stiffness, additional radicals formed during secondary photocrosslinking might be a confounding factor. While these dynamic material systems have demonstrated improvements over the conventional static cell culture systems, the stiffness of these hydrogels can only be decreased or increased irreversibly.

A hydrogel system with reversibly tunable matrix crosslinking and stiffness should be highly desirable in the study of cellular mechanobiology. An approach suitable for achieving reversible matrix crosslinking is the supramolecular host-guest interactions, which have been used extensively to enhance solubility of hydrophobic drugs and to design self-healing polymers [233-235]. For example, the hydrophobic cavity of macrocyclic molecules (e.g., CD, and cucurbit[8]uril) can reversibly bind to a variety of hydrophobic drug molecules (e.g., curcumin, paclitaxel, doxorubicin, etc.) [235-239]. In another example, light-responsive supramolecular hydrogels formed from azobenzene-functionalized hyaluronan (Azo-HA) and CD-functionalized polymers were used to encapsulate proteins and cells when Azo is in *trans* conformation, which permits CD/Azo complexation and network formation [240, 241]. Upon light exposure, Azo undergoes *trans*-to-*cis* isomerization, resulted in the disruption of CD/Azo complexes and the liberation of proteins and cells [240, 241]. Supramolecular ’host-guest‘ interactions between adamantane (AD) and CD have also been exploited for forming cell-laden hydrogels exhibiting injectable and shear-thinning properties [242-245]. To the best of our knowledge, however, supramolecular chemistry and host-guest interactions have not been exploited to induce reversible post-gelation hydrogel stiffening and/or softening in the presence of cells.

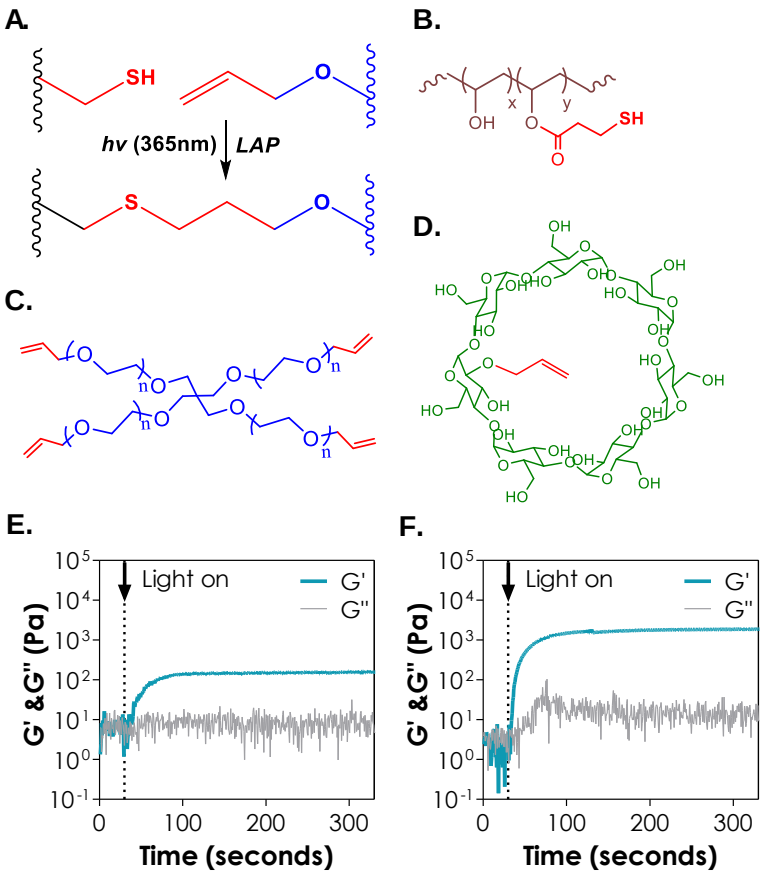

Figure 6.1. **(**A**)** Schematics of thiol-allylether photo-click reaction using photoinitiator LAP and long-wave ultraviolet light exposure (365 nm, 10 mW/cm^2). (B-D) Chemical structures of the major macromers used, including TPVA (B), PEG4AE (C), and βCDAE (D).

Here, we report the design of cell-laden hydrogels with reversibly tunable stiffness by means of non-covalent and reversible host-guest interactions between pendant βCD and soluble PEG4AD. The primary hydrogel network was prepared from thiol-allylether photopolymerization (Figure 6.1A) using TPVA (Figure 6.1B) and PEG4AE (Figure 6.1C) as the macromolecular crosslinkers. βCD-allylether (βCDAE, Figure 6.1D) was co-polymerized in the primary hydrogel network as pendant 'host' motifs that can form additional physical crosslinks in the presence of soluble PEG4AD. Thiol-allylether photopolymerization was used to create the primary hydrogel network due to its orthogonal crosslinking, as well as its facile and quantitative immobilization of pendant βCD. Through supramolecular host-guest interactions, chemically immobilized

'host' molecules (i.e., βCDAE, Figures 6.1D and 6.2) interact with user-supplied 'guest' macromolecules (i.e., PEG4AD), resulting in increased hydrogel crosslinking density and elastic modulus. When needed, this 'stiffened' hydrogel can be 'softened' thermodynamically or through competitive binding provided by soluble βCDs. In principle, the process of hydrogel stiffening or softening can be repeated indefinitely if no other degradation mechanism exists.

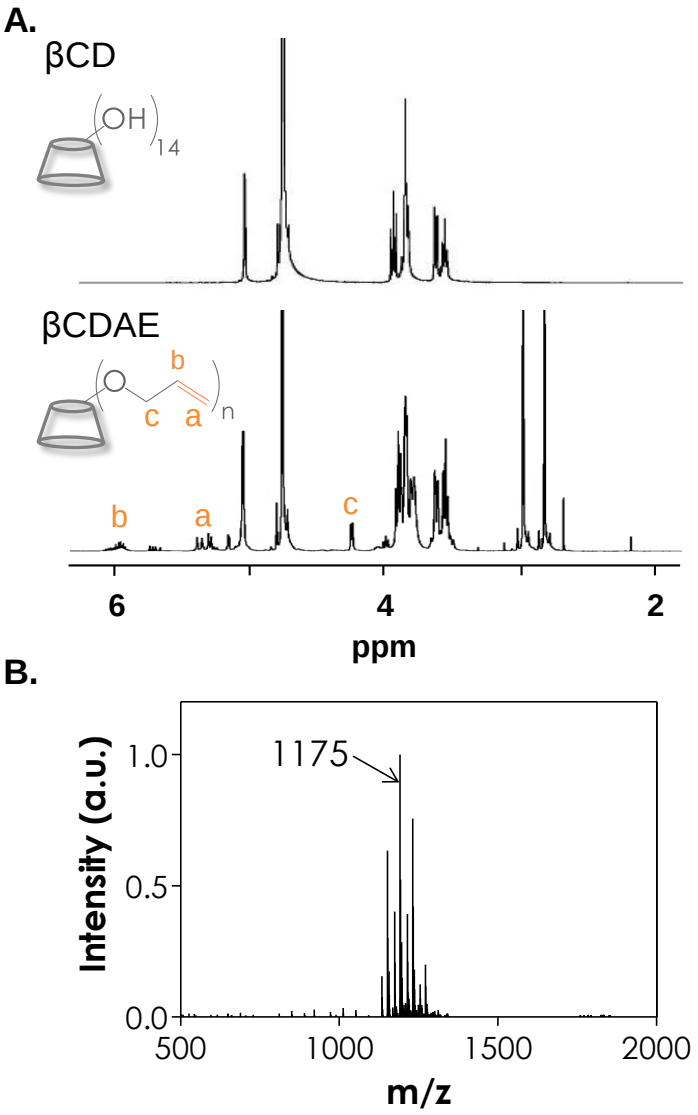

Figure 6.2. (A) ^{1}H NMR of βCD (top), and βCD-AE (bottom). Prepared with D_2O (at 4.79 ppm). (B) Mass spectroscopy of βCDAE.

6.3 Results and Discussion

To demonstrate the efficient crosslinking of orthogonal thiol-allylether hydrogels, we conducted *in situ* photorheometry using TPVA and PEG4AE in the absence (Figure 6.1E) or presence of βCDAE (Figure 6.1F). After the light was switched on, the thiol-allylether (TPVA-PEGAE) gelation occurred very rapidly (gel point: ~3 seconds) and the time required to reach 95% of ultimate stiffness was only ~2 minutes. The addition of βCDAE in the precursor solution led to a higher ultimate gel elastic modulus (G' ~ 2.4 kPa) and higher gel fraction (Figure 6.3A). One potential explanation for the higher initial gel stiffness in the presence of βCDAE (Figure 6.1F) is that some βCDAE might have more than two allylether motifs that contribute to additional crosslinking (Figure 6.2B). Another potential is that immobilized bulky βCDAE decreased chain flexibility of linear TPVA, thereby increasing hydrogel stiffness. It is worth noting that, compared with similar light-mediated step-growth gelation using PEG-thiol and PEG-allylether, the gelation using TPVA and PEG4AE was faster and with the use of a significantly lower macromer contents (i.e., 1.6 wt% of PEG4AE with 2.5 wt% TPVA) [150, 246]. This is likely due to the use of multi-functional TPVA (~10 thiol groups per molecule of PVA_{6kDa}). Overall, the use of efficient thiol-allylether photoclick reaction produces a stable βCD-immobilized hydrogel network for subsequent evaluation of hydrogel stiffening/softening using soluble PEG4AD macromers.

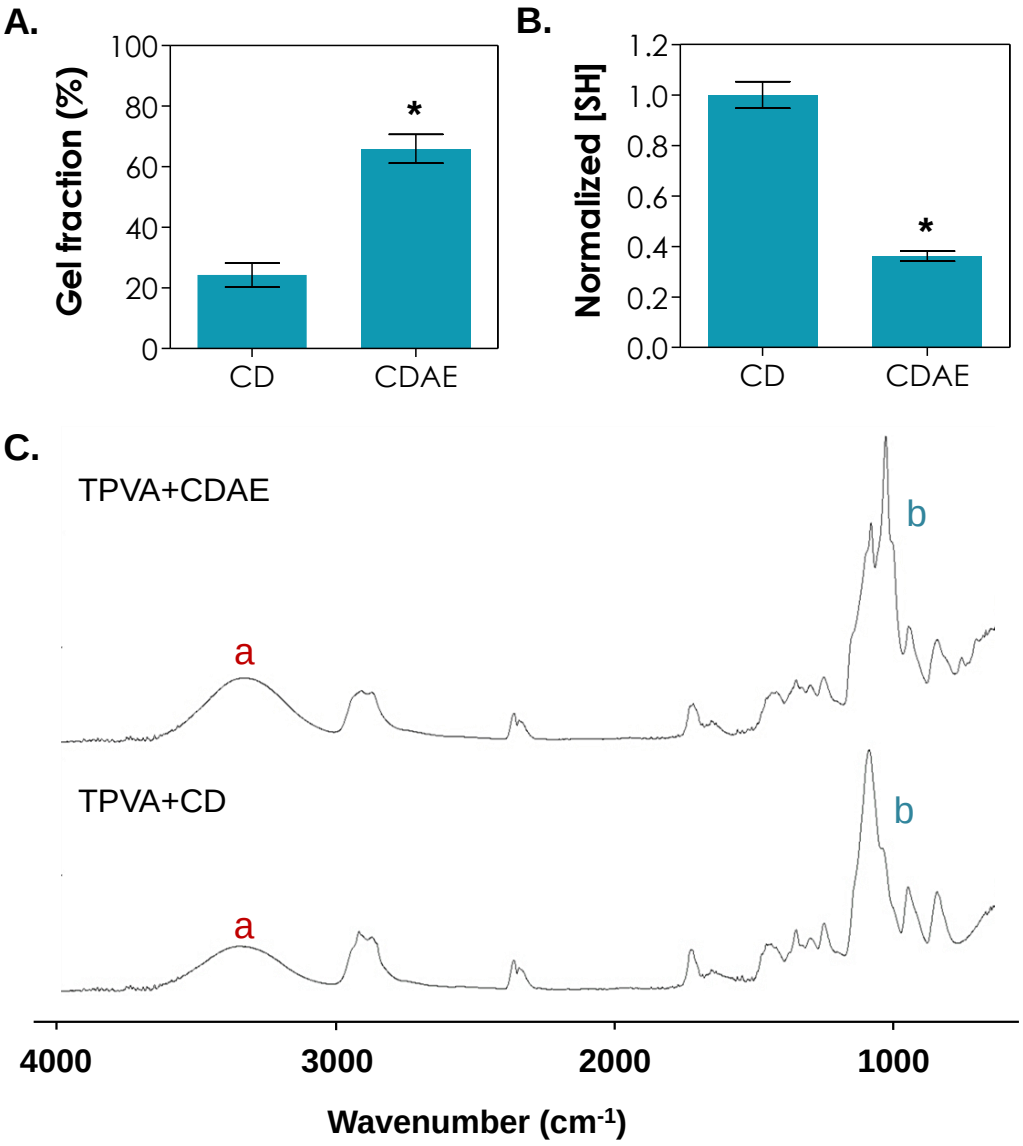

	Wavenumber (cm^{-1})	TPVA + CD	TPVA + CDAE
a	3700-3000	27.3 ± 1.5	39.8 ± 0.8
b	1050-970	0.4 ± 0.1	13.5 ± 0.5

Figure 6.3. Estimation of βCD-immobilization post-gelation: (A) gel fraction; (B) normalized thiol concentration measured by Ellman's assay; and (C) ATR-FTIR characterization. 2.5 wt% TPVA at 0.8 mM PEG4AE and 27.6 mM βCDAE ($R_{[allylether]/[thiol]}$ = 0.8) or βCD in the precursor solution (1 mM LAP, 365nm light at 10 mW/cm^2).

To ensure that βCDAE was successfully immobilized within the TPVA-PEG4AE hydrogel network, we prepared hydrogels using off-stoichiometric ratio of allylether to thiol (i.e., $R_{[allylether]/[thiol]}$ = 0.8). When compared with gelation using unmodified βCD, significantly lower free thiol was detected in the presence of βCDAE, indicative of βCDAE immobilization in the primary hydrogel network post-gelation (Figure 6.3B). ATR-FTIR characterization results also confirmed the immobilization of βCDAE in the thiol-allylether hydrogel network (1.5-fold and 34-fold increase in the areas under alcohol and carbonyl peaks, respectively. Figure 6.3C). We also conducted additional *in situ* photorheometry experiments to show that the gelation was indeed due to orthogonal thiol-allylether reaction between TPVA and PEG4AE and not a result of homopolymerization of allylether-macromers (i.e., βCDAE and PEG4AE, Figure 6.4A) or supramolecular 'threading' of βCDAE/TPVA or βCDAE/PEG4AE (Figure 6.4B). Another affirmation that βCD/PVA threading did not occur in this thiol-allylether gelation system (completing within 5 minutes) is that the threading events are typically achieved under extreme conditions such as high temperature (e.g., 90 °C), high βCD concentration (e.g., 70 wt%) or long incubation time (e.g., 2-72 hours) [247-250].

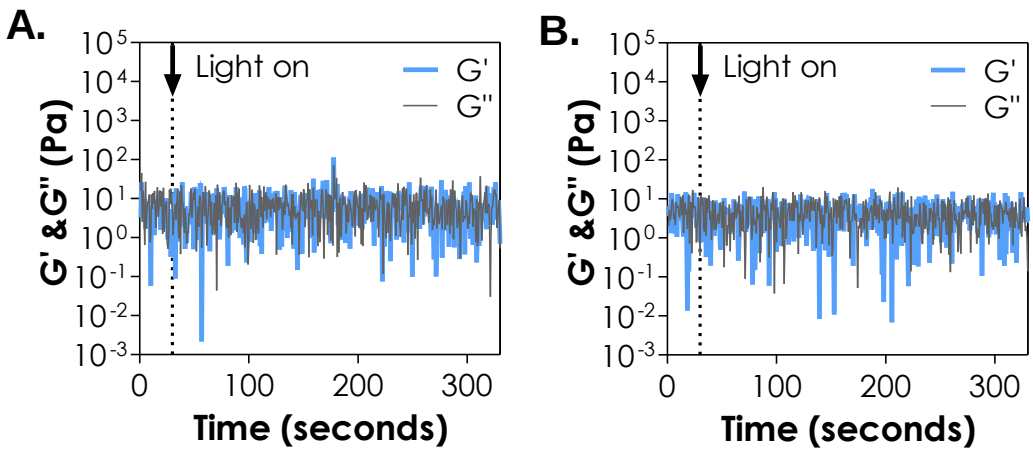

Figure 6.4. *In situ* photorheometry showing storage modulus (G') and loss modulus (G") of thiol-allylether photopolymerization (A) at 2.5wt% TPVA and 27.6 mM βCDAE; and (B) at 0.8 mM PEG4AE and 27.6 mM βCDAE in the precursor solution (1 mM LAP, 365nm light at 10 mW/cm^2). Light was turned on at 30 seconds (dotted line).

We hypothesized that the reversible association and dissociation between network-immobilized βCD and soluble multi-functional PEG4AD (MW: 10kDa) macromer (Figures 6.5A) could increase the crosslinking density, and hence elastic modulus, of this hydrogel [235, 251]. We first investigated the tunability of hydrogel stiffness by incubating βCD-immobilized hydrogels in solution containing PEG4AD (Figure 6.5B) at different concentrations. Since these thiol-allylether hydrogels were stiffened via host-guest supramolecular assembly, the amount of soluble PEG4AD supplemented to the βCD-immobilized hydrogels would affect the extent of host-guest interactions, and hence the degree of stiffening (Figure 6.5C). As expected, hydrogel stiffness increased from 1.6- to 2-fold when the concentration of PEG4AD was increased from 2.5 wt% (i.e., 10mM AD) to 5 wt% (i.e., 20mM AD) (Figure 6.5D). However, further increasing PEG4AD content to 10 wt% (i.e., 40mM AD) did not yield an even higher degree of stiffening because the concentration of AD at this condition exceeded the total βCD concentration (i.e., 27.6mM). As a result, additional PEG4AD became 'pendant' and did not contribute to the formation of additional crosslinking. We further evaluated the stiffening effect using TPVA-PEG4AE hydrogels with different initial gel stiffness. At a fixed TPVA content (2.5 wt%), increasing PEG4AE concentration yielded hydrogels with higher initial elastic modulus (Figure 6.5E, 0.9 kPa to 4 kPa for 0.6 mM to 1.1 mM of PEG4AE, respectively). These hydrogels were separately stiffened using PEG4AD solution. Regardless of the starting equilibrium shear modulus, the stiffening process yielded hydrogels with significantly increased final elastic moduli (Figure 6.5E, 2.3 kPa to 6.5 kPa). To evaluate the elastic nature of these hydrogels, we conducted frequency sweep oscillatory rheometry after incubating gels in the absence (Figure 6.6A) or presence (Figure 6.6B) of soluble PEG4AD. Results show that gel storage modulus (G') dominated loss modulus (G") over the range of frequency tested, indicating the elastic property of the thiol-allylether hydrogels pre- and post-incubation with PEG4AD.

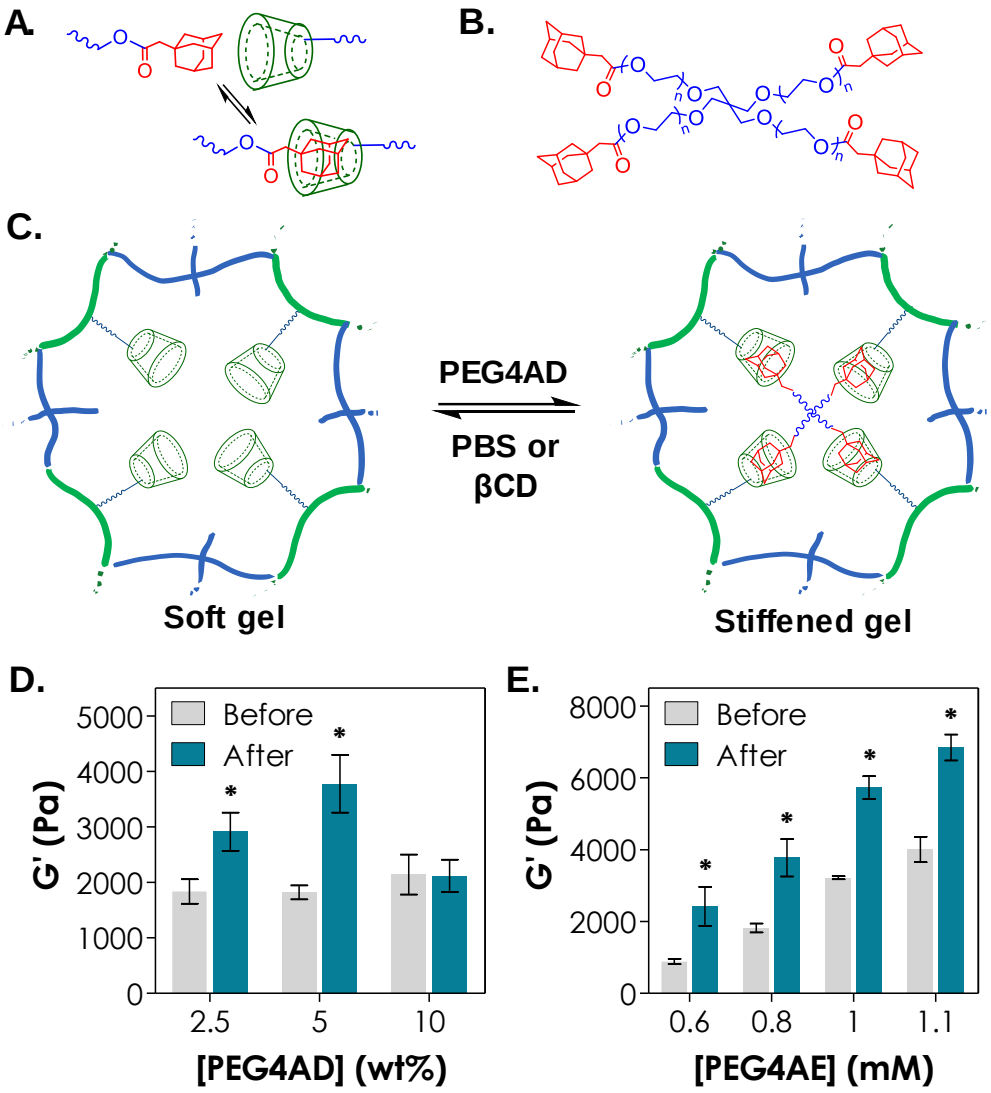

Figure 6.5. (A) Schematic of a reversible βCD/AD complex. (B) Chemical structure of PEG4AD. (C) *In situ* stiffening of hydrogel through incubating βCD-containing gel in PEG4AD solution. Gel softening could be achieved by incubating the stiffened gel in PBS or solution containing unmodified βCD. (D) *In situ* stiffening using PEG4AD (10 kDa) at different concentration. (E) Tuning the initial stiffness and dynamic stiffening of hydrogels through adjusting the content of PEG4AE in the pre-polymer solution. (Mean ± SD, N = 3, * indicates $p<0.05$).

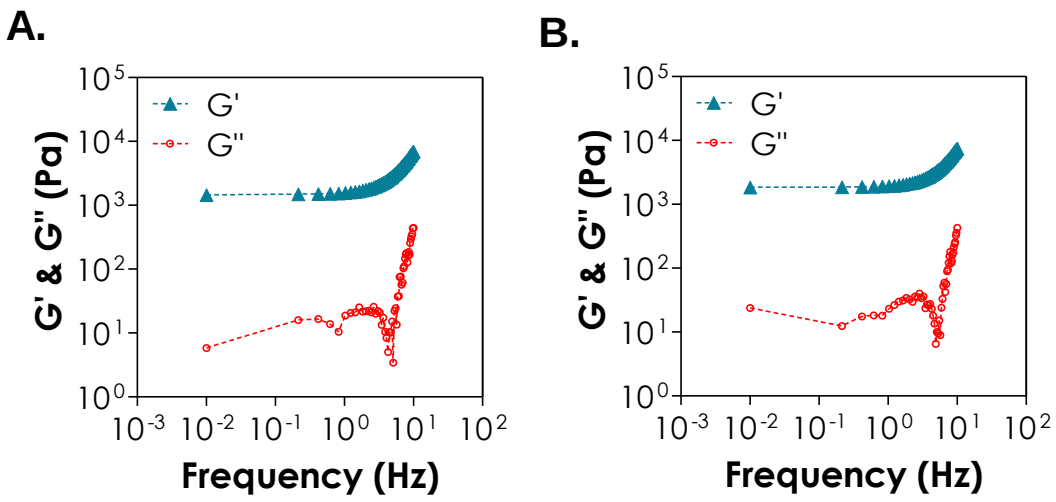

Figure 6.6. Frequency sweep rheometry of thiol-allylether hydrogels before (A), and after (B) incubating in PEG4AD. Error bars omitted for clarity.

Although results so far show that the range of elastic moduli of hydrogels before and after PEG4AD-stiffening could be tuned in a physiologically relevant range (i.e., elastic moduli ranging from 0.03 to 6 kPa) [216], it is necessary to determine the long-term stability of the *in situ* stiffened hydrogels. As shown in Figure 6.7A, PEG4AD-induced gel stiffening (from ~2 to 3.5 kPa) could be maintained for more than one month as long as the βCD-immobilized hydrogels were incubated in PEG4AD-containing solution. After one month, the moduli of PEG4AD-stiffened gels started to decrease, which could be attributed to the hydrolysis of ester bonds in PEG4AD macromers (Figure 6.5B). In a separate group where the stiffened hydrogels were transferred back to PBS following *in situ* stiffening, elastic moduli of the stiffened hydrogel decreased gradually (Figure 6.7A, from 3.5 to 2.2 kPa in 48 days), most likely a result of the thermal relaxation of the host-guest interaction. Control experiments show that hydrogels incubated in either 4-arm PEG or PBS solution had minimal change in stiffness throughout the study, suggesting that the specificity of βCD/AD binding is essential in the stiffening of the hydrogels.

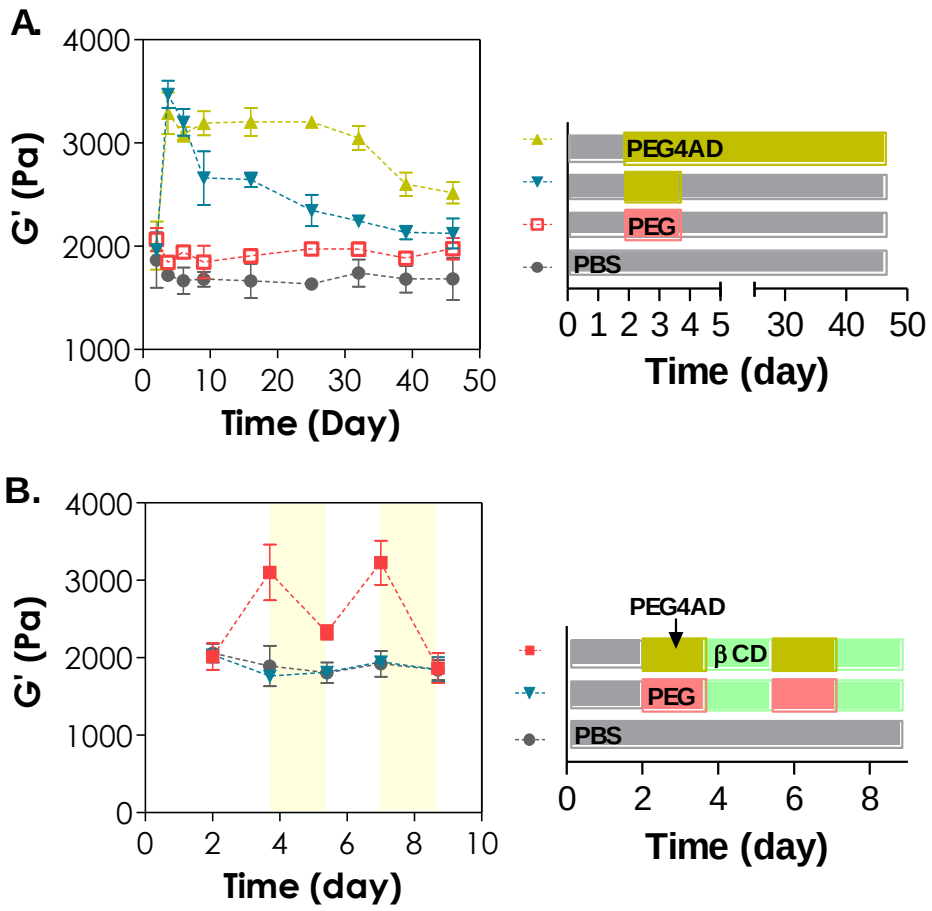

Figure 6.7. (A) Effect of gel treatment conditions on the elastic modulus of thiol-allylether hydrogel. Right panel: timeline for the treatments of hydrogels. (B) Reversibly tuning the elastic moduli of thiol-allylether hydrogel. 5 wt% of PEG4AD (10 kDa) and 5 wt% of 4-arm PEG (10 kDa), respectively. Right panel: timeline for the treatments of hydrogels (2.5 wt% TPVA, 0.8 mM PEG4AE and 27.6 mM βCDAE, Mean ± SD, N = 3, * indicates $p<0.05$).

βCD/AD interactions are non-covalent, reversible, and can be disrupted through thermal relaxation or through a competitive kinetic binding process. We have demonstrated that PEG4AD-stiffened gels took weeks to soften when placed in PBS (Figure 6.7A). This softening effect could be attributed to the dissociation and removal of PEG4AD from pendant βCD over time. Alternatively, a faster gel softening could be achieved by incubating the PEG4AD-stiffened hydrogels in solution containing unmodified βCD. Soluble βCD competes with PEG4AD for binding to immobilized βCD. As a result, the elastic moduli of PEG4AD-stiffened hydrogels incubated in βCD

solution decreased from 3.1 to 2.3 kPa within 40 hours (Figure 6.7B). When the *in situ* softened hydrogels were incubated in PEG4AD solution for another 40 hours, the hydrogels were stiffened again and the process of stiffening/softening was repeatable (Figure 6.7B). For gels incubated in either PBS or 4-arm PEG/βCD, the stiffness remained steady throughout the study (Figure 6.7B).

Comparing to other hydrogels with stiffening or softening potential [62, 209-213], our dynamic thiol-allylether hydrogel offers a wider range of stiffness tunability (i.e., from hundreds to thousands Pascals). For example, Rosales *et al.* prepared step-growth Michael-type hydrogels crosslinked with azobenzene-modified peptides that undergo *trans*-to-*cis* isomerization upon UV/visible light exposure [252]. The conformational change in azobenzene-containing peptide leads to changes in crosslinker length, and hence gel stiffness was controlled depending on light irradiation conditions. However, the magnitude of the elastic modulus change reported was about 100-200 Pa. Another difference between our approach and the light-responsive azobenzene-modified hydrogel or the secondary photo-crosslinking system was that the stiffening/softening of thiol-allylether hydrogels is a more gradual process (i.e., hours in our system vs. minutes in previous stiffening processes) that should be more relevant to the time scale of most cell fate processes [212].

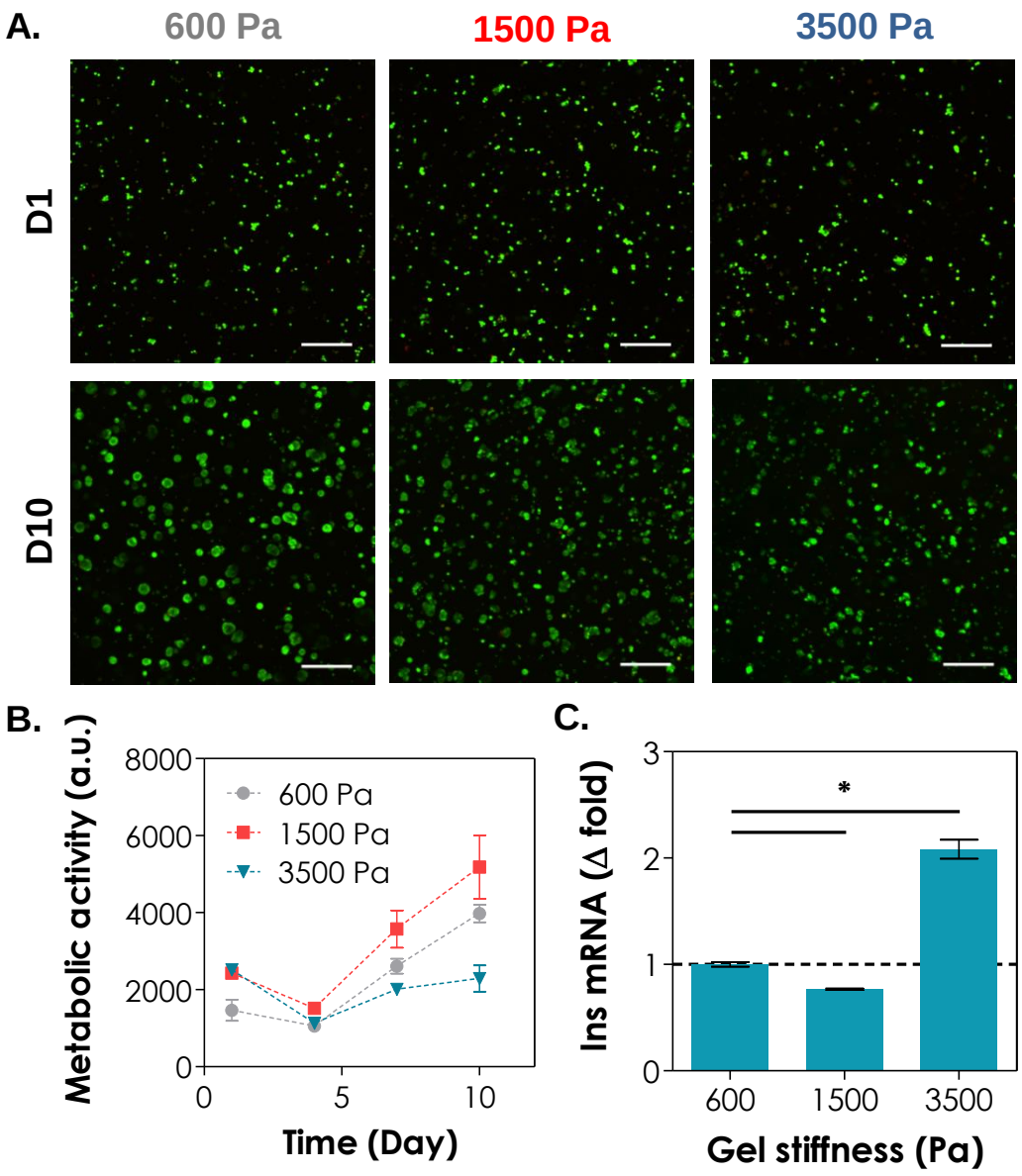

Figure 6.8. Effect of thiol-allylether hydrogel stiffness on the cytocompatibility of MIN6 β-cells. (A) Representative confocal z-stack images of MIN6 cells stained with live/dead staining kit on day 1 and day 10. MIN6 cells were encapsulated (2×10^6 cells/mL) in thiol-allylether hydrogels. (B) Cells viability as assessed by Alamarblue® reagent. (C) Normalized insulin mRNA expression on day 10. All gel formulations contained β-cells at 2×10^6 cells/mL, 2.5wt% TPVA, 0.6/0.8/1mM PEG4AE and 27.6 mM βCDAE, 1 mM LAP, and 365 nm light at 5 mW/cm^2 (Scales: 200 μm).

To evaluate the cytocompatibility of this dynamic thiol-allylether hydrogel system, we performed *in situ* encapsulation of pancreatic MIN6 β-cells at a relatively low

cell density (2×10^6 cells/mL). This cell density was used because a previous work has shown that MIN6 cells encapsulated in radical-mediated chain-growth photopolymerized PEG-diacrylate hydrogels did not survive well if the cell density was below 5×10^6 cells/mL [149]. We found that the step-growth thiol-allylether polymerization is highly cytocompatible for MIN6 β-cells as the encapsulated cells were viable regardless of the initial gel elastic modulus (0.6, 1.5 or 3.5 kPa, Figure 6.8A) [52, 246]. Furthermore, the encapsulated cells all formed multi-cell spheroids after 10 days of culture. While higher metabolic activity was detected in cells encapsulated in softer gel at day-10 post-encapsulation (Figure 6.8B), insulin mRNA level was lower in these cells (Figure 6.8C). Specifically, insulin expression was ~1.7-fold and 3.5-fold for soft and stiff gel, respectively (1-fold: insulin expression in cells encapsulated in 0.6 kPa gels). Another interesting phenomenon is that the sizes of cell spheroids formed within the stiffer hydrogels were noticeably smaller than those formed in the softer hydrogels, most likely because the stiffer hydrogels have higher crosslinking density that restricts the growth of the cell spheroids. The difference in cell spheroid sizes might be another confounding factor affecting insulin expression.

The higher insulin expression from cells encapsulated in stiffer hydrogel does not concord with a previous study conducted by Desai and colleagues, who cultured MIN6 β-cells using polymeric microwells with various moduli [163]. The conclusion from that study was that softer microwells promoted insulin expression in MIN6 β-cells and isolated islets. The discrepancy between current study and the reported results was likely due to the difference in cell-matrix interactions, because microwell does not provide uniform matrix contact for the cells. Furthermore, the function of β-cells in static thiol-allylether hydrogels might be affected by different amounts of radicals formed during cell encapsulation, different gel elastic moduli post-gelation, and/or different cell spheroids sizes.

Using the thiol-allylether dynamic hydrogel system, it is possible to study the influence of gel stiffness on cell fate without introducing additional radicals post cell encapsulation and without the confounding factor of cell spheroid sizes. Here, we encapsulated MIN6 β-cells in βCD-immobilized thiol-allylether hydrogels and cultured

the cells for 5 days to allow the formation of multi-cell spheroids (Figure 6.11A, condition ii). After *in situ* gel stiffening (Figure 6.9, from 1.8 kPa to 2.5 kPa), the viability of cells was evaluated using live/dead staining. Compared to cell-laden gels that did not undergo stiffening, cells encapsulated in PEG4AD stiffened gels had slightly more cell death as revealed by the confocal images of live/dead stained MIN6 β-cells (Figure 6.11A). Quantitative ATP assay showed a reduction (not statistically significant) in total intracellular ATP when cell-laden hydrogels were subjected to PEG4AD (Figure 6.11B, ~250 and 220 pmol of ATP/gel with and without exposure to PEG4AD, respectively). Since the concentration of PEG4AD selected was within the non-cytotoxic range (Figure 6.10A) and cells remained viable post-stiffening (Figure 6.11A), it is highly plausible that the increased gel stiffness altered intracellular metabolism/signalling that led to a lower intracellular ATP content. More interestingly, MIN6 β-cells encapsulated in PEG4AD-stiffened gels had a 1.5-fold higher insulin mRNA level when compared with cells encapsulated in gels that did not undergo stiffening process (Figure 6.11C). Results from control experiments show that PEG or PEG4AD did not induce up-regulation of insulin mRNA (Figure 6.10B). The effect of softening on cell fate was evaluated by incubating PEG4AD-stiffened gels in media containing βCD for 3 days (Figure 6.9). Compared to control gels that were not exposed to PEG4AD or βCD (Figure 6.11A, condition iii), MIN6 cells encapsulated in hydrogel that underwent stiffening/softening had similar viability (Figure 6.11A, condition iv) and ATP content (Figure 6.11B, ~180 pmol/gel). More importantly, there was a reduction in insulin mRNA expression after *in situ* softening (Figure 6.11C, from 1.5 to 1.2-fold for condition (ii) and (iv), respectively), suggesting that the effect of matrix mechanics on insulin expression can be reversed upon softening of the hydrogel matrix.

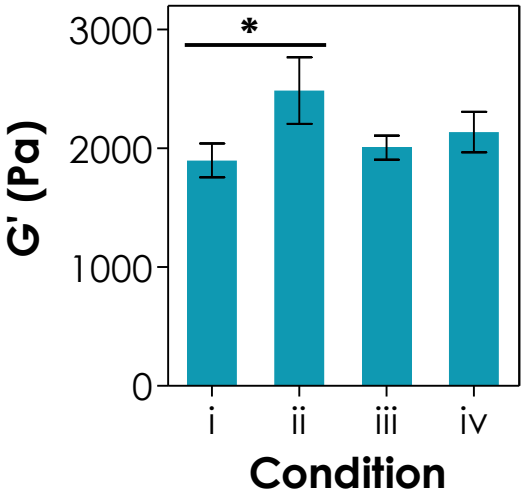

Figure 6.9. Effect of PEG4AD and βCD on the stiffening and softening of thiol-allylether hydrogel via CD-AD interactions. All gel formulations contained 2×10^6 cells/mL β-cells, 2.5 wt% TPVA, 0.8 mM PEG4AE and 27.6 mM βCDAE, 1 mM LAP, and 365 nm light at 10 mW/cm^2 (N = 3).

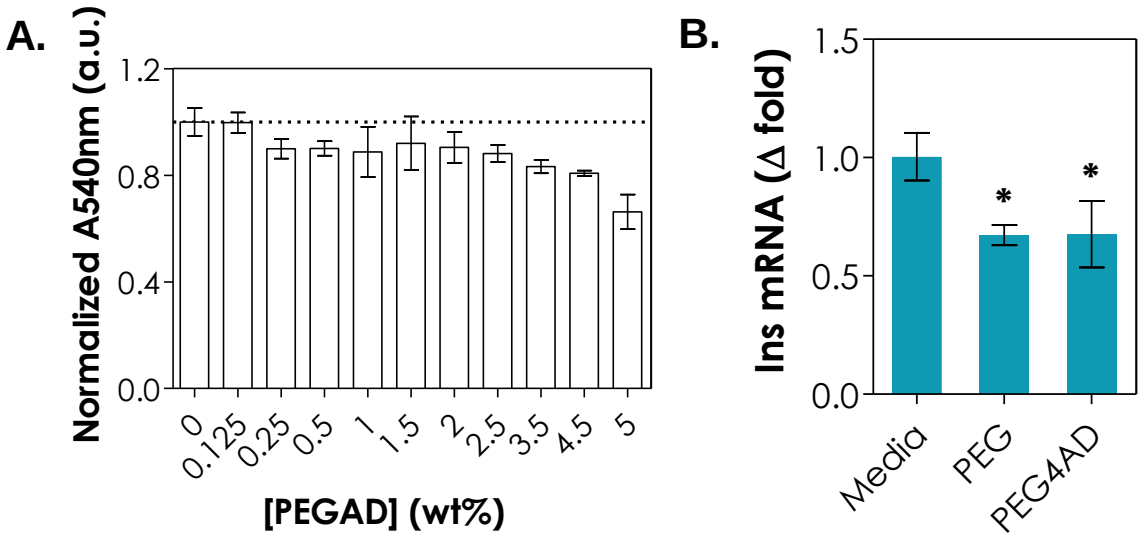

Figure 6.10. (A) Effect of PEGAD on the cytocompatibility of MIN6 β-cells. Cells viability as assessed by MTT. PEGAD (10 kda) was used. (B) Effect of PEG4AD (10 kDa) on the Ins mRNA expression. Cells were all cultured on 2D TCP.

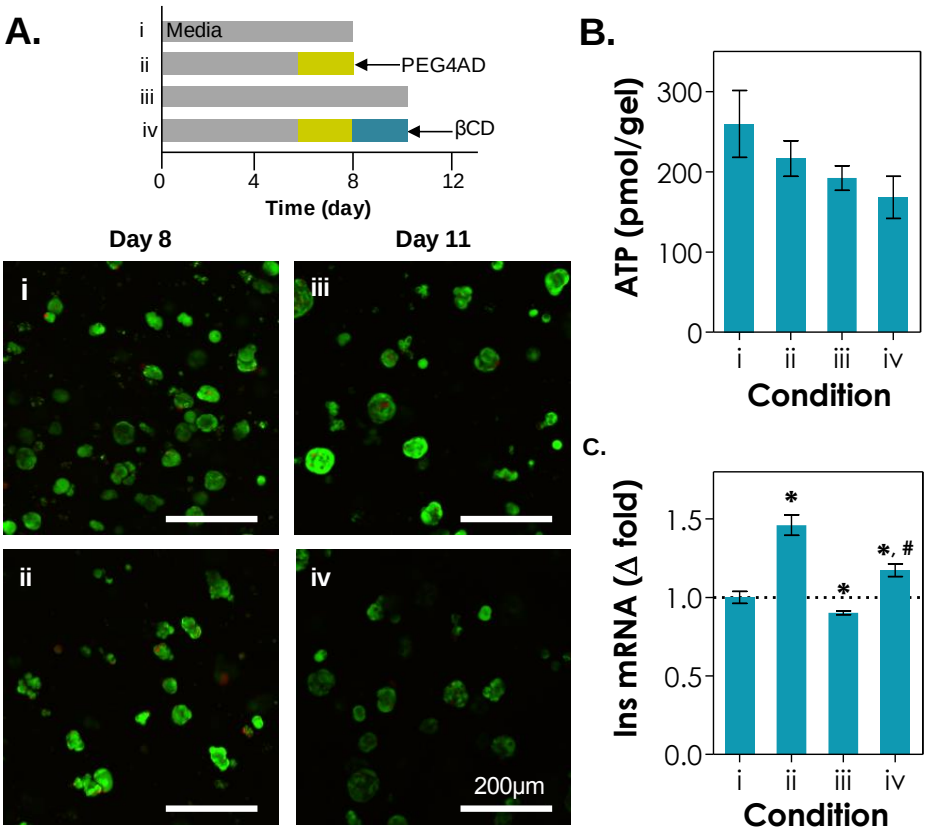

Figure 6.11. Effect of PEG4AD stiffening and βCD softening on the cytocompatibility and functions of MIN6 β-cells. (A) Representative confocal z-stack images of MIN6 cells stained with live/dead staining kit on day 8 with or without PEG4AD stiffening (i & ii) and on day 11 with or without βCD softening (iii & iv). (B) Cells viability as assessed by CellTiter Glo® reagent. (C) Insulin mRNA expression was normalized to condition (i). All gel formulations contained 2.5 wt% TPVA, 0.8 mM PEG4AE and 27.6 mM βCDAE, 1 mM LAP, 2×10^6 cells/mL, and 365 nm light at 5 mW/cm^2 (Scales: 200 μm). Mean ± SD, N = 3, * or $^{\#}$ indicate $p<0.05$ compared to condition i and iii, respectively.

Since the stiffening and softening of cell-laden thiol-allylether hydrogel did not introduce additional radicals and did not change the size of cell spheroids significantly, it is indicative that the insulin expression was affected in large part due to matrix stiffness. We hypothesize that the up-regulation of insulin in cells encapsulated in stiffened hydrogels was a collective result of altered cell-cell interactions [253-255], hypoxia-related gene expression [256, 257], or stiffness-induced mechanotransduction in the cells. In the stiffened gels, tighter gel networks might constrain the encapsulated cells to make close contact with their neighboring cells. Furthermore, the stiffened matrix may alter

other molecular targets downstream of mechanosensing pathways. While further investigations are required to elucidate the molecular mechanisms by which matrix stiffness affects mechanotransduction in cells encapsulated in this dynamic hydrogel, the current work demonstrates the concept and potential of using supramolecular host-guest interactions to tune matrix stiffness in cell-laden hydrogels.

6.4 Materials and Methods

Materials: 4-arm PEG-OH (10 and 20 kDa) was purchased from JenKem Technology USA. Poly(vinyl alcohol) (PVA, 6 kDa), 3-mercaptopropionic acid (MPA), βCD, 1-adamantaneacetic acid and all other chemicals were obtained from Fisher Scientific unless noted otherwise.

Synthesis of βCDAE, LAP, TPVA and PEG macromers: Poly(ethylene glycol)-tetra-allylether (PEG4AE, 20 kDa), poly(ethylene glycol)-adamantane (PEG4AD, 10 kDa), allylether functionalized βCD (βCDAE),[246] and photoinitiator lithium acylphosphinate (LAP) were synthesized using established protocols without modifications.[38] Functionalized βCDAE was analyzed with ^{1}H NMR (Figure 6.2A) and mass spectrometry (Agilent Technologies 6520 Accurate-Mass Q-TOF LC/MS, Figure 6.2B). TPVA was synthesized followed established protocol with modified purification method.[258, 259] Briefly, mixture of hydrochloric acid (5 ml, 12 N) and MPA (25 mL) was added slowly into PVA (5 g) pre-dissolved in 50 mL ddH_2O at 60 ^{o}C. After 24 hours of reaction (60 ^{o}C), the product was transferred to a dialysis bag (MWCO: 3600 Da, Spectrum lab) and dialyzed for 3 days in slightly acidic ddH_2O (pH 6.5). The TPVA product was recovered and lyophilized. The degree of thiolation was quantified by Ellman's assay to be about 16 mM of thiol per wt% of TPVA (Figure 6.12).

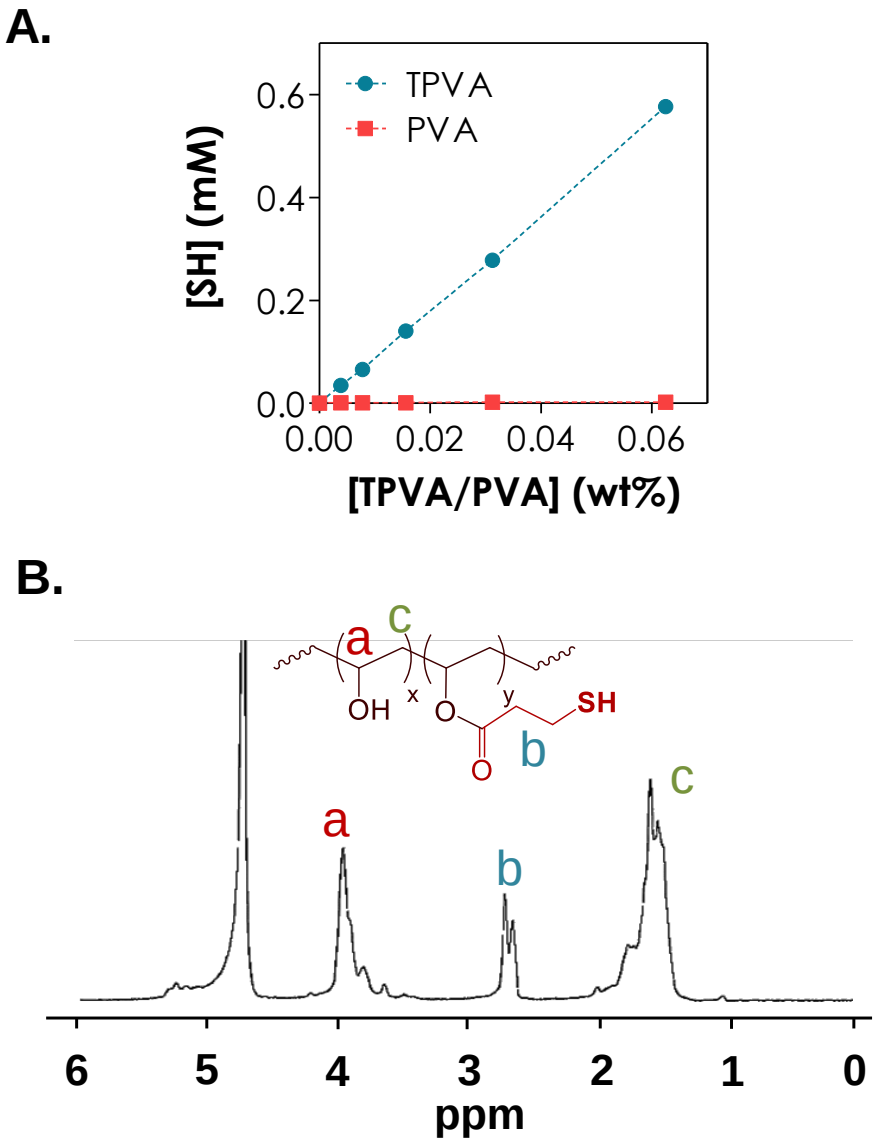

Figure 6.12. (A) Degree of TPVA thiolation measured by Ellman's assay. (B) ^{1}H NMR of TPVA prepared with D_2O (at 4.79 ppm).

4-arm PEG-allylether (PEG4AE, 20 kDa) was synthesized following a published protocol. Briefly, 4-arm PEG (20 kDa) was dissolved in anhydrous toluene, and dried with evaporation by reduced pressure. Dried PEG was re-dissolved in anhydrous tetrahydrofuran (THF). Sodium hydride (1.5-fold excess of hydroxyl group) was added slowly to the PEG solution under continuous nitrogen purging at 40 °C. Upon complete liberation of hydrogen gas, allylbromide (6-fold excess of hydroxyl group) was added slowly to the solution. After overnight reaction in dark, sodium bromide salt was filtered off to obtain a PEG4AE solution. PEG4AE was precipitated in cold ethyl ether, filtered and dried *in vacuuo*. The purity of PEG4AE product was verified with H^1 NMR in $CDCl_3$ (Figure 6.13A, 90 %, Bruker 500). 4-arm PEG-adamantane (PEG4AD, 10 kDa) was synthesized following an established protocol. In brief, 4-arm PEG and glassware were dried overnight in vacuum oven. Under continuous stirring and purging with nitrogen, dried PEG was dissolved in anhydrous dichloromethane (DCM). A required amount of 1-adamantaneacetic acid (2-fold excess of hydroxyl group), 4-dimethylaminopyridine (DMAP, 1-fold of hydroxyl group) and N,N-diisopropylcarbodiimide (DIC, 4-fold excess of hydroxyl group) were added to PEG solution. After an overnight reaction, PEG4AD was filtered, precipitated in cold ethyl ether and dried in vacuuo. Dried PEG4AD was redissolved in ddH_2O, filtered and transferred to a dialysis bag. After two days of dialysis in slightly acidic ddH_2O (~pH 6.8), PEG4AD were freeze-dried. The purity of PEG4AD product was verified with H^1 NMR in $CDCl_3$ (Figure 6.13B, >95 %, Bruker 500).

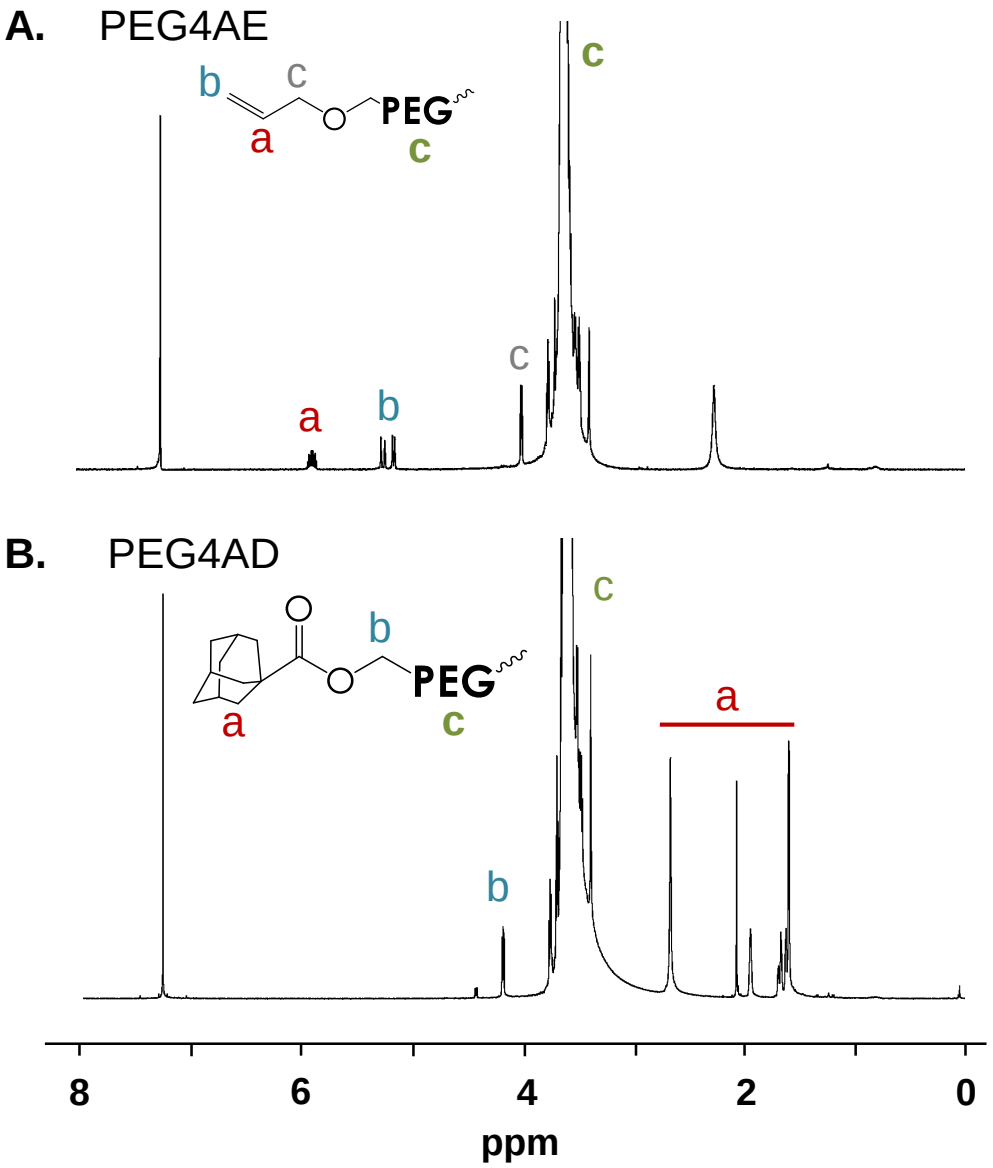

Figure 6.13. ^{1}H NMR of (A) PEG4AE (20 kDa), and (B) PEG4AD (10k Da). All dissolved in $CDCl_3$ (at 7.26 ppm).

Hydrogel fabrication and reversible stiffening: Thiol-allylether hydrogels (45 μL/gel) were formed by light mediated photo-click reactions using precursor solution prepared in the order of mixing pH 7.4 PBS, 1 mM LAP, PEG4AE, βCDAE and TPVA. Immediately after mixing the components, solution was injected in between two glass slides separated by 1 mm thick spacers. Hydrogel slabs were prepared by exposing the solution to 365 nm light at 10 mW/cm^2 for 5 minutes. The elastic moduli (G') of hydrogels were measured after 48 hours of swelling in PBS at 37 ºC. Hydrogel stiffening was achieved by incubating βCD-immobilized hydrogels in PEG4AD solution (48-well plate, 200 μL/well/gel) and placed on an orbital shaker (130 rpm) for 40 hours unless mentioned otherwise. After measuring the stiffness of hydrogels, gels were placed in either pH 7.4 PBS or 1 wt% of βCD (48-well plate, 400 μL/well/gel) for softening.

Rheometry: For rheometrical property measurements, hydrogel discs (8 mm in diameter and 1 mm in height) were fabricated as described previously and placed in pH 7.4 PBS for 48 hours. Frequency sweep (0.01 to 10 Hz, at 1 % strain) and strain sweep (0.1 % to 5 %, at 1 Hz frequency) oscillatory rheometry were performed on a Bohlin CVO 100 digital rheometer. Shear moduli of the hydrogels were measured using a parallel plate geometry (8 mm) with a gap size of 750 μm. The average of elastic moduli obtained from the linear viscoelastic region (LVR) was reported. *In situ* gelation rheometry for hydrogels was conducted in a light cure cell using a parallel plate geometry (25 mm) at room temperature. Briefly, the macromer solution was placed on a quartz plate in the light cure cell, and irradiated with liquid light guide (365 nm, 10 mW/cm^2). Light was turned on 30 seconds after the time sweep *in situ* rheometry (5 % strain, 1 Hz frequency, and a gap size of 90 μm). Gel point was determined at the time when G' surpassed loss modulus (G").

βCDAE immobilization efficiency: Following hydrogel preparation procedure as described previously, hydrogels (30 μL/gel) were fabricated using syringes with cut-off tips as molds. Hydrogels were synthesized in the presence of βCDAE or non-modified

βCD. To detect the concentration of non-reacted thiol after photopolymerization reaction, immediately after gel polymerization, hydrogels were individually placed in 48-well plate containing Ellman's reaction buffer (300 µL/well/gel). After 30 minutes of incubation at room temperature, these collected Ellman's reaction buffer was compared against a standard curve with known cysteine concentrations. In a separate experiment, immediately after polymerization, hydrogels were dried in a desiccator and the first dry mass were obtained. After incubating gels in ddH_2O for a day to allow sol fraction to leach out, gels were dried and the second dry mass were measured. Gel fraction of hydrogel was reported as the percentage of the second dry weight to the first dry weight. Furthermore, ATR-FTIR was used to detect the presence of immobilized βCDAE in the hydrogel.

Cytocompatibility of βCD and PEGAD: MIN6 β-cells were cultured on 96-well tissue culture treated plate for two days at 37 ^oC and 5 % of CO_2. β-cells were treated with different concentrations of soluble βCD and PEGAD (10 kDa) dissolved in media (high-glucose DMEM with L-glutamine and sodium pyruvate, 10 % FBS, β-mercaptoethanol and antibiotic-antimycotic) at 37 ^oC and 5 % of CO_2. After incubating for 40 hours, βCD and PEGAD containing media were removed, cells were supplemented with media containing 3-(4,5-dimethylthiazol-2-yl)-2,5-diphenyltetrazolium bromide (MTT) at 37 ^oC and 5 % of CO_2 (100 µL/well). After 4 hours of incubation, dimethyl sulfoxide (DMSO, 100 µL/well) was added to wells, and plate was further incubated in oven for 10 minutes (at 60 ^oC). The absorbance was measured at 540 nm and DMSO was used as a blank.

Cell encapsulation and cytocompatibility: MIN6 β-cells (final density 2×10^6 cells/mL) was suspended in polymer solutions (i.e., PBS, LAP, PEG4AE, βCDAE and TPVA) and exposed to light for 5 minutes (365 nm at 5 mW/cm^2). These MIN6 cell-laden hydrogels (20 µl/gel) were cultured in growth media (high-glucose DMEM with L-glutamine and sodium pyruvate, 10 % fetal bovine serum (FBS), β-mercaptoethanol and antibiotic-antimycotic) and maintained at 37 ^oC and 5 % of CO_2. Fresh media was changed every two days. After a week, cell-laden hydrogels were transferred to 48-well plate (2

gels/well), supplemented with media containing 5 wt% of PEG4AD (200 μL/well), and placed on a rotary platform in 37 ^{o}C and 5 % of CO_2 for 3 days. For quantitative cell viability study, cell-laden hydrogels were incubated in 500 μL Alamarblue® reagent (10 % in cell culture medium; AbD Serotec) at 37 ^{o}C and 5 % of CO_2. After 16 hours of incubation, 200 μl of incubated Alamarblue® media was transferred to a transparent 96-well plate. Using a microplate reader, the Alamarblue® fluorescence (excitation: 560 nm and emission: 590 nm) due to cell metabolic activity was determined. Cell viability was quantified by CellTiter Glo® assay (Promega). In addition, confocal imaging (FV1000 Laser Scanning Biological Microscope) of cell-laden hydrogels were stained with Biotium live/dead kit (Calcein AM stained live cells green and Ethidium homodimer-1 stained dead cells red) for an hour and washed with HBSS for 10 minutes. The confocal imaging was performed with a step size of 10 μm for a total image thickness of 100 μm. In preparation for RNA isolation, cell-laden gels were rapidly frozen using liquid nitrogen and stored in -80 ^{o}C until use. Collected samples were processed following NucleoSpin® RNA protocols (Clontech). The concentrations of pure RNA were determined using NanoDrop 2000 Spectrophotometer (Thermo Scientific). Reverse transcription PCR (rt-PCR) was performed on Applied Biosystems 2720 Thermal Cycler to convert RNA into cDNA using PrimeScript^{TM} RT Reagent Kit (Clontech). cDNA samples were further prepared with SYBR Premix Ex Taq II kit (Clontech) and primers (Sigma-Aldrich, Table S1) for quantitative real time PCR (Applied Biosystems 7500 Fast Real-Time PCR machine).

Table 6.1. Mouse primer sequences used in real time PCR.

Gene Symbol	Primer Sequence	Reference
Tbp	ACCCTTCACCAATGACTCCTATG	[205]
	ATGATGACTGCAGCAAATCGC	
Ins	TGGCTTCTTCTACACACCCAAG	[206]
	ACAATGCCACGCTTCTGCC	

6.5. Conclusion

In summary, we have synthesized a step-growth thiol-allylether photopolymerized hydrogel containing chemically immobilized βCD that complexes with soluble PEG4AD to form a dynamic hydrogel network with tunable stiffness. Thiol-allylether hydrogels crosslinked by TPVA, PEG4AE, and βCDAE exhibited rapid gelation kinetics and high tunability in crosslinking density. The process of gel stiffening/softening was repeatable by exposing gels in either PEGAD or βCD solutions, respectively. Most importantly, MIN6 β-cell fate is regulated in hydrogels that are stiffened *in situ*. Thiol-allylether hydrogel with immobilized βCD provided a wider range of stiffness tunability over existing dynamic hydrogels, and should be of great interest for studying the influence of biomechanical properties on cell fate processes.

CHAPTER 7
CONCLUSIONS AND RECOMMENDATION

In summary, thiol-ene hydrogels formed by radical mediated photopolymerizations have emerged as a versatile biomaterial platform for controlled release of therapeutics and tissue engineering applications. Thiol-ene hydrogels have improved network crosslinking than the conventional chain-growth PEGDA and step-groth Michael-type addition hydrogels. Type I and type II photoinitiator can be used to prepared thiol-ene hydrogels via UV light or visible light irradiation, respectively. In addition, thiol-ene hydrogels can be rendered completely non-degradable, or degradable only by hydrolysis, proteolysis, photolysis, or by the combination of different mechanisms. The diverse gelation and degradation of thiol-ene hydrogels offer researchers a new platform to design hydrogel matrices suitable for protein delivery and three dimensional cell culture. Using this thiol-ene hydrogelation scheme, the following objectives were met:

Objective 1: Establish a visible light mediated interfacial thiol-ene photopolymerization for microencapaulation of islets. I have developed a visible light-mediated thiol-norbornene interfacial coating process to prepare step-growth conformal hydrogel coating on islet surface. Using MIN6 β-cell aggregates as a model, I evaluated the parameters critical in determining coating thickness (e.g., molecular weight of PEGdSH, polymerization time, and macromer concentration). The results of live/dead staining and GSIS demonstrated high cytocompatibility of thiol-ene hydrogel coating on murine islets. This visible light mediated thiol-ene interfacial photopolymerization provides an alternate coating option and should be of great interest to the field of islet transplantation. Future work will focus on modifying thiol-ene gel formulation to create

multi-functional immuno-isolation barrier, and ondetermining the inflammatory response and long-term efficacy of the transplanted coated islets on maintaining euglycemia.

Objective 2: Synthesize biomimetic and anti-inflammatory thiol-ene hydrogel for macroencapsulation of β-cells. Step-growth thiol-ene photopolymerized hydrogel was synthesized using derivatives of βCD and PEG. Thiol-norbornene hydrogels crosslinked by βCD-SH and PEGNB exhibited faster gelation kinetics and higher crosslinking efficiency when comparing with thiol-allylether hydrogels crosslinked by PEGSH and βCD-AE. Furthermore, the gelation kinetics of thiol-norbornene depended highly on the functionality of macromer used. In addition, βCD/PEG hydrogels afforded higher loading, as well as prolonged and sustained delivery, of hydrophobic curcumin. The results of live/dead staining, cell viability assay, and GSIS demonstrated that cell viability was maintained in these hydrogels, but in some cases affected by hydrogel properties (e.g., stiffness).

In addition, I have explored the crosslinking of various bis-cysteine containing peptides with macromer 8-arm PEGNB to form biomimetic hydrogels suitable for in situ cell encapsulation. Initial efforts to polymerize thiol-norbornene PEG-peptide hydrogels through visible light and eosin-Y mediated crosslinking encountered challenges in gelation efficiency. During the optimization processes, I found that the addition of soluble tyrosine during polymerization significantly improved the crosslinking efficiency of PEG-peptide hydrogels. Furthermore, soluble tyrosine drastically enhanced the cytocompatibility of the resulting PEG-peptide hydrogels, as demonstrated by in situ encapsulation and culture of pancreatic β-cell line (MIN6) and primary mouse islets.

Objective 3: Investigate the effect of biomechanical stimulus on the survival of β-cells. A step-growth thiol-allylether photopolymerized hydrogel containing chemically immobilized βCD that complexes with soluble PEG4AD to form a dynamic hydrogel network with tunable stiffness. Thiol-allylether hydrogels crosslinked by TPVA, PEG4AE, and βCDAE exhibited rapid gelation kinetics and high tunability in

crosslinking density. The process of gel stiffening/softening was repeatable by exposing gels in either PEGAD or βCD solutions, respectively. Most importantly, MIN6 β-cell fate is regulated in hydrogels that are stiffened *in situ*. Thiol-allylether hydrogel with immobilized βCD provided a wider range of stiffness tunability over existing dynamic hydrogels, and should be of great interest for studying the influence of biomechanical properties on cell fate processes. Future work will focus on evaluating the molecular mechanisms by which matrix stiffness affects mechanotransduction, cell-cell interactions and their correlations with insulin expression in β-cells.

LIST OF REFERENCES

LIST OF REFERENCES

[1] R. P. Robertson, C. Davis, J. Larsen, R. Stratta, and D. E. Sutherland, "Pancreas and islet transplantation for patients with diabetes," *Diabetes Care,* vol. 23, pp. 112-6, 2000.

[2] K. M. Bratlie, R. L. York, M. A. Invernale, R. Langer, and D. G. Anderson, "Materials for diabetes therapeutics," *Adv Healthc Mater,* vol. 1, pp. 267-84, 2012.

[3] A. M. Shapiro, J. R. Lakey, E. A. Ryan, G. S. Korbutt, E. Toth, G. L. Warnock, *et al.*, "Islet transplantation in seven patients with type 1 diabetes mellitus using a glucocorticoid-free immunosuppressive regimen," *N Engl J Med,* vol. 343, pp. 230-8, 2000.

[4] E. A. Ryan, J. R. Lakey, R. V. Rajotte, G. S. Korbutt, T. Kin, S. Imes, *et al.*, "Clinical outcomes and insulin secretion after islet transplantation with the Edmonton protocol," *Diabetes,* vol. 50, pp. 710-9, 2001.

[5] P. Soon-Shiong, R. E. Heintz, N. Merideth, Q. X. Yao, Z. Yao, T. Zheng, *et al.*, "Insulin independence in a type 1 diabetic patient after encapsulated islet transplantation," *Lancet,* vol. 343, pp. 950-1, 1994.

[6] B. Nilsson, K. N. Ekdahl, and O. Korsgren, "Control of instant blood-mediated inflammatory reaction to improve islets of Langerhans engraftment," *Curr Opin Organ Transplant,* vol. 16, pp. 620-6, 2011.

[7] L. Moberg, H. Johansson, A. Lukinius, C. Berne, A. Foss, R. Kallen, *et al.*, "Production of tissue factor by pancreatic islet cells as a trigger of detrimental thrombotic reactions in clinical islet transplantation," *Lancet,* vol. 360, pp. 2039-45, 2002.

[8] A. M. Shapiro, C. Ricordi, B. J. Hering, H. Auchincloss, R. Lindblad, R. P. Robertson, *et al.*, "International trial of the Edmonton protocol for islet transplantation," *N Engl J Med,* vol. 355, pp. 1318-30, 2006.

[9] A. S. Sawhney and J. A. Hubbell, "Poly(ethylene oxide)-graft-poly(L-lysine) copolymers to enhance the biocompatibility of poly(L-lysine)-alginate microcapsule membranes," *Biomaterials,* vol. 13, pp. 863-70, 1992.

[10] T. Wang, I. Lacik, M. Brissova, A. V. Anilkumar, A. Prokop, D. Hunkeler, *et al.*, "An encapsulation system for the immunoisolation of pancreatic islets," *Nat Biotechnol,* vol. 15, pp. 358-62, 1997.

[11] T. M. Chang, "Therapeutic applications of polymeric artificial cells," *Nat Rev Drug Discov,* vol. 4, pp. 221-35, 2005.

[12] M. Y. Fan, Z. P. Lum, X. W. Fu, L. Levesque, I. T. Tai, and A. M. Sun, "Reversal of diabetes in BB rats by transplantation of encapsulated pancreatic islets," *Diabetes,* vol. 39, pp. 519-22, 1990.

[13] Y. Teramura and H. Iwata, "Bioartificial pancreas microencapsulation and conformal coating of islet of Langerhans," *Adv Drug Deliv Rev,* vol. 62, pp. 827-40, 2010.

[14] D. B. Jaroch, J. Lu, R. Madangopal, N. D. Stull, M. Stensberg, J. Shi, *et al.*, "Mouse and human islets survive and function after coating by biosilicification," *Am J Physiol Endocrinol Metab,* vol. 305, pp. E1230-40, 2013.

[15] E. S. O'Sullivan, A. Vegas, D. G. Anderson, and G. C. Weir, "Islets transplanted in immunoisolation devices: a review of the progress and the challenges that remain," *Endocr Rev,* vol. 32, pp. 827-44, 2011.

[16] M. Ma, A. Chiu, G. Sahay, J. C. Doloff, N. Dholakia, R. Thakrar, *et al.*, "Core-shell hydrogel microcapsules for improved islets encapsulation," *Adv Healthc Mater,* vol. 2, pp. 667-72, 2013.

[17] H. R. Rengifo, J. A. Giraldo, I. Labrada, and C. L. Stabler, "Long-Term Survival of Allograft Murine Islets Coated via Covalently Stabilized Polymers," *Adv Healthc Mater,* 2014.

[18] K. M. Gattás-Asfura and C. L. Stabler, "Bioorthogonal Layer-by-Layer Encapsulation of Pancreatic Islets via Hyperbranched Polymers," *ACS Applied Materials & Interfaces,* vol. 5, pp. 9964-9974, 2013.

[19] G. M. Cruise, O. D. Hegre, D. S. Scharp, and J. A. Hubbell, "A sensitivity study of the key parameters in the interfacial photopolymerization of poly(ethylene glycol) diacrylate upon porcine islets," *Biotechnol Bioeng,* vol. 57, pp. 655-65, 1998.

[20] Y. Teramura, O. P. Oommen, J. Olerud, J. Hilborn, and B. Nilsson, "Microencapsulation of cells, including islets, within stable ultra-thin membranes of maleimide-conjugated PEG-lipid with multifunctional crosslinkers," *Biomaterials,* vol. 34, pp. 2683-93, 2013.

[21] P. de Vos, M. M. Faas, B. Strand, and R. Calafiore, "Alginate-based microcapsules for immunoisolation of pancreatic islets," *Biomaterials,* vol. 27, pp. 5603-5617, 2006.

[22] M. Ma, A. Chiu, G. Sahay, J. C. Doloff, N. Dholakia, R. Thakrar, *et al.*, "Core–Shell Hydrogel Microcapsules for Improved Islets Encapsulation," *Advanced Healthcare Materials,* vol. 2, pp. 667-672, 2013.

[23] J. I. Lee, R. Nishimura, H. Sakai, N. Sasaki, and T. Kenmochi, "A Newly Developed Immunoisolated Bioartificial Pancreas With Cell Sheet Engineering," *Cell Transplantation,* vol. 17, pp. 51-59, 2008.

[24] Z. Qi, C. Yamamoto, N. Imori, A. Kinukawa, K.-c. Yang, G. Yanai, *et al.*, "Immunoisolation Effect of Polyvinyl Alcohol (PVA) Macroencapsulated Islets in Type 1 Diabetes Therapy," *Cell Transplantation,* vol. 21, pp. 525-534, 2012.

[25] A. C. Jen, M. C. Wake, and A. G. Mikos, "Review: Hydrogels for cell immobilization," *Biotechnol Bioeng,* vol. 50, pp. 357-64, 1996.

[26] C. C. Lin and K. S. Anseth, "PEG hydrogels for the controlled release of biomolecules in regenerative medicine," *Pharmaceutical Research,* vol. 26, pp. 631-643, 2009.

[27] K. T. Nguyen and J. L. West, "Photopolymerizable hydrogels for tissue engineering applications," *Biomaterials,* vol. 23, pp. 4307-14, 2002.

[28] M. B. Mellott, K. Searcy, and M. V. Pishko, "Release of protein from highly cross-linked hydrogels of poly(ethylene glycol) diacrylate fabricated by UV polymerization," *Biomaterials,* vol. 22, pp. 929-41, 2001.

[29] D. J. Quick and K. S. Anseth, "DNA delivery from photocrosslinked PEG hydrogels: encapsulation efficiency, release profiles, and DNA quality," *J Control Release,* vol. 96, pp. 341-51, 2004.

[30] B. V. Slaughter, S. S. Khurshid, O. Z. Fisher, A. Khademhosseini, and N. A. Peppas, "Hydrogels in regenerative medicine," *Adv Mater,* vol. 21, pp. 3307-29, 2009.

[31] C. R. Nuttelman, M. A. Rice, A. E. Rydholm, C. N. Salinas, D. N. Shah, and K. S. Anseth, "Macromolecular Monomers for the Synthesis of Hydrogel Niches and Their Application in Cell Encapsulation and Tissue Engineering," *Prog Polym Sci,* vol. 33, pp. 167-179, 2008.

[32] S. Salinas, C. Proukakis, A. Crosby, and T. T. Warner, "Hereditary spastic paraplegia: clinical features and pathogenetic mechanisms," *Lancet Neurol,* vol. 7, pp. 1127-38, 2008.

[33] S. J. Bryant, J. A. Arthur, and K. S. Anseth, "Incorporation of tissue-specific molecules alters chondrocyte metabolism and gene expression in photocrosslinked hydrogels," *Acta Biomater,* vol. 1, pp. 243-52, 2005.

[34] G. M. Cruise, O. D. Hegre, D. S. Scharp, and J. A. Hubbell, "A sensitivity study of the key parameters in the interfacial photopolymerization of poly(ethylene glycol) diacrylate upon porcine islets," *Biotechnology and Bioengineering,* vol. 57, pp. 655-665, 1998.

[35] A. S. Sawhney, C. P. Pathak, and J. A. Hubbell, "Interfacial photopolymerization of poly(ethylene glycol)-based hydrogels upon alginate poly(l-lysine) microcapsules for enhanced biocompatibility " *Biomaterials,* vol. 14, pp. 1008-1016, 1993.

[36] S. J. Bryant, C. R. Nuttelman, and K. S. Anseth, "Cytocompatibility of UV and visible light photoinitiating systems on cultured NIH/3T3 fibroblasts in vitro," *J Biomater Sci Polym Ed,* vol. 11, pp. 439-57, 2000.

[37] C. G. Williams, A. N. Malik, T. K. Kim, P. N. Manson, and J. H. Elisseeff, "Variable cytocompatibility of six cell lines with photoinitiators used for polymerizing hydrogels and cell encapsulation," *Biomaterials,* vol. 26, pp. 1211-8, 2005.

[38] B. D. Fairbanks, M. P. Schwartz, C. N. Bowman, and K. S. Anseth, "Photoinitiated polymerization of PEG-diacrylate with lithium phenyl-2,4,6-trimethylbenzoylphosphinate: polymerization rate and cytocompatibility," *Biomaterials,* vol. 30, pp. 6702-7, 2009.

[39] D. L. Elbert and J. A. Hubbell, "Conjugate addition reactions combined with free-radical cross-linking for the design of materials for tissue engineering," *Biomacromolecules,* vol. 2, pp. 430-41, 2001.

[40] J. D. McCall and K. S. Anseth, "Thiol-ene photopolymerizations provide a facile method to encapsulate proteins and maintain their bioactivity," *Biomacromolecules,* vol. 13, pp. 2410-7, 2012.

[41] K. S. Anseth, A. T. Metters, S. J. Bryant, P. J. Martens, J. H. Elisseeff, and C. N. Bowman, "In situ forming degradable networks and their application in tissue engineering and drug delivery," *J Control Release,* vol. 78, pp. 199-209, 2002.

[42] S. J. Bryant and K. S. Anseth, "Hydrogel properties influence ECM production by chondrocytes photoencapsulated in poly(ethylene glycol) hydrogels," *J Biomed Mater Res,* vol. 59, pp. 63-72, 2002.

[43] N. A. Peppas, J. Z. Hilt, A. Khademhosseini, and R. Langer, "Hydrogels in Biology and Medicine: From Molecular Principles to Bionanotechnology," *Advanced Materials,* vol. 18, pp. 1345-1360, 2006.

[44] C. C. Lin and K. S. Anseth, "PEG hydrogels for the controlled release of biomolecules in regenerative medicine," *Pharm Res,* vol. 26, pp. 631-43, 2009.

[45] A. T. Metters, K. S. Anseth, and C. N. Bowman, "A Statistical Kinetic Model for the Bulk Degradation of PLA-b-PEG-b-PLA Hydrogel Networks: Incorporating Network Non-Idealities," *The Journal of Physical Chemistry B,* vol. 105, pp. 8069-8076, 2001.

[46] A. T. Metters, C. N. Bowman, and K. S. Anseth, "A Statistical Kinetic Model for the Bulk Degradation of PLA-b-PEG-b-PLA Hydrogel Networks," *The Journal of Physical Chemistry B,* vol. 104, pp. 7043-7049, 2000.

[47] A. T. Metters, K. S. Anseth, and C. N. Bowman, "Fundamental studies of a novel, biodegradable PEG-b-PLA hydrogel," *Polymer,* vol. 41, pp. 3993-4004, 2000.

[48] S. He, M. D. Timmer, M. J. Yaszemski, A. W. Yasko, P. S. Engel, and A. G. Mikos, "Synthesis of biodegradable poly(propylene fumarate) networks with poly(propylene fumarate)–diacrylate macromers as crosslinking agents and characterization of their degradation products," *Polymer,* vol. 42, pp. 1251-1260, 2001.

[49] E. Cho, J. K. Kutty, K. Datar, J. S. Lee, N. R. Vyavahare, and K. Webb, "A novel synthetic route for the preparation of hydrolytically degradable synthetic hydrogels," *J Biomed Mater Res A,* vol. 90, pp. 1073-82, 2009.

[50] S. Lin-Gibson, R. L. Jones, N. R. Washburn, and F. Horkay, "Structure−Property Relationships of Photopolymerizable Poly(ethylene glycol) Dimethacrylate Hydrogels," *Macromolecules,* vol. 38, pp. 2897-2902, 2005.

[51] C. E. Hoyle and C. N. Bowman, "Thiol-ene click chemistry," *Angew Chem Int Ed Engl,* vol. 49, pp. 1540-73, 2010.

[52] C. C. Lin, A. Raza, and H. Shih, "PEG hydrogels formed by thiol-ene photo-click chemistry and their effect on the formation and recovery of insulin-secreting cell spheroids," *Biomaterials,* vol. 32, pp. 9685-9695, 2011.

[53] B. D. Fairbanks, S. P. Singh, C. N. Bowman, and K. S. Anseth, "Photodegradable, Photoadaptable Hydrogels via Radical-Mediated Disulfide Fragmentation Reaction," *Macromolecules,* vol. 44, pp. 2444-2450, 2011.

[54] S. B. Anderson, C. C. Lin, D. V. Kuntzler, and K. S. Anseth, "The performance of human mesenchymal stem cells encapsulated in cell-degradable polymer-peptide hydrogels," *Biomaterials,* vol. 32, pp. 3564-3574, 2011.

[55] M. P. Schwartz, B. D. Fairbanks, R. E. Rogers, R. Rangarajan, M. H. Zaman, and K. S. Anseth, "A synthetic strategy for mimicking the extracellular matrix provides new insight about tumor cell migration," *Integr Biol (Camb),* vol. 2, pp. 32-40, 2010.

[56] J. A. Benton, B. D. Fairbanks, and K. S. Anseth, "Characterization of valvular interstitial cell function in three dimensional matrix metalloproteinase degradable PEG hydrogels," *Biomaterials,* vol. 30, pp. 6593-603, 2009.

[57] A. A. Aimetti, A. J. Machen, and K. S. Anseth, "Poly(ethylene glycol) hydrogels formed by thiol-ene photopolymerization for enzyme-responsive protein delivery," *Biomaterials,* vol. 30, pp. 6048-54, 2009.

[58] H. Shih, A. K. Fraser, and C. C. Lin, "Interfacial thiol-ene photoclick reactions for forming multilayer hydrogels," *ACS Appl Mater Interfaces,* vol. 5, pp. 1673-80, 2013.

[59] H. Shih and C. C. Lin, "Visible-light-mediated thiol-ene hydrogelation using eosin-Y as the only photoinitiator," *Macromol Rapid Commun,* vol. 34, pp. 269-73, 2013.

[60] S. K. Reddy, N. B. Cramer, and C. N. Bowman, "Thiol−Vinyl Mechanisms. 1. Termination and Propagation Kinetics in Thiol−Ene Photopolymerizations," *Macromolecules,* vol. 39, pp. 3673-3680, 2006.

[61] M. P. Lutolf and J. A. Hubbell, "Synthesis and Physicochemical Characterization of End-Linked Poly(ethylene glycol)-co-peptide Hydrogels Formed by Michael-Type Addition," *Biomacromolecules,* vol. 4, pp. 713-722, 2003.

[62] H. Shih and C. C. Lin, "Cross-linking and degradation of step-growth hydrogels formed by thiol-ene photoclick chemistry," *Biomacromolecules,* vol. 13, pp. 2003-12, 2012.

[63] A. Metters and J. Hubbell, "Network formation and degradation behavior of hydrogels formed by Michael-type addition reactions," *Biomacromolecules,* vol. 6, pp. 290-301, 2005.

[64] P. Flory, *Principles in Polymer Chemistry*. Ithaca, NY: Cornell University Press, 1953.

[65] K. S. Anseth, C. N. Bowman, and L. Brannon-Peppas, "Mechanical properties of hydrogels and their experimental determination," *Biomaterials,* vol. 17, pp. 1647-57, 1996.

[66] A. E. Rydholm, S. K. Reddy, K. S. Anseth, and C. N. Bowman, "Development and Characterization of Degradable Thiol-Allyl Ether Photopolymers," *Polymer (Guildf),* vol. 48, pp. 4589-4600, 2007.

[67] J. E. Elliott, J. W. Anseth, and C. N. Bowman, "Kinetic modeling of the effect of solvent concentration on primary cyclization during polymerization of multifunctional monomers," *Chemical Engineering Science,* vol. 56, pp. 3173-3184, 2001.

[68] A. M. Kloxin, J. A. Benton, and K. S. Anseth, "In situ elasticity modulation with dynamic substrates to direct cell phenotype," *Biomaterials,* vol. 31, pp. 1-8, 2010.

[69] A. M. Kloxin, C. J. Kloxin, C. N. Bowman, and K. S. Anseth, "Mechanical Properties of Cellularly Responsive Hydrogels and Their Experimental Determination," *Advanced Materials,* vol. 22, pp. 3484-3494, 2010.

[70] A. E. Rydholm, C. N. Bowman, and K. S. Anseth, "Degradable thiol-acrylate photopolymers: polymerization and degradation behavior of an in situ forming biomaterial," *Biomaterials,* vol. 26, pp. 4495-4506, 2005.

[71] A. E. Rydholm, S. K. Reddy, K. S. Anseth, and C. N. Bowman, "Controlling Network Structure in Degradable Thiol−Acrylate Biomaterials to Tune Mass Loss Behavior," *Biomacromolecules,* vol. 7, pp. 2827-2836, 2006.

[72] A. E. Rydholm, K. S. Anseth, and C. N. Bowman, "Effects of neighboring sulfides and pH on ester hydrolysis in thiol–acrylate photopolymers," *Acta Biomaterialia,* vol. 3, pp. 449-455, 2007.

[73] S. P. Zustiak and J. B. Leach, "Hydrolytically degradable poly(ethylene glycol) hydrogel scaffolds with tunable degradation and mechanical properties," *Biomacromolecules,* vol. 11, pp. 1348-57, 2010.

[74] S. P. Zustiak and J. B. Leach, "Characterization of protein release from hydrolytically degradable poly(ethylene glycol) hydrogels," *Biotechnol Bioeng,* vol. 108, pp. 197-206, 2011.

[75] D. Klinger and K. Landfester, "Enzymatic- and light-degradable hybrid nanogels: Crosslinking of polyacrylamide with acrylate-functionalized Dextrans containing photocleavable linkers," *Journal of Polymer Science Part A: Polymer Chemistry,* vol. 50, pp. 1062-1075, 2012.

[76] A. E. Rydholm, K. S. Anseth, and C. N. Bowman, "Effects of neighboring sulfides and pH on ester hydrolysis in thiol-acrylate photopolymers," *Acta Biomater,* vol. 3, pp. 449-55, 2007.

[77] M. P. Lutolf, J. L. Lauer-Fields, H. G. Schmoekel, A. T. Metters, F. E. Weber, G. B. Fields, *et al.*, "Synthetic matrix metalloproteinase-sensitive hydrogels for the conduction of tissue regeneration: engineering cell-invasion characteristics," *Proc Natl Acad Sci U S A,* vol. 100, pp. 5413-8, 2003.

[78] A. Raza and C. C. Lin, "The influence of matrix degradation and functionality on cell survival and morphogenesis in PEG-based hydrogels," *Macromol Biosci,* vol. 13, pp. 1048-58, 2013.

[79] A. Raza, C. S. Ki, and C. C. Lin, "The influence of matrix properties on growth and morphogenesis of human pancreatic ductal epithelial cells in 3D," *Biomaterials,* vol. 34, pp. 5117-27, 2013.

[80] C. S. Ki, H. Shih, and C. C. Lin, "Facile preparation of photodegradable hydrogels by photopolymerization," *Polymer (Guildf),* vol. 54, pp. 2115-2122, 2013.

[81] A. M. Kloxin, A. M. Kasko, C. N. Salinas, and K. S. Anseth, "Photodegradable hydrogels for dynamic tuning of physical and chemical properties," *Science,* vol. 324, pp. 59-63, 2009.

[82] D. R. Griffin, J. T. Patterson, and A. M. Kasko, "Photodegradation as a mechanism for controlled drug delivery," *Biotechnol Bioeng,* vol. 107, pp. 1012-9, 2010.

[83] D. R. Griffin and A. M. Kasko, "Photodegradable Macromers and Hydrogels for Live Cell Encapsulation and Release," *J Am Chem Soc,* 2012.
[84] D. R. Griffin and A. M. Kasko, "Photoselective Delivery of Model Therapeutics from Hydrogels," *ACS Macro Letters,* vol. 1, pp. 1330-1334, 2012.
[85] S. Murayama, F. Ishizuka, K. Takagi, H. Inoda, A. Sano, T. Santa, *et al.*, "Small mesh size hydrogel for functional photocontrol of encapsulated enzymes and small probe molecules," *Anal Chem,* vol. 84, pp. 1374-9, 2012.
[86] R. P. Narayanan, G. Melman, N. J. Letourneau, N. L. Mendelson, and A. Melman, "Photodegradable iron(III) cross-linked alginate gels," *Biomacromolecules,* vol. 13, pp. 2465-71, 2012.
[87] B. Yan, J. C. Boyer, D. Habault, N. R. Branda, and Y. Zhao, "Near infrared light triggered release of biomacromolecules from hydrogels loaded with upconversion nanoparticles," *J Am Chem Soc,* vol. 134, pp. 16558-61, 2012.
[88] C. C. Lin and A. T. Metters, "Enhanced protein delivery from photopolymerized hydrogels using a pseudospecific metal chelating ligand," *Pharm Res,* vol. 23, pp. 614-22, 2006.
[89] N. A. Impellitteri, M. W. Toepke, S. K. Lan Levengood, and W. L. Murphy, "Specific VEGF sequestering and release using peptide-functionalized hydrogel microspheres," *Biomaterials,* vol. 33, pp. 3475-84, 2012.
[90] A. K. Fraser, C. S. Ki, and C.-C. Lin, "PEG-Based Microgels Formed by Visible-Light-Mediated Thiol-Ene Photo-Click Reactions," *Macromolecular Chemistry and Physics,* vol. 215, pp. 507-515, 2014.
[91] C. S. Ki, H. Shih, and C. C. Lin, "Effect of 3D matrix compositions on the efficacy of EGFR inhibition in pancreatic ductal adenocarcinoma cells," *Biomacromolecules,* vol. 14, pp. 3017-26, 2013.
[92] D. D. McKinnon, A. M. Kloxin, and K. S. Anseth, "Synthetic hydrogel platform for three-dimensional culture of embryonic stem cell-derived motor neurons," *Biomaterials Science,* vol. 1, pp. 460-469, 2013.
[93] V. Di Gialleonardo, E. F. de Vries, M. Di Girolamo, A. M. Quintero, R. A. Dierckx, and A. Signore, "Imaging of beta-cell mass and insulitis in insulin-dependent (Type 1) diabetes mellitus," *Endocr Rev,* vol. 33, pp. 892-919, 2012.
[94] R. M. Meloche, "Transplantation for the treatment of type 1 diabetes," *World J Gastroenterol,* vol. 13, pp. 6347-55, 2007.
[95] D. Daneman, "Type 1 diabetes," *Lancet,* vol. 367, pp. 847-58, 2006.
[96] P. R. Johnson and K. E. Jones, "Pancreatic islet transplantation," *Semin Pediatr Surg,* vol. 21, pp. 272-80, 2012.
[97] E. A. Ryan, B. W. Paty, P. A. Senior, D. Bigam, E. Alfadhli, N. M. Kneteman, *et al.*, "Five-year follow-up after clinical islet transplantation," *Diabetes,* vol. 54, pp. 2060-9, 2005.
[98] S. Kizilel, M. Garfinkel, and E. Opara, "The bioartificial pancreas: progress and challenges," *Diabetes Technol Ther,* vol. 7, pp. 968-85, 2005.
[99] J. T. Wilson and E. L. Chaikof, "Challenges and emerging technologies in the immunoisolation of cells and tissues," *Adv Drug Deliv Rev,* vol. 60, pp. 124-45, 2008.

[100] B. Thu, P. Bruheim, T. Espevik, O. Smidsrod, P. Soon-Shiong, and G. Skjak-Braek, "Alginate polycation microcapsules. I. Interaction between alginate and polycation," *Biomaterials,* vol. 17, pp. 1031-40, 1996.
[101] F. Lim and A. M. Sun, "Microencapsulated islets as bioartificial endocrine pancreas," *Science,* vol. 210, pp. 908-10, 1980.
[102] P. de Vos, M. M. Faas, B. Strand, and R. Calafiore, "Alginate-based microcapsules for immunoisolation of pancreatic islets," *Biomaterials,* vol. 27, pp. 5603-17, 2006.
[103] S. Kizilel, A. Scavone, X. Liu, J. M. Nothias, D. Ostrega, P. Witkowski, *et al.*, "Encapsulation of pancreatic islets within nano-thin functional polyethylene glycol coatings for enhanced insulin secretion," *Tissue Eng Part A,* vol. 16, pp. 2217-28, 2010.
[104] N. Marek, A. Krzystyniak, I. Ergenc, O. Cochet, R. Misawa, L. J. Wang, *et al.*, "Coating human pancreatic islets with CD4(+)CD25(high)CD127(-) regulatory T cells as a novel approach for the local immunoprotection," *Ann Surg,* vol. 254, pp. 512-8; discussion 518-9, 2011.
[105] V. Kozlovskaya, O. Zavgorodnya, Y. Chen, K. Ellis, H. M. Tse, W. Cui, *et al.*, "Ultrathin polymeric coatings based on hydrogen-bonded polyphenol for protection of pancreatic islet cells," *Adv Funct Mater,* vol. 22, pp. 3389-3398, 2012.
[106] V. Kozlovskaya, E. Kharlampieva, I. Drachuk, D. Cheng, and V. V. Tsukruk, "Responsive microcapsule reactors based on hydrogen-bonded tannic acid layer-by-layer assemblies," *Soft Matter,* vol. 6, pp. 3596-3608, 2010.
[107] B. S. Kim, H. I. Lee, Y. Min, Z. Poon, and P. T. Hammond, "Hydrogen-bonded multilayer of pH-responsive polymeric micelles with tannic acid for surface drug delivery," *Chem Commun (Camb),* pp. 4194-6, 2009.
[108] N. M. Luan and H. Iwata, "Inhibition of instant blood-mediated inflammatory responses by co-immobilization of sCR1 and heparin on islets," *Biomaterials,* vol. 34, pp. 5019-24, 2013.
[109] N. M. Luan, Y. Teramura, and H. Iwata, "Layer-by-layer co-immobilization of soluble complement receptor 1 and heparin on islets," *Biomaterials,* vol. 32, pp. 6487-6492, 2011.
[110] D. L. Elbert, A. B. Pratt, M. P. Lutolf, S. Halstenberg, and J. A. Hubbell, "Protein delivery from materials formed by self-selective conjugate addition reactions," *J Control Release,* vol. 76, pp. 11-25, 2001.
[111] M. A. Rubio, E. Lissi, H. Jorquera, E. Salinas, J. Castro, and M. Cadiz, "Carbon monoxide concentrations in Santiago City at street levels and their vertical gradient," *Environ Monit Assess,* vol. 140, pp. 161-73, 2008.
[112] G. M. Cruise, D. S. Scharp, and J. A. Hubbell, "Characterization of permeability and network structure of interfacially photopolymerized poly(ethylene glycol) diacrylate hydrogels," *Biomaterials,* vol. 19, pp. 1287-94, 1998.
[113] G. M. Cruise, O. D. Hegre, F. V. Lamberti, S. R. Hager, R. Hill, D. S. Scharp, *et al.*, "In vitro and in vivo performance of porcine islets encapsulated in interfacially photopolymerized poly(ethylene glycol) diacrylate membranes," *Cell Transplant,* vol. 8, pp. 293-306, 1999.

[114] A. S. Sawhney, C. P. Pathak, and J. A. Hubbell, "Interfacial photopolymerization of poly(ethylene glycol)-based hydrogels upon alginate-poly(l-lysine) microcapsules for enhanced biocompatibility," *Biomaterials,* vol. 14, pp. 1008-16, 1993.

[115] A. S. Sawhney, C. P. Pathak, and J. A. Hubbell, "Modification of islet of langerhans surfaces with immunoprotective poly(ethylene glycol) coatings via interfacial photopolymerization," *Biotechnol Bioeng,* vol. 44, pp. 383-6, 1994.

[116] C. Halberstadt and D. Emerich, in *Cellular Transplantation From Laboratory to Clinic*, ed: Academic Press, 2006.

[117] A. Shikanov, R. M. Smith, M. Xu, T. K. Woodruff, and L. D. Shea, "Hydrogel network design using multifunctional macromers to coordinate tissue maturation in ovarian follicle culture," *Biomaterials,* vol. 32, pp. 2524-2531, 2011.

[118] E. A. Phelps, N. O. Enemchukwu, V. F. Fiore, J. C. Sy, N. Murthy, T. A. Sulchek, *et al.*, "Maleimide Cross-Linked Bioactive PEG Hydrogel Exhibits Improved Reaction Kinetics and Cross-Linking for Cell Encapsulation and In Situ Delivery," *Advanced Materials,* vol. 24, pp. 64-70, 2012.

[119] T. Bal, B. Kepsutlu, and S. Kizilel, "Characterization of protein release from poly(ethylene glycol) hydrogels with crosslink density gradients," *Journal of Biomedical Materials Research Part A,* vol. 102, pp. 487-495, 2014.

[120] B. D. Fairbanks, M. P. Schwartz, A. E. Halevi, C. R. Nuttelman, C. N. Bowman, and K. S. Anseth, "A Versatile Synthetic Extracellular Matrix Mimic via Thiol-Norbornene Photopolymerization," *Advanced Materials,* vol. 21, pp. 5005-5010, 2009.

[121] M. A. von Mach, J. Schlosser, M. Weiland, P. J. Feilen, M. Ringel, J. G. Hengstler, *et al.*, "Size of pancreatic islets of Langerhans: a key parameter for viability after cryopreservation," *Acta Diabetol,* vol. 40, pp. 123-9, 2003.

[122] H. Shih, A. K. Fraser, and C.-C. Lin, "Interfacial Thiol-ene Photoclick Reactions for Forming Multilayer Hydrogels," *ACS Applied Materials & Interfaces,* vol. 5, pp. 1673-1680, 2013.

[123] P. J. Flory, *Principles of Polymer Chemistry*. Ithaca, NY: Cornell University Press, 1953.

[124] V. Banerjee, R. K. Kar, A. Datta, K. Parthasarathi, S. Chatterjee, K. P. Das, *et al.*, "Use of a Small Peptide Fragment as an Inhibitor of Insulin Fibrillation Process: A Study by High and Low Resolution Spectroscopy," *PLoS ONE,* vol. 8, p. e72318, 2013.

[125] N. D. Stull, A. Breite, R. McCarthy, S. A. Tersey, and R. G. Mirmira, "Mouse islet of Langerhans isolation using a combination of purified collagenase and neutral protease," *J Vis Exp,* 2012.

[126] K. E. Dionne, C. K. Colton, and M. L. Yarmush, "Effect of hypoxia on insulin secretion by isolated rat and canine islets of Langerhans," *Diabetes,* vol. 42, pp. 12-21, 1993.

[127] T. Kobayashi, G. Harb, R. V. Rajotte, G. S. Korbutt, A. G. Mallett, H. Arefanian, *et al.*, "Immune mechanisms associated with the rejection of encapsulated neonatal porcine islet xenografts," *Xenotransplantation,* vol. 13, pp. 547-59, 2006.

[128] V. Vaithilingam, C. Fung, S. Ratnapala, J. Foster, V. Vaghjiani, U. Manuelpillai, *et al.*, "Characterisation of the Xenogeneic Immune Response to Microencapsulated Fetal Pig Islet-Like Cell Clusters Transplanted into Immunocompetent C57BL/6 Mice," *PLoS ONE,* vol. 8, p. e59120, 2013.

[129] A. Amrani, S. Durant, M. Throsby, J. Coulaud, M. Dardenne, and F. Homo-Delarche, "Glucose Homeostasis in the Nonobese Diabetic Mouse at the Prediabetic Stage," *Endocrinology,* vol. 139, pp. 1115-1124, 1998.

[130] S. R. Lustig and N. A. Peppas, "Solute diffusion in swollen membranes. IX. Scaling laws for solute diffusion in gels," *Journal of Applied Polymer Science,* vol. 36, pp. 735-747, 1988.

[131] S. R. C. Peter Buchwald, "Glucose-stimulated insulin secretion in isolated pancreatic islets: Multiphysics FEM model calculations compared to results of perifusion experiments with human islets," *Journal of Biomedical Science and Engineering,* vol. 6, pp. 26-35, 2013.

[132] A. Vyas, S. Saraf, and S. Saraf, "Cyclodextrin based novel drug delivery systems," *Journal of Inclusion Phenomena and Macrocyclic Chemistry,* vol. 62, pp. 23-42, 2008.

[133] G. Tiwari, R. Tiwari, and A. K. Rai, "Cyclodextrins in delivery systems: Applications," *J Pharm Bioallied Sci,* vol. 2, pp. 72-9, Apr 2010.

[134] (2014, August 7). *GRAS Notices*. Available: http://www.accessdata.fda.gov/scripts/fdcc/?set=GRASNotices&sort=GRN_No&order=DESC&startrow=1&type=basic&search=cyclodextrin

[135] K. T. Savjani, A. K. Gajjar, and J. K. Savjani, "Drug solubility: importance and enhancement techniques," *ISRN Pharm,* vol. 2012, p. 195727, 2012.

[136] J. Szejtli, "Introduction and General Overview of Cyclodextrin Chemistry," *Chemical Reviews,* vol. 98, pp. 1743-1754, 1998.

[137] A. Douhal, *Cyclodextrin Materials Photochemistry, Photophysics and Photobiology*. Italy: Elsevier, 2006.

[138] J. Li and X. J. Loh, "Cyclodextrin-based supramolecular architectures: Syntheses, structures, and applications for drug and gene delivery," *Advanced Drug Delivery Reviews,* vol. 60, pp. 1000-1017, 2008.

[139] Z.-X. Zhang, K. L. Liu, and J. Li, "A Thermoresponsive Hydrogel Formed from a Star–Star Supramolecular Architecture," *Angewandte Chemie International Edition,* vol. 52, pp. 6180-6184, 2013.

[140] Y. Huang and X.-D. Fan, "Synthesis and properties of hydrogels of poly(acrylic-co-acroloyl β-cyclodextrin)," *Journal of Applied Polymer Science,* vol. 113, pp. 3068-3077, 2009.

[141] S. Tan, A. Blencowe, K. Ladewig, and G. G. Qiao, "A novel one-pot approach towards dynamically cross-linked hydrogels," *Soft Matter,* vol. 9, pp. 5239-5250, 2013.

[142] L. M. Gaetke and C. K. Chow, "Copper toxicity, oxidative stress, and antioxidant nutrients," *Toxicology,* vol. 189, pp. 147-163, 2003.

[143] D. Soriano del Amo, W. Wang, H. Jiang, C. Besanceney, A. C. Yan, M. Levy, *et al.*, "Biocompatible Copper(I) Catalysts for in Vivo Imaging of Glycans," *Journal of the American Chemical Society,* vol. 132, pp. 16893-16899, 2010.

[144] M. Arslan, T. N. Gevrek, A. Sanyal, and R. Sanyal, "Cyclodextrin mediated polymer coupling via thiol-maleimide conjugation: facile access to functionalizable hydrogels," *RSC Advances,* vol. 4, pp. 57834-57841, 2014.

[145] L. H. Jensen, A. Renodon-Corniere, I. Wessel, S. W. Langer, B. Sokilde, E. V. Carstensen, *et al.*, "Maleimide is a potent inhibitor of topoisomerase II in vitro and in vivo: a new mode of catalytic inhibition," *Mol Pharmacol,* vol. 61, pp. 1235-43, 2002.

[146] K. E. Machado, K. N. de Oliveira, H. M. S. Andreossi, L. d. S. Bubniak, A. C. R. de Moraes, P. C. Gaspar, *et al.*, "Apoptotic Events Induced by Maleimides on Human Acute Leukemia Cell Lines," *Chemical Research in Toxicology,* vol. 26, pp. 1904-1916, 2013.

[147] M. Arslan, T. N. Gevrek, R. Sanyal, and A. Sanyal, "Fabrication of poly(ethylene glycol)-based cyclodextrin containing hydrogels via thiol-ene click reaction," *European Polymer Journal,* vol. 62, pp. 426-434, 2015.

[148] C.-C. Lin, C. S. Ki, and H. Shih, "Thiol–norbornene photoclick hydrogels for tissue engineering applications," *Journal of Applied Polymer Science,* vol. 132, pp. 41563, 2015.

[149] C.-C. Lin and K. S. Anseth, "Cell–cell communication mimicry with poly(ethylene glycol) hydrogels for enhancing β-cell function," *Proceedings of the National Academy of Sciences,* vol. 108, pp. 6380-6385, 2011.

[150] L. A. Sawicki and A. M. Kloxin, "Design of thiol-ene photoclick hydrogels using facile techniques for cell culture applications," *Biomaterials Science,* vol. 2, pp. 1612-1626, 2014.

[151] N. B. Cramer, S. K. Reddy, A. K. O'Brien, and C. N. Bowman, "Thiol−Ene Photopolymerization Mechanism and Rate Limiting Step Changes for Various Vinyl Functional Group Chemistries," *Macromolecules,* vol. 36, pp. 7964-7969, 2003.

[152] C. Pradal, K. S. Jack, L. Grøndahl, and J. J. Cooper-White, "Gelation Kinetics and Viscoelastic Properties of Pluronic and α-Cyclodextrin-Based Pseudopolyrotaxane Hydrogels," *Biomacromolecules,* vol. 14, pp. 3780-3792, 2013.

[153] A. Singh, J. Zhan, Z. Ye, and J. H. Elisseeff, "Modular Multifunctional Poly(ethylene glycol) Hydrogels for Stem Cell Differentiation," *Advanced Functional Materials,* vol. 23, pp. 575-582, 2013.

[154] A. Metters and J. Hubbell, "Network Formation and Degradation Behavior of Hydrogels Formed by Michael-Type Addition Reactions," *Biomacromolecules,* vol. 6, pp. 290-301, 2004.

[155] M. M. Amoli, R. Mousavizadeh, R. Sorouri, M. Rahmani, and B. Larijani, "Curcumin Inhibits in Vitro MCP-1 Release From Mouse Pancreatic Islets," *Transplantation Proceedings,* vol. 38, pp. 3035-3038, 2006.

[156] M. Srinivasan, "Effect of curcumin on blood sugar as seen in a diabetic subject," *Indian Journal of Medical Sciences,* vol. 26, pp. 269-270, 1972.

[157] V. R. Yadav, S. Prasad, R. Kannappan, J. Ravindran, M. M. Chaturvedi, L. Vaahtera, *et al.*, "Cyclodextrin-complexed curcumin exhibits anti-inflammatory and antiproliferative activities superior to those of curcumin through higher cellular uptake," *Biochemical Pharmacology,* vol. 80, pp. 1021-1032, 2010.

[158] H. H. Tønnesen, M. Másson, and T. Loftsson, "Studies of curcumin and curcuminoids. XXVII. Cyclodextrin complexation: solubility, chemical and photochemical stability," *International Journal of Pharmaceutics,* vol. 244, pp. 127-135, 2002.

[159] M. El-Kemary and A. Douhal, "Chapter 4 - Photochemistry and Photophysics of Cyclodextrin Caged Drugs: Relevance to Their Stability and Efficiency," in *Cyclodextrin Materials Photochemistry, Photophysics and Photobiology*. vol. 1, A. Douhal, Ed., ed Amsterdam: Elsevier, pp. 79-105, 2006.

[160] M. M. Yallapu, M. Jaggi, and S. C. Chauhan, "Poly(beta-cyclodextrin)/curcumin self-assembly: a novel approach to improve curcumin delivery and its therapeutic efficacy in prostate cancer cells," *Macromol Biosci,* vol. 10, pp. 1141-51, 2010.

[161] Y. Jung, W. Xu, H. Kim, N. Ha, and L. Neckers, "Curcumin-induced degradation of ErbB2: A role for the E3 ubiquitin ligase CHIP and the Michael reaction acceptor activity of curcumin," *Biochimica et Biophysica Acta (BBA) - Molecular Cell Research,* vol. 1773, pp. 383-390, 2007.

[162] H. Rachmawati, C. A. Edityaningrum, and R. Mauludin, "Molecular inclusion complex of curcumin-beta-cyclodextrin nanoparticle to enhance curcumin skin permeability from hydrophilic matrix gel," *AAPS PharmSciTech,* vol. 14, pp. 1303-12, 2013.

[163] C. E. Nyitray, M. G. Chavez, and T. A. Desai, "Compliant 3D microenvironment improves beta-cell cluster insulin expression through mechanosensing and beta-catenin signaling," *Tissue Eng Part A,* vol. 20, pp. 1888-95, 2014.

[164] H. X. Chen, X. Y. Wang, S. Q. Wang, H. T. He, X. G. Luo, X. G. Chen, *et al.*, "Study on rhGM-CSF as adjuvant in revaccination among adults of non-and hyporesponders to hepatitis B vaccine," *Zhonghua Shi Yan He Lin Chuang Bing Du Xue Za Zhi,* vol. 23, pp. 177-9, 2009.

[165] D. A. Fulton and J. F. Stoddart, "An Efficient Synthesis of Cyclodextrin-Based Carbohydrate Cluster Compounds," *Organic Letters,* vol. 2, pp. 1113-1116, 2000.

[166] C. A. Simmons, E. Alsberg, S. Hsiong, W. J. Kim, and D. J. Mooney, "Dual growth factor delivery and controlled scaffold degradation enhance in vivo bone formation by transplanted bone marrow stromal cells," *Bone,* vol. 35, pp. 562-569, 2004.

[167] Y. Zhao, T. Nakajima, J. J. Yang, T. Kurokawa, J. Liu, J. Lu, *et al.*, "Proteoglycans and glycosaminoglycans improve toughness of biocompatible double network hydrogels," *Adv Mater,* vol. 26, pp. 436-42, 2014.

[168] W. Y. Chen and G. Abatangelo, "Functions of hyaluronan in wound repair," *Wound Repair Regen,* vol. 7, pp. 79-89, 1999.

[169] W. I. Choi, M. Kim, G. Tae, and Y. H. Kim, "Sustained release of human growth hormone from heparin-based hydrogel," *Biomacromolecules,* vol. 9, pp. 1698-704, 2008.

[170] J. Dudas, G. Ramadori, T. Knittel, K. Neubauer, D. Raddatz, K. Egedy, *et al.*, "Effect of heparin and liver heparan sulphate on interaction of HepG2-derived transcription factors and their cis-acting elements: altered potential of hepatocellular carcinoma heparan sulphate," *Biochem J,* vol. 350 Pt 1, pp. 245-51, 2000.

[171] G. N. Homminga, P. Buma, H. W. J. Koot, P. M. van der Kraan, and W. B. van den Berg, "Chondrocyte behavior in fibrin glue in vitro," *Acta Orthopaedica,* vol. 64, pp. 441-445, 1993.

[172] D. F. Thompson, N. A. Letassy, and G. D. Thompson, "Fibrin glue: a review of its preparation, efficacy, and adverse effects as a topical hemostat," *Drug Intell Clin Pharm,* vol. 22, pp. 946-52, 1988.

[173] Y. Murata, Y. Kontani, H. Ohmae, and S. Kawashima, "Behavior of alginate gel beads containing chitosan salt prepared with water-soluble vitamins," *European Journal of Pharmaceutics and Biopharmaceutics,* vol. 53, pp. 249-251, 2002.

[174] Y.-H. Lin, H.-F. Liang, C.-K. Chung, M.-C. Chen, and H.-W. Sung, "Physically crosslinked alginate/N,O-carboxymethyl chitosan hydrogels with calcium for oral delivery of protein drugs," *Biomaterials,* vol. 26, pp. 2105-2113, 2005.

[175] K. W. Lee, J. J. Yoon, J. H. Lee, S. Y. Kim, H. J. Jung, S. J. Kim, *et al.*, "Sustained release of vascular endothelial growth factor from calcium-induced alginate hydrogels reinforced by heparin and chitosan," *Transplantation Proceedings,* vol. 36, pp. 2464-2465, 2004.

[176] W. E. Hennink, S. J. De Jong, G. W. Bos, T. F. Veldhuis, and C. F. van Nostrum, "Biodegradable dextran hydrogels crosslinked by stereocomplex formation for the controlled release of pharmaceutical proteins," *Int J Pharm,* vol. 277, pp. 99-104, 2004.

[177] C. Mao and W. S. Kisaalita, "Characterization of 3-D collagen hydrogels for functional cell-based biosensing," *Biosens Bioelectron,* vol. 19, pp. 1075-88, 2004.

[178] Y. Tabata, S. Hijikata, M. Muniruzzaman, and Y. Ikada, "Neovascularization effect of biodegradable gelatin microspheres incorporating basic fibroblast growth factor," *J Biomater Sci Polym Ed,* vol. 10, pp. 79-94, 1999.

[179] M. Yamamoto, Y. Takahashi, and Y. Tabata, "Controlled release by biodegradable hydrogels enhances the ectopic bone formation of bone morphogenetic protein," *Biomaterials,* vol. 24, pp. 4375-83, 2003.

[180] M. Guvendiren and J. A. Burdick, "Engineering synthetic hydrogel microenvironments to instruct stem cells," *Current Opinion in Biotechnology,* vol. 24, pp. 841-846, 2013.

[181] E. Brinkman, L. van der Does, and A. Bantjes, "Poly(vinyl alcohol)-heparin hydrogels as sensor catheter membranes," *Biomaterials,* vol. 12, pp. 63-70, 1991.

[182] N. A. Peppas and J. E. Scott, "Controlled release from poly (vinyl alcohol) gels prepared by freezing-thawing processes," *Journal of Controlled Release,* vol. 18, pp. 95-100, 1992.

[183] S. R. Stauffer and N. A. Peppast, "Poly(vinyl alcohol) hydrogels prepared by freezing-thawing cyclic processing," *Polymer,* vol. 33, pp. 3932-3936, 1992.

[184] D. L. Hern and J. A. Hubbell, "Incorporation of adhesion peptides into nonadhesive hydrogels useful for tissue resurfacing," *Journal of Biomedical Materials Research,* vol. 39, pp. 266-276, 1998.
[185] C. N. Salinas and K. S. Anseth, "Mixed Mode Thiol−Acrylate Photopolymerizations for the Synthesis of PEG−Peptide Hydrogels," *Macromolecules,* vol. 41, pp. 6019-6026, 2008.
[186] C.-C. Lin and K. S. Anseth, "Glucagon-Like Peptide-1 Functionalized PEG Hydrogels Promote Survival and Function of Encapsulated Pancreatic β-Cells," *Biomacromolecules,* vol. 10, pp. 2460-2467, 2009.
[187] D. L. Elbert, A. B. Pratt, M. P. Lutolf, S. Halstenberg, and J. A. Hubbell, "Protein delivery from materials formed by self-selective conjugate addition reactions," *Journal of Controlled Release,* vol. 76, pp. 11-25, 2001.
[188] M. P. Lutolf, J. L. Lauer-Fields, H. G. Schmoekel, A. T. Metters, F. E. Weber, G. B. Fields, *et al.,* "Synthetic matrix metalloproteinase-sensitive hydrogels for the conduction of tissue regeneration: Engineering cell-invasion characteristics," *Proceedings of the National Academy of Sciences of the United States of America,* vol. 100, pp. 5413-5418, 2003.
[189] S. P. Zustiak and J. B. Leach, "Characterization of Protein Release From Hydrolytically Degradable Poly(Ethylene Glycol) Hydrogels," *Biotechnology and Bioengineering,* vol. 108, pp. 197-206, 2011.
[190] E. A. Phelps, K. L. Templeman, P. M. Thulé, and A. J. García, "Engineered VEGF-releasing PEG–MAL hydrogel for pancreatic islet vascularization," *Drug Delivery and Translational Research,* vol. 5, pp. 125-136, 2013.
[191] A. T. Metters, C. N. Bowman, and K. S. Anseth, "A statistical kinetic model for the bulk degradation of PLA-b-PEG-b-PLA hydrogel networks," *Journal of Physical Chemistry B,* vol. 104, pp. 7043-7049, 2000.
[192] A. T. Metters, K. S. Anseth, and C. N. Bowman, "A statistical kinetic model for the bulk degradation of PLA-b-PEG-b-PLA hydrogel networks: Incorporating network non-idealities," *Journal of Physical Chemistry B,* vol. 105, pp. 8069-8076, 2001.
[193] S. Lin-Gibson, R. L. Jones, N. R. Washburn, and F. Horkay, "Structure-property relationships of photopolymerizable poly(ethylene glycol) dimethacrylate hydrogels," *Macromolecules,* vol. 38, pp. 2897-2902, 2005.
[194] T.-Y. Lin, C. S. Ki, and C.-C. Lin, "Manipulating hepatocellular carcinoma cell fate in orthogonally cross-linked hydrogels," *Biomaterials,* vol. 35, pp. 6898-6906, 2014.
[195] G. Jones, II, C. W. Farahat, and C. Oh, "Photoinduced Electron Transfer Involving Eosin-Tryptophan Conjugates. Long-Lived Radical Pair States for Systems Incorporating Aromatic Amino Acid Side Chains," *The Journal of Physical Chemistry,* vol. 98, pp. 6906-6909, 1994.
[196] D. I. Pattison and M. J. Davies, "Actions of ultraviolet light on cellular structures," *EXS,* pp. 131-57, 2006.
[197] F. Rizzuto and J. D. Spikes, "THE EOSIN-SENSITIZED PHOTOOXIDATION OF SUBSTITUTED PHENYLALANINES AND TYROSINES*," *Photochemistry and Photobiology,* vol. 25, pp. 465-476, 1977.

[198] G. Jones, Z. Feng, and C. Oh, "Photoinduced Electron Transfer for an Eosin-Tyrosine Conjugate. Activity of the Tyrosinate Anion in Long Range Electron Transfer in a Protein-like Polymer Matrix," *The Journal of Physical Chemistry,* vol. 99, pp. 3883-3888, 1995.

[199] D. Creed, "THE PHOTOPHYSICS AND PHOTOCHEMISTRY OF THE NEAR-UV ABSORBING AMINO ACIDS–II. TYROSINE AND ITS SIMPLE DERIVATIVES," *Photochemistry and Photobiology,* vol. 39, pp. 563-575, 1984.

[200] U. Johansson, M. Ria, K. Åvall, N. Dekki Shalaly, S. V. Zaitsev, P.-O. Berggren, *et al.*, "Pancreatic Islet Survival and Engraftment Is Promoted by Culture on Functionalized Spider Silk Matrices," *PLoS ONE,* vol. 10, p. e0130169, 2015.

[201] T. Otonkoski, M. Banerjee, O. Korsgren, L. E. Thornell, and I. Virtanen, "Unique basement membrane structure of human pancreatic islets: implications for β-cell growth and differentiation," *Diabetes, Obesity and Metabolism,* vol. 10, pp. 119-127, 2008.

[202] M. Armanet, A. Wojtusciszyn, P. Morel, G. Parnaud, P. Rousselle, C. Sinigaglia, *et al.*, "Regulated laminin-332 expression in human islets of Langerhans," *The FASEB Journal,* vol. 23, pp. 4046-4055, December 1, 2009.

[203] Y. Li, X. Cao, L.-X. Li, P. L. Brubaker, H. Edlund, and D. J. Drucker, "β-Cell Pdx1 Expression Is Essential for the Glucoregulatory, Proliferative, and Cytoprotective Actions of Glucagon-Like Peptide-1," *Diabetes,* vol. 54, pp. 482-491, 2005.

[204] Sreenath S. Andrali, Megan L. Sampley, Nathan L. Vanderford, and S. Özcan, "Glucose regulation of insulin gene expression in pancreatic β-cells," *Biochemical Journal,* vol. 415, pp. 1-10, 2008.

[205] M. Ejarque, S. Cervantes, G. Pujadas, A. Tutusaus, L. Sanchez, and R. Gasa, "Neurogenin3 Cooperates with Foxa2 to Autoactivate Its Own Expression," *Journal of Biological Chemistry,* vol. 288, pp. 11705-11717, 2013.

[206] T. Iype, J. Francis, J. C. Garmey, J. C. Schisler, R. Nesher, G. C. Weir, *et al.*, "Mechanism of insulin Gene Regulation by the Pancreatic Transcription Factor Pdx-1: APPLICATION OF PRE-mRNA ANALYSIS AND CHROMATIN IMMUNOPRECIPITATION TO ASSESS FORMATION OF FUNCTIONAL TRANSCRIPTIONAL COMPLEXES," *Journal of Biological Chemistry,* vol. 280, pp. 16798-16807, 2005.

[207] D. B. Jaroch, J. Lu, R. Madangopal, N. D. Stull, M. Stensberg, J. Shi, *et al.*, "Mouse and human islets survive and function after coating by biosilicification," *American Journal of Physiology - Endocrinology and Metabolism,* vol. 305, pp. E1230-E1240, 2013.

[208] M. P. Lutolf and J. A. Hubbell, "Synthetic biomaterials as instructive extracellular microenvironments for morphogenesis in tissue engineering," *Nat Biotechnol,* vol. 23, pp. 47-55, 2005.

[209] P. M. Kharkar, K. L. Kiick, and A. M. Kloxin, "Designing degradable hydrogels for orthogonal control of cell microenvironments," *Chem Soc Rev,* vol. 42, pp. 7335-72, 2013.

[210] Y. Jiang, J. Chen, C. Deng, E. J. Suuronen, and Z. Zhong, "Click hydrogels, microgels and nanogels: emerging platforms for drug delivery and tissue engineering," *Biomaterials,* vol. 35, pp. 4969-85, 2014.

[211] A. M. Kloxin, M. W. Tibbitt, A. M. Kasko, J. A. Fairbairn, and K. S. Anseth, "Tunable Hydrogels for External Manipulation of Cellular Microenvironments through Controlled Photodegradation," *Advanced Materials,* vol. 22, pp. 61-66, 2010.

[212] M. Guvendiren and J. A. Burdick, "Stiffening hydrogels to probe short- and long-term cellular responses to dynamic mechanics," *Nat Commun,* vol. 3, p. 792, 2012.

[213] K. M. Mabry, R. L. Lawrence, and K. S. Anseth, "Dynamic stiffening of poly(ethylene glycol)-based hydrogels to direct valvular interstitial cell phenotype in a three-dimensional environment," *Biomaterials,* vol. 49, pp. 47-56, 2015.

[214] D. T. Butcher, T. Alliston, and V. M. Weaver, "A tense situation: forcing tumour progression," *Nat Rev Cancer,* vol. 9, pp. 108-122, 2009.

[215] A. M. Handorf, Y. Zhou, M. A. Halanski, and W.-J. Li, "Tissue Stiffness Dictates Development, Homeostasis, and Disease Progression," *Organogenesis,* vol. 11, pp. 1-15, 2015.

[216] A. J. Engler, S. Sen, H. L. Sweeney, and D. E. Discher, "Matrix Elasticity Directs Stem Cell Lineage Specification," *Cell,* vol. 126, pp. 677-689, 2006.

[217] N. Huebsch, P. R. Arany, A. S. Mao, D. Shvartsman, O. A. Ali, S. A. Bencherif, *et al.,* "Harnessing traction-mediated manipulation of the cell/matrix interface to control stem-cell fate," *Nat Mater,* vol. 9, pp. 518-526, 2010.

[218] M. Krieg, Y. Arboleda-Estudillo, P. H. Puech, J. Kafer, F. Graner, D. J. Muller, *et al.,* "Tensile forces govern germ-layer organization in zebrafish," *Nat Cell Biol,* vol. 10, pp. 429-436, 2008.

[219] J. D. Pajerowski, K. N. Dahl, F. L. Zhong, P. J. Sammak, and D. E. Discher, "Physical plasticity of the nucleus in stem cell differentiation," *Proceedings of the National Academy of Sciences,* vol. 104, pp. 15619-15624, October 2, 2007.

[220] C. M. Kraning-Rush and C. A. Reinhart-King, "Controlling matrix stiffness and topography for the study of tumor cell migration," *Cell Adhesion & Migration,* vol. 6, pp. 274-279, 2012.

[221] R. S. Stowers, S. C. Allen, and L. J. Suggs, "Dynamic phototuning of 3D hydrogel stiffness," *Proceedings of the National Academy of Sciences,* vol. 112, pp. 1953-1958, February 17, 2015.

[222] J.-H. Seo, S. Kakinoki, T. Yamaoka, and N. Yui, "Directing Stem Cell Differentiation by Changing the Molecular Mobility of Supramolecular Surfaces," *Advanced Healthcare Materials,* vol. 4, pp. 215-222, 2015.

[223] T. R. Cox and J. T. Erler, "Remodeling and homeostasis of the extracellular matrix: implications for fibrotic diseases and cancer," *Disease Models and Mechanisms,* vol. 4, pp. 165-178, 2011.

[224] S. Sharma, C. Santiskulvong, J. Rao, J. K. Gimzewski, and O. Dorigo, "The role of Rho GTPase in cell stiffness and cisplatin resistance in ovarian cancer cells," *Integrative Biology,* vol. 6, pp. 611-617, 2014.

[225] C. Liu, Y. Liu, H.-g. Xie, S. Zhao, X.-x. Xu, L.-x. Fan, *et al.*, "Role of three-dimensional matrix stiffness in regulating the chemoresistance of hepatocellular carcinoma cells," *Biotechnology and Applied Biochemistry,* vol. 62, pp. 556-562, 2015.

[226] M. Guvendiren, M. Perepelyuk, R. G. Wells, and J. A. Burdick, "Hydrogels with differential and patterned mechanics to study stiffness-mediated myofibroblastic differentiation of hepatic stellate cells," *J Mech Behav Biomed Mater,* vol. 38, pp. 198-208, 2014.

[227] H. Wang, M. W. Tibbitt, S. J. Langer, L. A. Leinwand, and K. S. Anseth, "Hydrogels preserve native phenotypes of valvular fibroblasts through an elasticity-regulated PI3K/AKT pathway," *Proc Natl Acad Sci U S A,* vol. 110, pp. 19336-41, 2013.

[228] H. Wang, S. M. Haeger, A. M. Kloxin, L. A. Leinwand, and K. S. Anseth, "Redirecting valvular myofibroblasts into dormant fibroblasts through light-mediated reduction in substrate modulus," *PLoS One,* vol. 7, p. e39969, 2012.

[229] R. G. Wells, "The role of matrix stiffness in regulating cell behavior," *Hepatology,* vol. 47, pp. 1394-1400, 2008.

[230] B. J. Gill, D. L. Gibbons, L. C. Roudsari, J. E. Saik, Z. H. Rizvi, J. D. Roybal, *et al.*, "A synthetic matrix with independently tunable biochemistry and mechanical properties to study epithelial morphogenesis and EMT in a lung adenocarcinoma model," *Cancer Res,* vol. 72, pp. 6013-23, 2012.

[231] C.-C. Lin, "Recent advances in crosslinking chemistry of biomimetic poly(ethylene glycol) hydrogels," *RSC Advances,* vol. 5, pp. 39844-39853, 2015.

[232] J. A. Burdick and W. L. Murphy, "Moving from static to dynamic complexity in hydrogel design," *Nat Commun,* vol. 3, p. 1269, 2012.

[233] J. Hu, "Supramolecular shape memory polymers," in *Advances in Shape Memory Polymers*, ed: Woodhead Publishing, pp. 111-127, 2013.

[234] H. Meng and G. Li, "A review of stimuli-responsive shape memory polymer composites," *Polymer,* vol. 54, pp. 2199-2221, 2013.

[235] X. Ma and Y. Zhao, "Biomedical Applications of Supramolecular Systems Based on Host–Guest Interactions," *Chemical Reviews,* vol. 115, pp. 7794-7839, 2015.

[236] B. W. Hwang, S. J. Kim, K. M. Park, H. Kim, J. Yeom, J.-A. Yang, *et al.*, "Genetically engineered mesenchymal stem cell therapy using self-assembling supramolecular hydrogels," *Journal of Controlled Release,* vol. 220, Part A, pp. 119-129, 2015.

[237] M. Cheng, F. Shi, J. Li, Z. Lin, C. Jiang, M. Xiao, *et al.*, "Macroscopic Supramolecular Assembly of Rigid Building Blocks Through a Flexible Spacing Coating," *Advanced Materials,* vol. 26, pp. 3009-3013, 2014.

[238] E. A. Appel, F. Biedermann, U. Rauwald, S. T. Jones, J. M. Zayed, and O. A. Scherman, "Supramolecular Cross-Linked Networks via Host−Guest Complexation with Cucurbit[8]uril," *Journal of the American Chemical Society,* vol. 132, pp. 14251-14260, 2010.

[239] E. A. Appel, R. A. Forster, M. J. Rowland, and O. A. Scherman, "The control of cargo release from physically crosslinked hydrogels by crosslink dynamics," *Biomaterials,* vol. 35, pp. 9897-9903, 2014.

[240] D. Wang, M. Wagner, H.-J. Butt, and S. Wu, "Supramolecular hydrogels constructed by red-light-responsive host-guest interactions for photo-controlled protein release in deep tissue," *Soft Matter,* vol. 11, pp. 7656-7662, 2015.
[241] L. Chen, X. Zhao, Y. Lin, Z. Su, and Q. Wang, "Dual stimuli-responsive supramolecular hydrogel of bionanoparticles and hyaluronan," *Polymer Chemistry,* vol. 5, pp. 6754-6760, 2014.
[242] F. van de Manakker, K. Braeckmans, N. e. Morabit, S. C. De Smedt, C. F. van Nostrum, and W. E. Hennink, "Protein-Release Behavior of Self-Assembled PEG–β-Cyclodextrin/PEG–Cholesterol Hydrogels," *Advanced Functional Materials,* vol. 19, pp. 2992-3001, 2009.
[243] C. B. Rodell, A. L. Kaminski, and J. A. Burdick, "Rational Design of Network Properties in Guest–Host Assembled and Shear-Thinning Hyaluronic Acid Hydrogels," *Biomacromolecules,* vol. 14, pp. 4125-4134, 2013.
[244] C. B. Rodell, J. W. MacArthur, S. M. Dorsey, R. J. Wade, L. L. Wang, Y. J. Woo, *et al.*, "Shear-Thinning Supramolecular Hydrogels with Secondary Autonomous Covalent Crosslinking to Modulate Viscoelastic Properties In Vivo," *Advanced Functional Materials,* vol. 25, pp. 636-644, 2015.
[245] T. Kakuta, Y. Takashima, and A. Harada, "Highly Elastic Supramolecular Hydrogels Using Host–Guest Inclusion Complexes with Cyclodextrins," *Macromolecules,* vol. 46, pp. 4575-4579, 2013.
[246] H. Shih and C.-C. Lin, "Photoclick Hydrogels Prepared from Functionalized Cyclodextrin and Poly(ethylene glycol) for Drug Delivery and in Situ Cell Encapsulation," *Biomacromolecules,* vol. 16, pp. 1915-1923, 2015.
[247] W. Zhang, M. Chen, and G. Diao, "Electrospinning β-cyclodextrin/poly(vinyl alcohol) nanofibrous membrane for molecular capture," *Carbohydrate Polymers,* vol. 86, pp. 1410-1416, 2011.
[248] M. Constantin, G. Fundueanu, F. Bortolotti, R. Cortesi, P. Ascenzi, and E. Menegatti, "Preparation and characterisation of poly(vinyl alcohol)/cyclodextrin microspheres as matrix for inclusion and separation of drugs," *International Journal of Pharmaceutics,* vol. 285, pp. 87-96, 2004.
[249] J. L. Manasco, C. Tang, N. A. Burns, C. D. Saquing, and S. A. Khan, "Rapidly dissolving poly(vinyl alcohol)/cyclodextrin electrospun nanofibrous membranes," *RSC Advances,* vol. 4, pp. 13274-13279, 2014.
[250] S. Das, M. T. Joseph, and D. Sarkar, "Hydrogen Bonding Interpolymer Complex Formation and Study of Its Host–Guest Interaction with Cyclodextrin and Its Application as an Active Delivery Vehicle," *Langmuir,* vol. 29, pp. 1818-1830, 2013.
[251] C. B. Rodell, J. E. Mealy, and J. A. Burdick, "Supramolecular Guest–Host Interactions for the Preparation of Biomedical Materials," *Bioconjug Chem,* 2015.
[252] A. M. Rosales, K. M. Mabry, E. M. Nehls, and K. S. Anseth, "Photoresponsive Elastic Properties of Azobenzene-Containing Poly(ethylene-glycol)-Based Hydrogels," *Biomacromolecules,* vol. 16, pp. 798-806, 2015.
[253] R. Jain and E. Lammert, "Cell-cell interactions in the endocrine pancreas," *Diabetes Obes Metab,* vol. 11 Suppl 4, pp. 159-67, 2009.

[254] A. Tomas, B. Yermen, L. Min, J. E. Pessin, and P. A. Halban, "Regulation of pancreatic beta-cell insulin secretion by actin cytoskeleton remodelling: role of gelsolin and cooperation with the MAPK signalling pathway," *J Cell Sci,* vol. 119, pp. 2156-67, 2006.

[255] D. C. Thurmond, C. Gonelle-Gispert, M. Furukawa, P. A. Halban, and J. E. Pessin, "Glucose-stimulated insulin secretion is coupled to the interaction of actin with the t-SNARE (target membrane soluble N-ethylmaleimide-sensitive factor attachment protein receptor protein) complex," *Mol Endocrinol,* vol. 17, pp. 732-42, 2003.

[256] L. Tillmar and N. Welsh, "Hypoxia may increase rat insulin mRNA levels by promoting binding of the polypyrimidine tract-binding protein (PTB) to the pyrimidine-rich insulin mRNA 3'-untranslated region," *Mol Med,* vol. 8, pp. 263-72, 2002.

[257] Y. Sato, H. Endo, H. Okuyama, T. Takeda, H. Iwahashi, A. Imagawa, *et al.*, "Cellular hypoxia of pancreatic beta-cells due to high levels of oxygen consumption for insulin secretion in vitro," *J Biol Chem,* vol. 286, pp. 12524-32, 2011.

[258] R. M. Dicharry, P. Ye, G. Saha, E. Waxman, A. D. Asandei, and R. S. Parnas, "Wheat Gluten−Thiolated Poly(vinyl alcohol) Blends with Improved Mechanical Properties," *Biomacromolecules,* vol. 7, pp. 2837-2844, 2006.

[259] B. Gupta, S. Anjum, and S. Ikram, "Preparation of thiolated polyvinyl alcohol hydrogels," *Journal of Applied Polymer Science,* vol. 129, pp. 815-821, 2013.

VITA

VITA

Education

Weldon School of Biomedical Engineering, Purdue University, West Lafayette, IN
PhD Candidate in Biomedical Engineering
Purdue Research Foundation Fellow — Expected Graduation: May 2016

Purdue School of Engineering and Technology, Indiana University-Purdue University Indianapolis (IUPUI), Indianapolis, IN
Master of Science in Biomedical Engineering
University Fellow — Graduated: May 2013

Purdue School of Engineering and Technology, Indiana University-Purdue University Indianapolis (IUPUI), Indianapolis, IN
Bachelor of Science in Biomedical Engineering
Minors in Mathematics & Chemistry — Graduated: May 2011

Research Experiences

Biomaterials and Tissue Engineering Lab, IUPUI
May, 2011 – Current
Graduate Research Assistant

- Developing biomaterial for encapsulating cells and delivering drugs for potential treatment of type I diabetes
- Planning and executing research experiments including chemical synthesis, material characterization, formulation, and cytocompatibility testing
- Writing proposals, publications, and book chapters
- Training and managing junior researchers and new members
- Troubleshooting and maintaining equipment
- Communicating and presentation at regional, national and international conferences

Department of Biomedical Engineering, IUPUI
August, 2011 – May, 2013
Teaching Assistant

- Developed experiments and lab guides for biomaterials lab
- Prepared and purchased materials for experiments
- Gave lectures and graded lab reports

Indiana University School of Dentistry
June, 2009 – January, 2011
Undergraduate Research Assistant

- Evaluated effect of oral bacteria on the mechanical properties of dental resin
- Planned and executed research experiments from bacteria culture to mechanical testing
- Presented at national and international conferences

Key Technical Skills

Biomaterial & Polymer Sciences: scaffold design, polymerization, hydrogel formulation, surface modifications, coating techniques, drug delivery, purification, photo-chemistry, lyophilization, solid phase peptide synthesis (SPPS), bioconjugation techniques, chemical synthesis and modifications (e.g., macromer, polymer or small molecules),
Analytical Chemistry: HPLC, MS, FT-IR, UV-vis, NMR
Biological Sciences: confocal microscopy, fluorescence microscopy, immunostaining, intracellular staining, RNA isolation, PCR, drug dosage assay, protein quantification assays, sterilization, cell encapsulation, cell culture, stem cell differentiation, bacterial culture, ELISA, cellular assays (e.g., proliferation & apoptosis), biocompatibility tests
Engineering Tools: rheometry, mechanical and microhardness testing, ChemDraw, MATLAB, ProE/Creo, basic C Programming and R programming, statistical analysis, GraphPad Prism, MS Office

Honors and Awards

2016
Outstanding Graduate Research Award (Purdue)
Joe Bourland Travel Award (Purdue)
A. H. Ismail Interdisciplinary Program Doctoral Research Travel Award (Purdue)

2015
Professional Grant from Purdue Graduate Student Government
Joe Bourland Travel Award (Purdue University)
Biomedical Engineering Research Symposium – Second place (IUPUI)

2014
Honorable Mention Student Travel Achievement Recognition (Society for Biomaterials)
A. H. Ismail Interdisciplinary Program Doctoral Research Travel Award (Purdue)
Graduate and Professional Education Grant (Purdue)
Biomedical Engineering Research Symposium – First place (IUPUI)
2013
Purdue School of Engineering and Technology Student Council Travel Grant
Graduate and Professional Enhancement Grant (IUPUI)

2012
Material Research Society Spring Meeting Travel Award

2011
TOP 100 Student – TOP 10 Female (IUPUI)
Biomedical Engineering Service Award (IUPUI)
Alfred R. and Janet H. Potvin Outstanding Student Leader & Scholar (IUPUI)
Commitment to Engineering Excellence Undergraduate Research Grant (IUPUI)
Imagine Cup Honorable Mention (Microsoft)

2010
TOP 100 Student – TOP 10 Female (IUPUI)
Purdue School of Engineering and Technology Outstanding Woman (IUPUI)
Commitment to Engineering Excellence Undergraduate Summer Research Grant (IUPUI)

Publications

1. **Shih H**, and **Lin CC**. Tuning stiffness of cell-laden hydrogels via host-guest interactions. *Journal of Materials Chemistry B*. 2016 (*In press*) DOI: 10.1039/C6TB00890A
2. **Shih H**, and Lin C. Photo-click hydrogels prepared from functionalized cyclodextrin and poly(ethylene glycol) for drug delivery and in situ cell encapsulation. *Biomacromolecules.* 2015(16)1915-1923.
3. **Shih H**, Mirmira RG, and Lin C. Visible light-initiated interfacial thiol-ene photopolymerization for forming islet surface conformal coating. *Journal of Material Chemistry B.* 2015(3)170-175.
4. Lin C, Ki CS, **Shih H**. Thiol-norbornene photo-click hydrogels for tissue engineering applications. *Journal of Applied Polymer Science*. 2015(132)41563. (Featured cover)
5. Munoz Z*, **Shih H***, and Lin C. Gelatin hydrogels formed by orthogonal thiol-norbornene photochemistry for cell encapsulation. *Biomaterials Science.* 2014(2)1063-1072. (Featured cover, * indicates equal contribution)
6. Hao Y*, **Shih H***, Munoz Z, Kemp A, and Lin C. Visible light curable thiol-vinyl hydrogels with tunable matrix stiffness and degradability for 3D cell culture. *Acta Biomaterialia.* 2014(10)104-114. (* indicates equal contribution)
7. Hamamura K, Zhang P, Zhao L, Shim JW, Chen A, Dodge TR, Wan Q, **Shih H**, Na S, Lin C, Sun HB, and Yokota H. Knee loading reduces MMP13 activity in the mouse cartilage. *BMC Musculoskeletal Disorders.* 2013(14)312.
8. Ki CS, **Shih H**, and Lin C. The influence of matrix stiffness and cell-matrix interaction on the efficacy of EGFR antagonist in pancreatic adenocarcinoma cells. *Biomacromolecules*. 2013(9)3017-3026.
9. Ki CS, **Shih H**, and Lin C. Facile preparation of photodegradable hydrogels by photopolymerization. *Polymer.* 2013(54)2115-2122.
10. **Shih H**, Fraser AK, and Lin C. Interfacial thiol-ene photo-click reactions for forming multilayer hydrogels. *ACS Applied Materials & Interfaces.* 2013(5)1673-1680.
11. **Shih H**, and Lin C. Visible light-mediated thiol-ene hydrogelation using eosin-Y as the only photoinitiator. *Macromolecular Rapid Communications*. 2013(34)269-273.
12. **Shih H**, and Lin C. Cross-linking and degradation of step-growth hydrogels formed by thiol-ene photo-click chemistry. *Biomacromolecules*. 2012(13)2003-2012.

13. Lin C, Raza A, and **Shih H**. PEG hydrogels formed by thiol-ene photo-click chemistry and their effect on the formation and recovery of insulin-secreting spheroids. *Biomaterials.* 2011(32)9685-9695.
14. Gregson KS, **Shih H**, and Gregory RL. The Impact of three strains of oral bacteria on the surface and mechanical properties of a dental resin material. *Clinical Oral Investigation.* 2011.

Invited Book Chapters

1. **Shih H** and Lin C. Dynamic controls in degradable hydrogels. Biodegradable Polymers: New Development, Editor: Chu CC. Nova Science Publishers.
2. Lin C and **Shih H**. Modeling drug release from synthetic hydrogels. Applications of Hydrogels in Drug Delivery and Biosensors, Editors: Khademhosseini A. and Demirci U. World Scientific Publishing.

Contributed Abstracts

1. **Shih H**, and Lin C. "Photo-click hydrogels prepared from functionalized cyclodextrin and poly(ethylene glycol) for drug delivery and *in situ* cell encapsulation" American Institute of Chemical Engineer Midwest Regional Conference, Chicago, IL, Mar. 2016. Oral presentation.
2. **Shih H**, and Lin C. "Tuning stiffness of cell-laden hydrogel by reversible host-guest interactions" American Chemical Society National Conference, San Diego, CA, Mar. 2016. Oral presentation.
3. **Shih H**, and Lin C. "Tuning stiffness of cell-laden hydrogel by photo-reversible host-guest interactions" Society for Biomaterials Annual Meeting and Exhibition, Charlotte, NC, Apr. 2015. Oral presentation.
4. **Shih H**, and Lin C. "Interfacial thiol-ene photochemistry for forming orthogonal immune-isolation coating on pancreatic islets" Society for Biomaterials Annual Meeting and Exhibition, Denvor, CO, Apr. 2014. Oral presentation.
5. Hao Y, **Shih H**, Munoz Z, Kemp AD, and Lin C. "Visible light cured thiol-vinyl hydrogels with tunable degradation for 3D cell culture" Society for Biomaterials Annual Meeting and Exhibition, Denvor, CO, Apr. 2014. Oral presentation.
6. Munoz Z, **Shih H**, and Lin C. "Gelatin hydrogels formed by orthogonal thiol-norbornene photochemistry for cell encapsulation" Society for Biomaterials Annual Meeting and Exhibition, Denvor, CO, Apr. 2014. Poster presentation.
7. **Shih H**, and Lin C. "Visible light-mediated multi-scale thiol-ene hydrogels for 3D cell culture" Society for Biomaterials Regional Conference, Cleveland, OH, Oct. 2013. Oral presentation.
8. **Shih H**, Fraser AK, and Lin C. "Visible light-mediated multi-scale thiol-ene hydrogels for 3D cell culture" Society for Biomaterials Annual Meeting and Exhibition, Boston, MA, Apr. 2013. Oral presentation.
9. Fraser AK, **Shih H**, and Lin C. "Preparation of microgels using thiol-ene "click" chemistry" Society for Biomaterials Annual Meeting and Exhibition, Boston, MA, Apr. 2013.

10. Ki CS, **Shih H**, and Lin C. "Facile preparation of photodegradable hydrogel by photo-mediated crosslinking" Society for Biomaterials Annual Meeting and Exhibition, Boston, MA, Apr. 2013.
11. Fraser AK, **Shih H**, and Lin C. "Preparation of photopolymerized dual-layer microgels" 18th IUURC, IUPUI, Indianapolis, IN, Nov. 2012.
12. **Shih H**, and Lin C. "Manipulating thiol-ene hydrogel degradation for controlling 3D cell morphogenesis" Material Research Society Spring Conference, San Francisco, CA, Apr. 2012. Oral presentation.
13. **Shih H**, and Lin C. "Dual-mode degradable hydrogels formed by thiol-ene photo-click reactions" Society for Biomaterials Regional Conference, West Lafayette, IN, Oct. 2011. Poster presentation.
14. Raza A, **Shih H**, and Lin C. "Thiol-ene hydrogels for generation and recovery of pancreatic beta-cell spheroids" Society for Biomaterials Regional Conference, West Lafayette, IN, Oct. 2011.
15. **Shih H**, Gregson KS, and Gregory RL. "Dental materials and oral bacterial interactions" Biomedical Engineering Society Annual Conference, Austin, TX, Oct. 2010. Poster presentation.
16. **Shih H**, Gregson KS, and Gregory RL. "Impact of oral bacteria on the surface and mechanical properties of a dental material" American Association for Dental Research Annual Conference, Washington, DC, Mar. 2010. Poster presentation.

Leadership Experience

2013 – 2014

President of Biomedical Engineering Graduate Student Association (IUPUI)

2010 – 2011

Treasurer of Society of Biomedical Engineering

Office of Student Involvement Leadership Consultant (IUPUI)

Community Services

- American Chemical Society National Conference (2014)
- Minority Engineering Advancement Program (2008-2013)
- Preparing Outstanding Women for Engineering Roles Summer Program (2010-2014)
- IUPUI Student Organizations Leadership Development Workshops (2009-2011)